

A Reproduced Copy
OF

Reproduced for NASA
by the
NASA Scientific and Technical Information Facility

DRF-05577

STUDIES TO DETERMINE THE FEASIBILITY
OF VARIOUS TECHNIQUES FOR MEASURING PROPELLANT
MASS ABOARD ORBITING SPACE VEHICLE

Volume 11

PHASE "B"

FINAL REPORT

PERIOD, June 3, 1966 to January 30, 1968

Contract No. NAS 8-18039

Prepared for

GEORGE C. MARSHALL SPACE FLIGHT CENTER
NATIONAL AERONAUTICS & SPACE ADMINISTRATION
Huntsville, Alabama

by

THE BENDIX CORPORATION
Instruments & Life Support Division
Davenport, Iowa

FACILITY FORM 602	N 69-12144	
	(ACCESSION NUMBER)	(THRU)
	310	1
	(PAGES)	(CODE)
	CR-97818	28
	(NASA CR OR TMX OR AD NUMBER)	(CATEGORY)

PUBLICATION NO. 3745-67
JUNE 1, 1968

TABLE OF CONTENTS

SECTION		PAGE NUMBER
FOREWORD		i
ABSTRACT		ii
SECTION I	INTRODUCTION	1-1, 2
SECTION II	PROGRAM OBJECTIVES	
2.1	INTRODUCTION	2-1
2.2	STUDY OF TANK CHARACTERISTICS	2-1, 2
2.3	STUDY OF PROPELLANT CHARACTERISTICS	2-2
2.4	STUDY OF HARDWARE CHARACTERISTICS	2-2
2.5	STUDY OF SYSTEM CHARACTERISTICS	2-2
SECTION III	THEORETICAL STUDIES	
3.1	INTRODUCTION	3-1
3.2	ANALYSIS - RECTANGULAR CAVITY	3-1 thru 3-5
3.3	ANALYSIS - CYLINDRICAL CAVITY	3-5 thru 3-11
3.4	ANALYSIS - SPHERICAL CAVITY	3-11 thru 3-15
3.5	ANALYSIS - ARBITRARY CAVITIES OF REVOLUTION	3-15 thru 3-19
3.6	FIELD PATTERNS AND ANTENNA LOCATION	3-20, 21
3.7	DEVELOPMENT OF VOLUME DEPENDENCE FORMULA	3-21 thru 3-23
3.8	RESONANCE DISTRIBUTION VERSUS FREQUENCY BAND	3-24
3.9	MODE MERGING AND 'Q' DEPENDENCE	3-24 thru 3-30
3.10	DEVELOPMENT OF STATISTICAL REPRESENTATION	3-30 thru 3-50

TABLE OF CONTENTS (Continued)

SECTION IV	EXPERIMENTAL STUDIES	
4.1	INTRODUCTION	4-1 thru 4-3
4.2	STANDARD CYLINDRICAL CAVITY TESTS	4-3 thru 4-8
4.2.1	TANK COUPLING	4-8 thru 4-11
4.2.2	ANTENNA SYSTEMS	4-11 thru 4-13
4.2.3	COMPARISON OF THE MONOPOLE AND CONE ANTENNAS IN A RESONANT CAVITY	4-13 thru 4-16
4.2.4	OPTIMUM MODE COUPLING WITH SMALL MONOPOLES	4-16, 17
4.3	S-IVB MATCHED TANK STUDY	4-17 thru 4-21
4.4	THERMO TANK TESTS (2/5 SCALE MODEL)	4-21 thru 4-42
4.5	THERMO TANK TESTS (1/3 SCALE MODEL)	4-43 thru 4-45
4.6	SIMULATED SPACECRAFT TANK TESTS	4-46 thru 4-51
SECTION V	COMPARISON OF EXPERIMENTAL RESULTS TO THEORETICAL PREDICTIONS	
5.1	INTRODUCTION	5-1
5.2	COMPUTER CALCULATED LOADING DEPENDANCIES COMPARISONS	5-2
5.2.1	1/3 SCALE THERMO TANK COMPARISONS	5-2
5.2.2	2/5 SCALE THERMO TANK COMPARISONS	5-2 thru 5-6
5.3	MATHEMATICAL FORMULA LOADING DEPENDANCIES COMPARISONS	5-6
5.3.1	S-IVB TANK COMPARISONS	5-6 thru 5-9
5.3.2	LOADING RESPONSE SPACECRAFT TANK	5-9

TABLE OF CONTENTS (Continued)

5.3.3	LOADING RESPONSE 1/3 SCALE THERMO	5-9 thru 5-15
5.3.4	LOADING DEPENDANCIES OF SIMULATED SPACECRAFT TANK	5-15 thru 5-20
5.3.5	LOADING RESPONSE 2/5 SCALE THERMO TANK	5-20
5.4	CONCLUSIONS	5-20 thru 5-24
SECTION VI	GENERALIZED RF GAGING HANDBOOK	6-1 thru 6-6
SECTION VII	CONCLUSIONS	7-1
SECTION VIII	RECOMMENDATIONS	8-1, 2

TABLE OF CONTENTS (Continued)

SECTION IX	REFERENCES	9-1
APPENDICES		
APPENDIX A	THEORETICAL ANALYSIS OF CAVITIES	
SECTION I	THEORETICAL ANALYSIS OF A RECTANGULAR CAVITY	A-1 thru A-8
SECTION II	THEORETICAL ANALYSIS OF A CYLINDRICAL CAVITY (EXACT)	A-9 thru A-16
SECTION III	THEORETICAL ANALYSIS OF A SPHERICAL CAVITY (EXACT)	A-17 thru A-21
APPENDIX B	COMPUTER PROGRAMS	
SECTION I	PROGRAM FOR PARTIALLY FILLED RECTANGULAR CAVITY	B-1 thru B-8
SECTION II	PROGRAM FOR PARTIALLY FILLED CYLINDRICAL CAVITY (VARIATIONAL TECHNIQUE)	B-9 thru B-18
SECTION III	PROGRAM FOR PARTIALLY FILLED CYLINDRICAL CAVITY (EXACT)	B-19 thru B-28
SECTION IV	SPHERICAL CAVITY PROGRAM	B-29 thru B-34
SECTION V	STATISTICAL PROGRAM	B-35 thru B-36
SECTION VI	BESSEL ZERO PROGRAM	B-47 thru B-50
APPENDIX C	ANALYTICAL DATA	
SECTION I	FIELD PATTERNS FOR VARIOUS MODES IN A CYLINDRICAL CAVITY	C-1 thru C-8
SECTION II	TRANSFER CHARACTERISTICS OF ADJACENT MODES	C-9 thru C-42
APPENDIX D	STATISTICAL PROGRAM ANALYSIS	D-1 thru D-31

LIST OF FIGURES

FIGURE NUMBER		PAGE NUMBER
3-1	RECTANGULAR CAVITY PARTIALLY FILLED WITH DIELECTRIC	3-1
3-2	THEORETICAL LOADING DEPENDENCE - RECTANGULAR CAVITY NO. 1	3-4
3-3	THEORETICAL LOADING DEPENDENCE - RECTANGULAR CAVITY NO. 2	3-6
3-4	THEORETICAL LOADING DEPENDENCE - STANDARD CYLINDRICAL CAVITY	3-8
3-5	CIRCULAR CYLINDRICAL PROPELLANT TANK CONTAINING FLAT END-PLATES	3-10
3-6	THEORETICAL LOADING DEPENDENCE - CYLINDRICAL CAVITY	3-12
3-7	SPHERICAL CAVITY PARTIALLY FILLED WITH DIELECTRIC	3-13
3-8	GENERALIZED SPACECRAFT TANK	3-14
3-9	ELECTRIC FIELD STRENGTH (MM MODES)	3-16
3-10	MAGNETIC FIELD STRENGTH (ME MODES)	3-18
3-11	THEORETICAL MODE DISTRIBUION NORMALIZED TO FULL RESONANCE COUNT	3-24
3-12	ΔN Vs. FREQUENCY CYLINDRICAL CAVITY	3-26
3-13	THEORETICAL LOADING DEPENDENCE - STANDARD CYLINDRICAL TANK	3-27
3-14	OVERLAP OF ADJACENT MODES	3-28
3-15	RESONANCE OVERLAP DEFINITION	3-29
3-16	EXACT COMPUTER SOLUTION - STANDARD CYLINDRICAL CAVITY	3-32
3-17	SYSTEM 'Q' EFFECT ON LOADING - STANDARD CYLINDRICAL TANK (1-2 GHz)	3-35

LIST OF FIGURES (Continued)

FIGURE NUMBER		PAGE NUMBER
3-18	SYSTEM 'Q' EFFECT ON LOADING - STANDARD CYLINDRICAL TANK (2-3 GHz)	3-36
3-19	SYSTEM 'Q' EFFECT ON LOADING - STANDARD CYLINDRICAL TANK (2-4 GHz)	3-37
3-20	SYSTEM 'Q' EFFECT ON LOADING - STANDARD CYLINDRICAL TANK (1-4 GHz)	3-38
3-21	SYSTEM 'Q' EFFECT ON LOADING - THERMO TANK (1/3 SCALE) 1-2 GHz	3-39
3-22	SYSTEM 'Q' EFFECT ON LOADING - THERMO TANK (1/3 SCALE) 2-4 GHz	3-40
3-23	SYSTEM 'Q' EFFECT ON LOADING - THERMO TANK (1/3 SCALE) 1-4 GHz	3-41
3-24	SYSTEM 'Q' EFFECT ON MODE DISTRIBUTION - STANDARD CYLINDRICAL TANK (Q=500)	3-42
3-25	SYSTEM 'Q' EFFECT ON MODE DISTRIBUTION - STANDARD CYLINDRICAL TANK (Q=2000)	3-43
3-26	SYSTEM 'Q' EFFECT ON MODE DISTRIBUTION - STANDARD CYLINDRICAL TANK (Q=5000)	3-44
3-27	SYSTEM 'Q' EFFECT ON MODE DISTRIBUTION - STANDARD CYLINDRICAL TANK (Q=10,000)	3-45
3-28	SYSTEM 'Q' EFFECT ON MODE DISTRIBUTION - STANDARD CYLINDRICAL TANK (Q=20,000)	3-46
3-29	SYSTEM 'Q' EFFECT ON MODE DISTRIBUTION - STANDARD CYLINDRICAL TANK (Q=∞)	3-47
3-30	UPPER CUTOFF FREQUENCY Vs. SYSTEM 'Q' - STANDARD CYLINDRICAL TANK	3-48
4-1	THERMO 2/5 SCALE MODEL TANK	4-2
4-2	DRAWING - SIMULATED THERMO TANK	4-4
4-3	THERMO 1/3 SCALE MODEL TANK FOR LN ₂ TESTS	4-5

LIST OF FIGURES (Continued)

FIGURE NUMBER		PAGE NUMBER
4-4	LH ₂ TEST DEWAR	4-6
4-5	STANDARD CYLINDRICAL CAVITY	4-7
4-6	CAVITY SHOWING LOCATION OF ANTENNA HOLES	4-9
4-7	TANK 'Q' LIMITS, STANDARD CYLINDRICAL CAVITY	4-10
4-8	FREE SPACE ANTENNA CHARACTERISTICS	4-12
4-9	BROAD AND NARROW BAND ANTENNA	4-14
4-10	IMPEDANCE CHARACTERISTICS OF CONE ANTENNA	4-15
4-11	STATIC LOADING TEST, S-IVB TANK (1/20 SCALE)	4-18
4-12	ANTENNA POSITION 1/20 SCALE S-IVB TANK	4-20
4-13	ANTENNA POSITION 2/5 SCALE THERMO TANK	4-21
4-14	OPTIMIZED ANTENNA LENGTH, THERMO TANK (2/5 SCALE)	4-22
4-15	STATIC LOADING TEST, THERMO TANK (2/5 SCALE), NO PROBE GUARDS	4-24
4-16	STATIC LOADING TEST, THERMO TANK (2/5 SCALE), PROBE GUARDS	4-25
4-17	EFFECT OF PERTURBATIONS ON RESONANCE COUNT, THERMO TANK (2/5 SCALE)	4-26
4-18	EFFECT OF PERTURBATIONS ON RESONANCE COUNT, THERMO TANK (2/5 SCALE)	4-27
4-19	REFLECTED ENERGY SYSTEM	4-29
4-20	STATIC LOADING TEST, THERMO TANK (2/5 SCALE)	4-30
4-21	MODIFICATION OF RE-ENTRANT SECTION, ALUMINUM PLATE	4-32
4-22	MODIFICATION OF RE-ENTRANT SECTION, ALUMINUM FOIL	4-32

LIST OF FIGURES (Continued)

FIGURE NUMBER		PAGE NUMBER
4-23	STATIC LOADING TEST, THERMO TANK (2/5 SCALE), MODIFIED RE-ENTRANT SECTION	4-34
4-24	MODIFIED RE-ENTRANT SECTION, PLUMBER'S WOOL	4-33
4-25	STATIC LOADING TEST, THERMO TANK (2/5 SCALE), MODIFIED RE-ENTRANT SECTION (PLUMBER'S WOOL)	4-36
4-26	STATIC LOADING TEST, THERMO TANK (2/5 SCALE), FINAL FREQUENCY BAND	4-37
4-27	BLOCK DIAGRAM - DYNAMIC FLOW TEST HARDWARE	4-38
4-28	DYNAMIC FLOW TEST SET-UP (PHOTOGRAPH)	4-40
4-29	DYNAMIC FLOW TEST (2/5 SCALE THERMO)	4-42
4-30	STATIC LOADING TEST, THERMO TANK (1/3 SCALE), BENZENE DIELECTRIC	4-44
4-31	STATIC LOADING TEST, THERMO TANK (1/3 SCALE), LN ₂ DIELECTRIC	4-45
4-32	STATIC ORIENTATIONS, SIMULATED SPACECRAFT TANK	4-46
4-33	STATIC ORIENTATION TEST, SIMULATED SPACECRAFT TANK, BENZENE DIELECTRIC	4-48
4-34	MODE RINGING	4-49
4-35	STATIC LOADING TEST, SIMULATED SPACECRAFT TANK, LH ₂ DIELECTRIC	4-51
5-1	LOADING RESPONSE - THERMO TANK (1/3 SCALE) LN ₂	5-3
5-2	THEORETICAL LOADING RESPONSE - THERMO TANK (1/3 SCALE)	5-4
5-3	STATIC LOADING TEST - SIMULATED SPACECRAFT TANK - LH ₂	5-5
5-4	SYSTEM 'Q' EFFECT ON MODE DISTRIBUTION - THERMO TANK (2/5 SCALE)	5-7
5-5	STATIC ORIENTATION TEST - THERMO TANK (2/5 SCALE) BENZENE	5-8

LIST OF FIGURES (Continued)

FIGURE NUMBER		PAGE NUMBER
5-6	STATIC LOADING TEST 1/20 SCALE S-IVB TANK	5-10
5-7	SPACECRAFT TANK BENZENE LOADING	5-11
5-8	SPACECRAFT TANK FREON LOADING	5-12
5-9	SPACECRAFT TANK FREON LOADING	5-13
5-10	SPACECRAFT TANK POLYSTYRENE LOADING	5-14
5-11	THEORETICAL LOADING RESPONSE 1/3 SCALE THERMO	5-16
5-12	LOADING RESPONSE 1/3 SCALE THERMO	5-17
5-13	STATIC LOADING TEST 1/3 SCALE THERMO	5-18
5-14	STATIC LOADING TEST SIMULATED SPACECRAFT TANK	5-19
5-15	STATIC ORIENTATION TEST SIMULATED SPACECRAFT TANK	5-21
5-16	STATIC LOADING TEST 2/5 SCALE THERMO TANK	5-22
5-17	STATIC LOADING TEST 2/5 SCALE THERMO TANK	5-23
6-2	f_{min} AND f_{max} DETERMINATION	6-4
6-3	DETERMINATION OF RESONANCE COUNT	6-4
6-4	LOADING RESPONSE $N_{1,2}$ CONCAVE AND CONVEX w.r.t. α AXIS	6-5

LIST OF TABLES

TABLE NUMBER		PAGE NUMBER
3-1	LOADING DEPENDENCY - RECTANGULAR	3-3
3-2	LOADING DEPENDENCE - RECTANGULAR	3-5
3-3	LOADING DEPENDENCY - 1/3 SCALE THERMO TANK	3-22
3-4	COMPARISON OF MODIFIED VOLUME DEPENDENCY FORMULA	3-23
3-5	RESONANCE BOUNDS STANDARD CYLINDRICAL CAVITY	3-31
3-6	RESONANCE DISTRIBUTION - STANDARD CYLINDRICAL CAVITY	3-31
4-1	STATIC ORIENTATION TEST - S-IVB (1/20 SCALE)	4-19
4-2	FREQUENCY BAND VERSUS MODE COUNT	4-28
4-3	STATIC LOADING TEST 2/5 SCALE THERMO, (FLAT- END INSTEAD OF LOWER HEMISPHERE)	4-31
4-4	STATIC ORIENTATION TEST, 2/5 SCALE THERMO, (LOWER HEMISPHERE MODIFIED WITH ALUMINUM FOIL TAPE)	4-33
4-5	STATIC ORIENTATION TEST 2/5 SCALE THERMO, (LOWER HEMISPHERE MODIFIED WITH PLUMBER'S WOOL)	4-35
4-6	STATIC ORIENTATION TEST, 2/5 SCALE THERMO, (FINAL FREQUENCY BAND)	4-35
4-7	INCREMENTAL LOADINGS, SMALL ANGULAR POSITIONS, 2/5 SCALE THERMO	4-39
4-8	FLOW TEST RESULTS, 2/5 SCALE THERMO	4-41
4-9	STATIC ORIENTATION TEST, SIMULATED SPACE- CRAFT TANK	4-47
4-10	LH ₂ STATIC LOADING TEST	4-50

FOREWORD

This report was prepared by the Instruments and Life Support Division of the Bendix Corporation under Contract NAS 8-18039, "Studies to Determine the Feasibility of Various Techniques for Measuring Propellant Mass Aboard Orbiting Space Vehicle." The work was administered under the direction of the National Aeronautics and Space Administration - George C. Marshall Space Flight Center, Lawrence Garrison, Contracting Officer.

This report covers work conducted from June 3, 1967 to January 30, 1968.

Prepared by *D. Passeri*
D. Passeri
Project Engineer *JPW*

Reviewed by *T. A. Loftus*
T. A. Loftus
Principal Investigator

J. W. Zorbell
J. W. Zorbell
Program Manager

D. A. Paustian
D. A. Paustian
Administrative Engineer

Approved by *N. F. Hosford*
N. F. Hosford
Director of Engineering

ABSTRACT

The feasibility of applying the Radio Frequency Resonance Counting Technique to generalized tank configurations was investigated. When a given tank was excited over a band of radio frequencies, a number of frequencies were found to exist where the tank acted as a cavity resonator. As the tank was loaded with a fuel simulant, the number of resonant frequencies contained in the band increased, dependent on the quantity and dielectric constant of the simulant. The change in the number of resonant frequencies was related to the quantity and mass of fuel simulant in the tank.

A theoretical analysis was performed on rectangular, cylindrical, spherical, and generalized propellant tank configurations to predict the dependence of the number of resonant frequencies on the fuel quantity, dielectric constant, mass and tank characteristics. These predictions were then evaluated in a series of experiments. Scale models of the fuel tanks were constructed and loaded under conditions simulating zero gravity and applied accelerations for typical fuels. The experiments verified the theoretical predictions and established the basic feasibility of the Radio Frequency Mass Gaging Technique. It is recommended that a breadboard prototype RF Mass Gaging System be fabricated.

SECTION 1

INTRODUCTION

The Bendix Corporation, Instruments & Life Support Division, respectfully submits Volume II of a two volume report to George C. Marshall Space Flight Center (MSFC). Volume II documents the progress made during the period June 3, 1967 through January 30, 1968 on NASA Contract NAS 8-18039 for "Studies to Determine the Feasibility of Various Techniques for Measuring Propellant Mass Aboard Orbiting Space Vehicles".

The initial study program performed under Phase A was directed toward the study of the feasibility of using a Radio Frequency (RF) resonance counting technique for gaging propellant mass in S-1B/S-1VB tank configurations under zero gravity conditions. The contract was later expanded to include a feasibility study of propellant mass gaging in the THERMO tank configuration. The basis of the work performed under both feasibility studies was the use of the propellant tank as a microwave cavity and counting the number of resonant frequencies that exist in the cavity between two fixed frequencies.

Generally, theoretical and experimental results were obtained simultaneously. Often, as theoretical results were being calculated, experiments were conducted on a trial and error basis until such time as the results were completed. Upon completion, the SST tank was matched by the information generated solely in the theoretical analysis.

In order to provide background information, a summary of the work accomplished during Phase A concerning the use of the propellant tank as a microwave cavity will be discussed.

A closed metallic tank of any shape and size has the property of resonance when excited with electromagnetic energy. The property of resonance is defined in the following manner: Suppose two comparatively small holes are drilled into the tank and RF power is then fed through one hole and an attempt to detect the radio frequency energy is made at the other hole. With DC and low RF frequencies, the tank will act either as a complete short circuit or a complete open circuit, the difference depending upon the type of coupling used. However, as we increase the frequency a frequency is reached where power is detected at the second hole or port. At this frequency, the tank allows power to enter and electromagnetic standing waves are set up in the tank. The existence of standing waves allows the output port to couple some of this power out of the tank. The tank is said to behave as a resonator at the frequency at which electromagnetic standing waves set up in the tank. The frequency at which a tank becomes a resonator is called a resonant frequency. The configuration of electromagnetic standing waves set up in the tank is called a mode pattern, and the tank is said to be operated in a particular mode. If the operating frequency is incrementally increased from this resonant frequency, the tank again reverts to being an open or closed circuit. Increasing the frequency again will produce a second resonant frequency. Again, the tank accepts power from the generator and again the power may be coupled out of the tank. The standing wave pattern at this resonant frequency as well as the

amount of the power coupled into and out of the tank will be different than the previous condition. Continually increasing the frequency reveals that more resonant frequencies exist, each having different transmission properties. The resonant frequencies in the tank primarily depend on the physical size of the tank and to a lesser extent on the dielectric constant of the material in the tank. The problem of the propellant tank partially filled with propellant under zero gravity conditions becomes, in microwave terms, a study of a inhomogenously filled cavity.

In performing the study of an inhomogenously filled cavity in Phase A, a mathematical RF system model of a given tank and propellant was formulated and experimental data was obtained using scale model tanks to evaluate the model's predictions. The most salient information developed during Phase A was the verification that the RF gaging technique employed was independent of mass position within the propellant tank. In summary, when a given tank was excited over a band of frequencies, a number of frequencies was found to exist. As the tank was loaded with a dielectric material, the number of resonant frequencies in the tank increased, dependent on the quantity and dielectric constant of the material. The change in the number of resonant frequencies was related to the quantity and mass of fuel material in the tank. The development made during Phase A relates the number of resonant frequencies in the cavity to its volume & the propellant fractional filling. The loading response of the tank is given by:

$$N = \frac{8\pi V}{3c^3} (f_2^3 - f_1^3) [1 + (\epsilon_r - 1)\alpha]^{3/2} \beta$$

where:

- N = number of resonances
- V = volume of the tank
- f_2 = upper frequency limit
- f_1 = lower frequency limit
- ϵ_r = dielectric constant of the propellant material
- α = fractional filling (0 to 1.0)
- β = mode reduction factor

The experimental data generated during Phase A showed that the general theory was adaptable to the S-1B/S-1VB tank. Experiments showed that when a scale model S-1B/S-1VB tank was gaged by RF techniques, the number of resonances was independent of dielectric position for any fractional filling. The extension of the theory to the THERMO tank was not successful and ultimately led to Phase B of the basic study contract.

SECTION II

PROGRAM OBJECTIVES

2.1 Introduction

The objective of the Phase B study program was to perform a feasibility study of Radio Frequency techniques for gaging mass in a generalized tank configuration and the THERMO tank configuration. The generalized tanks to be studied were:

- A) Cylindrical tank with flat ends.
- B) Spherical tank.
- C) Cylindrical tank with one hemisphere.
- D) Cylindrical tank with two hemispheres.
- E) THERMO tank complete with internal perturbations.

The combinations of these tanks along with internal perturbations comprised a THERMO tank configuration. In all cases the tanks were experimental scale models.

The work performed in Phase B utilized both analytical and experimental techniques to evaluate the effects of generalized tank components on the performance of the mass gage.

Within the scope of the general program outline and this contract, the program was divided into four basic study areas:

- 1) The study of spacecraft tank characteristics
- 2) The study of propellant characteristics
- 3) The study of hardware characteristics
- 4) The study of system characteristics

2.2 Study of Tank Characteristics

The study of tank characteristics concentrated upon the effect of the tank's geometric properties when the tank is used as a resonant cavity.

The geometric properties were:

- 1) The volume of the tank
- 2) The geometric shape of the tank
- 3) Internal perturbations contained within the tank

Theoretical studies were made of the tank shapes in order to determine their behavior as resonant cavities and to determine if the mathematical formulas previously formulated are dependent on these shapes.

2.3 Study of Propellant Characteristics

The study of propellant characteristics concerned itself with the radio frequency behavior of rocket propellants and their effect on the modes in a cavity or propellant tank.

2.4 Study of Hardware Characteristics

The study of hardware characteristics concerned itself with those discrete elements or circuits necessary to implement the RF gaging system. Contained in this study is the evaluation and design of any specialized circuitry required to determine when modes exist in the tank.

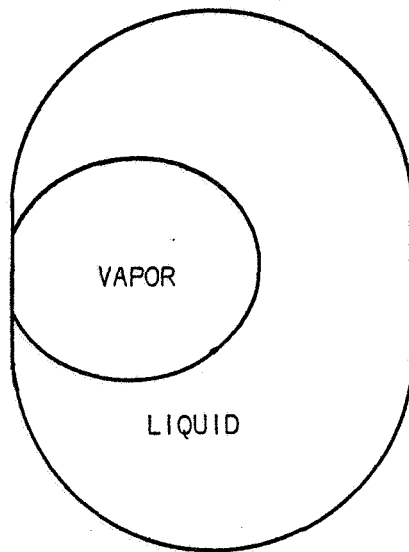
2.5 Study of System Characteristics

The study of system characteristics concerns itself with the external properties that the system imposes upon the tank, the effect of these properties on the tank resonances. The results of this study were used to determine what the system must contain in order to provide a mass gage under zero gravity conditions. The study of system characteristics integrates the study of tank characteristics, propellant characteristics and hardware characteristics in order that the final result is a system design capable of gaging propellant mass under zero gravity conditions.

The basic design goals of the mass gaging system as specified by NASA-MSFC relative to the feasibility determination were:

- 1) Mass Accuracy - $\leq \pm 2\%$ of full scale
- 2) Response Time - ≤ 0.5 seconds
- 3) Acceleration 0 to 5 g's; propellant location as shown in Figure 2-1.

"STEADY STATE" PROPELLANT LOCATION
FOR
FOR PLANETARY COAST



1. Bubble is somewhat **random in** location. Probably attached to wall on sun side.
2. APS, crew movement can cause bubble to move.
3. Bubble shape and location is somewhat dependent on tank shape and bubble volume.
4. Bubble size increases as liquid is depleted.

FIGURE 2-1a

"STEADY STATE" PROPELLANT LOCATION
FOR
100 NM ORBIT W/O CONTINUOUS THRUST

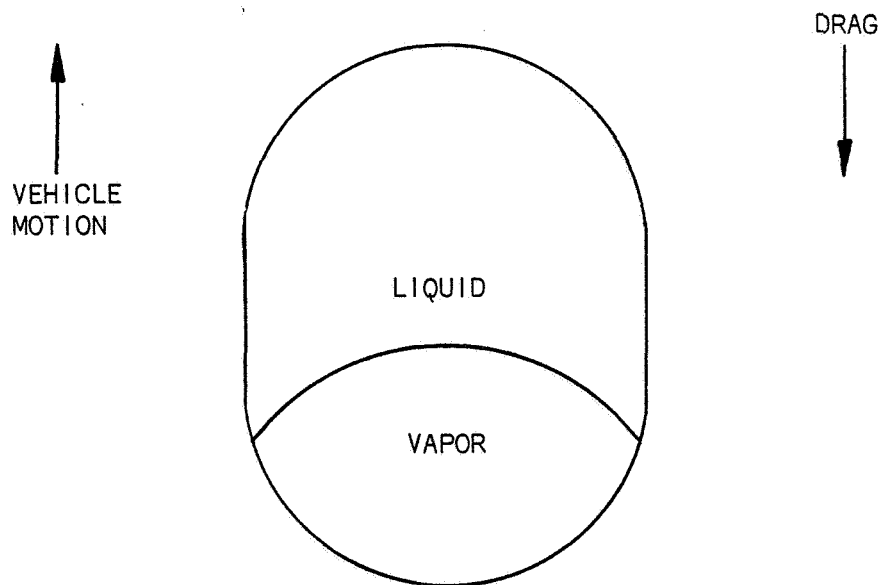


FIGURE 2-1b

SECTION III

THEORETICAL STUDIES

3.1 Introduction

The purpose of the theoretical study was to relate the information developed in Phase A to generalized spacecraft tanks. The information developed in Phase A relating the resonant count in a cavity of arbitrary shape to the volume of the cavity, the dielectric constant of the fluid that is to be used in the cavity and the system losses, was expanded in Phase B by considering simple geometric tank shapes.

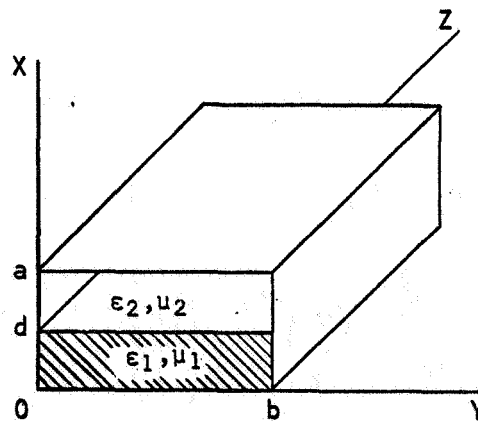
The theoretical study made on the simple geometries was expanded to fit tanks of arbitrary volumes of revolution, thereby leading to mathematical models of complex tank shapes.

The objective of the theoretical study was to establish a basis for predicting the actual response and performance of the Zero G gaging technique when applied to realistic tank configurations and geometries. A second basis for the theoretical study was to provide a mathematical model that would specify design parameters for the gaging system, as well as gaging system limitations.

3.2 Analysis-Rectangular Cavity

In order to verify the general theory that the RF gaging concept was independent of dielectric position in a resonant cavity, a theoretical analysis was performed on a rectangular cavity partially filled with a dielectric material.

Consider the rectangular cavity configuration shown in Figure 3-1 filled to a height 'd' with dielectric ' ϵ_1 '.



RECTANGULAR CAVITY PARTIALLY FILLED WITH DIELECTRIC

FIGURE 3-1

The resonances that exist in the cavity can be characterized into standing waves in both the dielectric and air, and standing waves in the dielectric only.

The basic equations for transverse magnetic (TM) modes existing in both the dielectric and air with the direction of propagation taken along the 'X' axis are:

TM^x Modes

$$\psi_1 = C_1 \cos k_{x1} x \sin \frac{n\pi y}{b} \sin \frac{p\pi z}{c} \quad (3-1)$$

$$\psi_2 = C_2 \cos k_{x2} (a - x) \sin \frac{n\pi y}{b} \sin \frac{p\pi z}{c} \quad (3-2)$$

where: ψ_1 is the wave function in dielectric

ψ_2 is the wave function in air

The basic equations for transverse electric (TE) modes to the direction of propagation are:

TE^x Modes

$$\psi_1 = C_1 \sin k_{x1} x \cos \frac{n\pi y}{b} \cos \frac{p\pi z}{c} \quad (3-3)$$

$$\psi_2 = C_2 \sin k_{x2} (a - x) \cos \frac{n\pi y}{b} \cos \frac{p\pi z}{c} \quad (3-4)$$

The equations for resonance can now be determined as,

$$k_{x1}^2 + \left(\frac{n\pi}{b}\right)^2 + \left(\frac{p\pi}{c}\right)^2 = \epsilon_r \left(\frac{\omega}{c}\right)^2 \quad (3-5)$$

$$k_{x2}^2 + \left(\frac{n\pi}{b}\right)^2 + \left(\frac{p\pi}{c}\right)^2 = \left(\frac{\omega}{c}\right)^2 \quad (3-6)$$

At the dielectric-air interface we must have continuity of the tangential E & H fields. This boundary condition leads to the development of transcendental equations that must be solved in

order to determine the modes of the cavity. The transcendental equations are:

$$-k_{x1} \tan k_{x1} d = \epsilon_r k_{x2} \tan k_{x2} (a - d) \quad (3-7)$$

$$-k_{x1} \cot k_{x1} d = k_{x2} \cot k_{x2} (a - d) \quad (3-8)$$

The solution of Equations 3-1, 3-2, and 3-7 generate the 'TM' modes; while the solution of Equations 3-1, 3-2, and 3-8 generate the 'TE' modes.

A similar development can be made for modes existing in the dielectric only. A complete analysis of the modes in a rectangular cavity partially filled with dielectric is given in Appendix A, Section I. Since the equations involved were transcendental, a computer solution to the problem was made. See Appendix B, Section I.

The independence of mass position within the cavity was verified by theoretically orientating the dielectric along each mutually perpendicular axis and performing partial loading with respect to each axis.

The computer program was run on two rectangular tanks. The calculations were made neglecting loss tangent effects. (i.e., β , the mode reduction value, equals 1.) Tank one had dimensions of 7.88" X 18" X 35.2" and was filled with a dielectric having $\epsilon_r = 2.25$. The results are shown in Figure 3-2 and Table 3-1.

TABLE 3-1

LOADING DEPENDENCY RECTANGULAR CAVITY

Fractional Filling	Resonant Count			
	⊥ to 7.88 in	⊥ to 18 in	⊥ to 35.2 in	Volume Dependency
Empty	1419	1419	1419	1423
0.01	1421	1426	1431	1431
0.10	1707	1733	1745	1700
0.20	2042	2039	2080	1995
0.30	2392	2388	2417	2300
0.40	2738	2745	2745	2605
0.50	3076	3078	3091	2890
0.60	3400	3412	3428	3290
0.70	3750	3759	3767	3680
0.80	4087	4093	4095	4020
0.90	4446	4424	4438	4420
1.00	4764	4764	4764	4781

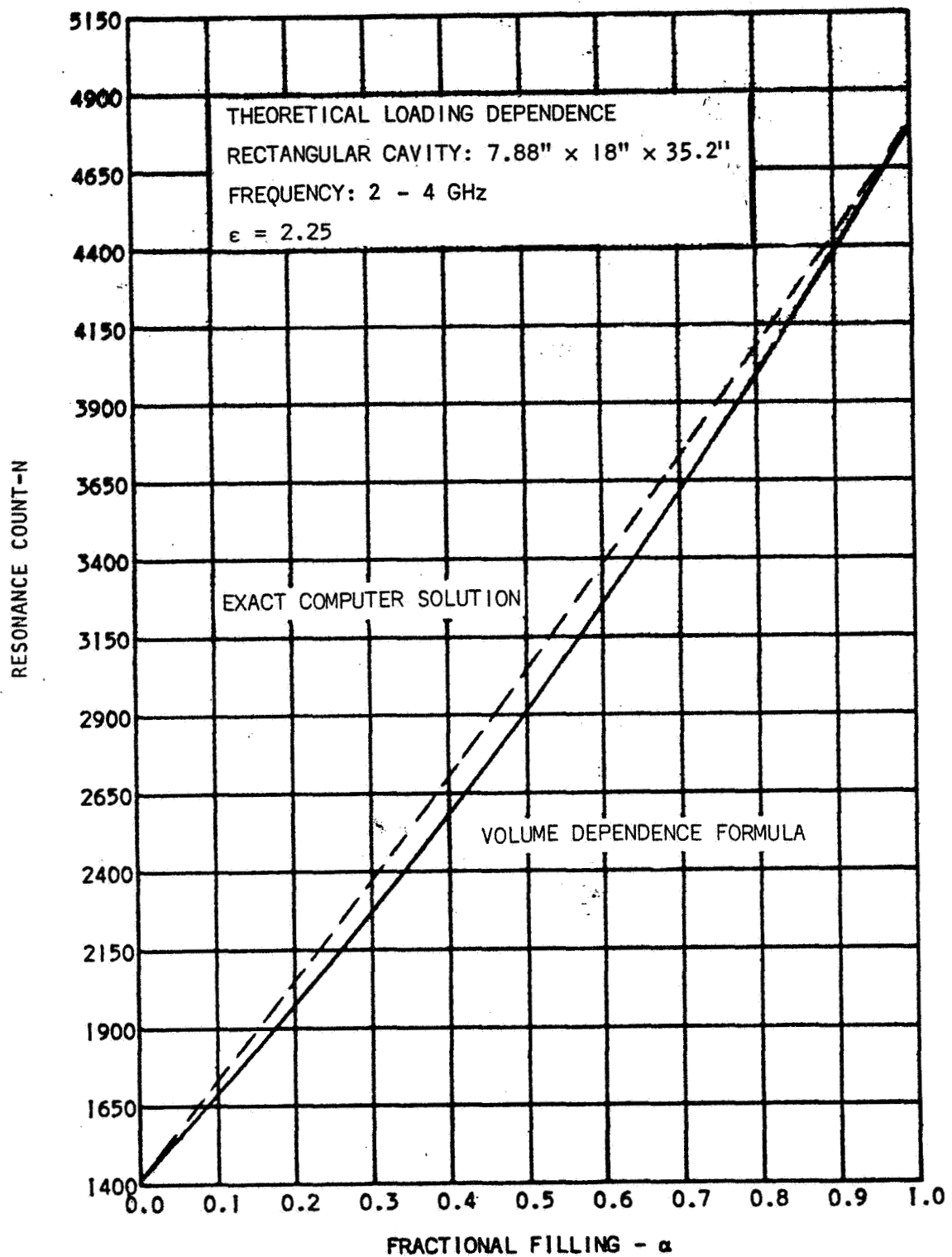


FIGURE 3-2

The second rectangular cavity had two equal sides (square) in order to provide a first order approximation to the basic S-IVB, THERMO tank configuration. The demension of the cavity was 15.36" X 15.36" X 9.6". The volume of the tank is equivalent to the 1/3 scale THERMO tank. The results of the computer program are shown in Figure 3-3 and Table 3-2.

TABLE 3-2

LOADING DEPENDENCE RECTANGULAR CAVITY

Fractional Filling	Resonant Count			Volume Dependency
	⊥ to 9.6 in	⊥ to 15.36 in	⊥ to 15.36 in	
0.0	292	292	292	296
0.1	362	360	360	356
0.2	428	430	430	420
0.3	509	511	511	482
0.4	579	577	577	551
0.5	654	658	658	621
0.6	724	722	722	696
0.7	798	804	804	775
0.8	863	871	871	857
0.9	944	951	951	935

The data shows that the resonant count versus fractional filling is linear and that the resonant count in a partially filled cavity is indeed independent of dielectric position. The 1.00 fractional fill point is not identical in all orientations due to variance in the stepping function in the computer program. An interesting comparison can be made to the volume dependency formula developed in Phase A.

$$N = \frac{8\pi}{3c^3} V (f_2^3 - f_1^3) [1 + (\epsilon_r - 1) \alpha]^{3/2}$$

It can be seen that a good correspondence exists between the volume dependency formula and the results obtained by a direct calculation of the number of resonances within the cavity, for the empty and full loading cases. However, there is a distinct nonlinearity in the volume dependence formula. This nonlinearity has its maximum deviation at the 50% fractional filling point.

3.3 Analysis-Cylindrical Cavity

The analysis of a right circular cylindrical cavity was made in Phase A using variational techniques. A computer program was written to calculate

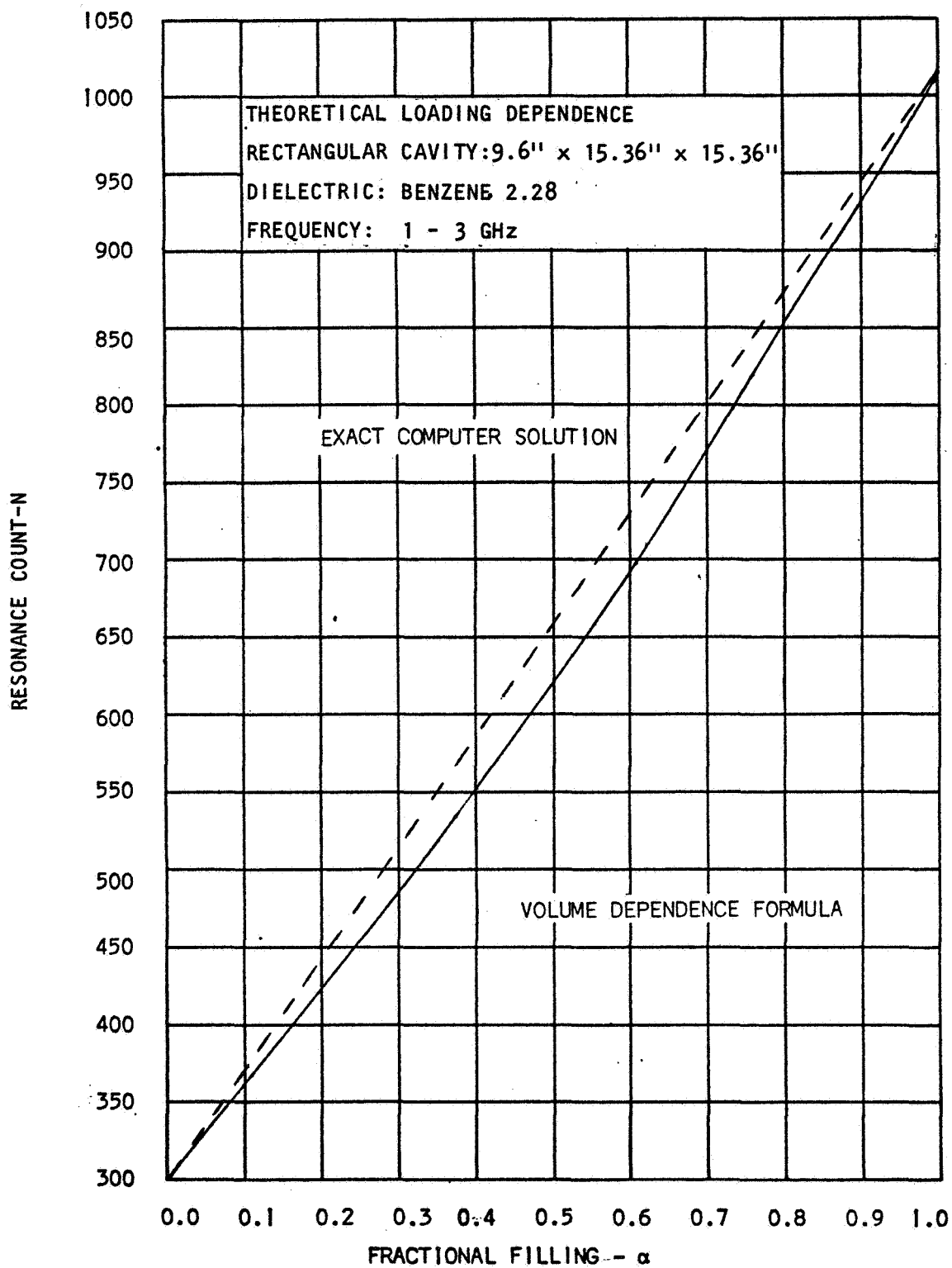


FIGURE 3-3

the modes in a partially filled cavity. The equations for resonance are given as:

$$TE_{\omega_{mnp}} = \left(C \frac{X_{mn}^2}{a^2} + \frac{p^2 \pi^2}{L^2} \right)^{1/2} \left[1 + (\epsilon_r - 1) \left(\frac{d}{L} - \frac{1}{2p\pi} \sin \frac{2p\pi d}{L} \right) \right]^{-1/2}$$

$$TM_{\omega_{mnp}} = C \left\{ \left[\left(\frac{X_{mn}}{a} \right)^2 + \left(\frac{p\pi}{L} \right)^2 \right] \left[1 - \frac{d}{L} \left(1 - \frac{1}{\epsilon_r} \right) \right] - \frac{1}{2p\pi} \left[\left(\frac{X_{mn}}{a} \right)^2 - \left(\frac{p\pi}{L} \right)^2 \right] \dots \right. \\ \left. \dots \left(1 - \frac{1}{\epsilon_r} \right) \sin \frac{2p\pi d}{L} \right\}^{1/2}$$

$$m = 0, 1, 2, \dots$$

$$n = 1, 2, 3, \dots$$

$$p = 1, 2, 3, \dots$$

$$TM_{\omega_{mnp}} = \frac{CX_{mn}}{a} \left[1 - \frac{d}{L} \left(1 - \frac{1}{\epsilon_r} \right) \right]^{1/2}$$

$$m = 0, 1, 2, 3, \dots$$

$$n = 1, 2, 3, \dots$$

$$p = 0$$

For a complete development of the modes in a cylindrical cavity by use of the variational technique, see Appendix A, Volume 1. The loading dependence for a cylindrical cavity filled with a material having a dielectric constant of 2.25 is shown in Figure 3-4. Although the curve is nonlinear in nature, the empty and full values are in close agreement with the volume dependence formula. Since the variational technique is the basis for the development of the volume dependency formula, a close agreement with the end points and curve form would be expected.

Because of the nonlinear nature of both loading curves for the cylindrical cavity, two basic questions had to be answered: 1) is the nonlinear loading response due to the geometry of the tank or 2) is the nonlinear loading response due to the volume dependence and the variational technique? In order to resolve this problem an exact solution to a partial loading cylindrical tank was attempted.

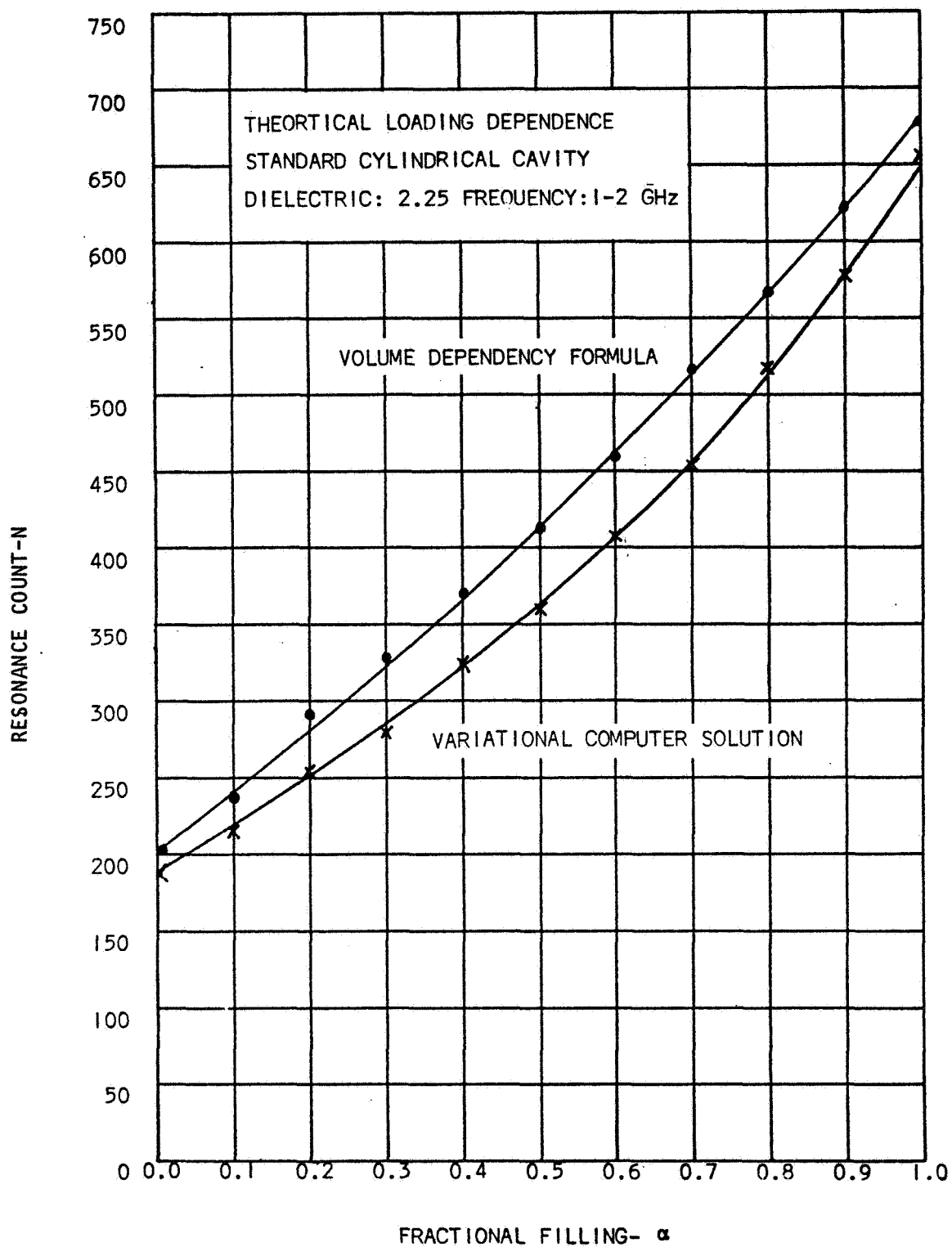


FIGURE 3-4

As in the rectangular cavity, two distinct set of resonances exist in the cavity; resonances having standing waves in both the liquid and the air and resonances having standing waves in liquid that are supported by exponential type waves in the air dielectric. See Figure 3-5. The equations for resonances having standing waves in both the dielectric and air are:

For TM modes:

$$k_1^2 + \left(\frac{X_{np}}{a}\right)^2 = \left(\frac{\omega}{c}\right)^2$$

$$k_2^2 + \left(\frac{X_{np}}{a}\right)^2 = \epsilon_r \left(\frac{\omega}{c}\right)^2$$

$$k_2 \sin k_2 c \cos k_1 b + \epsilon_r k_1 \cos k_2 c \sin k_1 b = 0$$

For TE Modes:

$$k_1^2 + \left(\frac{X'_{np}}{a}\right)^2 = \left(\frac{\omega}{c}\right)^2$$

$$k_2^2 + \left(\frac{X'_{np}}{a}\right)^2 = \epsilon_r \left(\frac{\omega}{c}\right)^2$$

$$k_2 \cos k_2 c \sin k_1 b + k_1 \sin k_2 c \cos k_1 b = 0$$

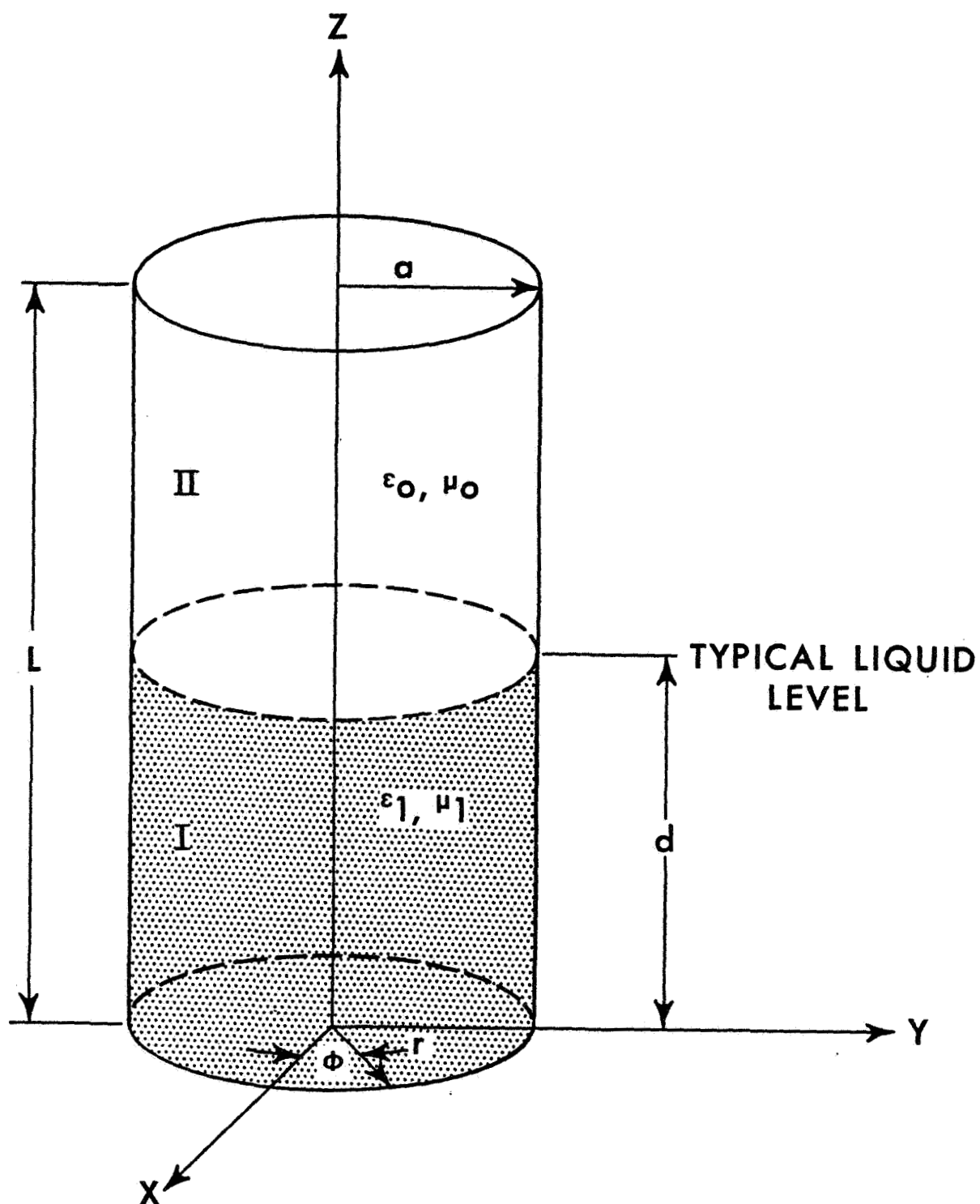
For resonances having standing waves in the dielectric we have:

For TM modes:

$$-k_1^2 + \left(\frac{X_{np}}{a}\right)^2 = \left(\frac{\omega}{c}\right)^2$$

$$k_2^2 + \left(\frac{X_{np}}{a}\right)^2 = \epsilon_r \left(\frac{\omega}{c}\right)^2$$

$$k_2 \sin k_2 c \cosh k_1 b - \epsilon_r k_1 \cos k_2 c \sinh k_1 b = 0$$



CIRCULAR CYLINDRICAL PROPELLANT TANK
CONTAINING FLAT END-PLATES

FIGURE 3-5

A-3521-67-304

For TE modes:

$$-k_1^2 + \left(\frac{X'_{np}}{a} \right)^2 = \left(\frac{\omega}{c} \right)^2$$

$$k_2^2 + \left(\frac{X'_{np}}{a} \right)^2 = \epsilon_r \left(\frac{\omega}{c} \right)^2$$

$$k_2 \cos k_2 c \sinh k_1 b + k_1 \sin k_2 c \cosh k_1 b = 0$$

A complete solution and development of the partially filled cylindrical cavity will be found in Appendix A, Section II. The exact solution to a partially filled cylindrical cavity was obtained through the use of a computer program. Figure 3-6 shows the loading dependence of an 0.15448 meters radius, 0.49434 meters height cylindrical tank when filled with a material having a dielectric constant of 2.28. The immediate conclusions that can be drawn from the data is that the volume dependency formula and the variational technique developed in Phase A does not provide an adequate mathematical model for a right circular cylinder. Secondary conclusions are: 1) the loading dependence is linear, and 2) there is good correspondence between the volume dependence formula and the exact solution's end points.

3.4 Analysis Spherical Cavity

The basic development of the modes that exist in a spherical cavity can be found in Volume I, Appendix B. This development is suitable only for determining the number of resonances in an empty or full spherical cavity. The comparison of the empty and full resonant count with the volume dependency formula is in good agreement as in the case of the rectangular and cylindrical cavities. Extracting from Volume I, Appendix B we can compare the resonant count obtained using both techniques for a spherical cavity 7 feet in diameter.

Volume Dependence Formula

$$N_{\text{empty}} = 1,382 \text{ resonances}$$

$$N_{\text{full}} = 1,881 \text{ resonances}$$

Spherical Cavity Solutions

$$N_{\text{empty}} = 1,326 \text{ resonances}$$

$$N_{\text{full}} = 1,817 \text{ resonances}$$

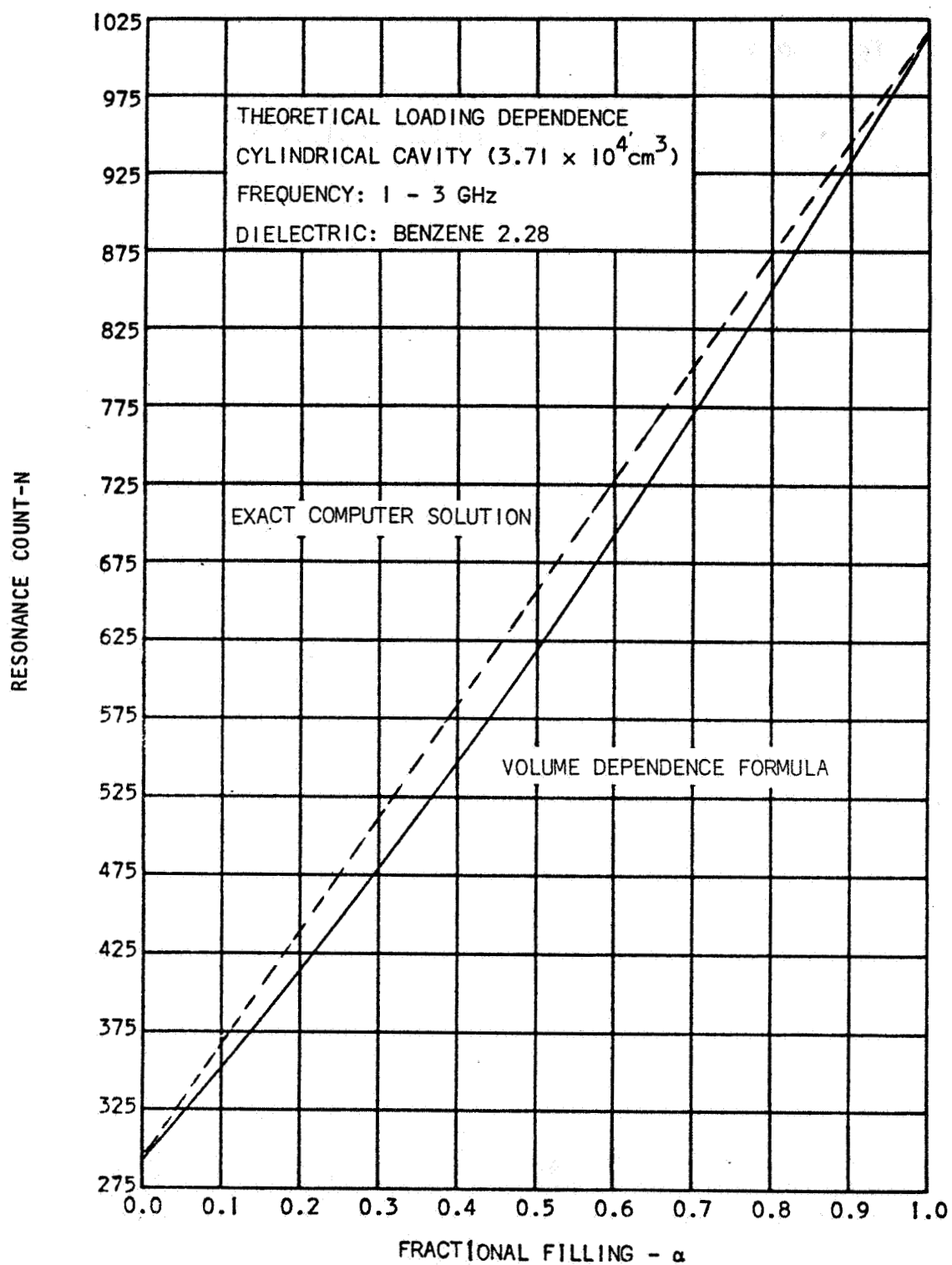


FIGURE 3-6

The resonant count difference between empty and full is within $\pm 2\%$ between the two techniques. It is beneficial to develop the necessary equations to determine the loading dependence of a spherical cavity partially filled with a dielectric material. See Figure 3-7.

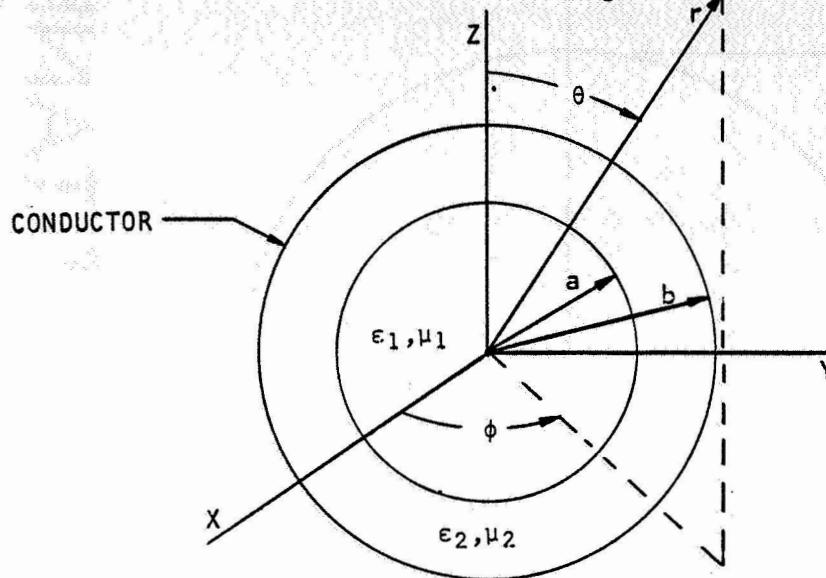


FIGURE 3-7

SPHERICAL CAVITY PARTIALLY FILLED WITH DIELECTRIC

A complete development of the characteristic equations needed to determine the modes is found in Appendix A, Section III. The necessary equations for resonances are:

For TE^r modes:

$$\frac{\eta_1}{\eta_2} \frac{\hat{J}_n(k_1 a)}{\hat{J}'_n(k_1 a)} = \frac{\hat{N}_n(k_2 b) \hat{J}_n(k_2 a) - \hat{J}_n(k_2 b) \hat{N}_n(k_2 a)}{\hat{N}_n(k_2 b) \hat{J}'_n(k_2 a) - \hat{J}'_n(k_2 b) \hat{N}'_n(k_2 a)}$$

For TM^r modes:

$$\frac{\eta_1}{\eta_2} \frac{\hat{J}'_n(k_1 a)}{\hat{J}_n(k_1 a)} = \frac{\hat{N}'_n(k_2 b) \hat{J}'_n(k_2 a) - \hat{J}'_n(k_2 b) \hat{N}'_n(k_2 a)}{\hat{N}'_n(k_2 b) \hat{J}_n(k_2 a) - \hat{J}_n(k_2 b) \hat{N}_n(k_2 a)}$$

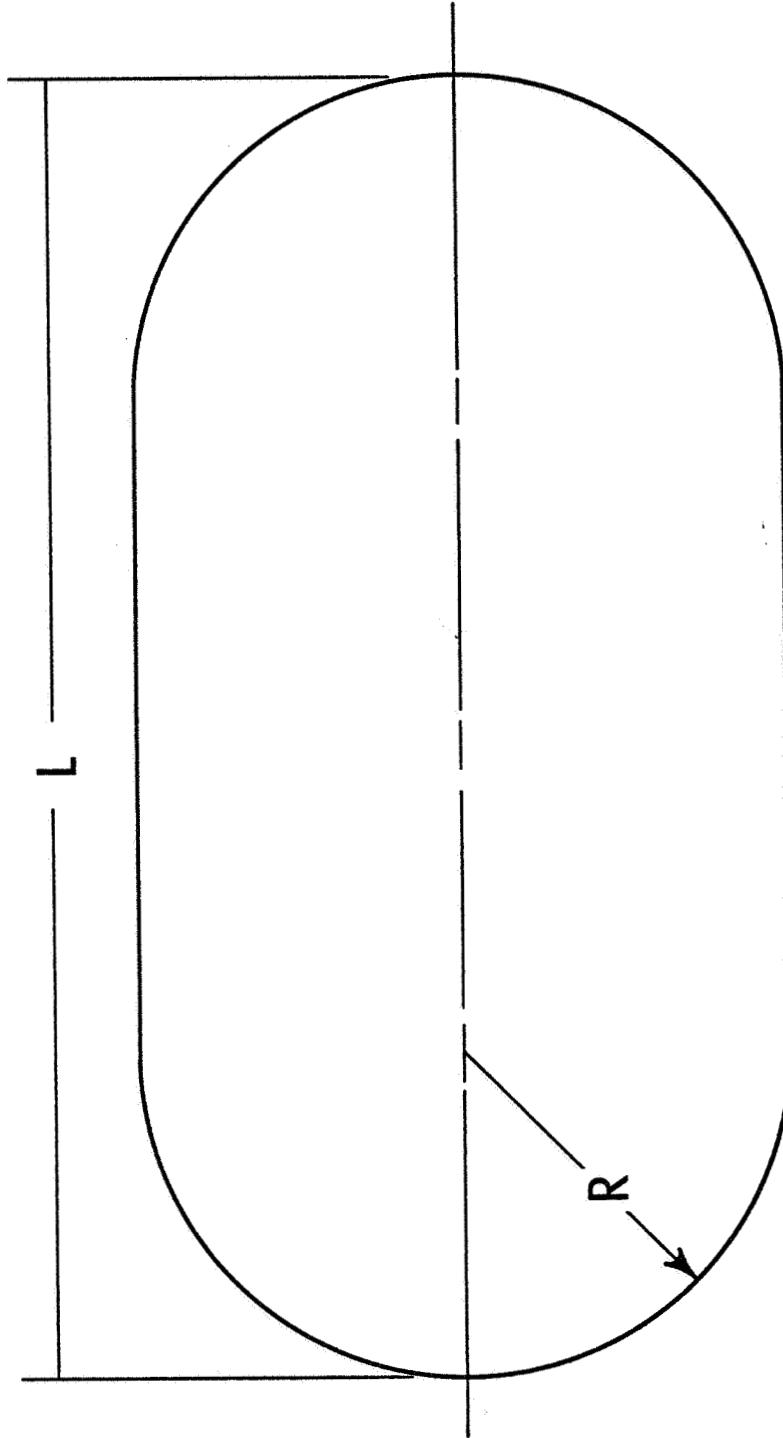


FIGURE 3-8

GENERALIZED SPACECRAFT TANK

A-3521-67-294

where

$$\begin{aligned}
 k_1 &= \omega \sqrt{\epsilon_1 \mu_1} & \eta_1 &= \sqrt{\mu_1 / \epsilon_1} \\
 k_2 &= \omega \sqrt{\epsilon_2 \mu_2} & \eta_2 &= \sqrt{\mu_2 / \epsilon_2}
 \end{aligned}$$

In the above equations, \hat{J}_n and \hat{N}_n are spherical Bessel functions. The solution of the partially loaded spherical cavity must be performed with the aid of a computer. Due to the complexity of the computer program and the indirect application of this type tank configuration to the THERMO tank geometry no further development was performed in this area.

3.5 Analysis Arbitrary Cavities of Revolution

A particular problem in the study of modes in general cavities has been the extension of the wave equations for rectangular, cylindrical or spherical tanks to cavities of revolution.

Previously this problem has been solved by representing a cigar-shaped cavity (see Figure 3-8) by a cylinder of equal volume. The number of resonances are found for the cylinder and then postulated to be equal in number to those of the cigar-shaped cavity. An alternate solution is to separate the cavity into two hemispheres and a cylinder and to obtain the total number of resonances by adding the modes for each separate section. This technique has been shown to be approximately correct for several different cylinder-hemisphere combinations. However, the location of probes, effects of reentrant sections, prediction of fuel loading characteristics, etc., are hampered by the lack of knowledge of the field distribution within the cavity.

A set of wave functions, which are appropriate for general volumes of revolution such as cigar-shaped cavities are those of modes of revolution. These modes constitute a portion of a more general class of modes having an azimuthal dependence. The modes of revolution do not have a ϕ or azimuthal dependence and are generally the dominant or lowest frequency modes of this cavity.

The modes of revolution are divided into two types. Modes of the first type are called meridian magnetic modes, and are characterized by the magnetic field lying entirely in the meridian plane. The associated electric field is perpendicular to the meridian plane. Here, the electric field is given by $g_m(r, z) \underline{u}_\phi$ and the magnetic field by $\nabla \times (g_m \underline{u}_\phi)$. Our function $g_m(r, z)$ satisfies the differential equation.

$$\frac{\partial^2 g_m}{\partial r^2} + \frac{1}{r} \frac{\partial g_m}{\partial r} + \frac{\partial^2 g_m}{\partial z^2} \left(K_m - \frac{1}{r^2} \right) g_m = 0 \quad (3-9)$$

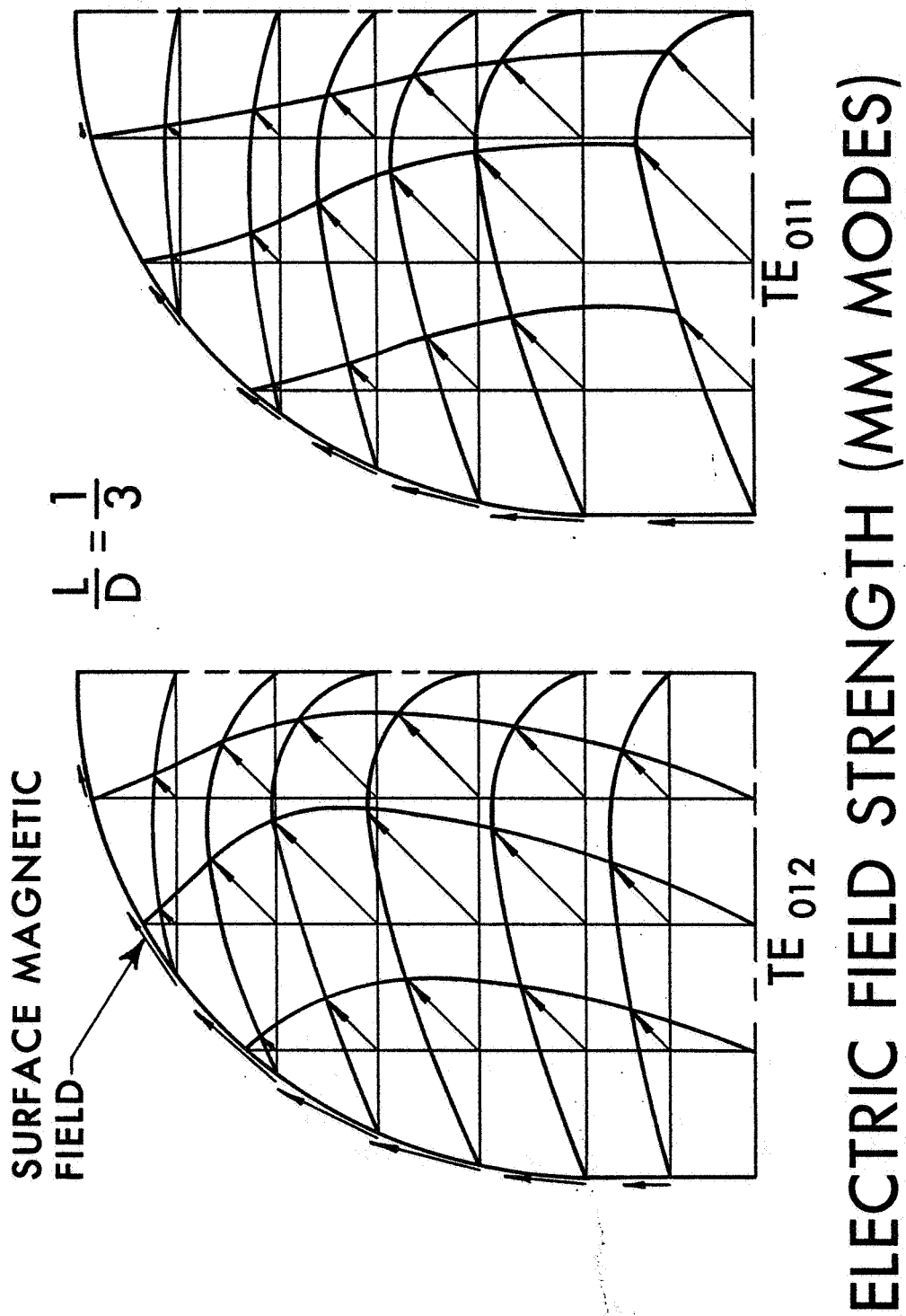


FIGURE 3-9

with the boundary conditions: $g_m = 0$ on the axis on the walls.

The K_m are the eigenvalues for each eigenfunction g_m . The resonant frequency of each mode is given by:

$$f_r = \frac{K_m}{2\pi\sqrt{\epsilon\mu}}$$

where μ and ϵ are the pertinent parameters of the cavity material.

For modes of the second type or meridian electric modes, the electrical field lies entirely in the meridian plane with the associated magnetic field perpendicular to the meridian plane. The magnetic field is given by $h_m(r,z) \underline{u}_\phi$ and the electric field by $\nabla \times (n_m \underline{u}_\phi)$. This function h_m also satisfies Equation 3-9 with the boundary conditions now being

$$\frac{\partial(h_m r)}{\partial r} = 0$$

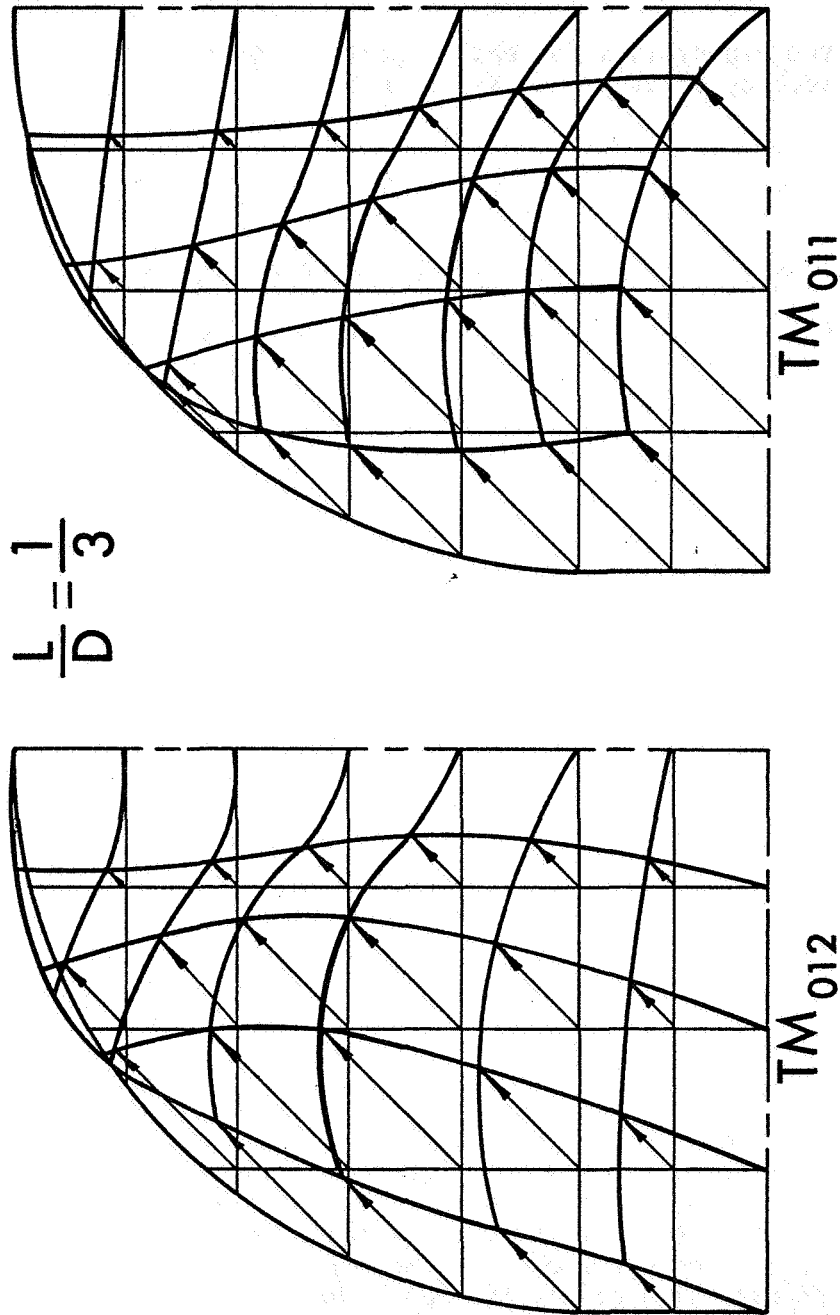
on the walls, $h_m = 0$ on the axis. Again, there exists a set of resonant frequencies given by:

$$\frac{K_m}{2\pi\sqrt{\epsilon\mu}}$$

A solution for the two correct "MM" and "ME" modes for a cigar-shaped cavity of variable aspect ratio (L/D) is shown in Figures 3-9 and 3-10. It can be seen from these figures that with a knowledge of the field distribution, probe placement for coupling to the electric or magnetic field is straightforward. Without this knowledge, the placement becomes largely a hit or miss procedure with little or no possibility for optimum field coupling.

The effect of dielectric material in the cavity can also be studied and a connection obtained between the amount and placement of this material and the resonant count for the cavity. This information can then be used to predict the loading response for partially filled cavities and to check the predictions made by assuming the loading dependence to follow a general function independent of tank geometry. A check may also be made on the effects of geometry changes on the overall excitation response of a cavity to provide a more complete catalog on shapes suitable for RF Gaging System application.

It should be noted that the cigar-shaped cavity is only one of many figures of revolution for which the field distribution and resonant frequencies can be found. Tanks having inward convex surfaces, doubly-connected surfaces, toroidal shapes, etc., lend themselves to an analysis of the type applied to the cigar-shaped cavity.



MAGNETIC FIELD STRENGTH (ME MODES)

FIGURE 3-10

A-3521-67-315

In general, the procedure for a general cavity is to set up the differential equation for the modes, replace these differential equations by difference equations, and then use variational principles for the calculation of the eigenvalues (resonant frequencies). There will be a triple infinity of eigenvalues corresponding to the number of field variations along the radius, axis, and circumference for a particular mode. Thus, as with the rectangle, cylinder or sphere, the last two of which are included in the volume of revolution class, a volume dependency for the total number of excitable resonances in a given tank should be found.

A further use for setting up the modes of revolution is the similarity in the boundary conditions $g_m = 0$ or $\partial g_m / \partial n = 0$ on the walls of the container, with those for acoustic modes in the same cavities. It has been shown by Roe(2) that for rectangular, cylindrical, spherical, prism, half cylinder, and hemispherical shaped cavities that

$$N(f) = \frac{4\pi V f^3}{3c^3} + \frac{\pi A f^2}{4c^2} \quad \text{for } \psi = 0 \text{ on walls}$$

$$= \frac{4\pi V f^3}{4c^3} - \frac{\pi A f^2}{4c^2} \quad \text{for } \frac{\partial \psi}{\partial n} = 0 \text{ on walls} \quad (3-10)$$

where

$$\nabla^2 \psi + \frac{4\pi^2 f^2}{c^2} \psi = 0 \quad (3-11)$$

or

$$N(f) = \frac{8\pi V f^3}{3c^3} \quad \text{for both classes} \quad (3-12)$$

If our modes can be shown to belong to this class also, then a strong case may be made that N is dependent only on the volume and frequency of excitation as given in Equation 3-12 for an empty cavity.

This is very important, as we now can be assured that if all modes are separable, or detectable in a cavity then the effect of cavity perturbations can be analyzed on the basis of volume alone, if the perturbation is metallic.

By adding the generalized loading dependence which depends on the bulk dielectric constants and mass of material in the cavity, a general relationship for the excitable resonances in a cavity independent of cavity geometry or mass content position is obtained. With this formula for N , the specification of the RF system parameters for a particular application becomes an engineering task.

3.6 Field Patterns and Antenna Location

Since the geometry of both the S-IVB and THERMO tanks have a significant cylindrical section, a simulation of the entire THERMO and S-IVB tanks was attempted through the use of equivalent volume cylinders. In order to determine the best possible antenna position for optimum probe coupling, the field patterns of a number of modes were drawn. See Appendix C, Section 1. A careful study of the field patterns shows that for a transmitted energy system; i.e., one excitation probe and one detection probe, the probes should be 180° apart with respect to the θ coordinate of the cylinder. All that remains is to determine the optimum probe location along the z and r axis.

The optimum location of the probe along the z axis of an empty right cylindrical tank is determined by first finding the highest number of p variations of the "TM_{mnp}" or "TE_{mnp}" modes for the frequency band used. Dividing the height of the tank by two times the value of the highest p , gives the optimum distance from the end of the tank to the highest p mode. All of the lower p modes (p greater than 0) will be coupled into the tank at this point at least slightly. In order to couple into lower p modes better, the locating point is modified by multiplying by 1.414. In equation form:

$$L.P. = (d/2p) 1.414$$

where p is defined as the number of half-wavelength variations of the field in the z direction and L.P. is defined as the locating point from the bottom or top of the cylinder.

The optimum location for the probe radially can be determined by inspection of the field equations. This requires a trial solution.

Take the five highest Bessel zeros (X_{mn}) that will be encountered in the frequency range used for both "TE" and "TM" modes, and determine X_{mn} with the two lowest m 's (usually $m = 0$ or 1).

For example:

a) $X_{04} = 11.792$

b) $X_{23} = 11.620$

Finding the value of $X_{m(n-1)}$ we have:

a) $X_{03} = 8.654$

b) $X_{22} = 8.417$

Solve the following expression for R in each case:

$$X_{mn}(R) X_{m(n-1)}(A)$$

where:

A = radius of cylinder

$$a) \quad X_{04}(R) = X_{03}(A)$$

$$R = 8.654(A) / 11.792 - 0.734A$$

$$b) \quad X_{23}(R) = X_{22}(A)$$

$$R = 8.417(A) / 11.620 - 0.725A$$

The largest R gives the desired case. Next find the half-distance from the edge of the cylinder for the given R where: H.D. is defined as the half-distance from the edge of the cylinder

$$H.D. = (A - R) / 2$$

For our case:

$$H.D. = (A - 0.734A) / 2$$

This results in the best probe location for the mode for which the zero occurs nearest the edge (all have to go to zero at the edge). Again, multiply the H.D. by 1.414 to give a position with better coupling to other modes without seriously affecting worst case mode coupling.

The position determined may not be physically realizable unless probes can actually be located within the tank. While this position is optimum for coupling to all modes, the coupling may be so weak that the mode is nondetectable. Nevertheless, probes in this vicinity, whether along the cylinder wall or end, have experimentally been coupled to a majority of the maximum number of resonances (90% or greater).

3.7 Development of Volume Dependence Formula

In order to establish an independence of resonant count to cavity geometry and develop a volume dependence relationship that would better fit the theoretical data, computer programs were run on two equal volume cavities having different geometries. The two geometries chosen were rectangular and cylindrical with volumes equal to those of the 1/3 scale THERMO tank. The rectangular tank had the following dimensions 15.36" X 9.6" X 15.36" and the cylindrical cavity had a radius of 0.15448 m and a height of 0.49434 m. Table 3-3 shows the fractional loading dependence when the cavities are filled with a propellant having a dielectric constant of 2.28 (Benzene). The calculations were made neglecting loss tangent effects. Therefore, β , the mode reduction value, equals 1.

TABLE 3-3
LOADING DEPENDENCY 1/3 SCALE THERMO TANK

Fractional Filling	Resonant Count			
	⊥ to 15.36"	⊥ to 9.6"	Cylinder	Volume Dependency
0.0	292	292	288	296
0.1	360	362	353	356
0.2	430	428	434	420
0.3	511	509	507	482
0.4	577	579	574	551
0.5	658	654	651	621
0.6	722	724	719	696
0.7	804	798	793	775
0.8	871	863	867	857
0.9	951	944	943	935
1.0	1022	1008	1014	1015

Again the volume dependence formula developed during Phase A is in error. The key to the refinement of the volume dependence formula lies in the containment of specific mode sets within the propellant dielectric and the air dielectric. See Appendix A. The number of resonances contained in the propellant dielectric is directly proportional to the dielectric constant of the propellant and as the propellant fractional filling increases, the number of resonances must increase in a linear manner. Therefore, the volume dependence formula must be modified accordingly. Since the empty and full cases agree in all instances, the fractional filling dependence " α " must be in error. The basic formula developed in Phase A is:

$$N = \frac{8\pi V}{3c^3} (f_2^3 - f_1^3) [1 + (\epsilon_r - 1)\alpha]^{3/2}$$

For the empty case this reduces to:

$$N = \frac{8\pi V}{3c^3} (f_2^3 - f_1^3) [1]^{3/2}$$

For the full case this reduces to:

$$N = \frac{8\pi V}{3c^3} (f_2^3 - f_1^3) \epsilon_r^{3/2}$$

In both cases, "α" the fractional filling has been removed. Inspection of the volume dependence formula for fractional filling shows a $3/2 \alpha$ dependence as the variational technique also indicated. If the fractional filling is to be linear, as the exact cavity solutions show, the basic formula must be modified. Postulating a new volume dependence formula we have:

$$N = N_o [1 + (\epsilon_r^{3/2} - 1)\alpha]$$

where:

$$N_o = \frac{8\pi V}{3c^3} (f_2^3 - f_1^3)$$

A comparison of the loading dependence generated by the postulated formula with the exact solution of the equivalent volume tanks is given in Table 3-4.

TABLE 3-4
COMPARISON OF MODIFIED VOLUME DEPENDENCY FORMULA

Fractional Filling	Resonance Count			
	⊥ to 15.36"	⊥ to 9.6"	Cylinder	Modified Volume Dependence
0.0	292	292	288	296
0.1	360	362	353	368
0.2	430	428	434	440
0.3	511	509	507	513
0.4	577	579	574	584
0.5	658	654	651	656
0.6	722	724	719	728
0.7	804	798	793	801
0.8	871	863	867	872
0.9	951	944	943	945
1.0	1022	1008	1014	1015

It can be seen that a good correspondence now exists between the exact solutions and the approximate volume dependence solution.

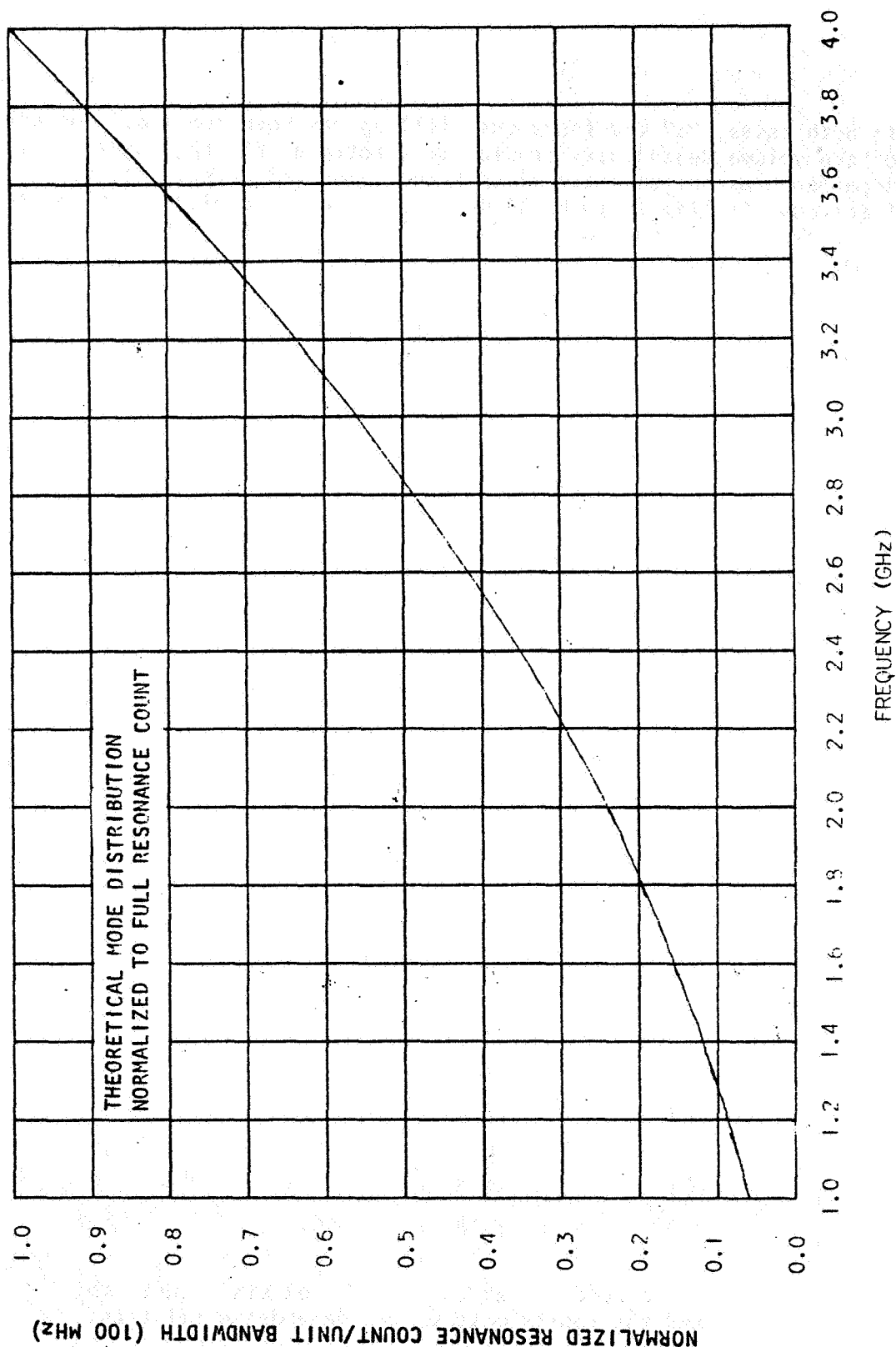


FIGURE 3-11

3.8 Resonance Distribution Versus Frequency Band

The Phase A report stated that the differential number of resonances dN , excited in a cavity for a fixed frequency band should follow the relationship,

$$\frac{dN}{df} = \text{constant} \times f^2$$

This relationship is based on the volume dependence formula and a plot of the relationship is shown in Figure 3-11. It was postulated that in a matched tank the resonance distribution would follow the differential distribution curve. Since an exact mode solution was obtained through the use of computer programs, it was desirable to plot the actual resonance distribution for a cylindrical cavity. The differential resonance distribution for the standard cylindrical cavity is shown in Figure 3-12. It can be seen that a least squares approximation to the actual resonance distribution does agree with the postulated mode distribution. That is, the average resonance distribution does follow a square law. Plots were made of the resonance distribution for partial fillings of the standard cylindrical cavity with both Benzene and LH_2 . In all cases for each of the partial fillings, the resonance distributions followed the square law response. What remains to be proven is that a resonance distribution that follows the square law response is indicative of a matched tank. This will be shown in Paragraph 3.10 and the experimental section of this report.

3.9 Mode Merging and 'Q' Dependency

Up to this point we have considered only ideal cases with regard to resonant count "N" versus fractional filling " α ". In actual practice, it would be impossible to detect and count each and every mode due to mode degeneracies and individual mode overlap. Mode degeneracies being defined as modes that exist at the same frequencies, and mode overlap being defined as the merging of modes due to finite mode "Q".

Figure 3-13 shows the upper and lower bounds that the resonant count can have due solely to mode degeneracies, ie; a infinite system "Q" is still being assumed. These bounds were established through the analysis of the exact solution of the number of modes contained in a cylindrical cavity. Note that the upper bound is in agreement with the postulated volume dependence formula. This is the maximum possible number of resonances that could exist in a cavity.

The lower bound is indicative of the loading response that would exist if the cavity were a perfect cylinder since the degeneracies would be inseparable. In essence, bounds have been established which include the detectability of mode degeneracies. In an actual tank such as the S-1VB or THERMO, the nonsymmetrical geometry as well as the internal perturbations would cause a portion of the mode degeneracies to split and the loading curves would be contained somewhere within the bounds shown in Figure 3-13.

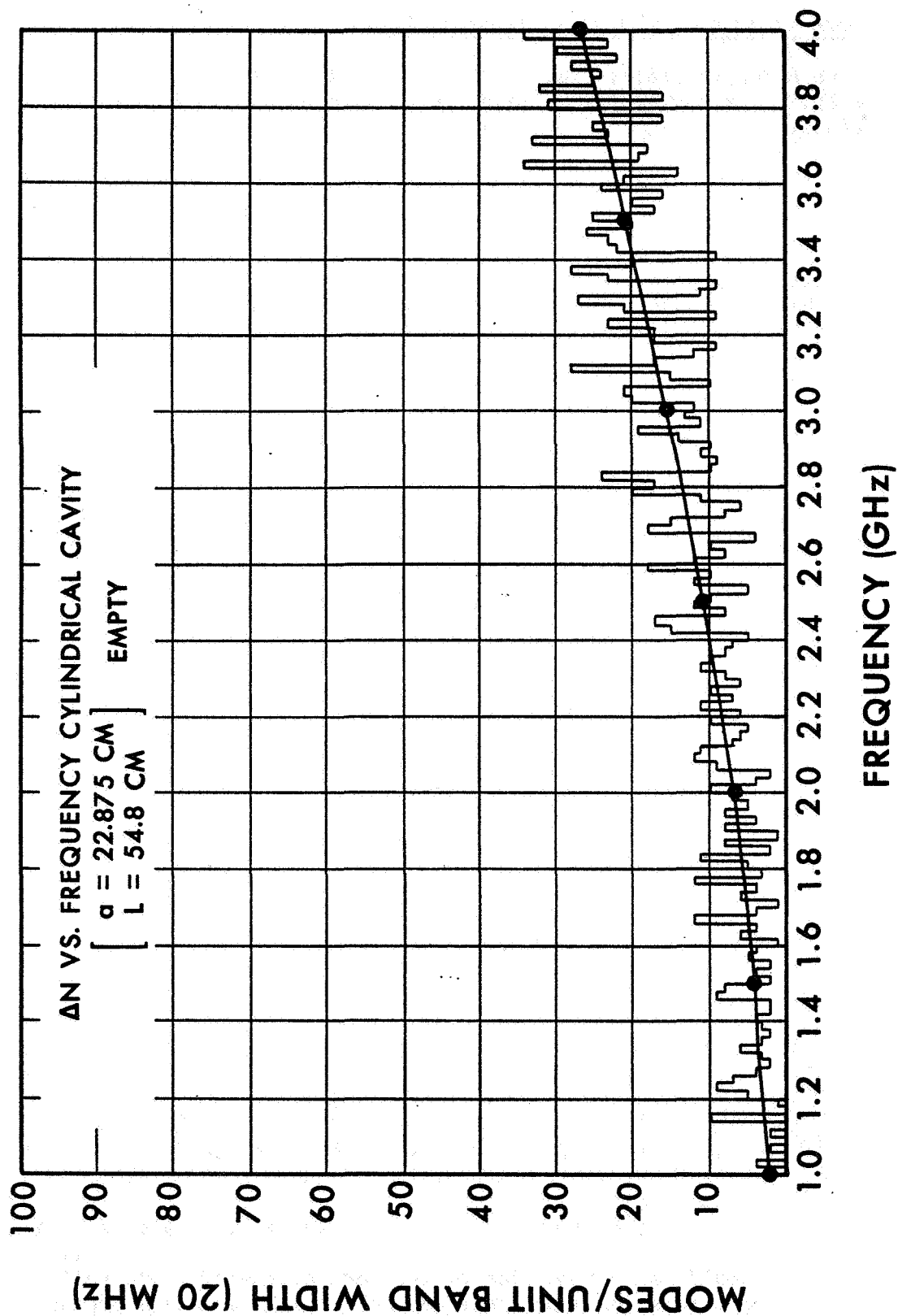


FIGURE 3-12

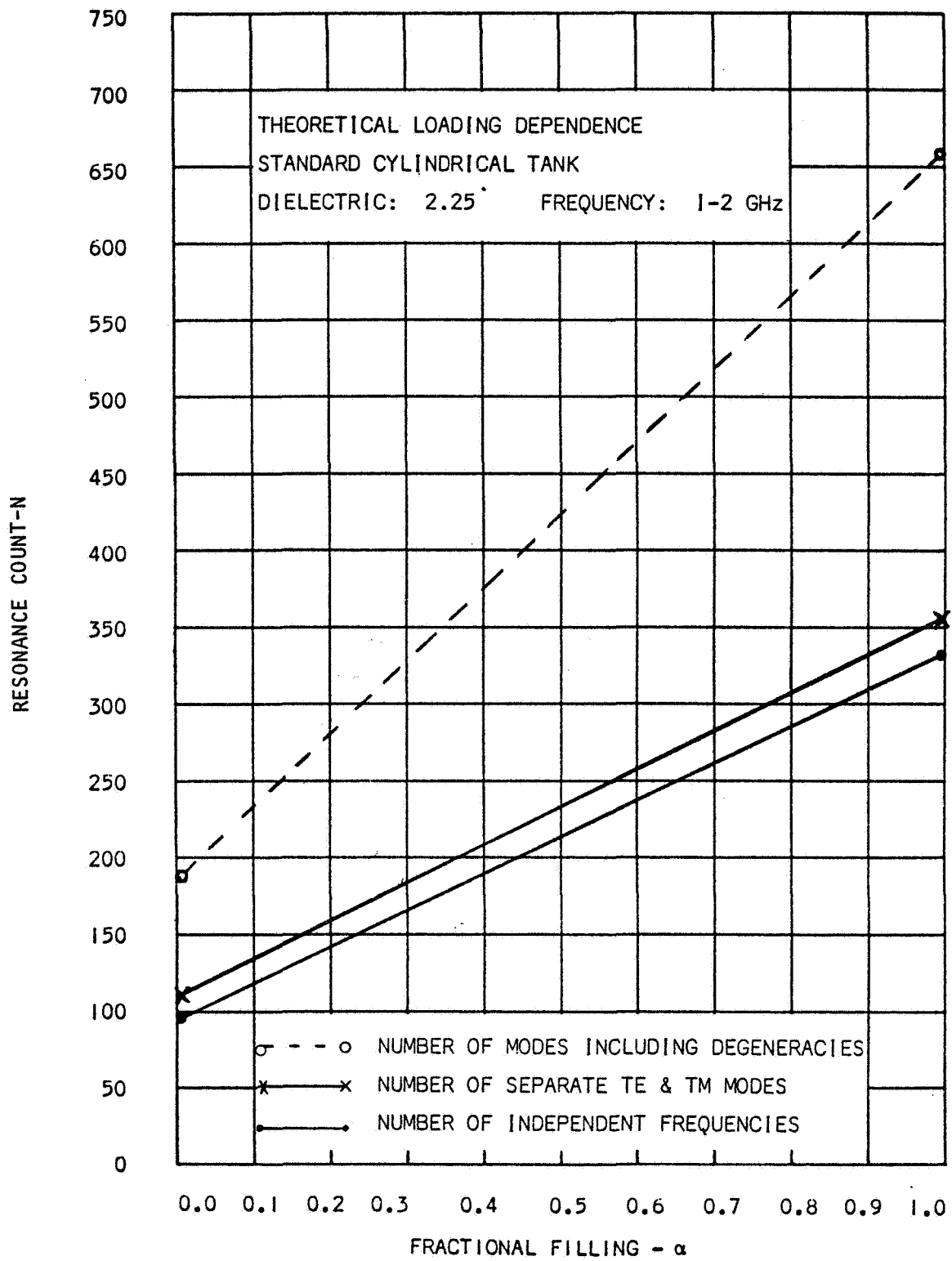


FIGURE 3-13

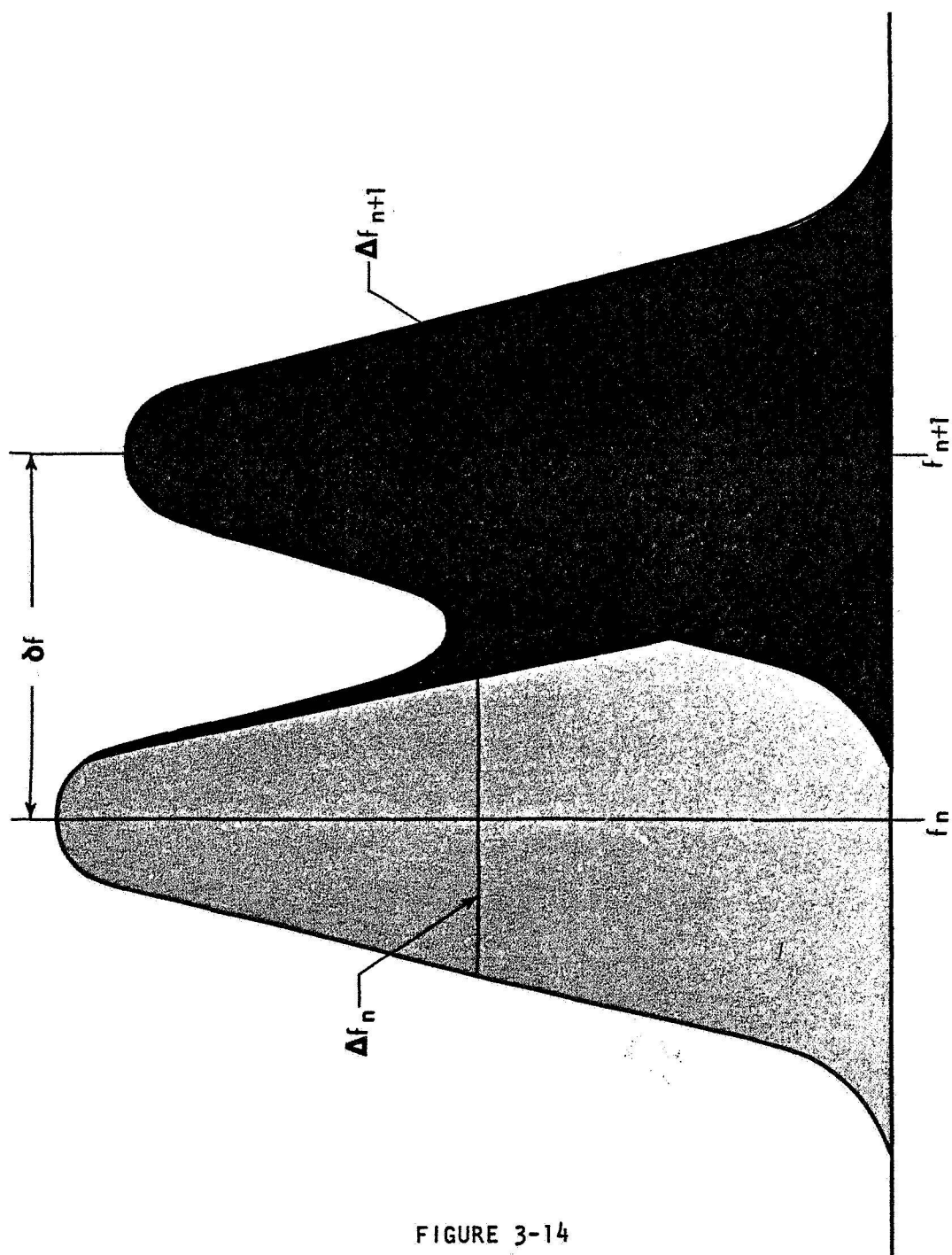


FIGURE 3-14

OVERLAP OF ADJACENT MODES

The second phenomenon of concern is that of resonance merging due to overlap of adjacent resonances. See Figure 3-14.

The overlap of adjacent resonances is caused by finite resonance "Q" due to cavity absorption of RF energy. "Q" is a measure of the sharpness of response of the cavity to external excitation. The common definition of "Q" relates the energy stored in the cavity to the energy loss per cycle.

$$Q = \frac{\omega_o}{2\pi} \left(\frac{\text{energy stored}}{\text{energy loss}} \right)$$

For a realistic system, all system losses must be considered. The total overall system "Q" factor from all loss sources is:

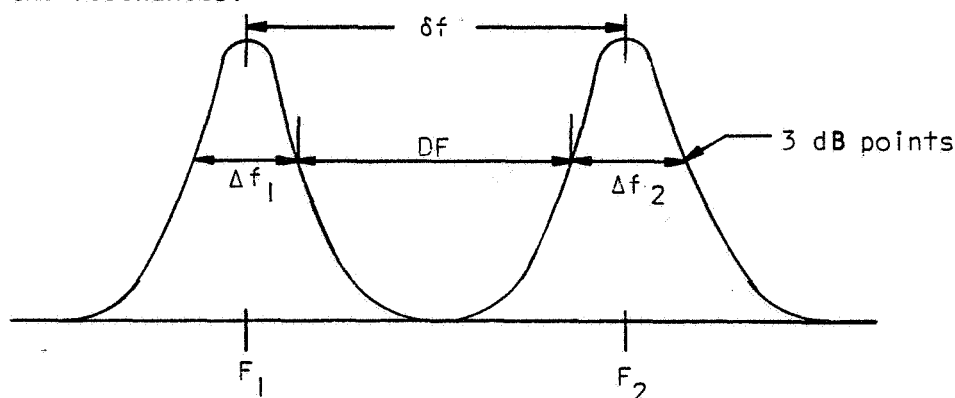
$$\frac{1}{Q_{\text{system}}} = \frac{1}{Q_{\text{tank}}} + \frac{1}{Q_{\text{dielectric}}} + \frac{1}{Q_{\text{external}}}$$

"Q" is directly related to the loss tangent; therefore:

$$\tan\delta_{\text{system}} = \tan\delta_{\text{tank}} + \tan\delta_{\text{dielectric}} + \tan\delta_{\text{external}}$$

where $\tan\delta_{\text{external}}$ includes cable losses, generator "Q", and connector losses. A complete discussion of "Q" effects can be found in Volume I Appendix F. In order to determine the effects of resonance overlap, a computer program was developed that would compute the transfer characteristics of a resonant cavity when two adjacent resonances overlap. Transfer characteristics were determined for adjacent resonances having variations in resonance "Q", resonance amplitude, and resonance separation frequency. Appendix C, Section II shows the transfer characteristics of a number of adjacent resonances having a variety of parameter variations. In all cases, the system "Q" or total "Q" has been used. Inspection of these curves allows the formulation of a figure of merit concerning the proportions of resonance overlap.

Figure 3-15 shows two adjacent resonances and the interrelationship between the resonances.



RESONANCE OVERLAP DEFINITION
FIGURE 3-15

The half power points or 3dB points, Δf_1 and Δf_2 can be related to the resonance "Q" by the following expression:

$$\Delta f_1 = \frac{f_1}{Q_1}$$

$$\Delta f_2 = \frac{f_2}{Q_2}$$

The separation of the adjacent resonances $\delta f = F_2 - F_1$ can now be used in conjunction with the resonance "Q" to determine the overlap factor, DF, between the two resonances; that is,

$$DF = \delta f - \left(\frac{F_1}{2Q_1} + \frac{F_2}{2Q_2} \right)$$

or

$$DF = F_2 - F_1 - \left(\frac{F_1}{2Q_1} + \frac{F_2}{2Q_2} \right)$$

This expression for resonance separation provides a figure of merit with regard to resonance detectability that is directly related to resonance "Q". What now remains is to combine the effect of resonance degeneracies and resonance overlap in a statistical manner that is indicative of the actual detectability of the resonances. The development of such a statistical program will be discussed in Paragraph 3.10.

3.10 Development of Statistical Representation

In order to formulate an empirical relationship between the actual number of resonances detectable in a cavity and resonances merging, experimental data on a cylindrical cavity was analyzed with respect to theoretical predictions. A computer program was run on a cylindrical cavity 22.875 cm in radius and 54.8 cm in height. Individual resonances were identified as being either "TE" or "TM", degenerate or nondegenerate, separate or identical frequencies. A summary of the breakdown for the cavity excited in the frequency band of 1-2 GHz and filled with a dielectric of 2.28 is given in Table 3-5.

TABLE 3-5

RESONANCE BOUNDS STANDARD CYLINDRICAL CAVITY

Condition/Fractional Filling	$\alpha = 0.0$	$\alpha = 1.0$
Number of Resonances Including Degeneracies	190	659
Number of Separate "TE" and "TM" Resonances	106	355
Number of Individual Separate Frequencies	99	333

An experimental cavity was constructed and excited over the frequency band 1-2 GHz. The resonance pattern was recorded by means of a strip chart and a direct comparison of the theoretical resonance frequencies to the experimental results made. Table 3-6 shows the comparison made for the empty standard cylindrical cavity.

TABLE 3-6

RESONANCE DISTRIBUTION STANDARD CYLINDRICAL CAVITY

Frequency (GHz)	Resonance Count (Empty)	
	Analysis	Experimental
1.0 - 1.1	6	6
1.1 - 1.2	13	14
1.2 - 1.3	12	12
1.3 - 1.4	15	14
1.4 - 1.5	17	15
1.5 - 1.6	25	25
1.6 - 1.7	17	15
1.7 - 1.8	26	29
1.8 - 1.9	27	26
1.9 - 2.0	32	28
TOTAL	190	184

EXACT COMPUTER SOLUTION - STANDARD CYLINDRICAL CAVITY

		BESSEL											
M		N		ZERO		P		f		Q			
0.30000E 01	0.10000E 01	0.42010E 01	0.20000E 01	0.10330E 10	0.44707E 05	1	2						
0.20000E 01	0.10000E 01	0.30540E 01	0.30000E 01	0.10388E 10	0.54260E 05	1	4						
0.20000E 01	0.10000E 01	0.51360E 01	0.00000E-05	0.10713E 10	0.64058E 05	2	6						
0.20000E 01	0.10000E 01	0.51360E 01	0.10000E 01	0.11057E 10	0.50273E 05	2	8						
0.40000E 01	0.10000E 01	0.53180E 01	0.10000E 01	0.11425E 10	0.40886E 05	1	10						
0.10000E 01	0.20000E 01	0.53320E 01	0.10000E 01	0.11453E 10	0.91411E 05	1	12						
0.10000E 01	0.10000E 01	0.38320E 01	0.30000E 01	0.11455E 10	0.51171E 05	2	14						
0.00000E-09	0.10000E 01	0.38320E 01	0.30000E 01	0.11455E 10	0.10259E 06	1	15						
0.00000E-10	0.20000E 01	0.55200E 01	0.00000E-05	0.11514E 10	0.66410E 05	2	16						
0.10000E 01	0.10000E 01	0.18410E 01	0.40000E 01	0.11596E 10	0.74294E 05	1	18						
0.00000E-10	0.20000E 01	0.55200E 01	0.10000E 01	0.11834E 10	0.52011E 05	2	19						
0.30000E 01	0.10000E 01	0.42010E 01	0.30000E 01	0.12005E 10	0.48953E 05	1	21						
0.20000E 01	0.10000E 01	0.51360E 01	0.20000E 01	0.12029E 10	0.52437E 05	2	23						
0.00000E-10	0.10000E 01	0.24050E 01	0.40000E 01	0.12036E 10	0.52453E 05	2	24						
0.40000E 01	0.10000E 01	0.53180E 01	0.20000E 01	0.12368E 10	0.42969E 05	1	26						
0.10000E 01	0.20000E 01	0.53320E 01	0.20000E 01	0.12394E 10	0.97248E 05	1	28						
0.20000E 01	0.10000E 01	0.30540E 01	0.40000E 01	0.12661E 10	0.60647E 05	1	30						
0.00000E-10	0.20000E 01	0.55200E 01	0.20000E 01	0.12747E 10	0.53980E 05	2	31						
0.30000E 01	0.10000E 01	0.63800E 01	0.00000E-05	0.13308E 10	0.71396E 05	2	33						
0.20000E 01	0.10000E 01	0.51360E 01	0.30000E 01	0.13495E 10	0.55540E 05	2	35						
0.10000E 01	0.10000E 01	0.38320E 01	0.40000E 01	0.13550E 10	0.55653E 05	2	37						
0.00000E-09	0.10000E 01	0.38320E 01	0.40000E 01	0.13550E 10	0.11444E 06	1	38						
0.30000E 01	0.10000E 01	0.63800E 01	0.10000E 01	0.13586E 10	0.55727E 05	2	40						
0.50000E 01	0.10000E 01	0.64150E 01	0.10000E 01	0.13657E 10	0.40344E 05	1	42						
0.40000E 01	0.10000E 01	0.53180E 01	0.30000E 01	0.13798E 10	0.45912E 05	1	44						
0.10000E 01	0.20000E 01	0.53320E 01	0.30000E 01	0.13821E 10	0.10543E 06	1	46						
0.30000E 01	0.10000E 01	0.42010E 01	0.40000E 01	0.14018E 10	0.53536E 05	1	48						
0.00000E-10	0.20000E 01	0.55200E 01	0.30000E 01	0.14139E 10	0.56850E 05	2	49						
0.10000E 01	0.10000E 01	0.18410E 01	0.50000E 01	0.14205E 10	0.82624E 05	1	51						
0.20000E 01	0.20000E 01	0.67060E 01	0.10000E 01	0.14253E 10	0.95946E 05	1	53						
0.30000E 01	0.10000E 01	0.63800E 01	0.20000E 01	0.14388E 10	0.57349E 05	2	55						
0.50000E 01	0.10000E 01	0.64150E 01	0.20000E 01	0.14456E 10	0.41786E 05	1	57						
0.00000E-10	0.10000E 01	0.24050E 01	0.50000E 01	0.14568E 10	0.57705E 05	2	58						
0.10000E 01	0.20000E 01	0.70160E 01	0.00000E-05	0.14634E 10	0.74870E 05	2	60						
0.10000E 01	0.20000E 01	0.70160E 01	0.10000E 01	0.14888E 10	0.58336E 05	2	62						
0.00000E-10	0.20000E 01	0.70160E 01	0.10000E 01	0.14888E 10	0.10764E 06	1	63						
0.20000E 01	0.20000E 01	0.67060E 01	0.20000E 01	0.15019E 10	0.99942E 05	1	65						
0.20000E 01	0.10000E 01	0.30540E 01	0.50000E 01	0.15087E 10	0.66712E 05	1	67						
0.20000E 01	0.10000E 01	0.51360E 01	0.40000E 01	0.15313E 10	0.59163E 05	2	69						
0.40000E 01	0.10000E 01	0.53180E 01	0.40000E 01	0.15581E 10	0.49294E 05	1	71						
0.10000E 01	0.20000E 01	0.53320E 01	0.40000E 01	0.15601E 10	0.11471E 06	1	73						
0.10000E 01	0.20000E 01	0.70160E 01	0.20000E 01	0.15623E 10	0.59760E 05	2	75						
0.00000E-10	0.20000E 01	0.70160E 01	0.20000E 01	0.15623E 10	0.11192E 06	1	76						
0.30000E 01	0.10000E 01	0.63800E 01	0.30000E 01	0.15634E 10	0.59781E 05	2	78						
0.50000E 01	0.10000E 01	0.64150E 01	0.30000E 01	0.15696E 10	0.43916E 05	1	80						
0.40000E 01	0.10000E 01	0.75880E 01	0.00000E-05	0.15827E 10	0.77862E 05	2	82						
0.10000E 01	0.10000E 01	0.38320E 01	0.50000E 01	0.15841E 10	0.60175E 05	2	84						

FIGURE 3-16

A number of observations can be made: 1) the average modal frequency distribution compares favorably with the predicted distribution, 2) the total number of resonances is in correspondence with the theoretical maximum, and 3) due to the construction of the cylindrical cavity, most degenerate resonances split. A careful study of the resonance pattern obtained yielded a number of general guidelines to determine whether or not a certain set of resonances would be physically detectable. The computer program, Figure 3-16, contains a number of resonance sets in which "TE" and "TM" resonances exist at the same identical frequency with the "TE" resonances being degenerate to itself. The four blocks of the figure shows the cases where the TE(2) and TM(1) resonances occur at the same frequency (f) thus having a maximum number of three resonances occurring at one frequency. However, since they occur at the same frequency they are not all readily detectable.

This implies that a maximum number of three (3) resonances can possibly exist at this frequency and that a minimum number of one (1) resonance be detectable. Careful study of this particular resonance set by use of strip charts shows that in a majority of instances, the set of three resonances is detected as two. A second case of interest is one in which individual resonances are quite close to each other. Because of the finite system "Q", these resonances tend to merge together and be counted as one. Study of experimental data in conjunction with the resonance transfer characteristics previously developed (See Appendix C, Section II), instigated a set of weighing factors that could be applied to the maximum theoretical resonance count. These weighing factors would modify the theoretical resonance count to a practical obtainable resonance count. The weighing factors incorporating the empirical results obtained on the standard cylindrical cavity are:

For Degenerate Resonance Sets

- a) For all degenerate resonance sets where overlap factor is positive, the weighing factor is two (2).
- b) For all degenerate "TE" and "TM" resonance sets whose overlap factor is positive, the weighing factor is two (2).
- c) For all degenerate mode sets whose overlap factor is negative, the following cases apply;
 - 1) if $(F_2 - F_1) > |2 \times DF|$ the weighing factor is one (1)
 - 2) if $(F_2 - F_1) \leq |2 \times DF|$ the weighing factor is zero (0)

For Non-degenerate Resonance Sets

- a) For all non-degenerate resonance sets whose overlap factor is negative, the weighing factor is zero (0).
- b) For all non-degenerate resonance sets whose overlap factor is positive, the weighing factor is one (1).

A computer program was written that combined the exact resonant frequency solution to a cavity and the weighing factors. Since the weighing factors are "Q" dependent, this allowed for the establishment of a loading dependence that is "Q" dependent. This program was used in conjunction with cylindrical and rectangular tanks that were equivalent in volume to the Phase A THERMO tank and the Phase B THERMO tank as well as other simulated spacecraft type tanks. The computer programs were run for the following dielectrics, Liquid Hydrogen, LH₂ (1.23), Liquid Nitrogen, LH₂ (1.46) and Benzene (2.28). System "Q" values ranged from ∞ to 500 and the frequency bands of RF excitation ranged from 1 to 4 GHz. The loading dependence (sensitivity) curves for the standard cylindrical cavity are shown in Figures 3-17 through 3-20, using the average "Q" value.

The most important conclusion that can be made from these plots is that the system sensitivity or loading dependence can be determined for a propellant tank having a finite system "Q". The system "Q"; being defined as:

$$\frac{1}{Q_{\text{system}}} = \frac{1}{Q_{\text{tank}}} + \frac{1}{Q_{\text{dielectric}}} + \frac{1}{Q_{\text{external}}}$$

where the external "Q" includes the effects of cable losses, probe losses, and RF generator losses. The graphs show that when the system "Q" is low (1000 to 500), the loading response becomes nonlinear regardless of the dielectric used in filling the cavity.

By observing the loading response of a given tank for various frequency ranges, a lower frequency bound can be established. For example, a computer program was executed for a cylindrical tank equivalent in volume to the 1/3 scale THERMO tank, partially filled with LH₂, and excited in the frequency bands 1-2 GHz, 2-4 GHz, and 1-4 GHz. Inspection of the loading dependence curves, Figures 3-21 thru 3-23 points out that the theoretical loading dependence curve ($Q = \infty$) is extremely nonlinear in the frequency range from 1-2 GHz. The frequency range from 2-4 GHz for this volume tank gives a linear response and it can be concluded that a lower frequency bound for this tank is at 2 GHz if a linear loading response curve is desired. Establishment of an upper frequency bound is graphically illustrated in the resonance distribution curves for the standard cylindrical tank partially filled with Benzene. Since a maximum number of resonances will always occur at the high fractional filling, the resonance distribution at these points is critical. The resonance distribution curves for a 90% filling are shown in Figures 3-24 through 3-29. For various system "Q's" it can be seen that the resonance distribution deviates from the square law distribution curve at distinct frequencies.

A deviation from the square law response being defined as a point at which the average resonance distribution no longer has a positive slope,

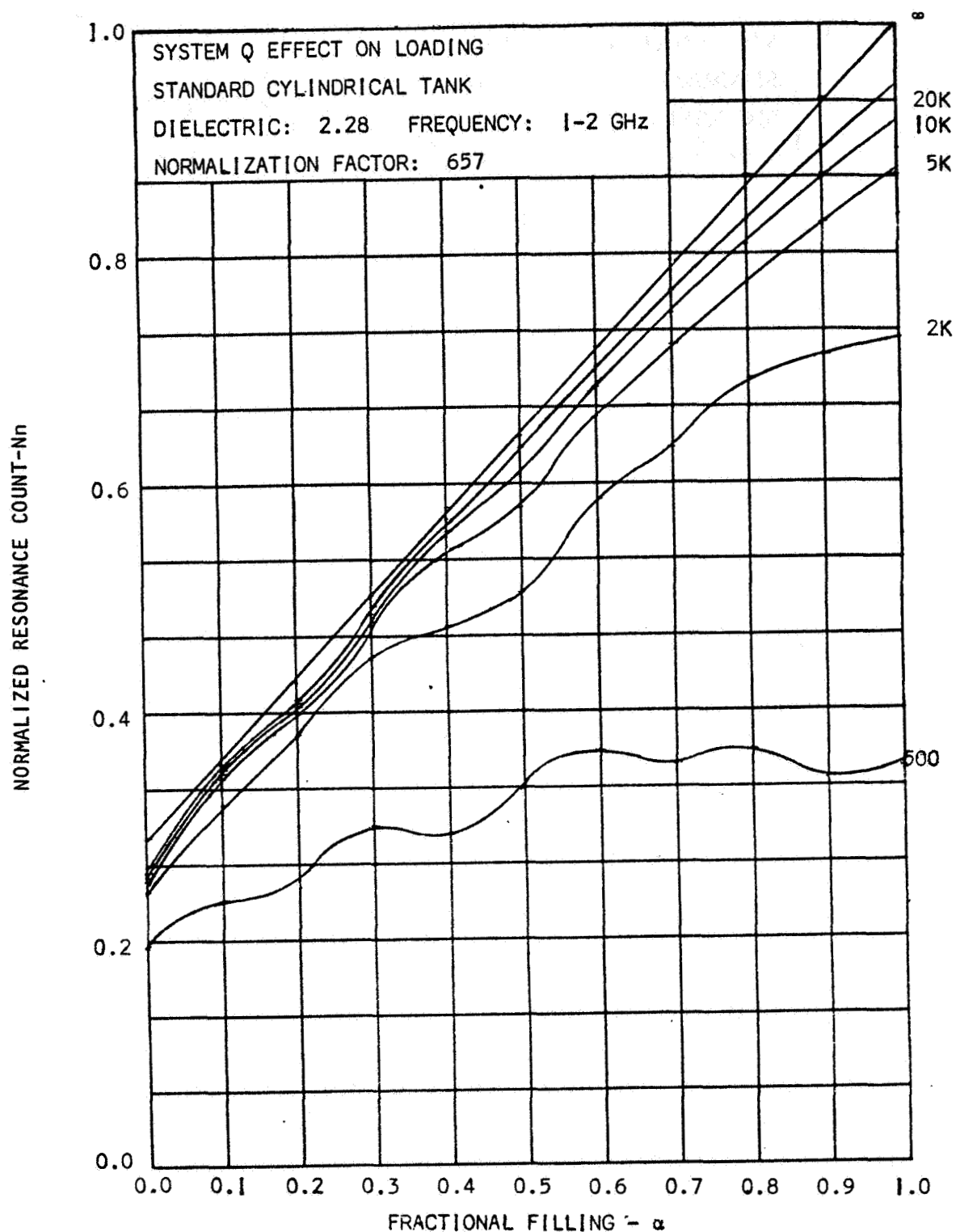


FIGURE 3-17

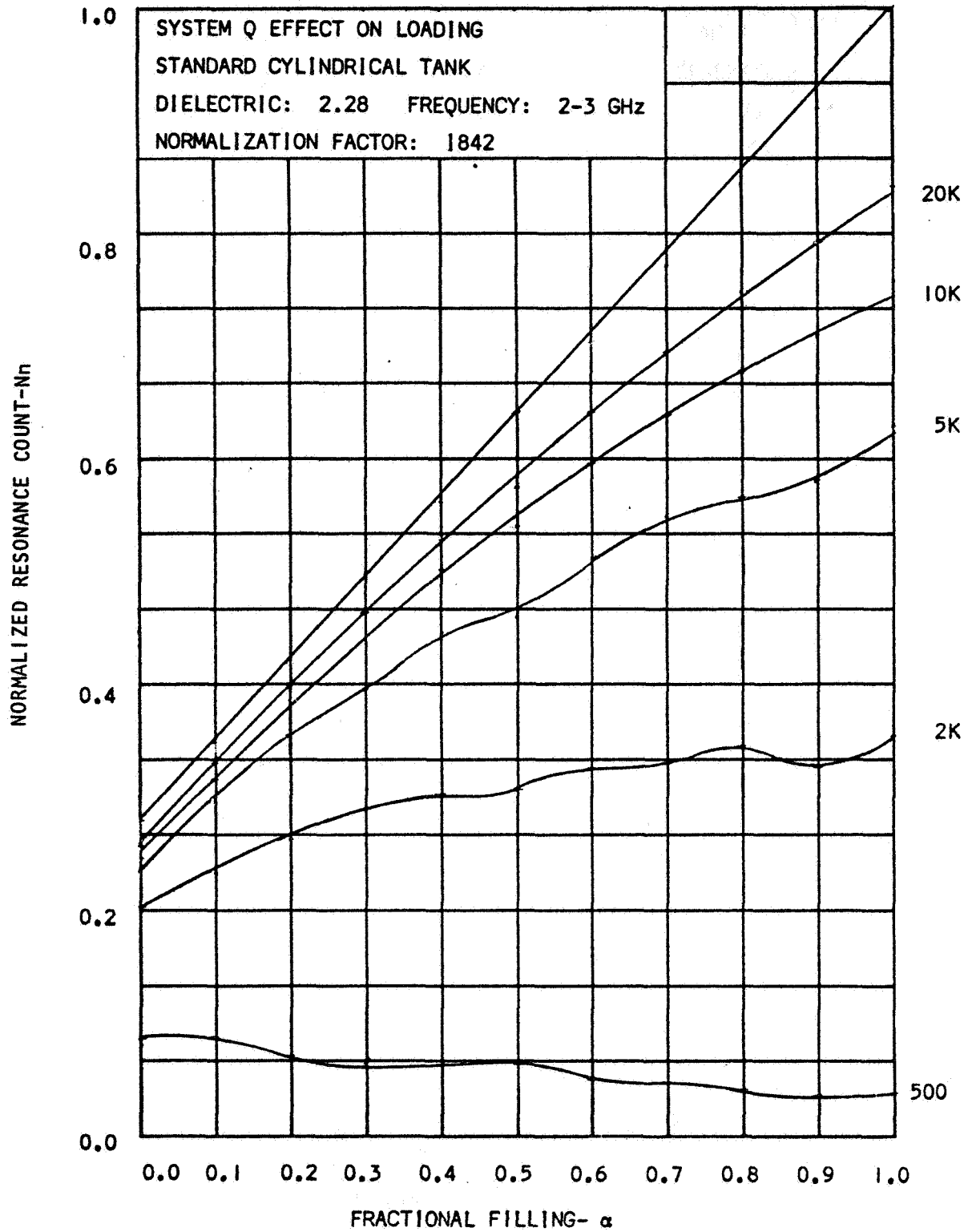


FIGURE 3-18

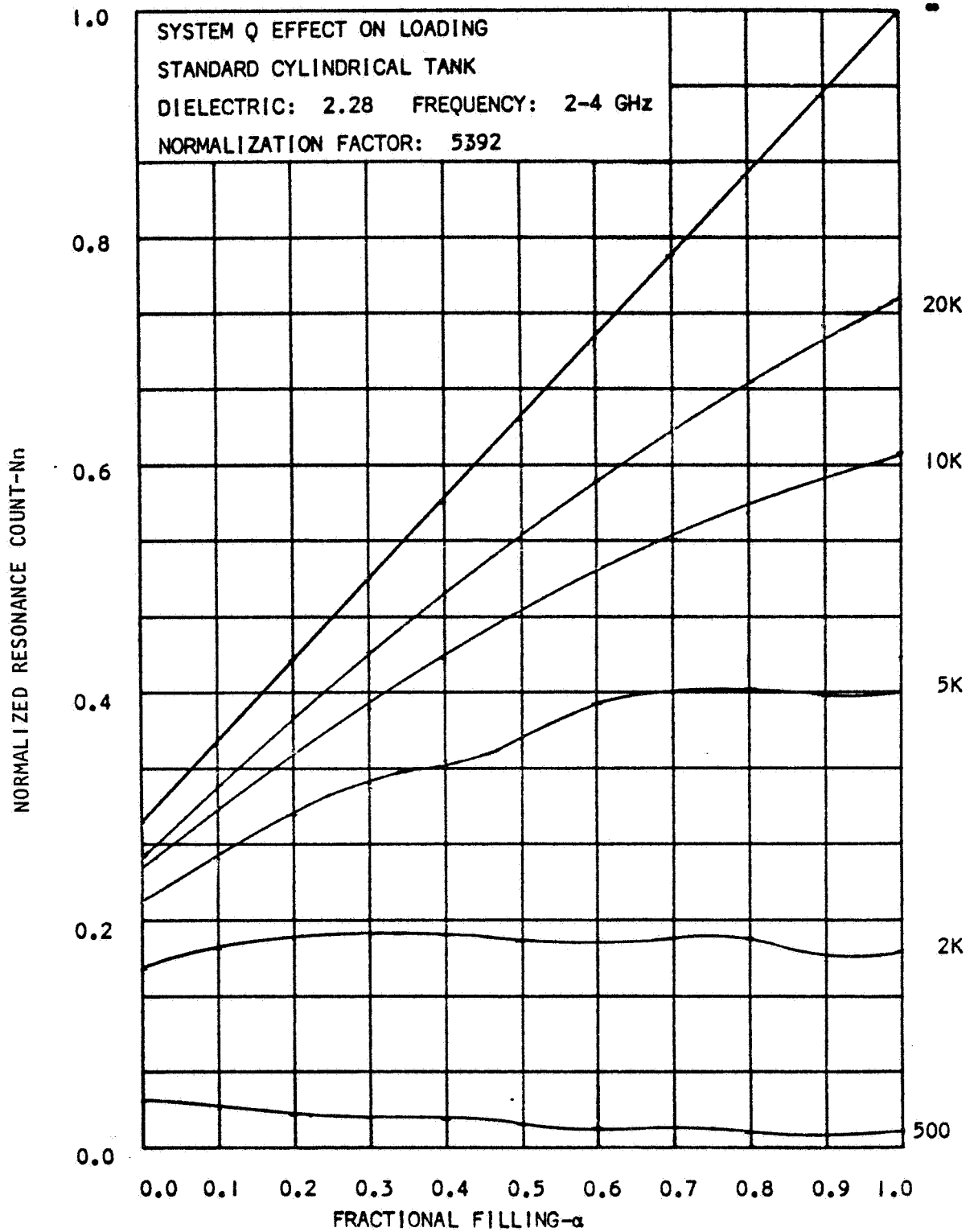


FIGURE 3-19

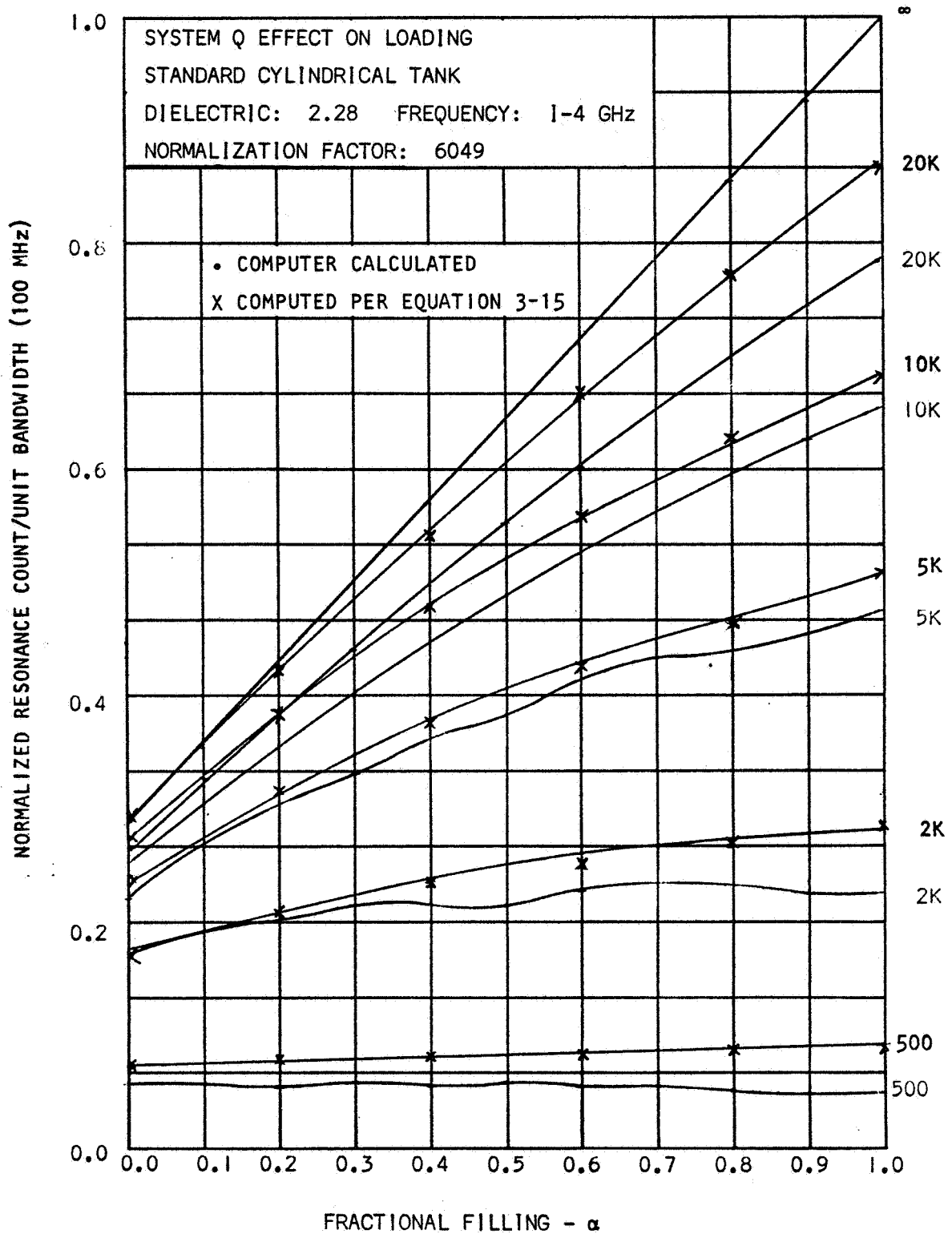


FIGURE 3-20

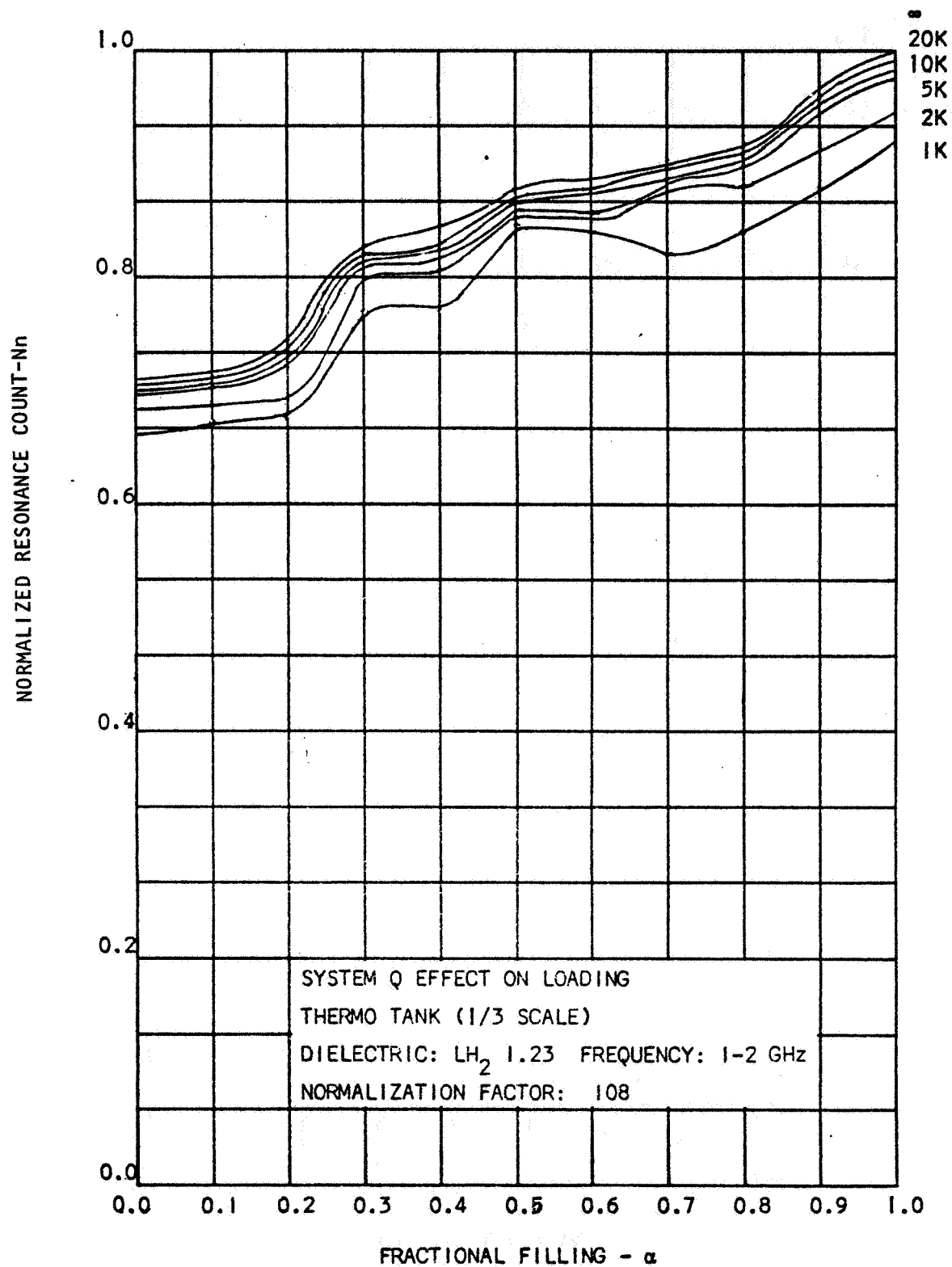


FIGURE 3-21

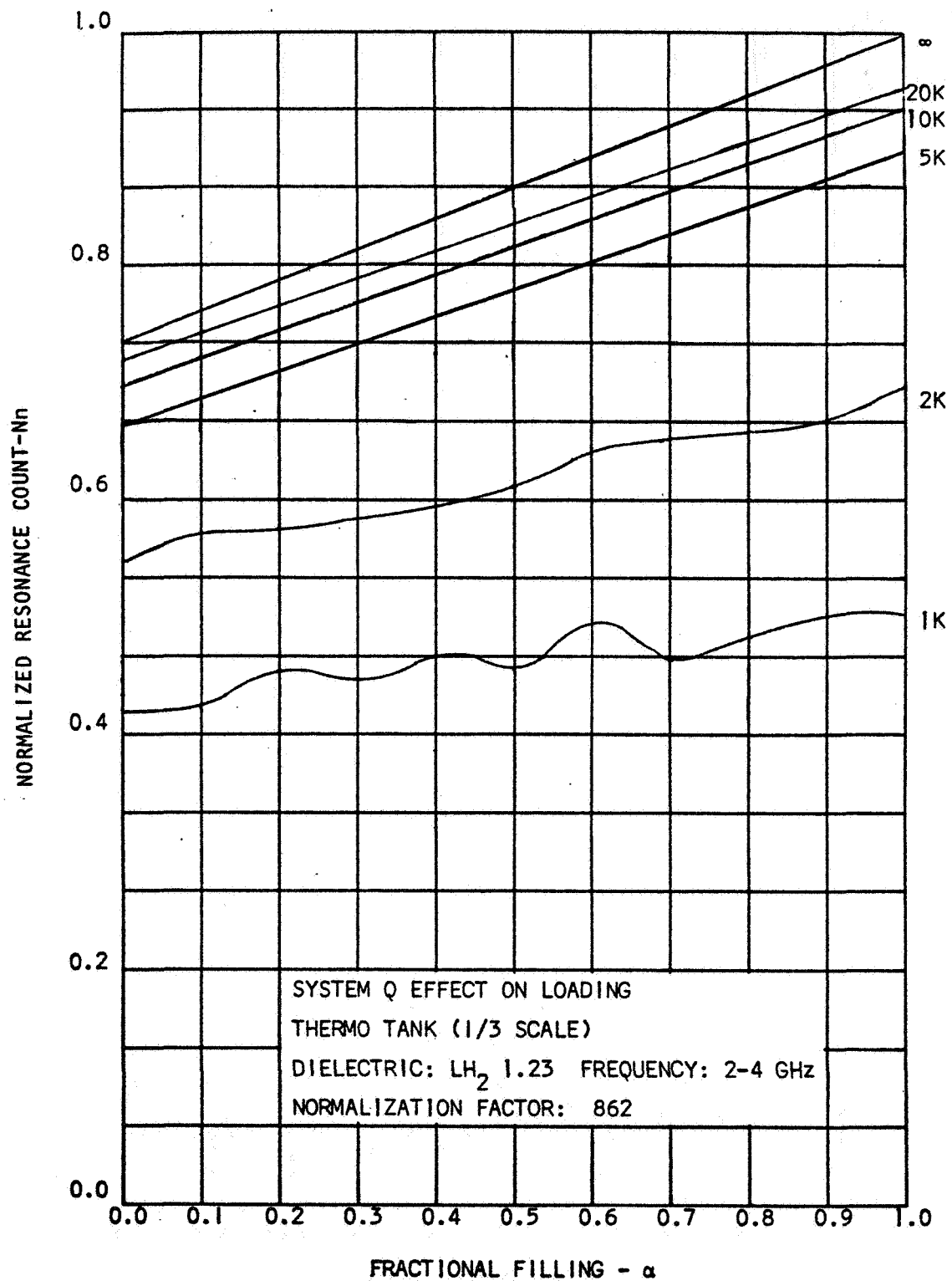


FIGURE 3-22

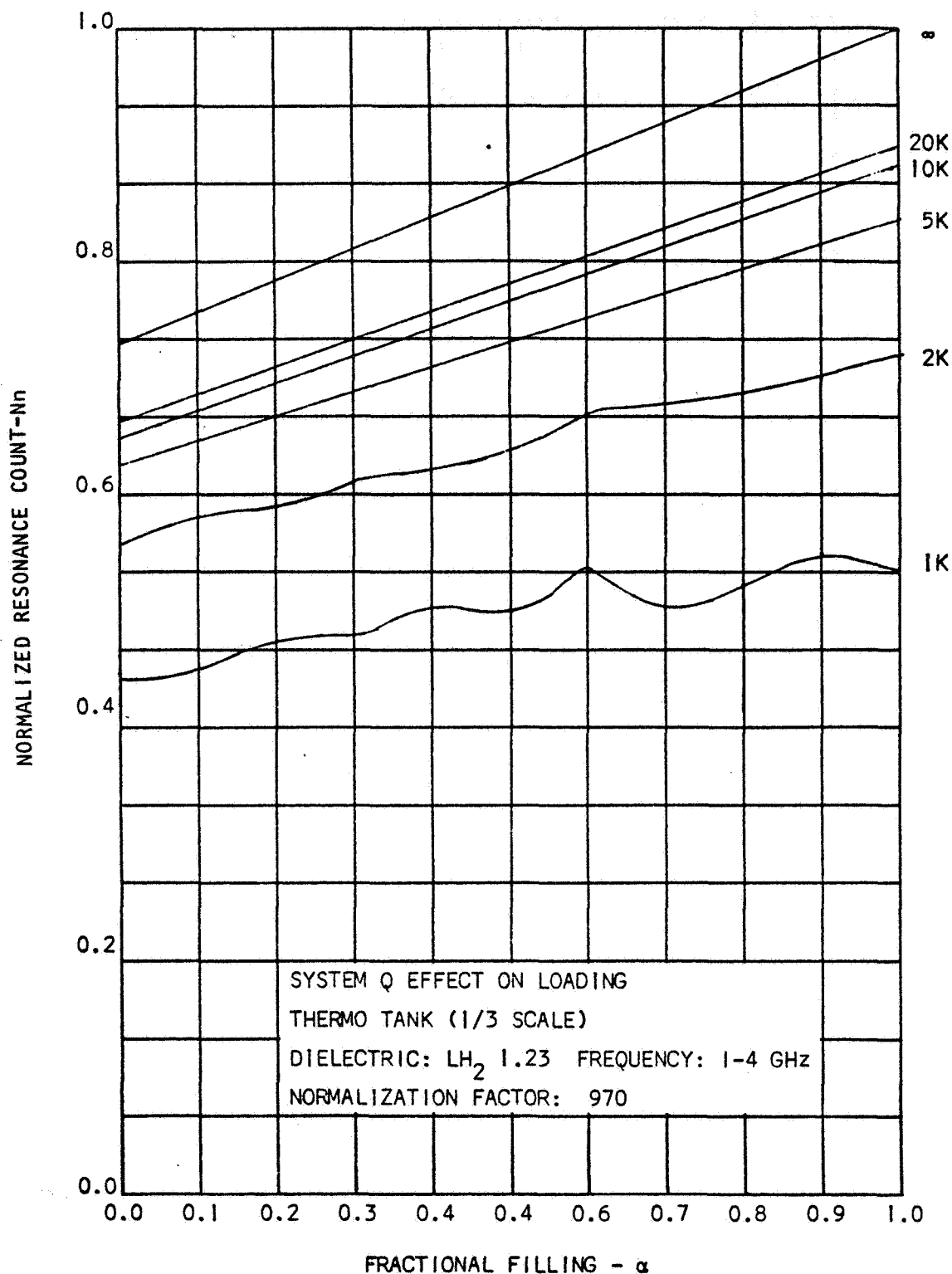


FIGURE 3-23

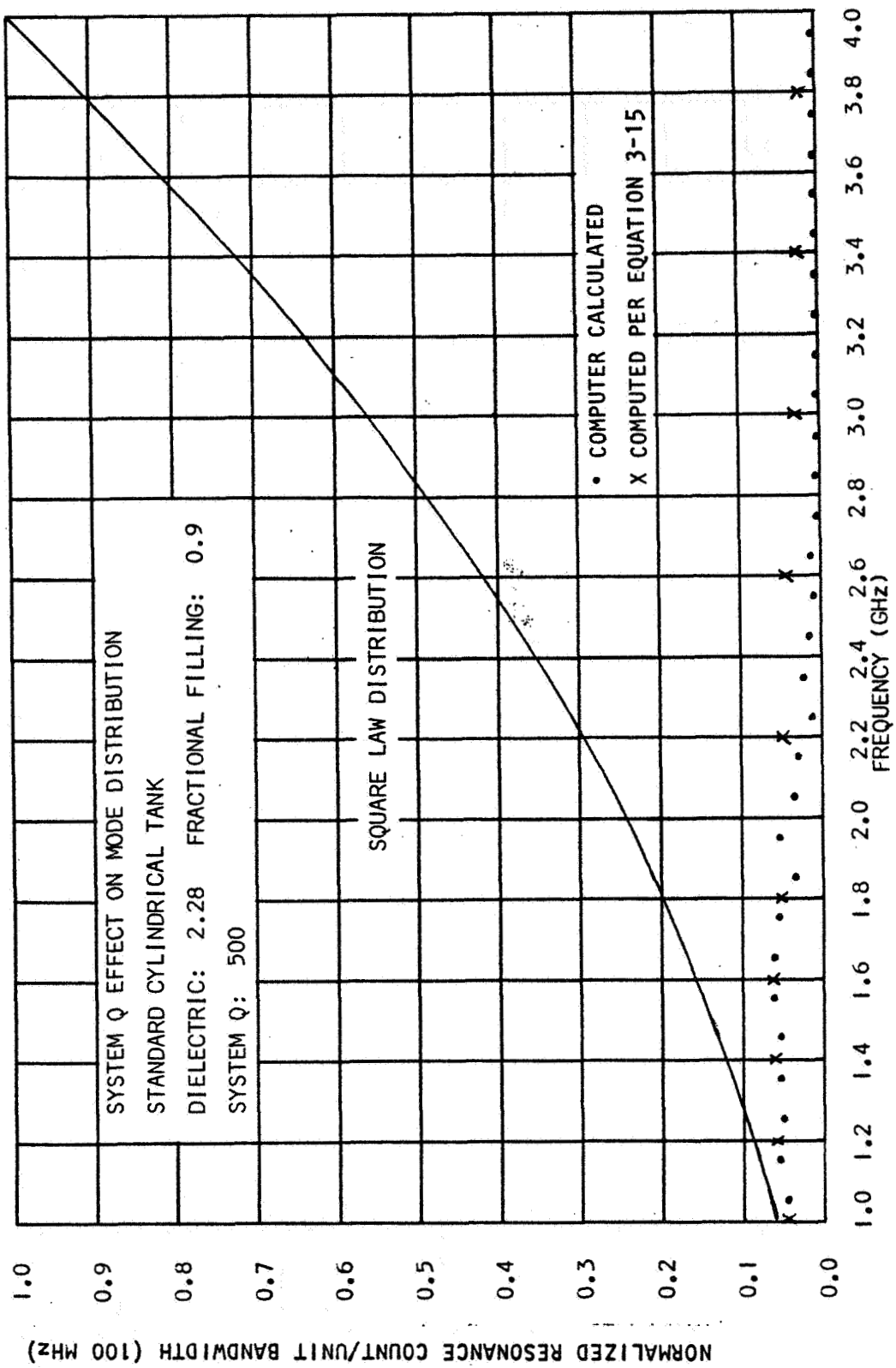


FIGURE 3-24

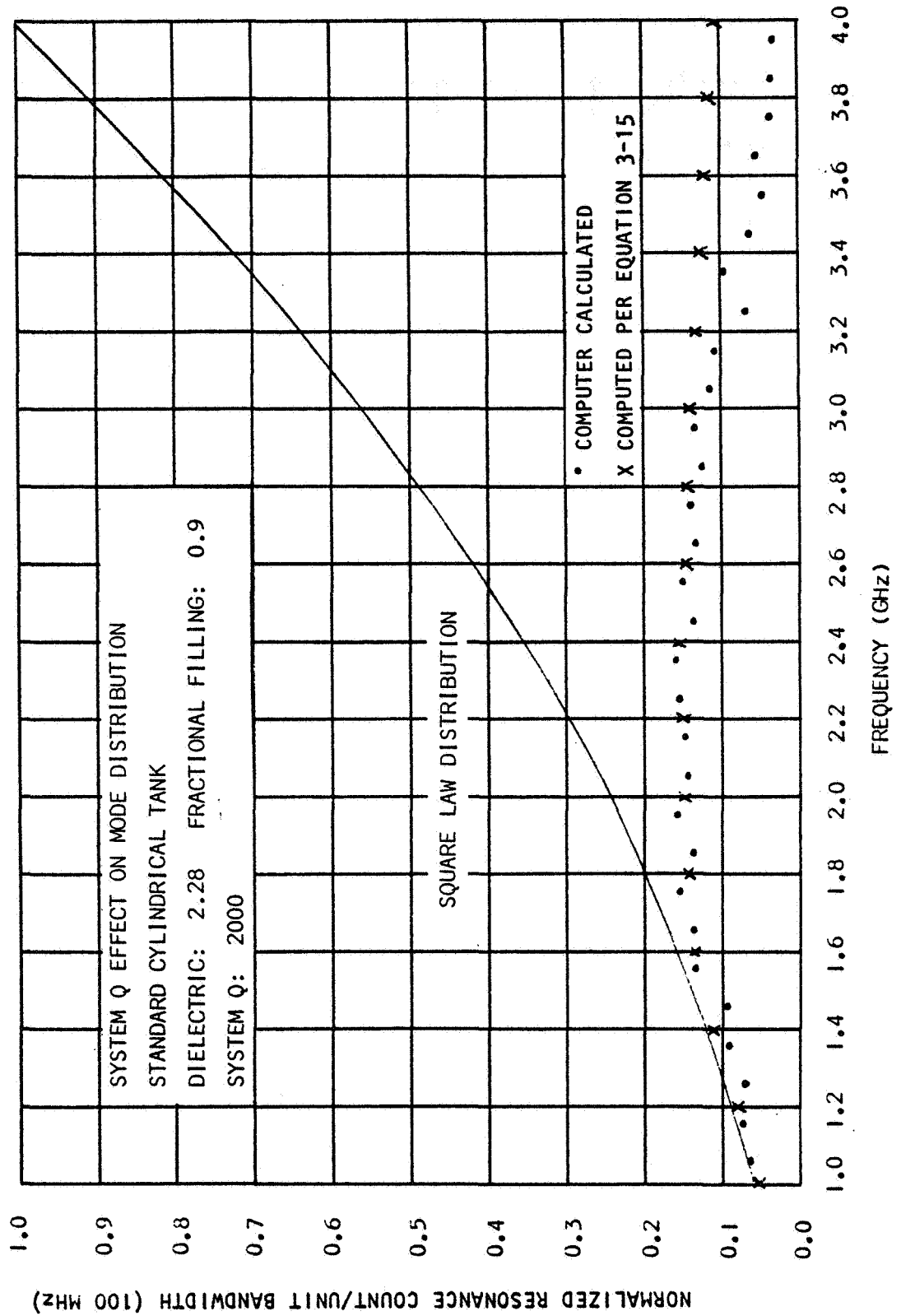


FIGURE 3-25

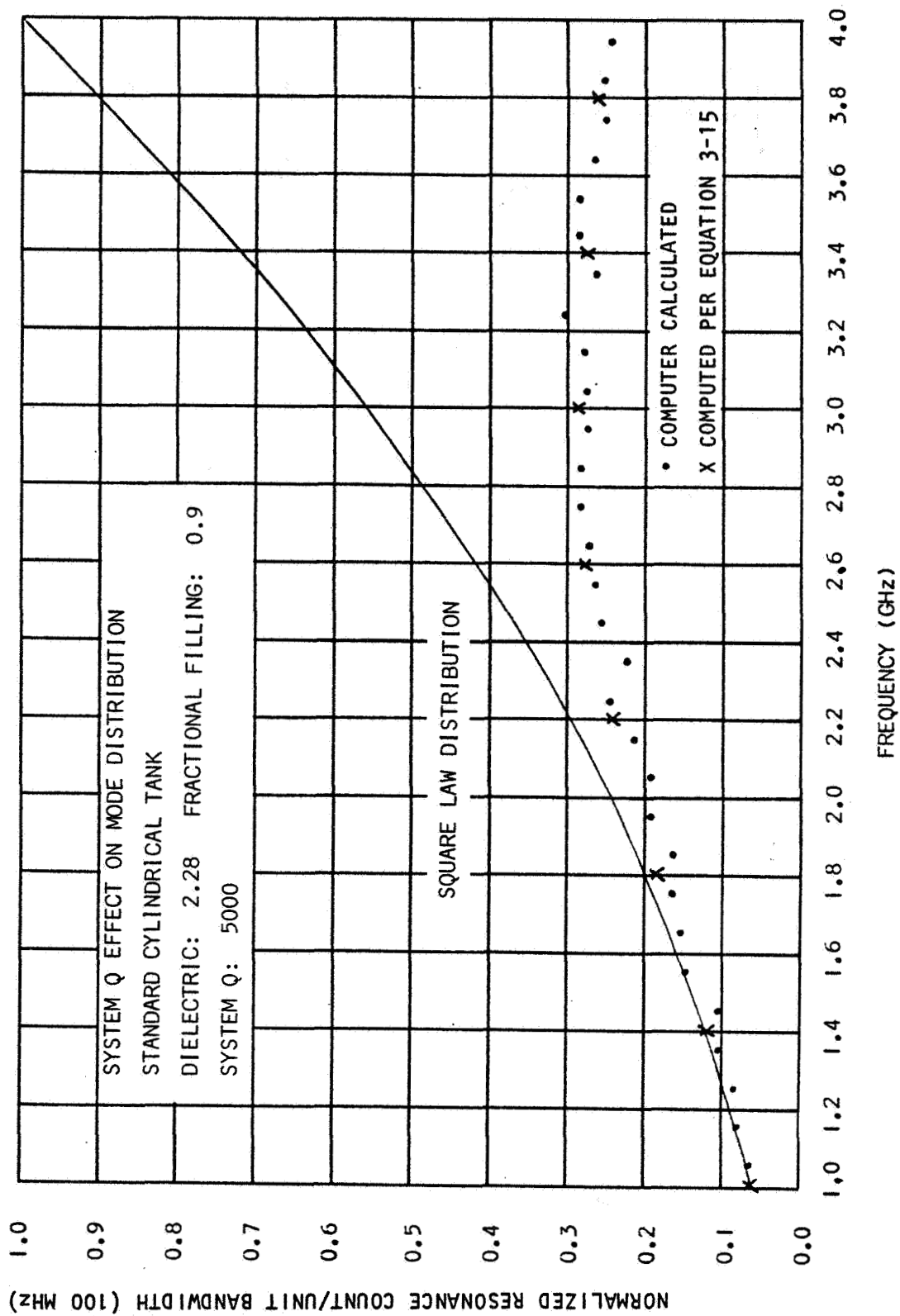


FIGURE 3-26

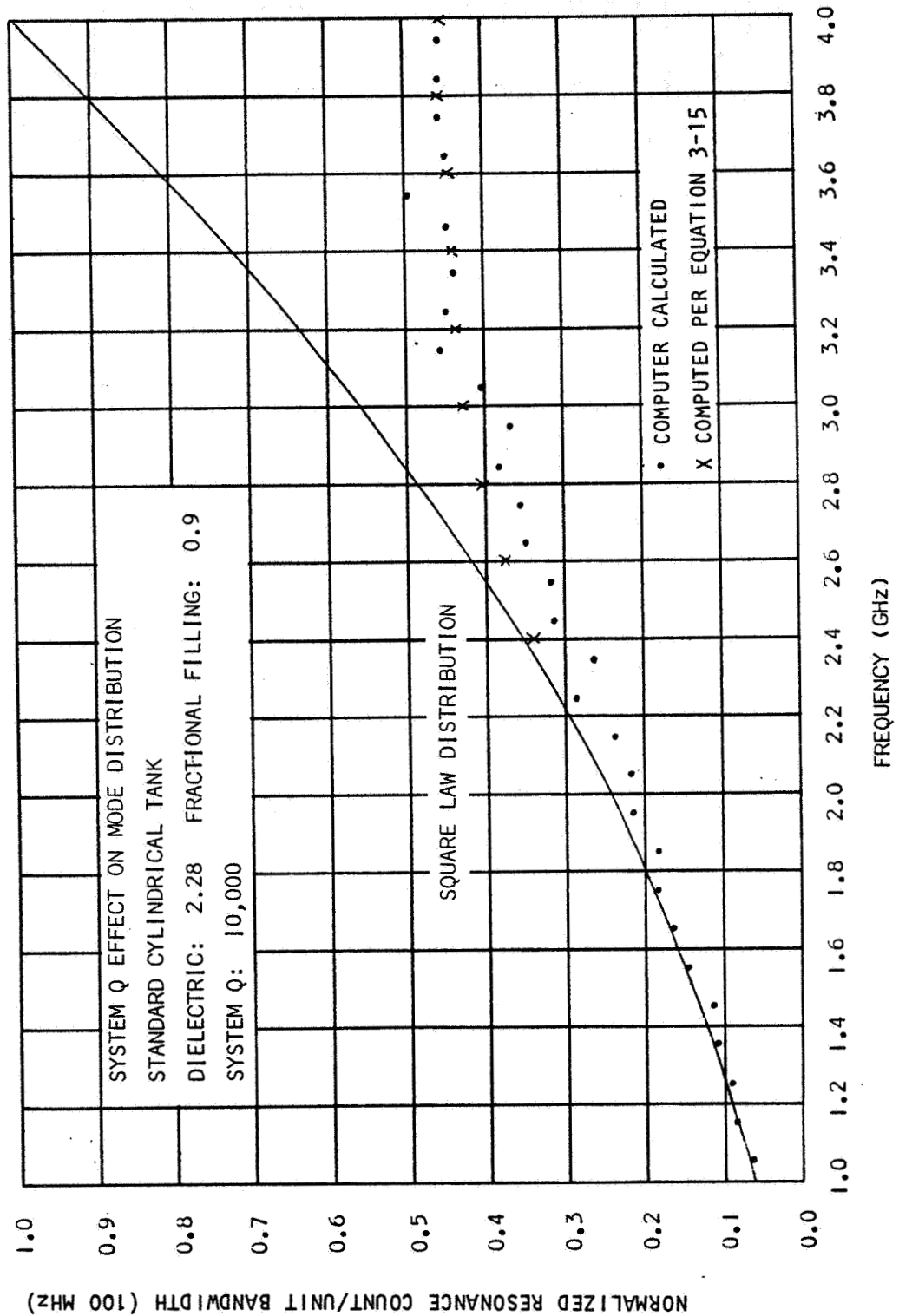


FIGURE 3-27

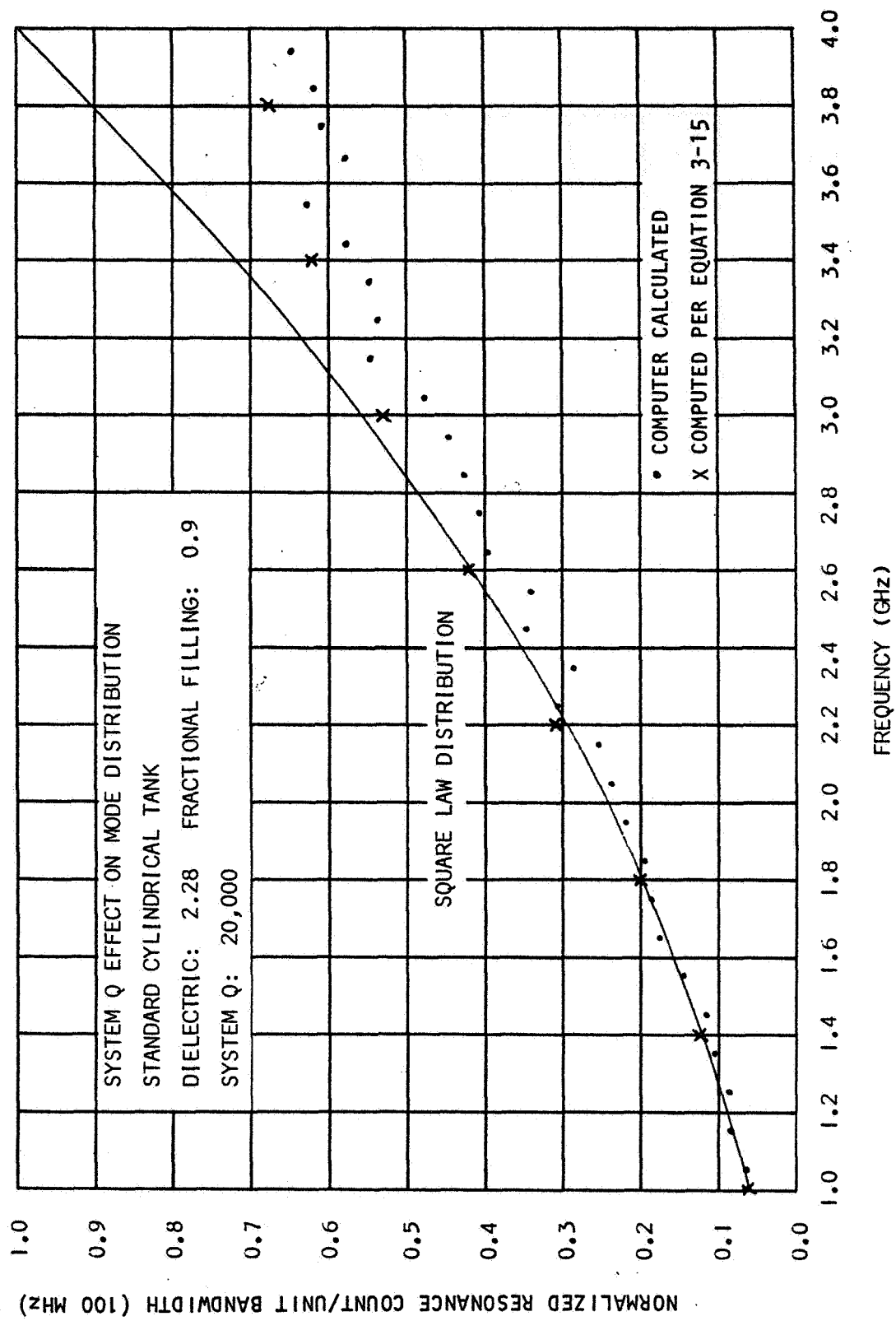


FIGURE 3-28

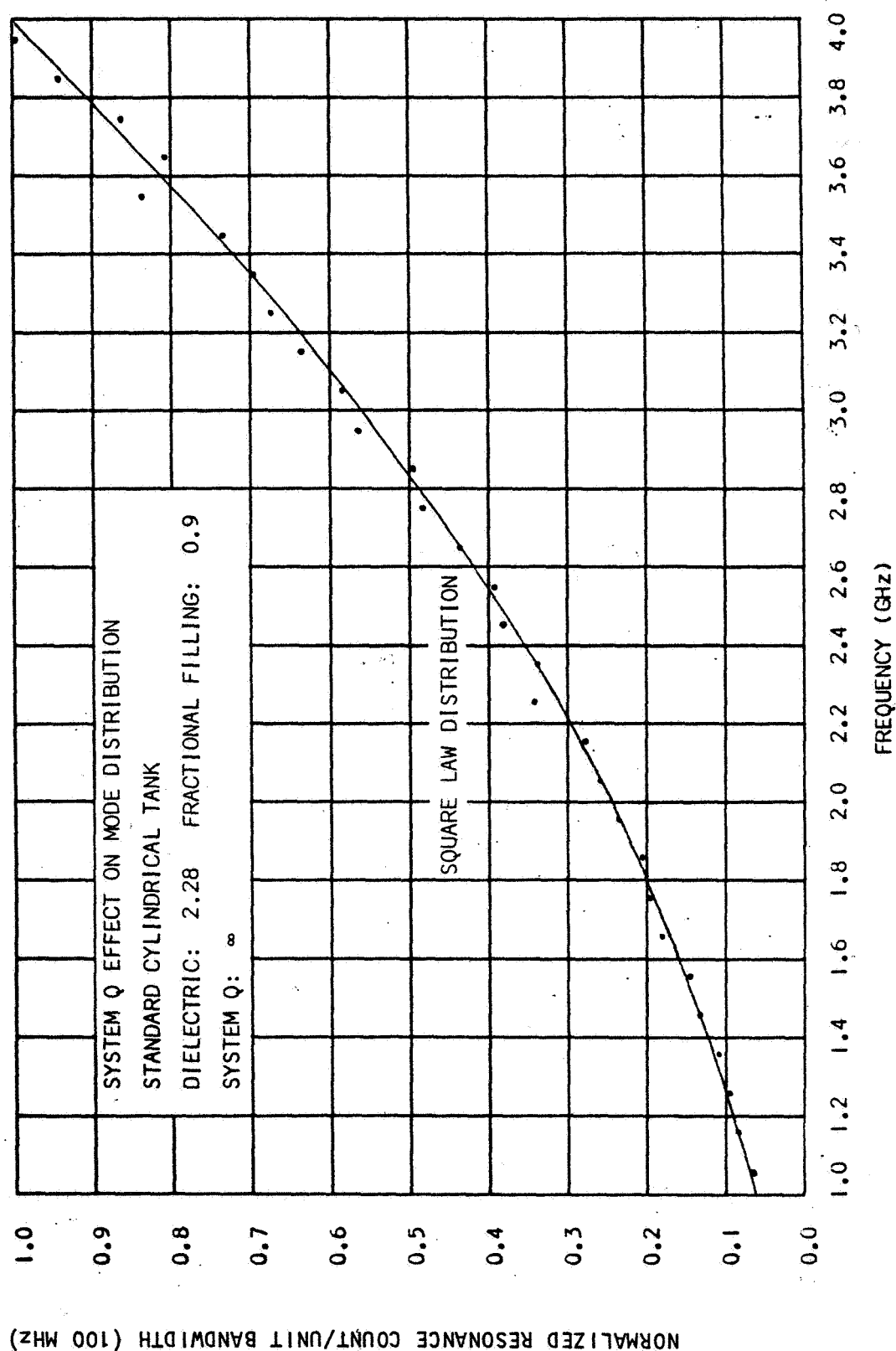


FIGURE 3-29

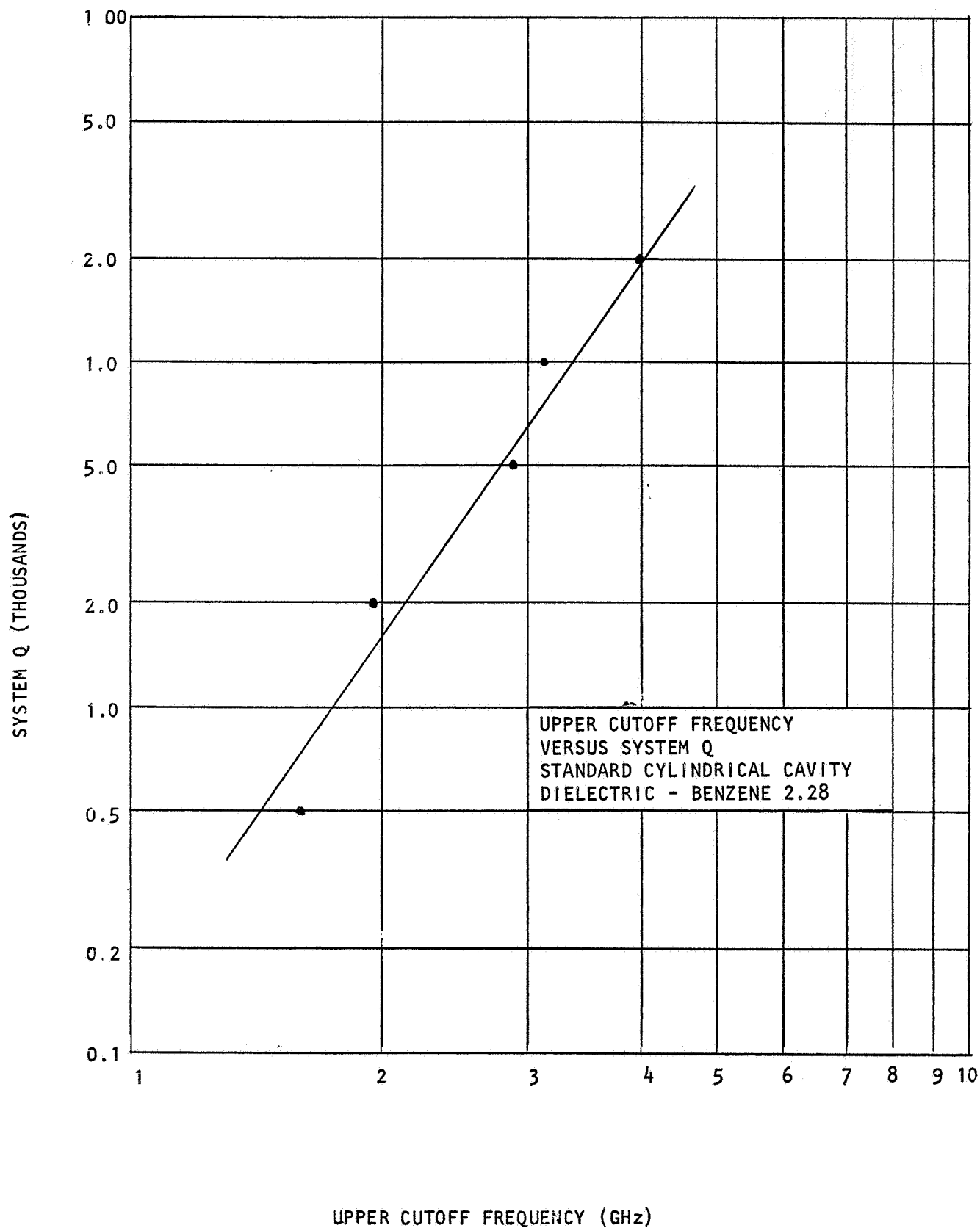


FIGURE 3-30

i.e., the point of zero slope. The mathematical expression is:

$$\frac{d^2N}{df^2} = 0$$

For a tank having a specific system "Q", the upper frequency limit can be determined as the point where:

$$\frac{d^2N}{df^2} = 0$$

For the standard cylindrical tank, the upper frequency limit is plotted as a function of "Q" as shown in Figure 3-30.

In practice, the lower frequency limit is not dependent on mode overlap to any great extent. Rather, it is an indication of a sufficient number of modes to uniformly illuminate the tank interior. Whether the lower frequency limit is best obtained by looking at a loading curve for octave bandwidths or by computing the total number of modes up to the lower frequency limit has not been determined. Present indications are that it would be best to set a lower frequency limit from the total number of modes excitable if the cavity were sweep from the cutoff frequency to the minimum sweep frequency.

A mathematical relationship has been derived for the normalized mode count/unit bandwidth, which is in approximate agreement with the computer derived results. This relation is:

$$\frac{dN}{df} = \frac{dN'}{df} \left(1 - \exp\left(\frac{-Q}{3N'}\right) \right) \quad (3-13)$$

where:

$$N' = \frac{8\pi}{3} \frac{V}{c^3} f^3 (1 + (\epsilon_r^{3/2} - 1) \alpha) \quad (3-14)$$

= Theoretical number of modes excitable in a partially loaded tank from cutoff frequency up to frequency f.

N = Number of resonances excitable for a tank of finite Q.

Comparison of the results of this calculation and the computer calculations is shown in Figures 3-24, 3-25, 3-26, 3-27 and 3-28.

This formula is seen to have an approximate agreement with the computer calculations and, therefore, is a useful tool for determining: 1) The number of excitable modes (N') and 2) The number of detectable resonances (N) up to a given frequency f. When the previous differential formula is integrated, it takes the form:

$$N = N' \left[1 - \exp\left(-\frac{Q}{3N'}\right) + \frac{Q}{3N'} E_1\left(\frac{Q}{3N'}\right) \right] \quad (3-15)$$

$$E_1(X) = -\gamma - \ln X + \sum_{n=1}^{\infty} \frac{(-1)^n X^n}{n!n} \quad (3-16)$$

= Exponential Integral

γ = Euler's Constant

= .5772

A comparison between the loading dependence obtained by the above equation and computer calculations for the standard cylindrical cavity, is shown in Figure 3-20. As the figure shows, a good agreement exists between the two types of calculation procedures.

The final choice of method to calculate N will depend on comparisons between the two methods and experimental results.

The techniques developed here are powerful tools, in that they give a means of establishing the system operating parameters, frequency band and system sensitivity. Both of these parameters are directly related to the system "Q", which can be experimentally measured or mathematically calculated.

A complete set of statistical data for the Phase A THERMO tank partially filled with LN_2 can be found in Appendix D.

SECTION IV

EXPERIMENTAL STUDIES

4.1 Introduction

In order to verify the theoretical predictions made and to prove the feasibility of a Zero "G" mass gaging system, a number of experiments were conducted on scale model spacecraft type tanks. The scale model tanks were tested with simulated fuels (Benzene and LN_2) as well as an actual fuel (LH_2). The simulated fuels were selected for their similarity to the actual fuel's electrical properties and for handling ease.

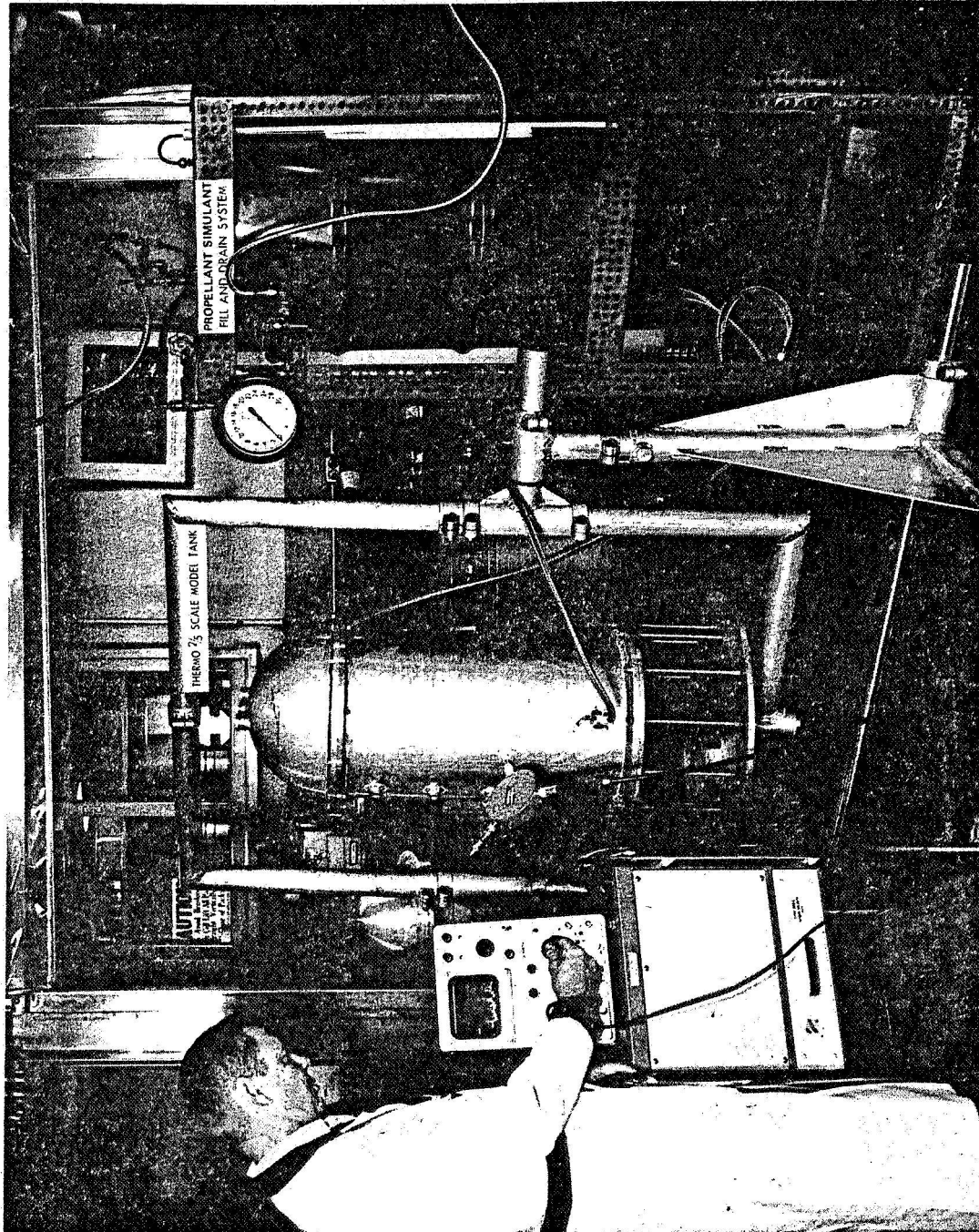
Simulation of the expected propellant configuration under low gravity conditions was performed by reorientation of the tank for a number of constant loadings. A vertical loading response was chosen as a basis to compare experimental results to theoretical predictions, since the loading response was theoretically analyzed in this orientation.

The objectives of the experimental work were:

- a) to verify the prediction that the resonant count remains invariant with redistribution of the dielectric content.
- b) to correlate theoretical predictions of loading dependence with experimental results.
- c) to evaluate the RF gaging system under operating conditions that could not be determined theoretically; that is, static loading, incremental positioning, slosh and flow tests.
- d) to specify system design parameters that could only be determined experimentally.

The brunt of the experimental work was performed on two laboratory type tanks. Both tanks were constructed of aluminum and were designed to incorporate the utilization of an automatic fill and drain system. Physical design size of the tanks was limited by handling facilities (considering tank weight when filled with simulated propellants) however, the tank volume was made as large as possible in order to use a lower frequency bandwidth.

An aluminum, cylindrical tank with flat ends (18 in. diameter by 22.312 in. height) was fabricated in order to provide a laboratory standard cavity that could be used to directly verify the theoretical analysis performed. This laboratory standard was used to make basic measurements and was always retained in its standard form for purposes of performance confirmation and data repetition.



THERMO 2/5 SCALE MODEL TANK

Figure 4-1

A second multi-purpose aluminum tank was constructed that could be used for a number of various tank geometries. The various sections of the tank could be recombined so that the following basic tank shapes could be studied:

- a) cylindrical tank with flat ends
- b) spherical tank
- c) cylindrical tank with one external hemisphere
- d) cylindrical tank with two external hemispheres
- e) cylindrical tank with one internal hemisphere
- f) two-fifths scale THERMO tank complete with internal perturbations

Figure 4-1 shows the multi-purpose tank assembled to the basic THERMO configuration. All the internal perturbations are removable and bosses are provided for the addition of other perturbations not distinct to the THERMO tank. See Figure 4-2.

Both tanks were designed to incorporate the utilization of an automatic fill and drain system suitable for use with the storable simulant (Benzene). The automatic fill and drain system consisted of a drum reservoir with suitable valving for draining and filling the test tanks under pressure. A sight glass attached to the drum reservoir provided quantity calibration for fractional fillings, "α", in the test tanks.

In order to provide a LH_2 test fixture, the 1/3 scale THERMO tank, constructed for laboratory testing during Phase A of this contract, was selected since its smaller size would provide the least difficulty in terms of the thermodynamics involved in the storage of cryogenic fluids. A cryostat was fabricated to insulate the 1/3 scale THERMO tank. The tank was stripped of all internal and external hardware and a fill tube, vent line and GH_2 external precooling coil were added. See Figure 4-3. The tank was able to retain nitrogen in liquid form but proved to be an inadequate cryogenic test fixture for the storage of LH_2 .

At Bendix expense a simulated spacecraft tank was constructed from a laboratory dewar in order to provide a test tank for LH_2 . Figure 4-4 shows the construction of the 25 liter LH_2 simulated spacecraft tank.

4.2 Standard Cylindrical Cavity Tests

To provide a sound foundation on which to expand the RF gaging concept to complex tank geometries, the initial phase of the experimental program concerned itself with a simple cylindrical tank that could be theoretically analyzed and also the experimental study of the RF properties of the S-IVB tank.

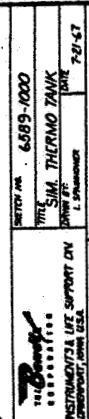


FIGURE 4-2

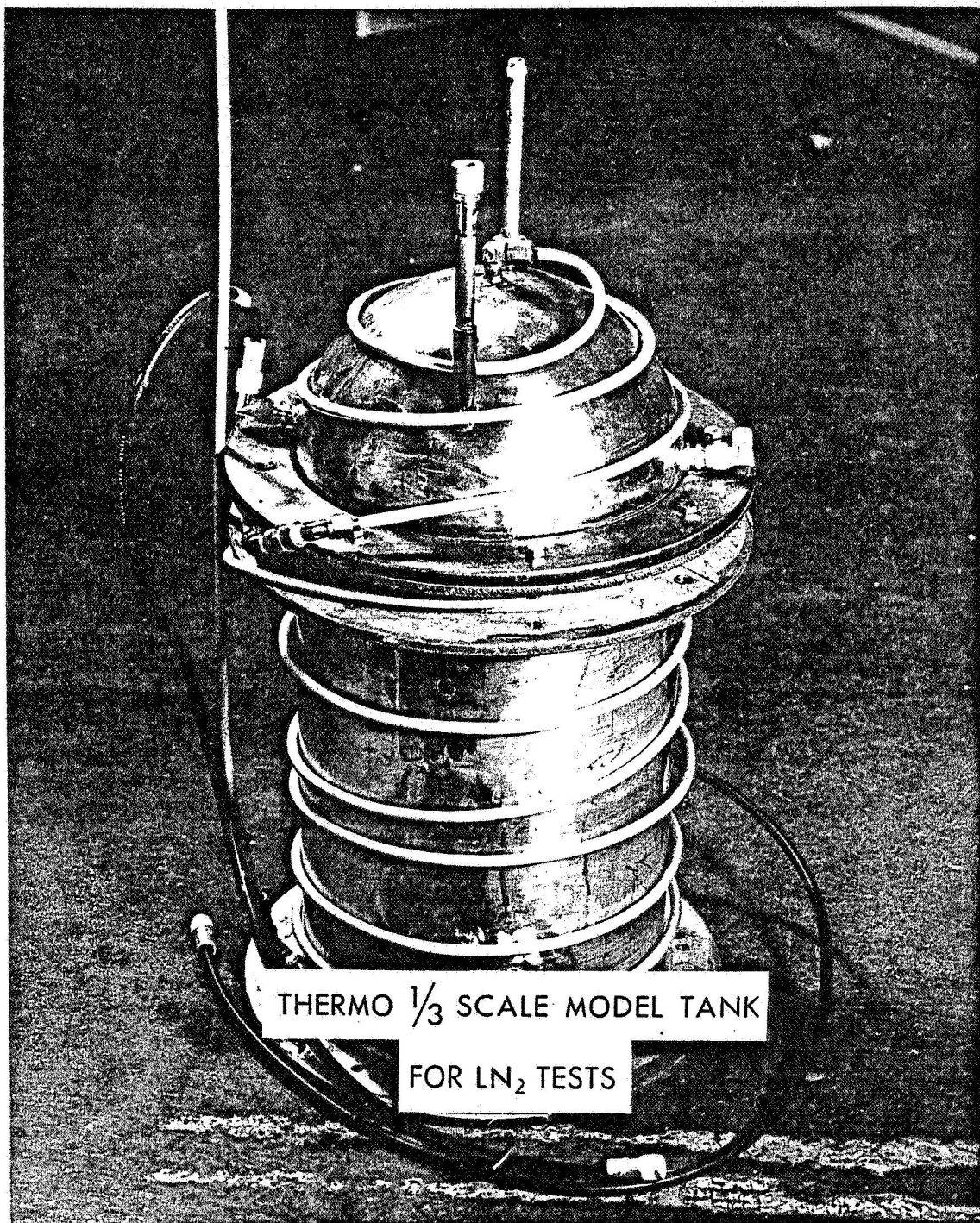
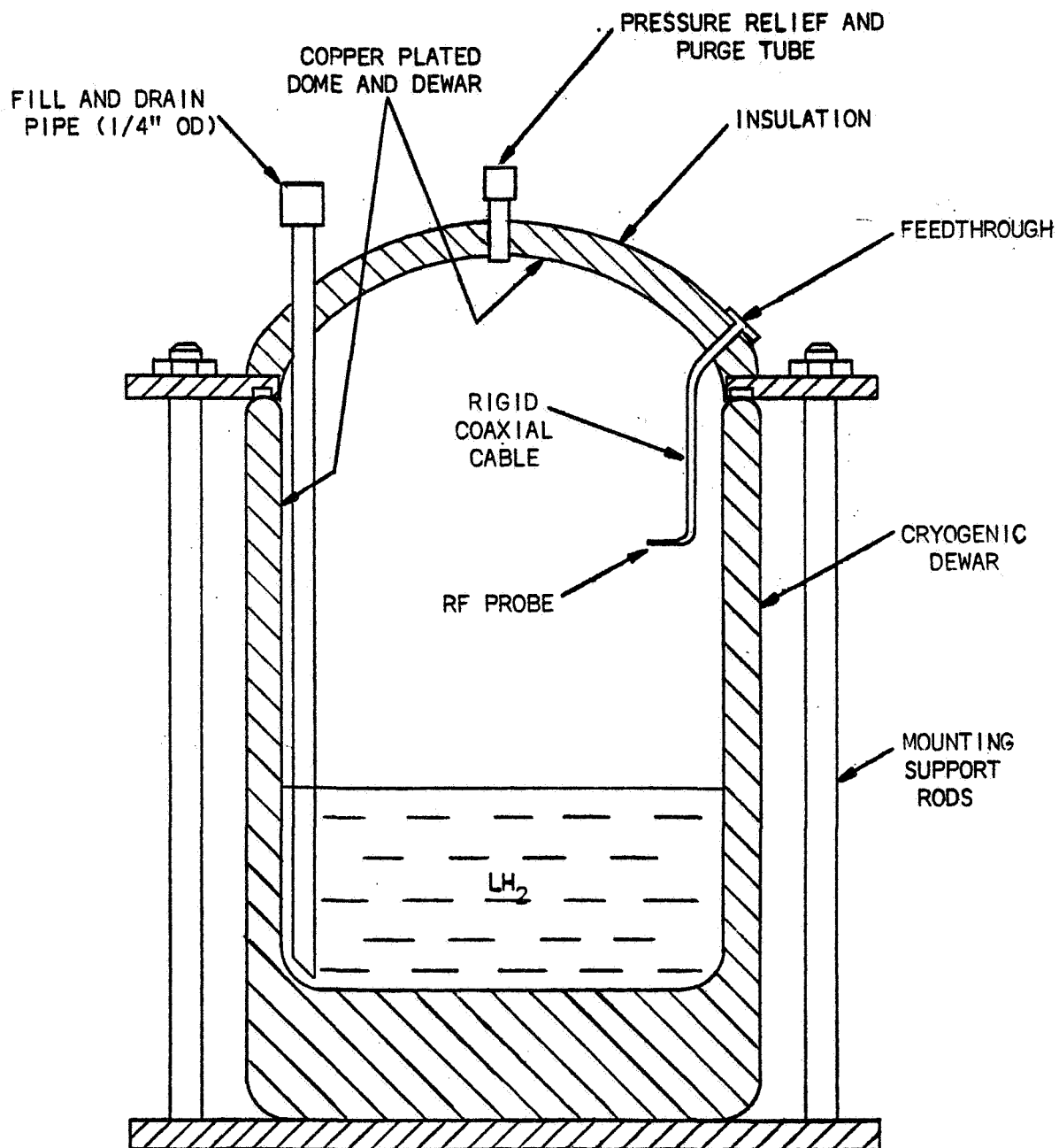


FIGURE 4-3



LH₂ TEST DEWAR

FIGURE 4-4

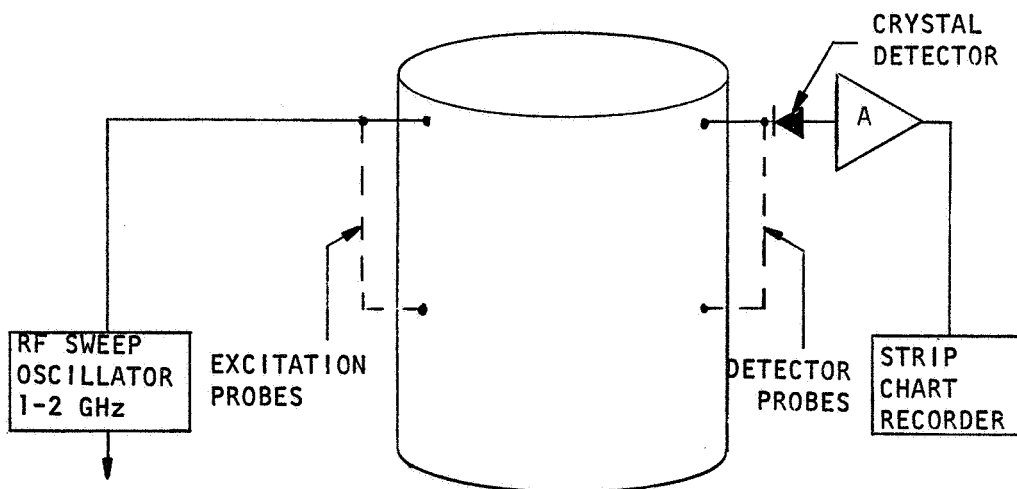
An exact computer solution of the resonant frequencies was obtained for the standard cylindrical tank and experiments were initiated to answer the following basic questions:

- a) Does the experimental number of excitable resonances agree with the theoretical predictions?
- b) Does the experimental resonant distribution agree with the theoretical distribution?
- c) What parameters govern probe coupling into the tank?
- d) What type of probes provide optimum resonant coupling?

The theoretical resonant frequencies were plotted on a length of strip chart paper in ascending frequency order with spacing being proportional to the sweep time required to transverse from the lower frequency bound, f_1 to the upper frequency bound, f_2 . Each resonant mode was identified as being "TE" or "TM", degenerate or nondegenerate.

Prior work accomplished during Phase A had employed a transmission type RF system to obtain a matched tank. A matched tank being defined as a tank whose resonant count is insensitive to dielectric position for any given fractional filling " α ". The transmission type RF system uses one or more excitation probes which insert RF energy into the cavity and one or more detection probes which extract RF energy from the cavity. The initial experiments performed on the standard cylindrical tank utilized the transmission method of RF resonant mode detection using one excitation probe and one detection probe.

Figure 4-5 shows the experimental setups used to verify the theoretical analysis made on the cavity, with various possible positions of excitation and detection probes, though only one was used in experiments, i.e., reflected energy technique.



STANDARD CYLINDRICAL CAVITY

FIGURE 4-5

The prime purpose of the experimental tests was to verify the input prediction of an empty mode count of 190 modes for the cavity when excited in the frequency range of 1-2 GHz.

In the implementation of this task, a number of holes were drilled into the cavity, as shown in Figure 4-6, in order to allow for various combinations of exciter and detector probes. The holes are labeled A through F, and M through R as shown in the figure. Before the location of the coupling system could be chosen, the type of tank coupling had to be determined.

4.2.1 Tank Coupling

The input and output coupling method for a microwave system consists of antennas a few centimeters in length. The antennas may, for coaxial leads, be either electrical field probes in the form of monopoles, or magnetic field probes in the form of loops, or a compound antenna made up of these elements. The criterion for the antenna is that it should couple to all the modes in the cavity, and the "Q" of the whole system should be sufficiently high to allow the output power for each resonance to be detected and distinguished from the neighboring resonances.

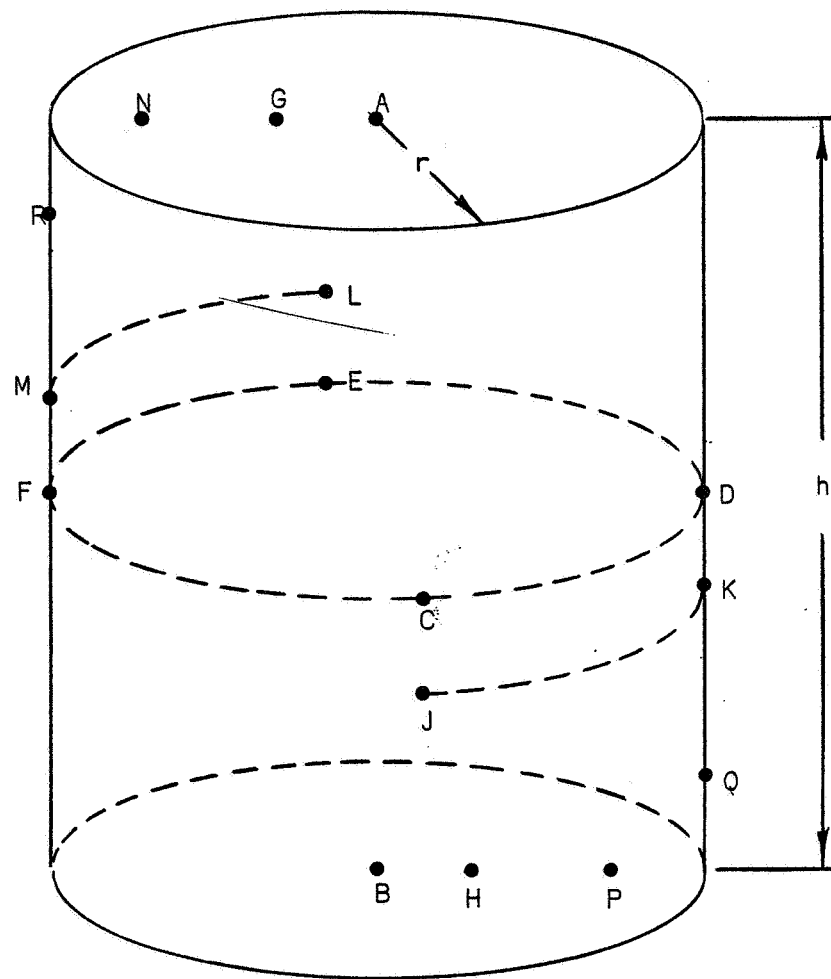
The variation of transmitted power with various coupling systems may be derived from Equation 4-1 with Δf_o made equal to zero.

$$\frac{P_2}{P_o} = \frac{4Q_L^2}{Q_1 Q_2} \left[\frac{1}{1 + \left(\frac{2\Delta f_o Q_L}{f_o} \right)^2} \right] \quad (4-1)$$

where: P_2 = transmitted power
 P_o = incident power
 Q_L = Loaded "Q"
 Q_1 = input port coupling "Q"
 Q_2 = output port coupling "Q"
 f_o = resonant frequency

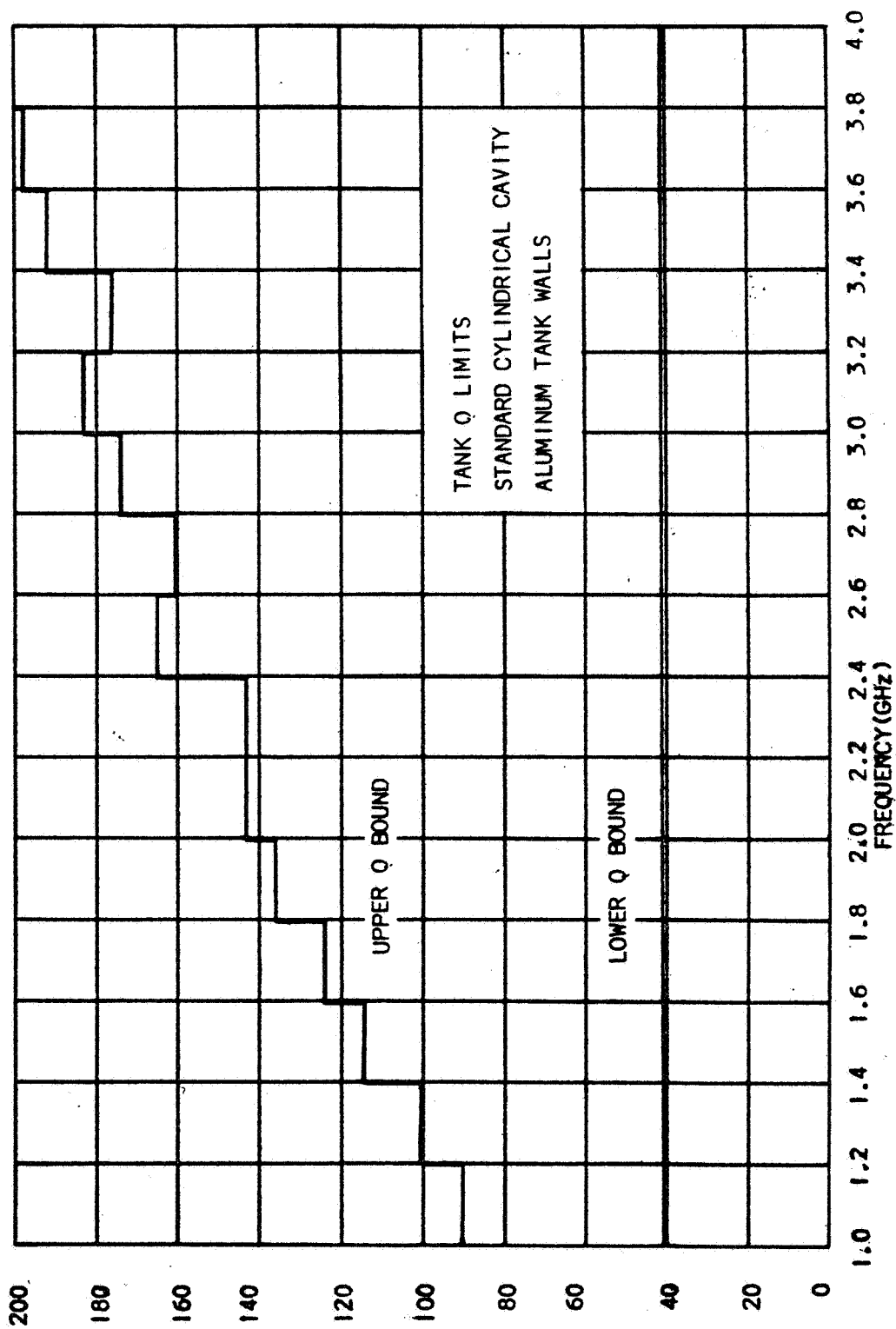
At resonance we have:

$$\frac{P_2}{P_o} = \frac{4Q_L^2}{Q_1 Q_2} \quad (4-2)$$



CAVITY SHOWING LOCATION OF ANTENNA HOLES

FIGURE 4-6



(0001) 0 030V07NU

FIGURE 4-7

This shows that for a given loaded "Q", maximum transmission occurs when $Q_1 = Q_2$. Also maximum possible transmission occurs when Q_1 and Q_2 are as small as possible, meaning that the probes should be as lightly coupled to the cavity as possible.

The general coupling "Q" is a function of the electric field within the cavity at the position of the probe, in the form:

$$Q \propto \frac{1}{|E|^2} \quad (4-3)$$

Consequently, at the point of low electric field, the coupling "Q" will be very high, and the transmitted power will be very low. Since all the resonances will have different values of electric field at a given probe position, the value of E is likely to vary from one resonance to the next. Thus, the coupling "Q" and the transmitted power will vary widely.

The theoretical unloaded "Q's" of the resonances in the standard cavity were calculated and are shown in Figure 4-7 for the empty cavity excited in the frequency range of 1-4 GHz. Although the unloaded "Q" was high, 40,000 or greater, measurements of Q_L ranged from 5000 to 1000 with an average Q_L of approximately 2000 to 3000 with a monopole antenna system.

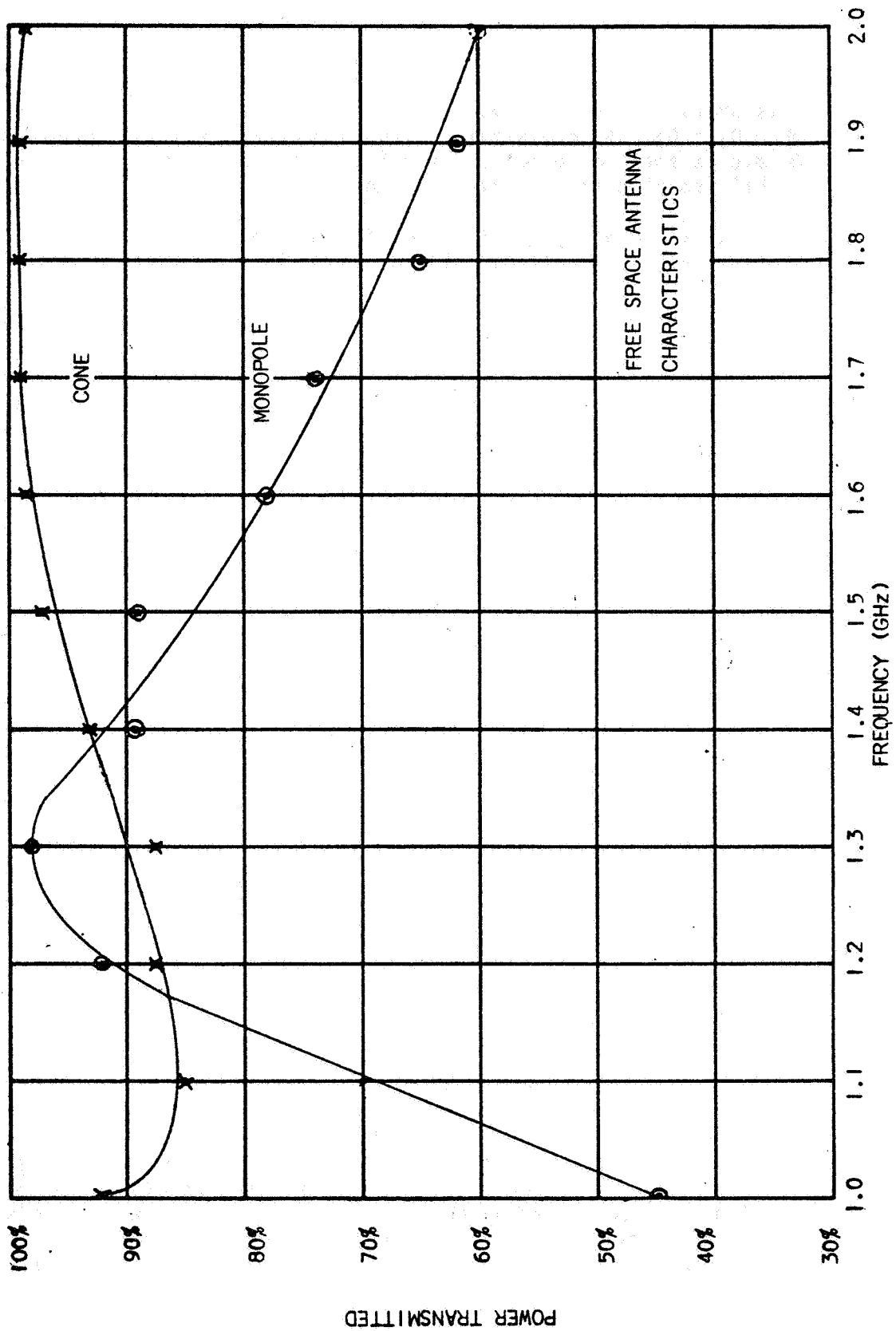
The antenna system used in coupling to the tank is instrumental in its effect on the system "Q" or loaded "Q"; therefore, care must be exercised in the selection of the antenna system that is used.

4.2.2 Antenna Systems

Antenna systems may be considered as either narrow band or broad band systems. The narrow band antennas are resonant antennas such as simple monopoles or loops. Monopoles were chosen for experimental work because; 1) they facilitate experimentation, and 2) the loop does not have such a great advantage over the monopole for wide band applications.

4.2.2.1 A Narrow Band Antenna

A monopole antenna radiates best into free space at a frequency for which the length of the monopole is approximately one quarter wavelength. For frequencies remote from this resonant frequency, the antenna is a poor radiator. For a resonant antenna radiating into a cavity which has dimensions larger than the wavelength of operation, the same property may be approximately true. For example, a frequency of 1.5 GHz had a wavelength of 20 cm. A monopole radiator for this frequency is thus approximately 5 centimeters long. The standard cylindrical cavity dimensions are 55 cm long by 46 cm in diameter. Thus, it may be argued that the antenna properties will be roughly similar to operation in free space. A monopole antenna slight longer than 5 cm was constructed. The reflected power from the antenna



POWER TRANSMITTED

FIGURE 4-8

was measured in order to determine the amount of power radiated into free space across the frequency band. A plot of transmitted power versus frequency is shown in Figure 4-8. It is noted that the monopole transmits twice as much power at a frequency of 1.3 GHz, than at the ends of the band. Consequently, a cavity coupling system employing transmitting and receiving monopoles of equal lengths may be capable of transmitting four times as much power at the middle of the band as compared to the power transmitted at the ends of the band. Using monopoles of suitable unequal lengths will make the transmission out of the cavity more level across the band, but even then it may be expected that more than half the power from the generator will be reflected back from the cavity.

4.2.2.2 A Broad Band Antenna

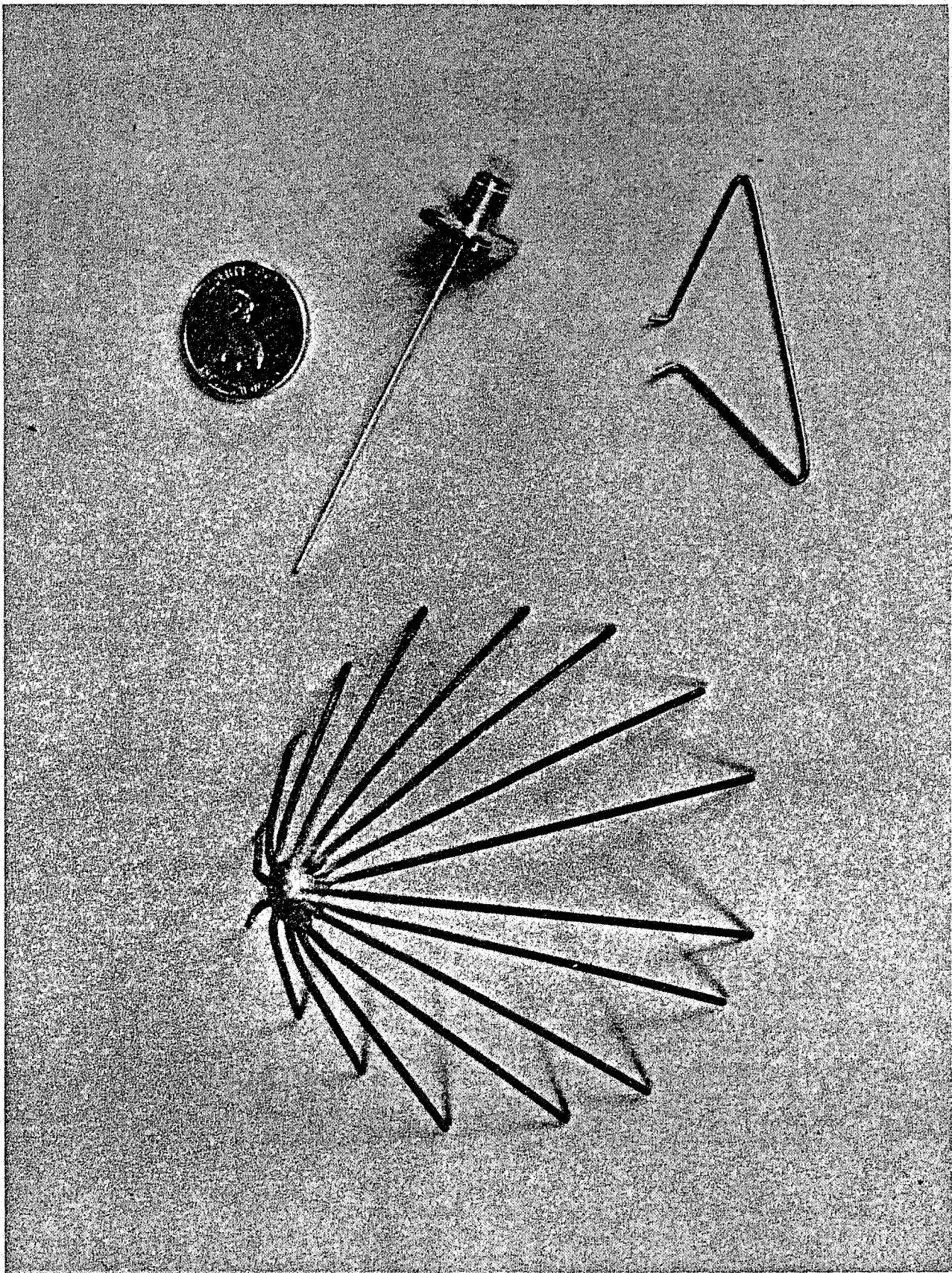
The monopole is a poor radiator over a wide frequency band because it is a resonant circuit element. The simplest form of broad band antennas is the metal cone. To investigate the properties of the cone antenna, some 20 cones were fabricated in order to find the best design for radiation into free space in the 1-2 GHz region. The best cone design was found to be approximately a 60° angle and 3 inches in length. By virtue of being a broad band antenna, the size of the cone is not so critical a factor as for the monopole. One of the cones, a sixteen-spoke wire cone, is shown in Figure 4-9, together with a monopole and triangular probe for comparison. The power transmission properties of the cone in free space are shown in Figure 4-8. It is noted that the cone is capable of transmitting over 85% of the incident power across the frequency band. The properties of both the cone and the monopole were measured using standard standing wave measurements. A Smith chart impedance plot for the cone is shown in Figure 4-10.

To test the relative performance of the monopole and cone antennas, the antennas were located in each of the holes drilled into the standard cavity and comparisons were made of the strip chart recordings with regard to mode detectability and mode number.

4.2.3 Comparison of the Monopole and Cone Antennas in a Resonant Cavity

Various combinations of monopoles and cones were inserted into the cavity and the transmitted energy was recorded for each location. Two phenomena were immediately apparent: 1) when the cavity was "overcoupled" the resonant pattern tended to merge and identification of the individual resonances with the theoretical analysis was impossible, and 2) when the cavity was "undercoupled" the individual resonances were distinguishable but the amplitude of the transmitted power was low.

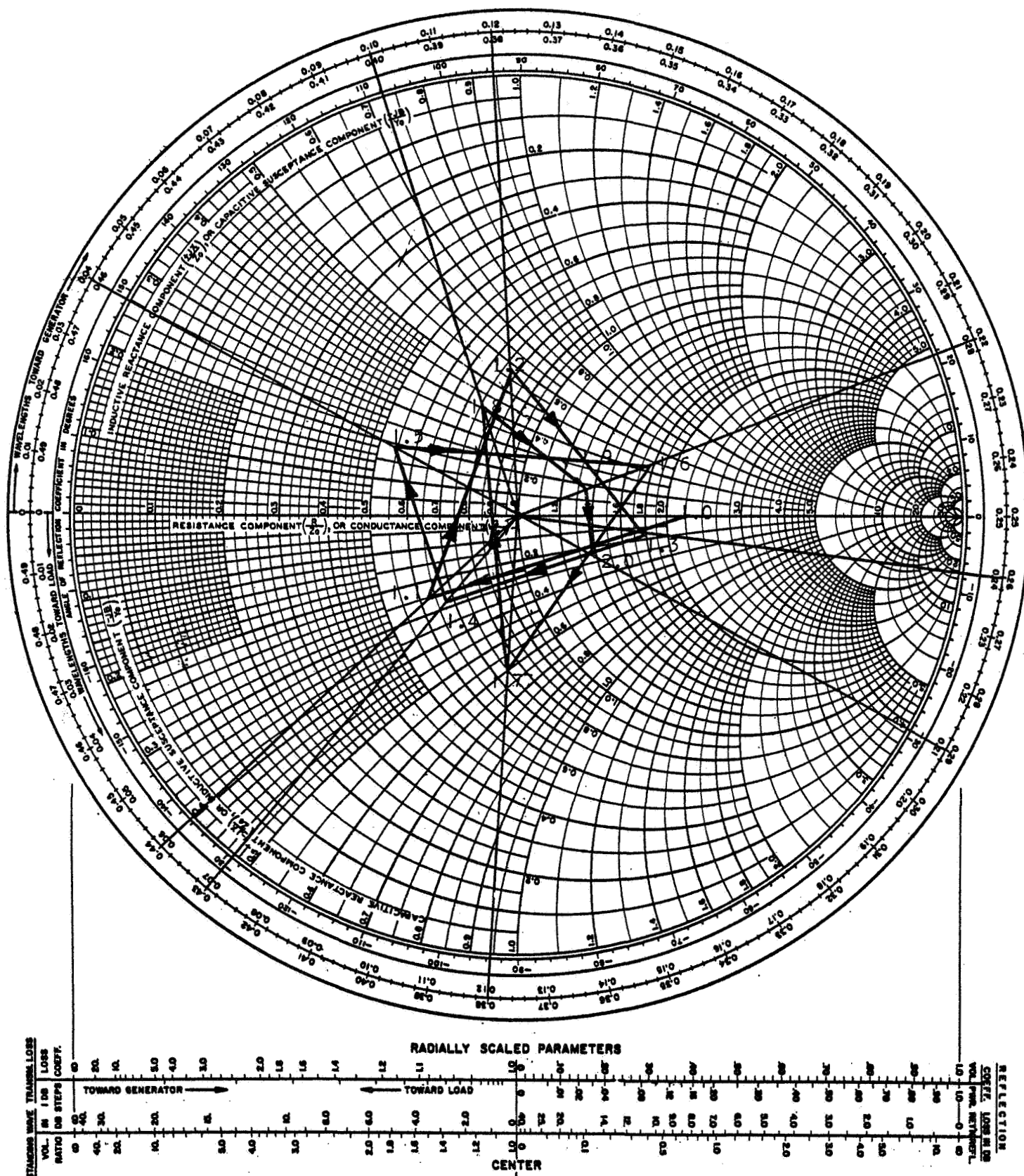
Experiments confirming the merits of cones and monopoles showed that the cone was capable of transmitting much more power through the cavity than the monopole. Consequently, the monopoles led to a much cleaner picture of the modes across the band, but many of the



BROAD AND NARROW-BAND ANTENNAS

FIGURE 4-9

IMPEDANCE OR ADMITTANCE COORDINATES



IMPEDANCE CHARACTERISTICS OF CONE ANTENNA

FIGURE 4-10

resonances could not be detected because they were of such small amplitude. The cone, on the other hand, transmitted much more power, and more resonances could be seen, but there was much difficulty in distinguishing the individual resonances from each other.

Since a direct correlation between the theoretical analysis and the experimental work was desired, it was decided to determine the best length of monopole which gave the clearest response as far as individual resonances were concerned. In this manner individual resonances could be identified.

4.2.4 Optimum Resonant Coupling With Small Monopoles

With monopoles in the various hole locations marked A through F in Figure 4-6, the transmitted power was recorded on a strip chart recorder. The length of the monopoles was then reduced and the recordings were repeated. It was decided from the recordings that the monopoles giving the best response, as far as mode clarity was concerned, were about 3/8" long for a frequency range of 1-2 GHz. These produced only a small amount of resonance merging at the high end of the frequency band. With this length of monopole, it was found that only about half of the resonances in the cavity could be detected, since the coupling was so small. Other holes were then drilled in the cavity at locations G through M in Figure 4-6. These holes were spaced 2 inches from the original holes. Holes G and H formed a plane with the holes A and B and were on opposite sides of the line AB. Holes J and K were vertically below holes C and D respectively, while holes L and M were vertically above holes E and F respectively. With probes in several of these positions another 25% of the resonances could be coupled. At this point, theoretical probes should not be placed at positions of symmetry in the cavity. Consequently, the holes A through F were not used again. Four other holes were drilled in the cavity at positions indicated by theory for coupling to the maximum number of resonances. These are labeled N through R in Figure 4-6.

Holes N and R are four centimeters from their common edge and holes P and Q are four centimeters from their common edge. Coupling via these positions in fact did not produce an appreciable increase in the number of resonances. Finally in an attempt to produce as many resonances as possible, all 10 probes were tied together, four to radiate power into the cavity, and six to receive power from the cavity. By this method 90% of the resonances were coupled and were identifiable with the computer program. Table 3-6 shows the experimental results compared to the theoretical solution of the resonances.

The conclusions derived from the work performed on the standard cylindrical cavity can be summarized as follows:

- a) 90% of the tank empty count can be obtained through the use of both multiple antenna systems (undercoupled) as well as single antenna systems (overcoupled).
- b) In an overcoupled antenna system, identification of individual resonances is impossible. A maximum resonant count can be more easily attained using an overcoupled system but at a sacrifice of lowering the system "Q".
- c) In an undercoupled antenna system, identification of individual resonances can be made. A maximum resonant count can only be achieved through the use of a multiple antenna system. Although the system "Q" is high, the relative resonance amplitudes are small and system sensitivity or resonant detectability suffers. Maximum resonant count can only be achieved through use of multiple antenna system when an under coupled antenna system is used.
- d) A monopole antenna provides the best response with respect to resonant "Q" and resonant amplitude. The optimum length of a monopole is a quarter wavelength at the mid-point of the operating frequency band. There is no optimum number of antennas in the transmission mode of detection; since it is not the ideal mode of coupling into the cavity.
- e) The experimental resonance distribution per unit bandwidth is in agreement with the predicted distribution.

With the establishment of these basic premises, an experimental study was made of the S-IVB tank which was matched during Phase A of this contract. This study was made in order to test the validity of the conclusions; and to isolate any other phenomenon a matched tank exhibited.

4.3 S-IVB Matched Tank Study

The purpose of the S-IVB matched tank study was to isolate the parameters that provide a matched tank condition. The 1/20 scale model S-IVB tank was excited in the frequency band of 2-4 GHz and its static loading response was determined for fractional fillings with Benzene (dielectric constant = 2.28). Figure 4-11 shows the static response and Table 4-1 shows the deviation in resonant count, for a static orientation test. The resonance distribution for the tank follows a square law response. These results agree with the results obtained during Phase A. The system or loaded "Q" was measured for a number of resonances with the average system "Q" being approximately 1000 to 2500. Since the original antennas that were used during Phase A were retained in the tank for this study, it would be of interest to compare their lengths to the antennas used in the standard cylindrical cavity. A transmitted energy system was used and the antennas were located on the tank as shown in Figure 4-12.

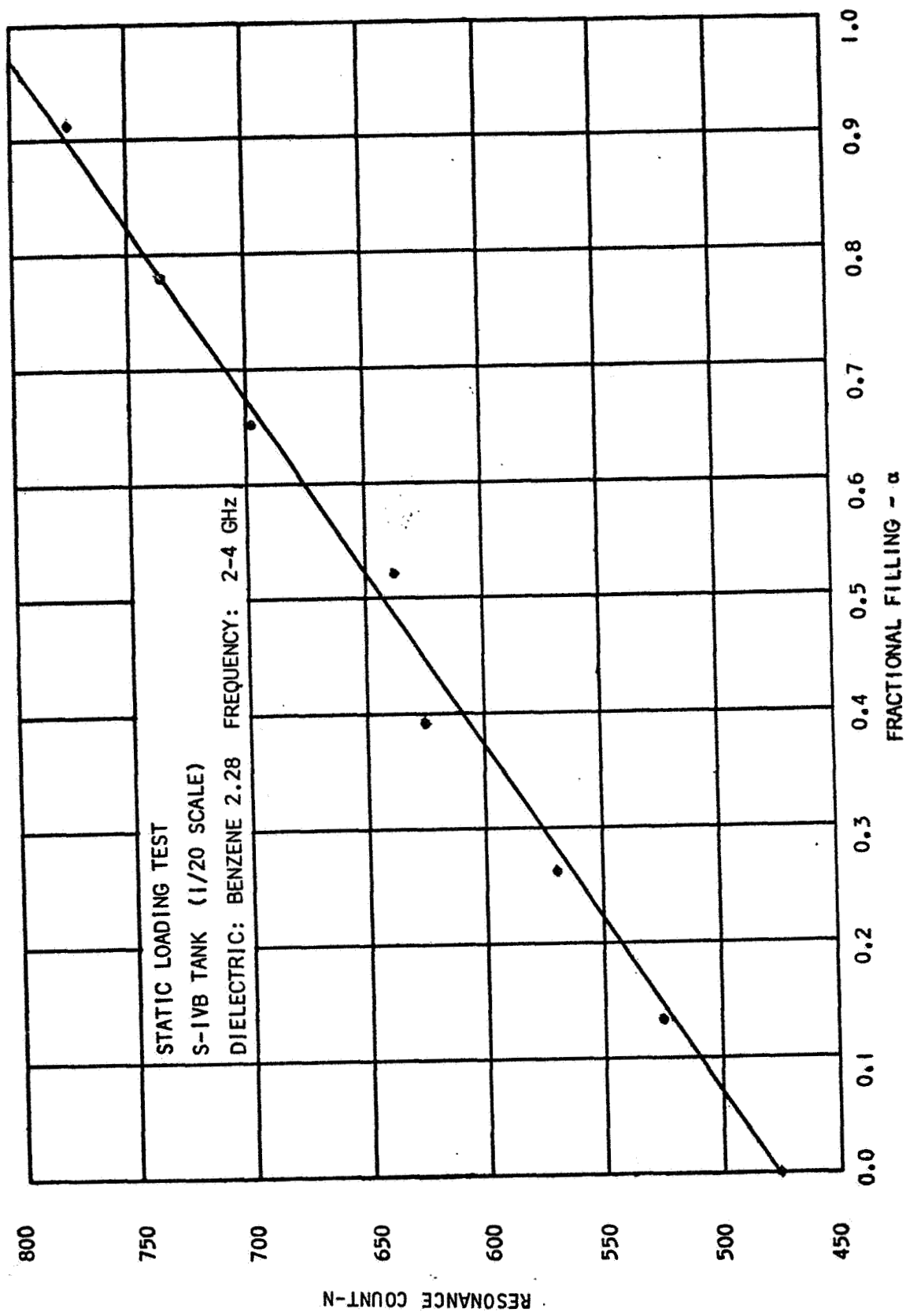


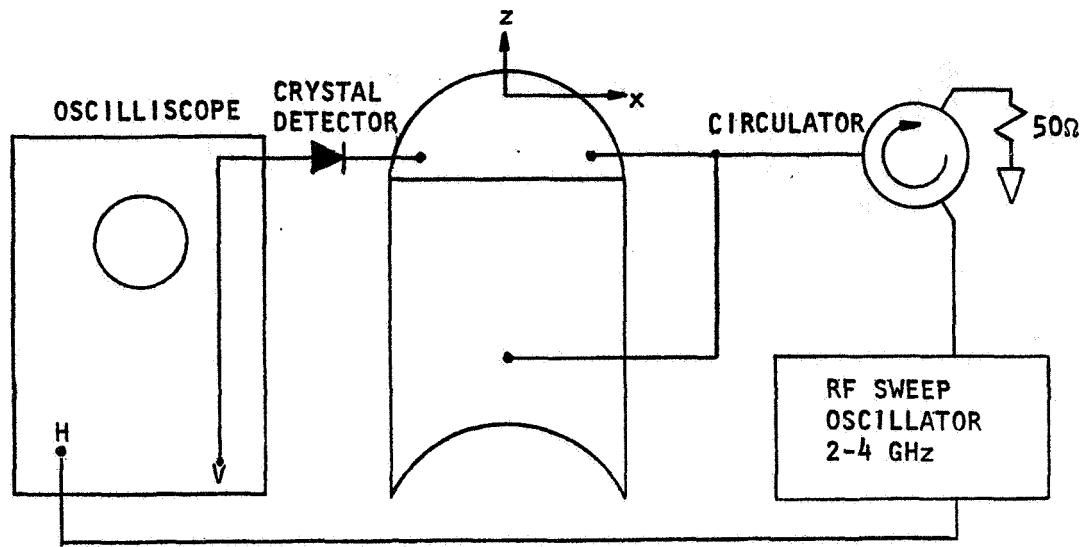
FIGURE 4-11

TABLE 4-1

STATIC ORIENTATION TEST - S-IVB (1/20 SCALE)

TANK POSITION	FREQUENCY (GHz)												TOTAL RESONANCE COUNT
	2.0	2.2	2.4	2.6	2.8	3.0	3.2	3.4	3.6	3.8	4.0		
0° VERTICAL		46	47	46	54	52	63	66	61	71	80		586
10°		45	42	47	53	53	66	69	68	76	68		587
20°		36	46	46	51	58	62	62	69	78	81		588
30°		43	40	47	57	55	68	68	66	71	73		588
40°		36	47	51	52	51	60	70	69	74	76		586
50°		44	47	48	52	57	62	67	66	73	68		584
60°		43	46	47	53	54	68	62	68	81	66		588
70°		40	39	47	55	56	60	67	70	77	78		589
80°		47	41	49	50	55	58	63	66	75	80		584
90° HORIZONTAL		37	43	51	52	57	57	66	70	71	82		586

DIELECTRIC: BENZENE 2.28



ANTENNA POSITION 1/20 SCALE S-IVB TANK

FIGURE 4-12

The RF probes are located as follows:

Dome input probe - along "z" axis	length = 2.5 cm
Side input probe - along "y" axis	length = 2.0 cm
Dome output probe - along "-z" axis	length = 2.1 cm

All of the above antenna lengths are in good agreement with the $1/4$ wavelength supposition determined on the cylindrical cavity.

The following conclusions can be made from the S-IVB matched tank study:

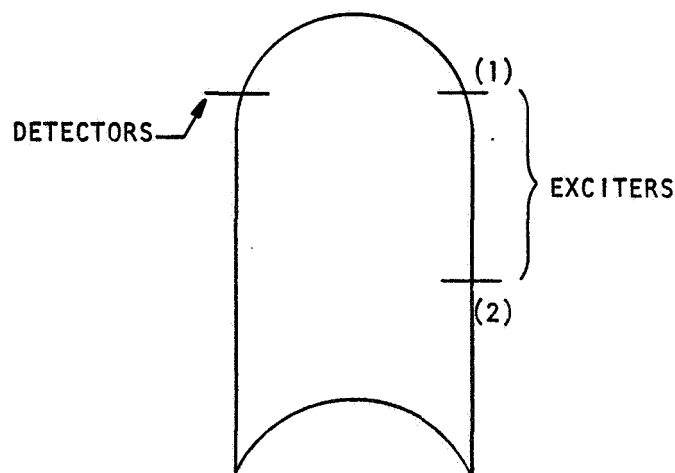
- The empty resonant count represented 90% of the maximum number of resonances that are the theoretical excitable.
- The antennas lengths used were $1/4$ wavelength of the center frequency (3 GHz). The location of the antennas at the cylindrical section boundaries is in good agreement with the theoretical analysis made in Section III, Paragraph 3.5.
- The experimental resonance distribution follows a $2f$ law distribution.
- The external "Q" has the largest effect on reducing the system "Q", since the external "Q" refers to "Q" of cables, tank and propellant.

Since these parameters were in accord with the results obtained on the standard cylindrical cavity, it was felt that these parameters completely specified a matched tank condition. Consequently, work was started on

the 2/5 scale THERMO tank using Benzene as a simulated propellant. The probe configuration and frequency range used on the 1/20 scale S-IVB tank were retained as being a key to the matched condition.

4.4 THERMO Tank Tests (2/5 Scale Model)

The 2/5 scale THERMO Tank was assembled from the multi-purpose tank minus all internal perturbations. Antennas were located at positions equivalent to the antenna positions on the S-IVB 1/20 scale tank. In order to find an optimum antenna length with respect to maximizing the empty resonant count, three (3) antennas were mounted on the tank. The antennas were mounted on the tank as shown in Figure 4-13 with the bottom exciter being positioned on a plane 90° to the top exciter.



ANTENNA POSITION 2/5 SCALE THERMO TANK

FIGURE 4-13

Each antenna was varied in length, in turn, while the others were kept constant until a maximum resonant count was obtained in an empty tank over the frequency range of 2-4 GHz.

Extracting from the experimental data shown in Figure 4-14 the optimum length of the antennas is determined as:

Exciter 1 = 0.984 inches/2.5 cm

Exciter 2 = 0.794 inches/2.02 cm

Detector = 0.827 inches/2.1 cm

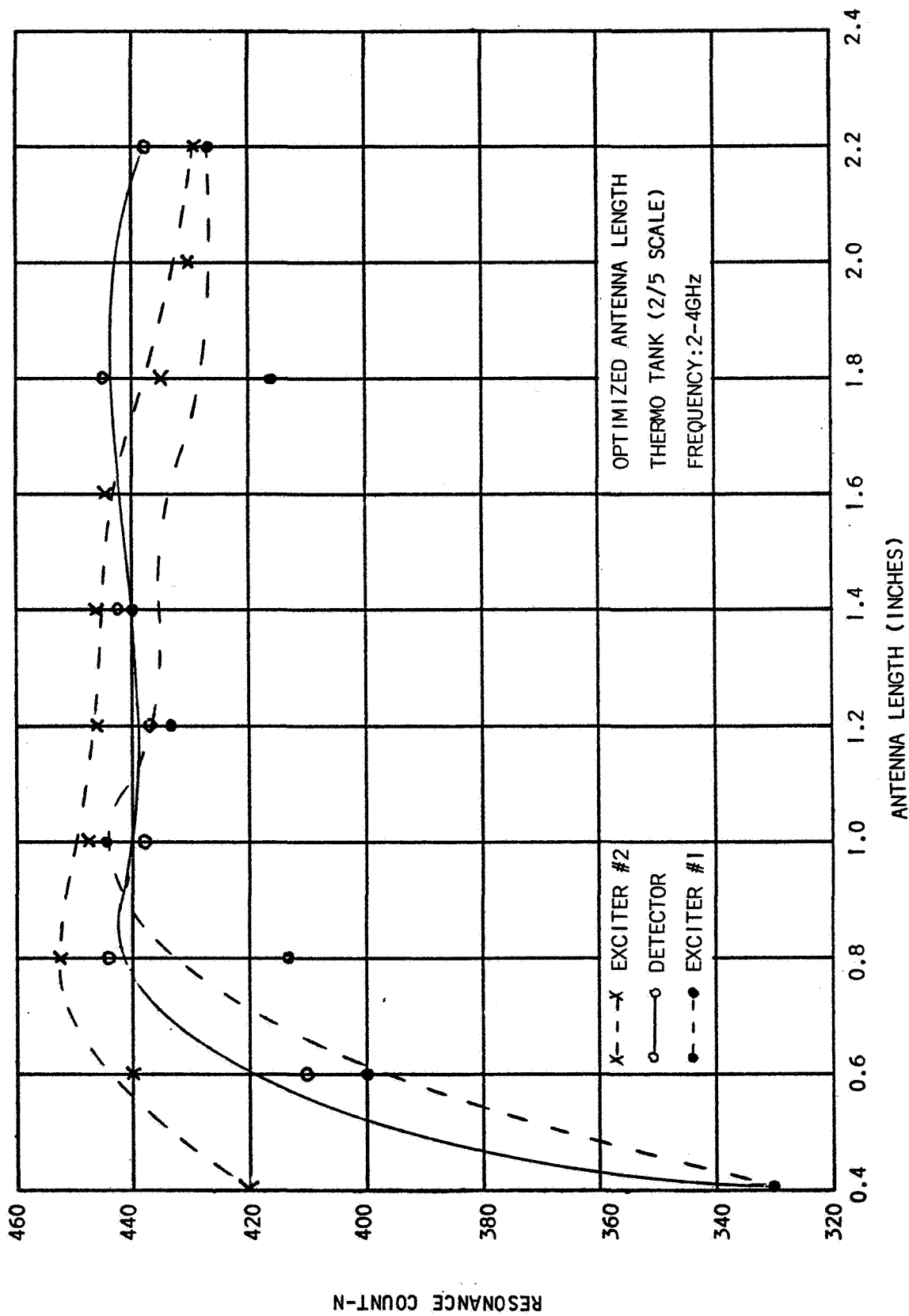


FIGURE 4-14

The antenna lengths are identical to the S-IVB antenna lengths. This suggests that the antenna length is strictly a function of operating frequency band and is independent of tank geometry.

These antenna lengths gave a maximum resonant count over a frequency range of 2-4 GHz. The maximum resonant count under these conditions for an empty tank was 439, and with a fractional filling of 1.0 (full), was 770. In comparison with a theoretical count for an empty tank (exclusive of all perturbations), the resonant count obtained represented approximately 35% of the theoretical empty count.

The full tank resonant count obtained represented 16% of the theoretical tank resonant count.

The optimum antenna length having been evaluated, a loading test was conducted with the tank in two different orientations, i.e., horizontal and vertical.

It was found that the presence of liquid near the antenna distorted the resonant count. Thus, a different reading was obtained depending on whether the antenna was above or below the liquid level. This is shown in Figure 4-15. The antennas were covered with a Teflon probe guard and the experiment repeated. The results shown in Figure 4-16 signify that the Teflon guard rectified this error, and the liquid level with respect to antenna position had no effect. However, the resonant count for the different orientations exhibited wide deviations which is indicative of an unmatched tank.

In a symmetrical tank, the theoretical studies showed that certain degeneracies occur over the frequency band; i.e., resonances overlap at certain discrete frequencies, and these resonances cannot be individually distinguished. It was felt that internal tank perturbations, such as side wall sensors, and other tank perturbations would break up the overlapping resonance, and as a result obtain a higher resonant count.

In an attempt to obtain a higher empty resonant count, the internal perturbations were added to the THERMO tank. Figures 4-17 and 4-18 show that the addition of internal perturbations in all cases causes the resonant count to increase. However, even with the increased resonant count, the tank remained unmatched for static orientations. Various other probe lengths were tried, perturbations were removed; but the tank remained unmatched. An analysis of the situation was made in order to determine what effect the THERMO configuration could have on a matched tank condition.

Experiments conducted with the 2/5 Scale THERMO tank, had a resonant count in an empty tank of approximately 400, and a resonant count in a full tank of approximately 800. In comparison with the theoretical maximum assuming no losses, the count obtained in an empty tank represents 30% and in a full tank, 20% of the theoretical maximum. The theoretical maximum in a full tank was 4,300. This number is far too high for

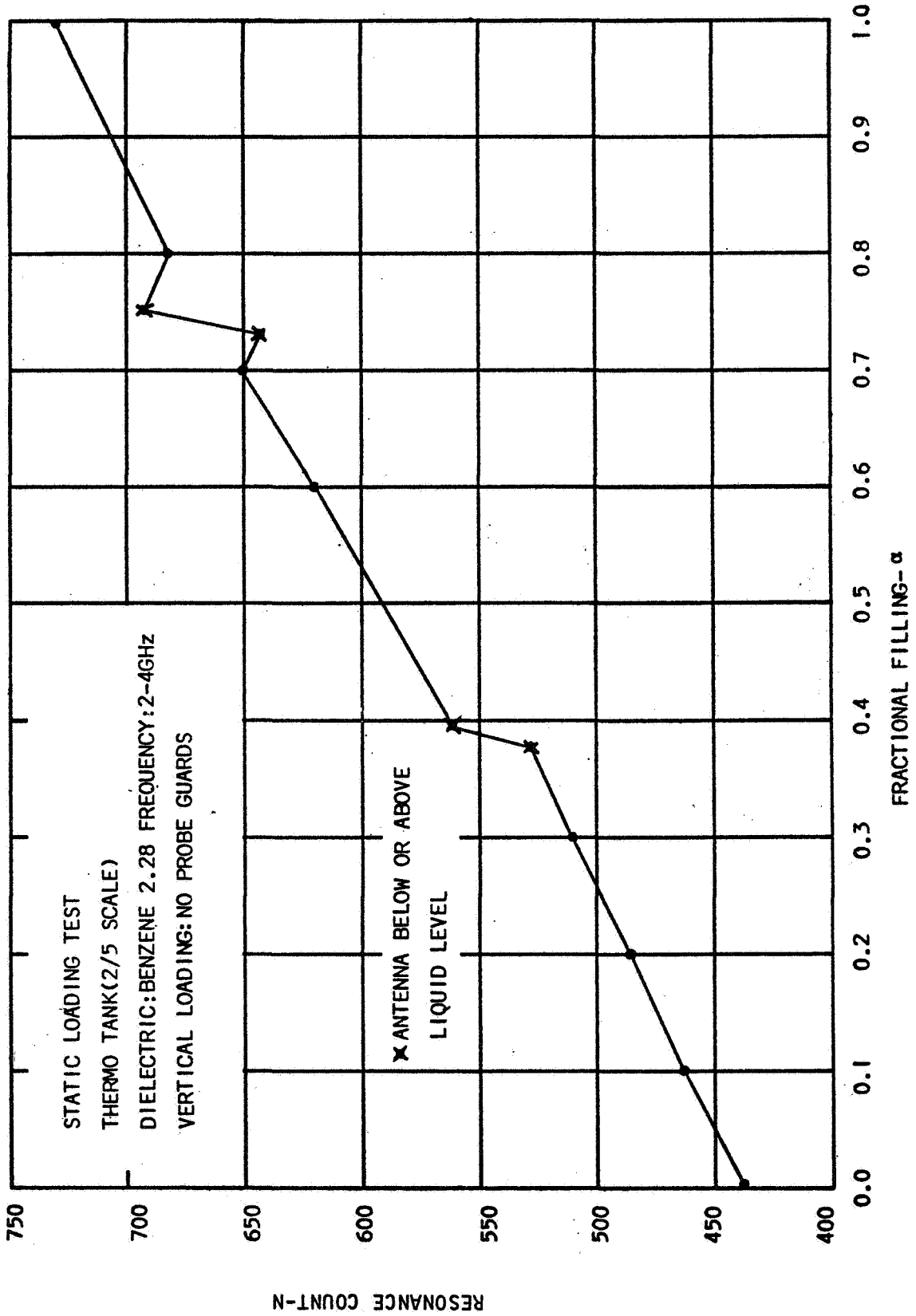


FIGURE 4-15

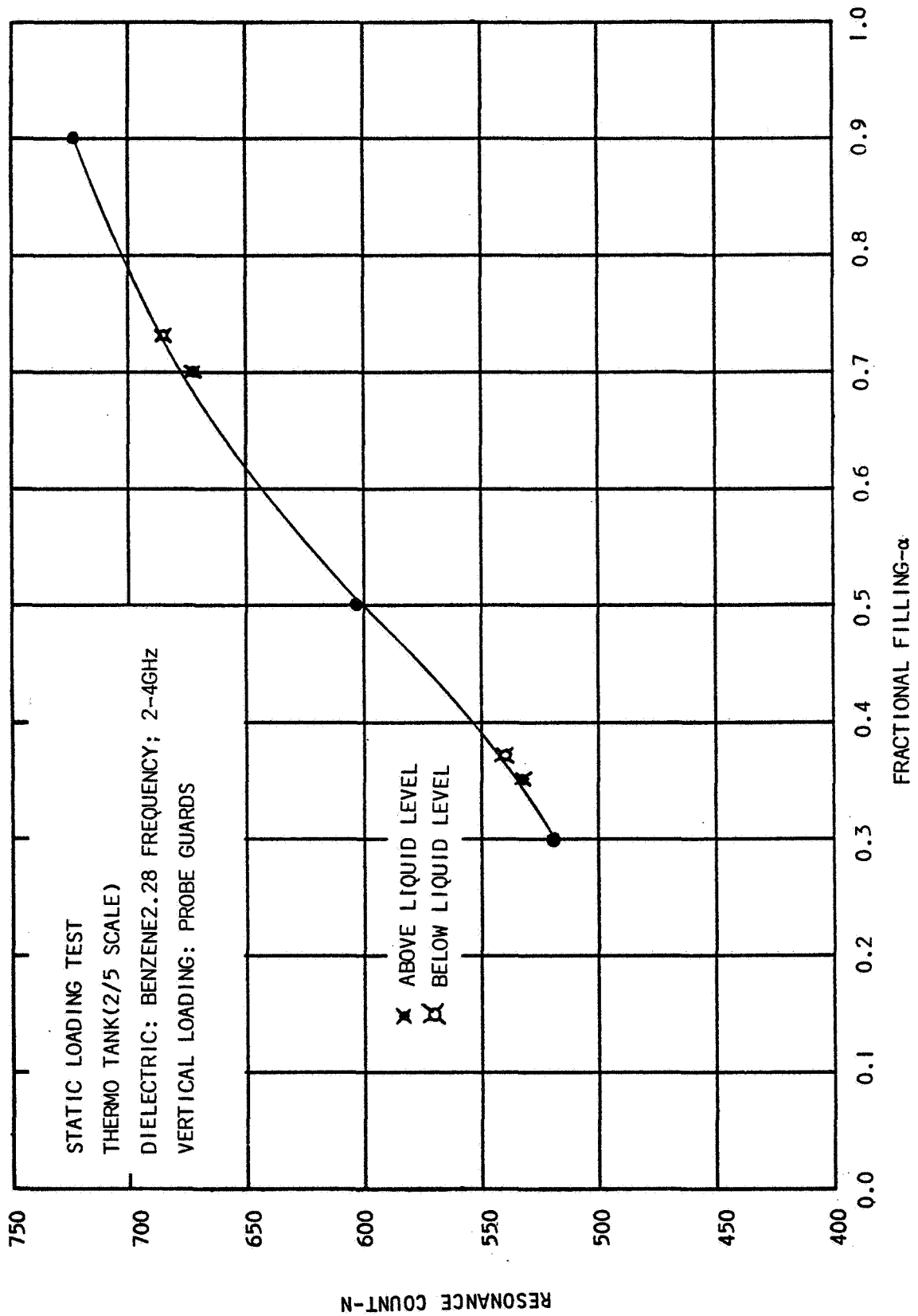


FIGURE 4-16

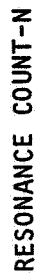


FIGURE 4-17

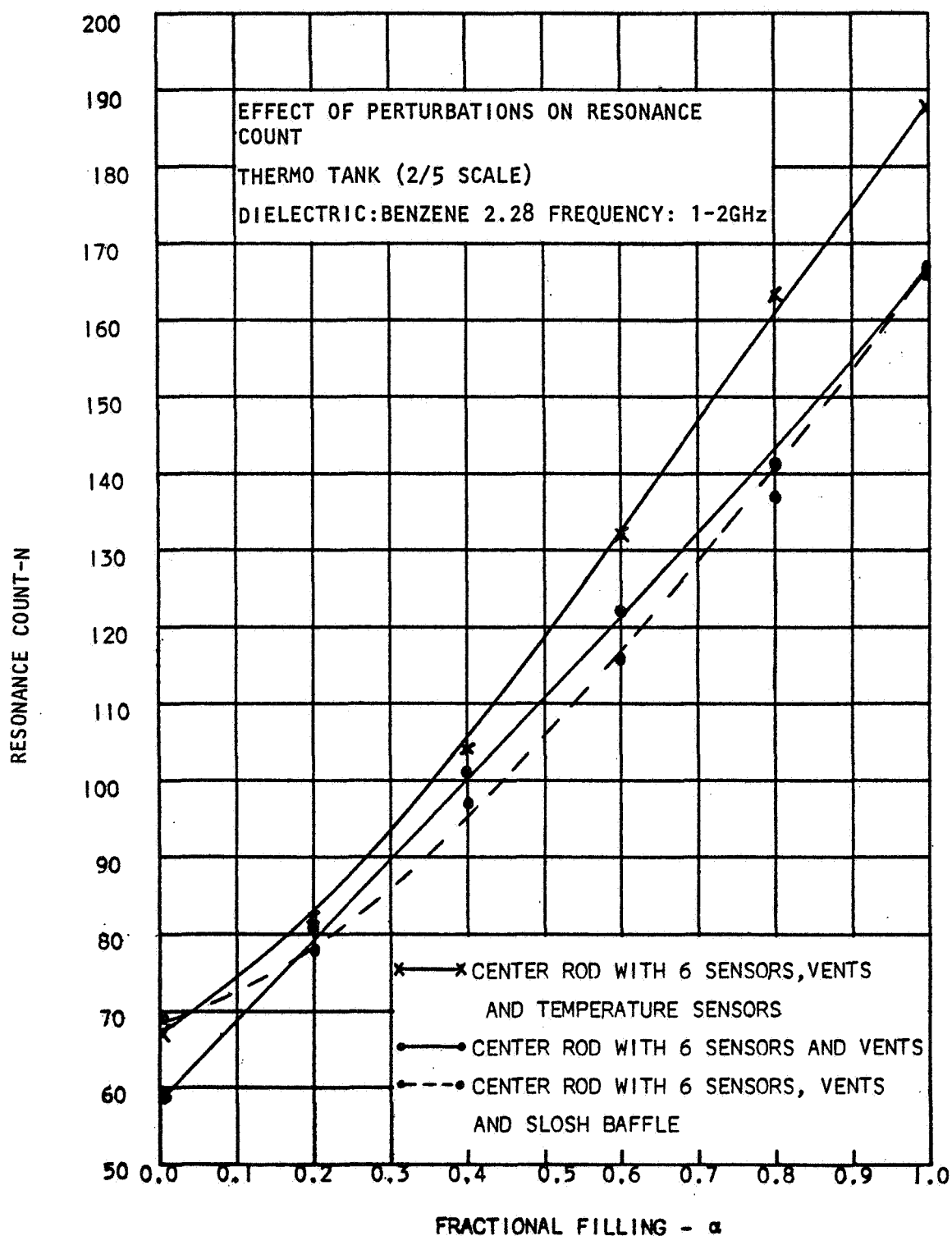


FIGURE 4-18

satisfactory detection, due to merging of resonances. This suggested that the frequency range i.e., 2-4 GHz, was unsatisfactory for operation of this tank. A comparison of the operating frequency band for the 1/20 scale S-IVB to the 1/3 and 2/5 scale THERMO tanks in relationship to the full tank resonant count was made.

Table 4-2 shows the relationship between operating frequency band and resonant count.

TABLE 4-2

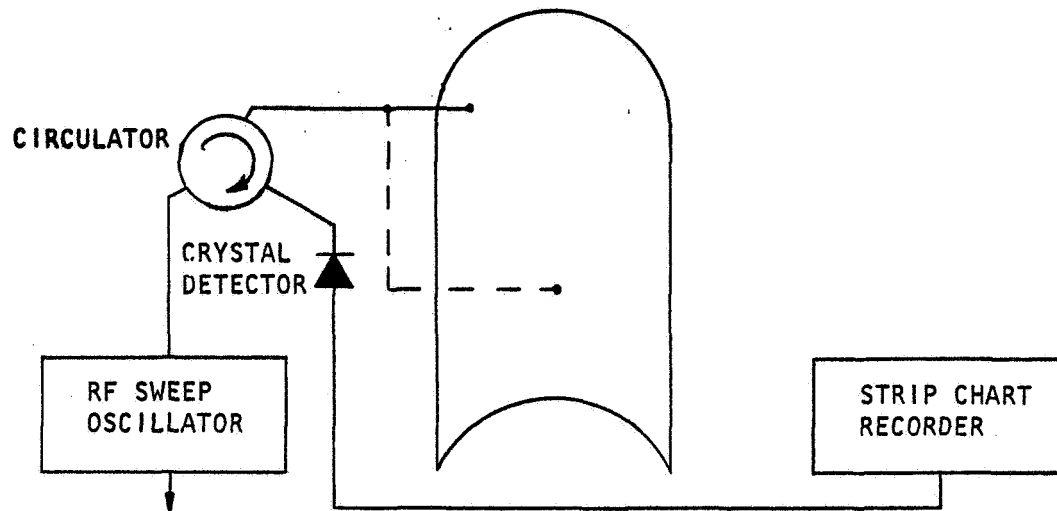
FREQUENCY BAND VERSUS RESONANCE COUNT

TANK	FREQUENCY RANGE (GHz)	RESONANCE COUNT	SPREAD
S-IVB	2-4	1200 Theoretical 800 Experimental	2 Mc/Resonance
1/3 THERMO	2-4	2200 Theoretical 600 Experimental	1 Mc/Resonance
2/5 THERMO	2-4	4300 Theoretical 770 Experimental	0.4 Mc/Resonance

Since the resonance spread was greatest for the S-IVB matched tank, it was decided that the operating frequencies for both the 1/3 scale THERMO tank and the 2/5 scale THERMO tank were too high. A new frequency band for the 2/5 THERMO tank was selected on the basis of 1000 resonances for a full tank. The frequency range was altered to 1-2.4 GHz to produce a full tank mode count of 1000 for more practical detection. A quarter wave length (center frequency 1.7 GHz) was used for the antenna lengths and the resonant count for an empty tank increased to 55% of the theoretical count.

The new operating frequency band of 1-2.4 GHz substantially improved the empty resonant count, but did not achieve a matched tank condition.

The failure of the transmitted energy type of resonance excitation prompted the use of a reflected energy technique. The reflected energy technique utilizes a circulator in order to detect the reflected energy from the tank. The implementation of a reflected energy system is shown in Figure 4-19.



REFLECTED ENERGY SYSTEM

FIGURE 4-19

At resonance the tank absorbs RF energy; therefore, the amount of reflected energy seen by the crystal detector decreases. The reflected energy resonance pattern is the direct inverse of the transmitted energy resonance pattern.

Two important results were obtained through the use of the reflected energy technique. In previous experimental tests using the transmission technique a number of excitation and detection antennas were used. The multiple antenna system introduced phase cancellation of RF signals at the T-Junctions, consequently obtaining a matched tank configuration was extremely difficult. It was found that a single antenna using the reflected energy technique produced a higher resonance count than a multiple antenna system. The second significant result was that the RF power required to excite the tank was considerably less than the power required for a transmission type system.

The reflected energy technique using multiple antennas was used on the 2/5 scale THERMO tank. This increased the empty tank resonant count to 60% of the theoretical count. A single antenna system using the reflection technique increased the empty resonant count to 75% of the theoretical count.

Further increases in the resonant count could not be achieved, and it was suspected that the geometry of the tank; that is, the spacing between the cylinder wall and the bottom dome prevent uniform illumination of the tank. The bottom dome was removed and replaced with a flat plate. The resonant count obtained with the tank in this configuration was 90% of the theoretical empty count. This was also the condition of the S-IVB tank when it was matched.

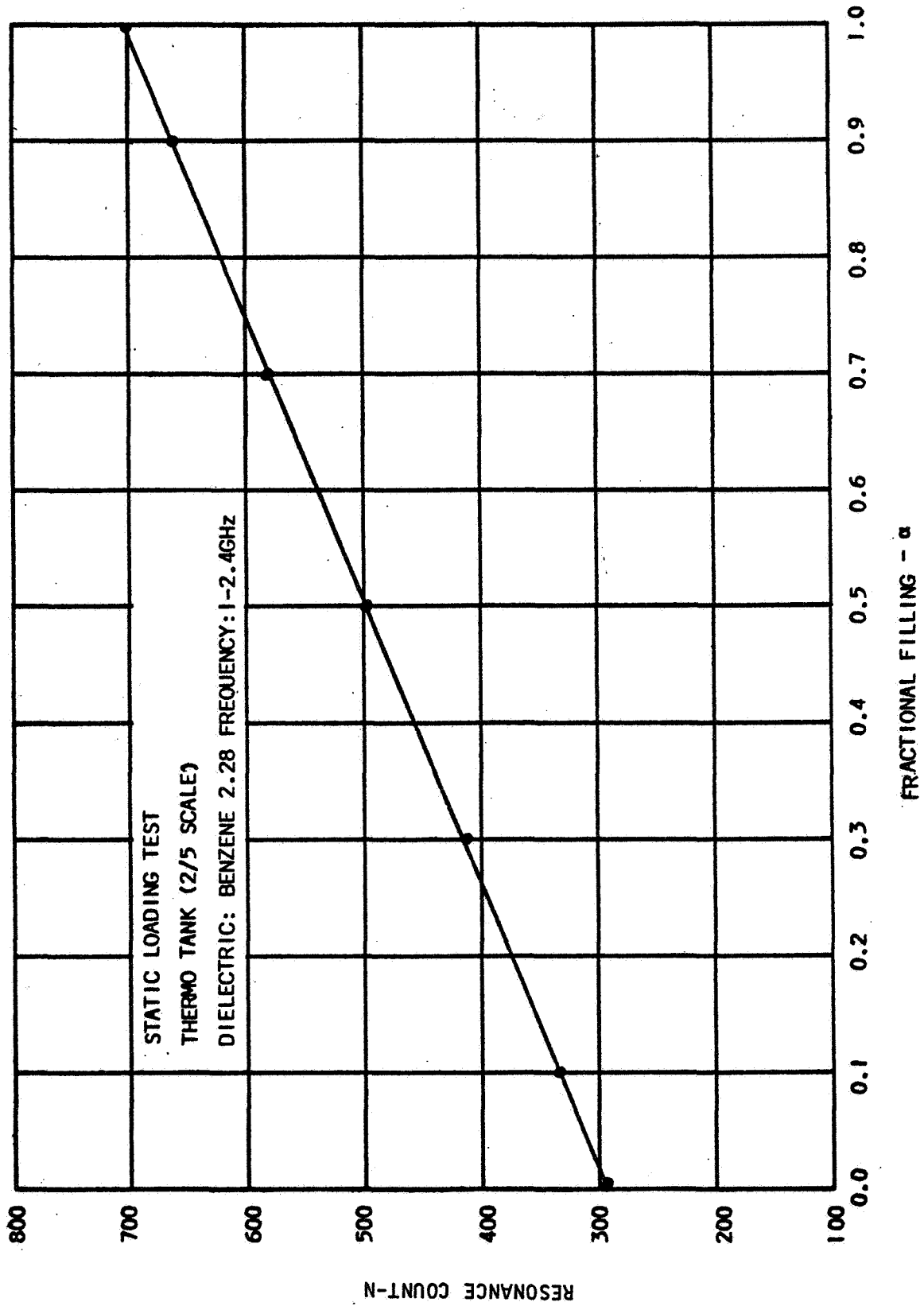


FIGURE 4-20

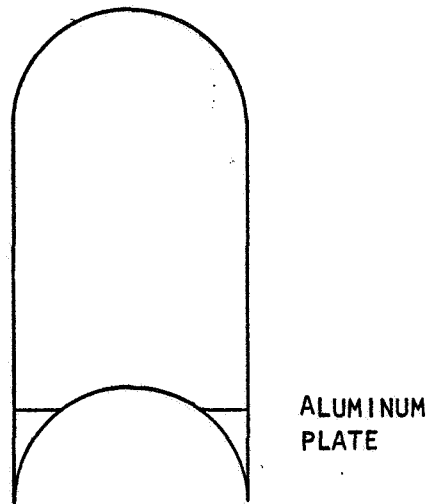
The tank was filled with Benzene and a static loading curve obtained. The loading dependence versus fractional filling was determined and a linear plot was obtained. This is shown in Figure 4-20. The resonant count is the average value of the resonant count obtained with the tank in three different orientations (vertical, horizontal and inverted) for a given fractional filling. The deviation due to orientation was within $\pm 3\%$ of the full tank resonant count. Table 4-3 shows the results of the static orientation test.

TABLE 4-3
STATIC ORIENTATION TEST, 2/5 SCALE THERMO

FRACTIONAL FILLING	RESONANT COUNT				
	CALCULATED	HOR.	VERT.	INVERT.	AVG.
0.0	334	295	295	295	295
0.1	415	340	333	332	335
0.3	579	421	399	418	413
0.5	742	498	489	504	497
0.7	905	570	580	591	580
0.9	1069	651	659	669	660

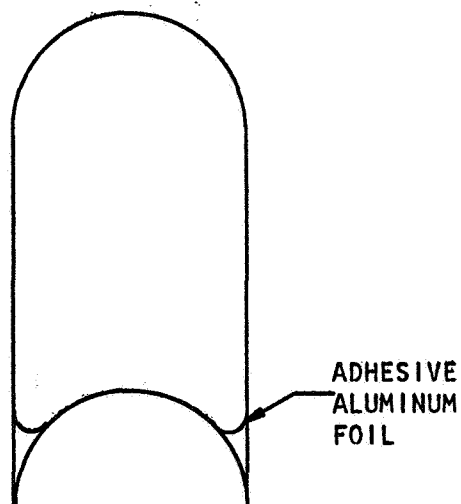
These results show that the basic THERMO tank configuration can be matched and that the reentrant section was a source of possible trouble.

The flat end plate was removed and the bottom dome replaced. A thin sheet of aluminum was placed over the reentrant dome, as shown in Figure 4-21 in order to modify the geometry of the section to achieve an empty tank resonant count of 90% of the theoretical resonant count.



MODIFICATION OF REENTRANT SECTION
FIGURE 4-21

This configuration achieved the required condition, but was impractical since this would require an excessive loss of available tank volume. Adhesive aluminum foil was then placed along the dome and cylinder, as shown in Figure 4-22:



MODIFICATION OF REENTRANT SECTION
FIGURE 4-22

This gave the required condition of an empty resonant count of 90% of the theoretical resonant count. A static loading test was conducted. A linear loading dependence was obtained, using the average value of the resonant counts for the three different orientations. See Figure 4-23. The maximum count variation was $\pm 8\%$ with respect to orientation for a particular fractional filling.

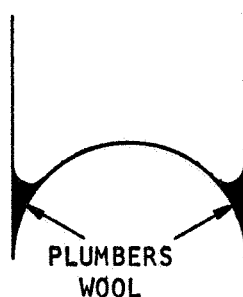
This large error could be attributed to the deformation of the aluminum foil under liquid, since the error was more significant at higher values of filling.

Table 4-4 presents the data obtained for the THERMO tank whose reentrant section was modified with adhesive aluminum foil.

TABLE 4-4
STATIC ORIENTATION TEST, 2/5 SCALE THERMO

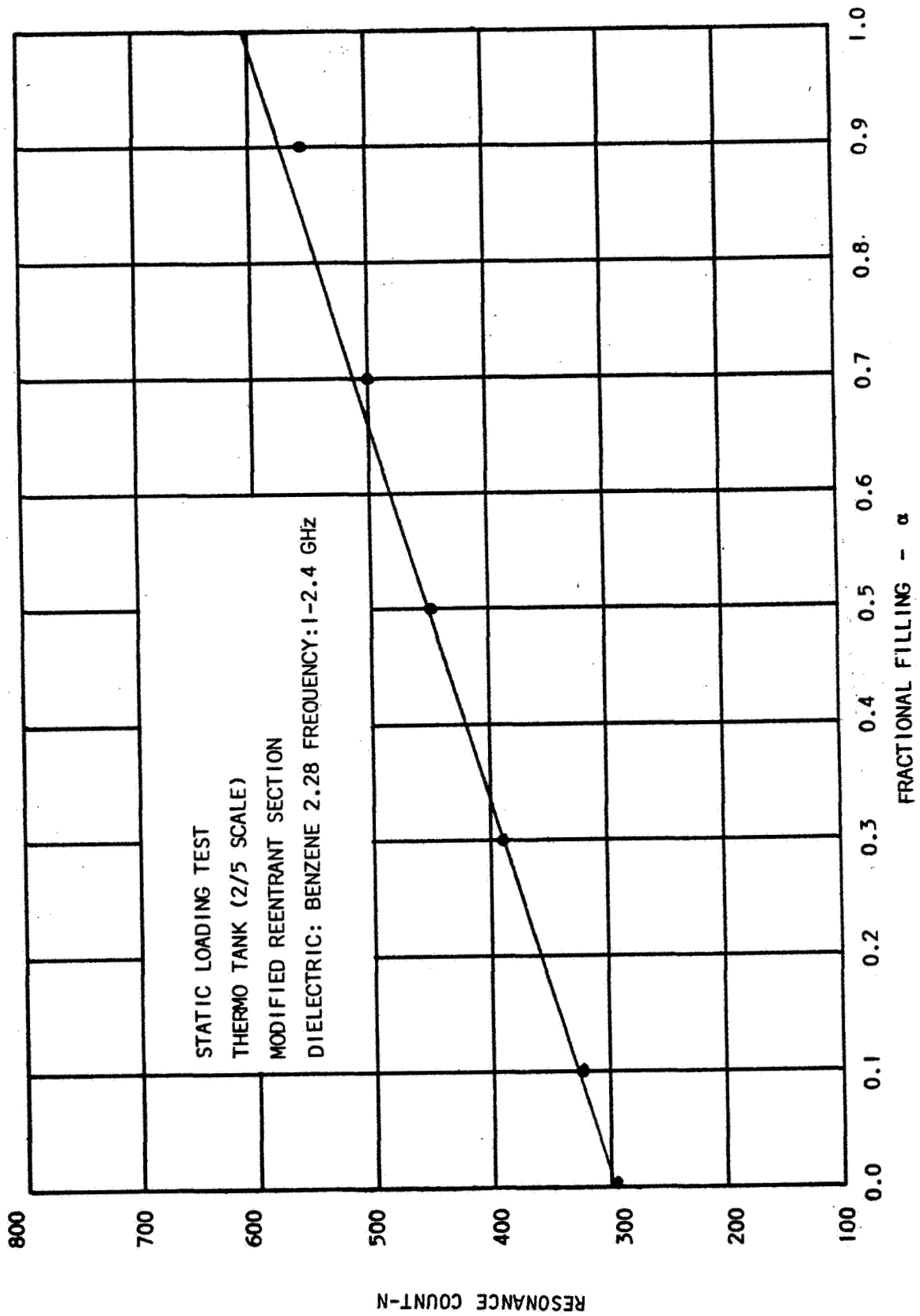
FRACTIONAL FILLING	RESONANT COUNT				
	CALCULATED	HOR.	VERT.	INVERT.	AVG.
0.0	334	295	295	295	295
0.1	415	335	315	323	324
0.3	579	401	387	389	390
0.5	742	462	450	443	451
0.7	905	522	487	491	497
0.9	1069	570	546	552	556

In order to provide structural integrity, the tank was modified to meet the required condition simulated by the adhesive aluminum foil by filling the reentrant section with plumbers wool. See Figure 4-24. The plumber's wool did not change the tank "Q" noticeably.



MODIFIED REENTRANT SECTION

FIGURE 4-24



RESONANCE COUNT-N

FIGURE 4-23

The configuration reduced the volume of the tank by 2% but the required condition for matching the tank was achieved (a 90% empty count was realizable). A static loading test was performed. Figure 4-25 shows the results of this test. The values at each particular loading are the average value of the resonant count obtained at the three different orientations. Table 4-5 indicates the resonant count data obtained for various percentage fillings. This test was a system verification. However, this test was repeated in detail and the results are shown in Table 4-6.

TABLE 4-5
STATIC ORIENTATION TEST, 2/5 SCALE THERMO

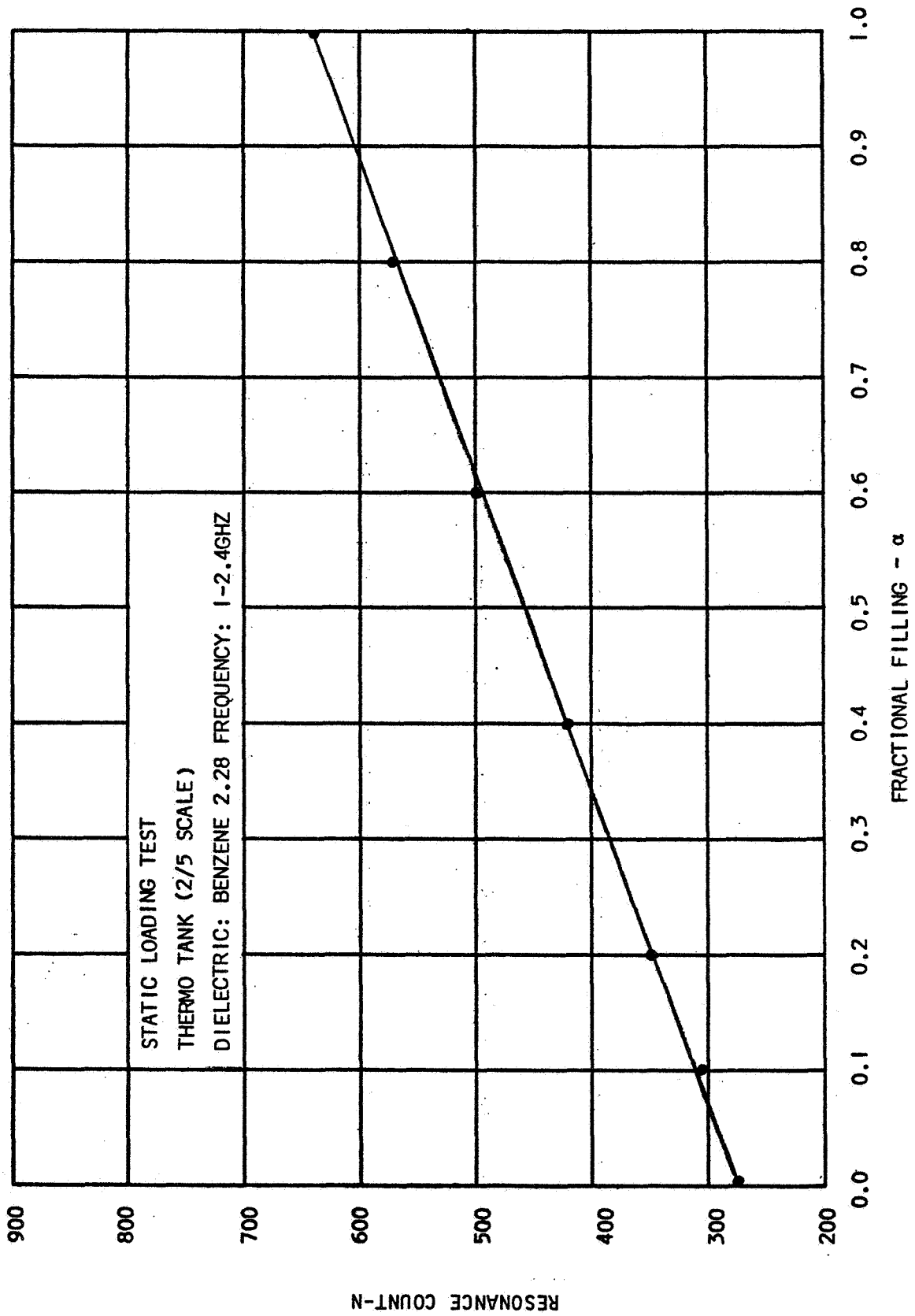
FRACTIONAL FILLING	RESONANT COUNT			
	HOR.	VERT.	INVERT.	AVG.
0.0	273	273	273	273
0.1	303	304	309	305
0.2	356	343	344	348
0.4	423	435	409	422
0.6	502	504	495	500
0.8	573	577	558	569

In all of the previous experimental work two sweep generators were used to obtain the sweep frequency band from 1-2.4 GHz. Because of the problem of performing dynamic tests on the 2/5 scale THERMO tank, the sweep generators were replaced with a voltage-tunable magnetron. The magnetron could be swept over a frequency band from 1.2-2.4 GHz. Static loading and orientation tests were then repeated on the 2/5 scale THERMO tank using the new frequency band. Table 4-6 shows the results of these tests and Figure 4-26 shows the loading dependence.

TABLE 4-6
STATIC ORIENTATION TEST, 2/5 SCALE THERMO
ANGULAR POSITIONS TO THE HORIZONTAL

FRACTIONAL FILLING	RESONANT COUNT								
	HOR.	22-1/2°	45°	67-1/2°	VERT.	INVERT.	1*	2*	AVG.
0.0	230	230	230	230	230	230	230	230	230
0.1	266	267	264	257	259	262	270	265	264
0.2	316	316	309	308	308	314	307	308	308
0.4	378	386	388	379	374	378	380	382	378
0.6	451	453	444	453	446	449	443	437	449
0.7	495	498	486	487	484	480	497	483	485
0.9	543	542	544	556	548	554	547	540	548
1.0	580	580	581	582	582	582	582	582	582

* Rotated 90° to horizontal position.



RESONANCE COUNT-N

FIGURE 4-25

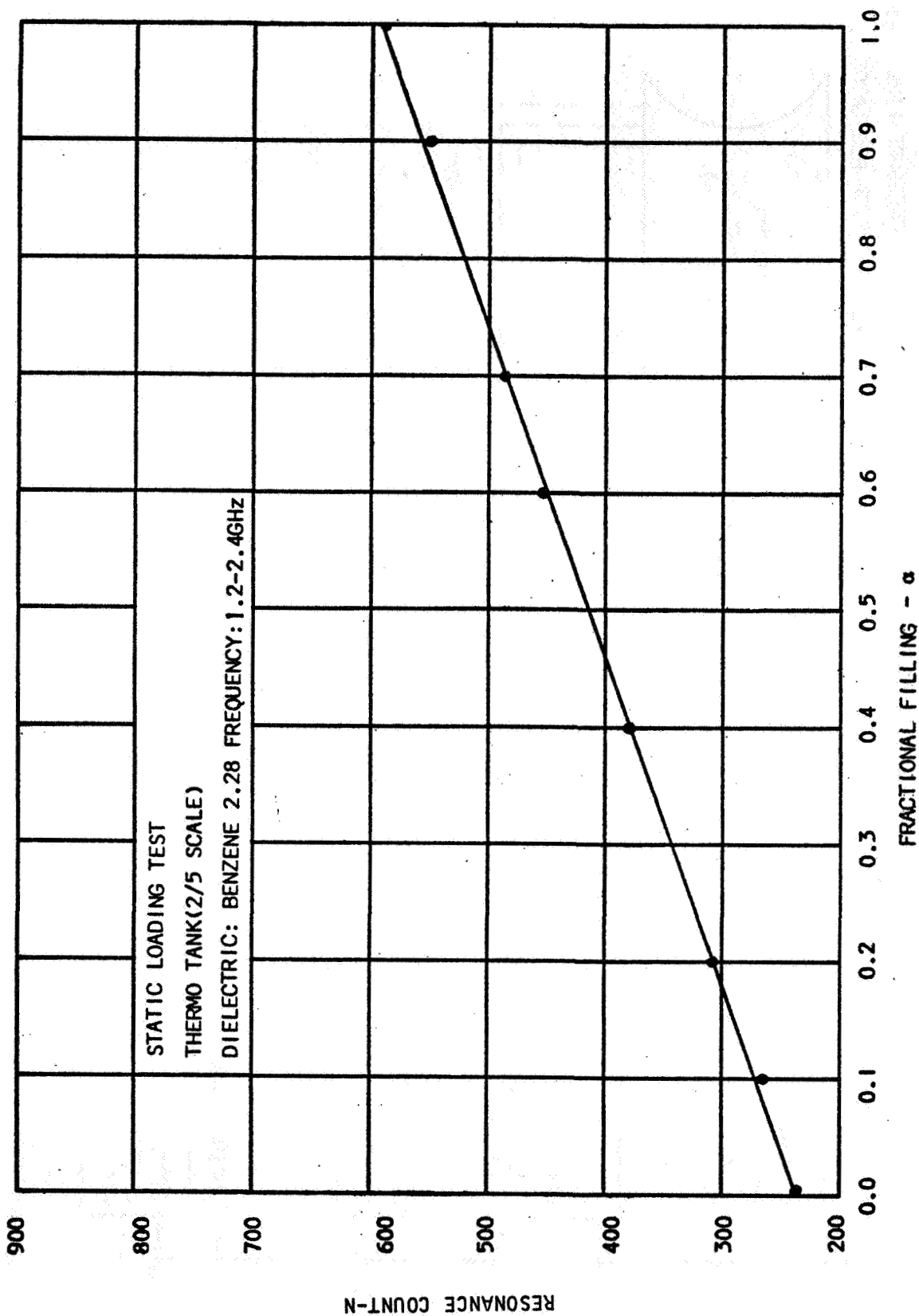


FIGURE 4-26

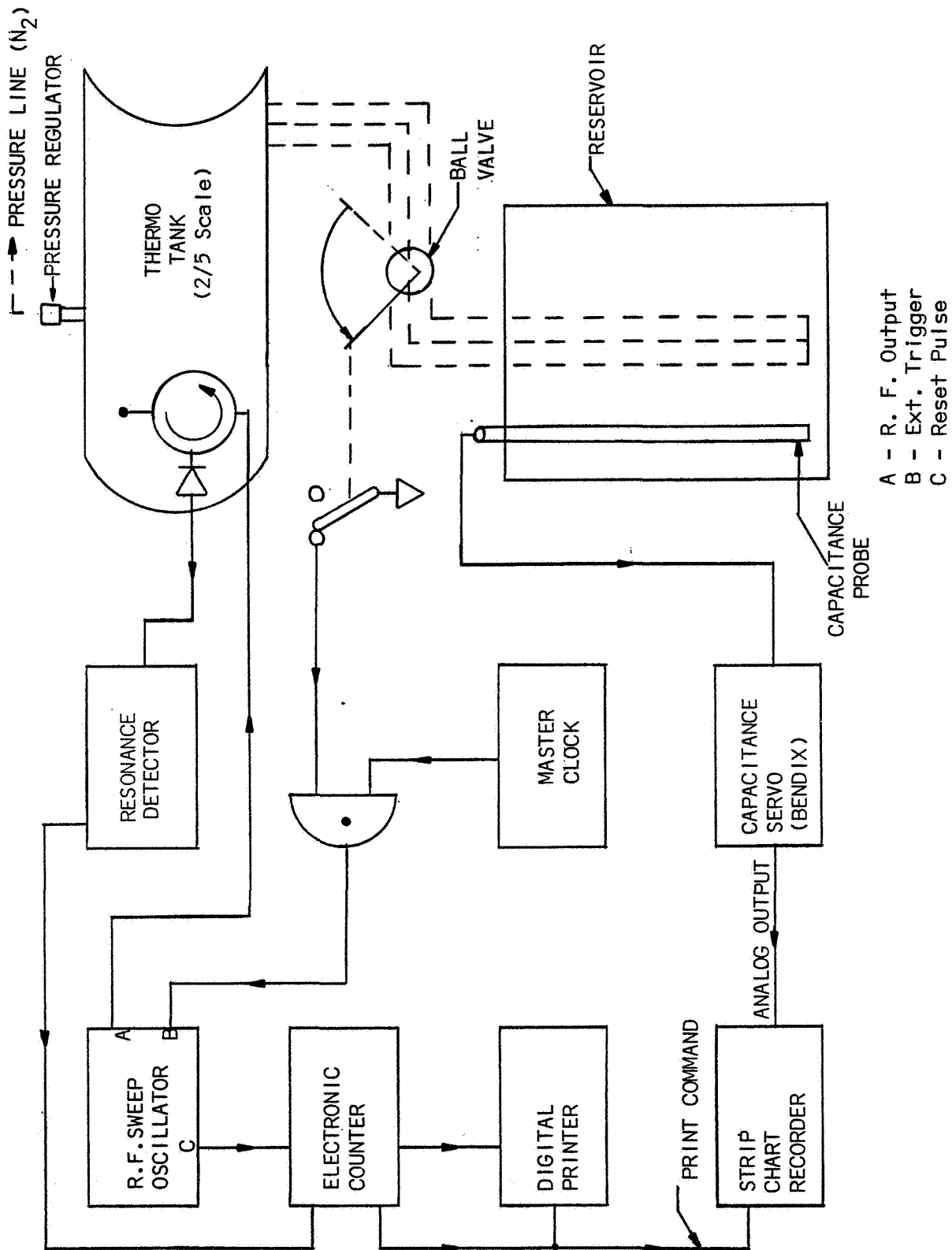


FIGURE 4-27

Tests were also conducted for small increment loadings at small angular positions. The results of these tests are shown in Table 4-7. This test simulates slosh conditions.

TABLE 4-7
INCREMENTAL LOADINGS - SMALL ANGULAR POSITIONS - 2/5 SCALE THERMO

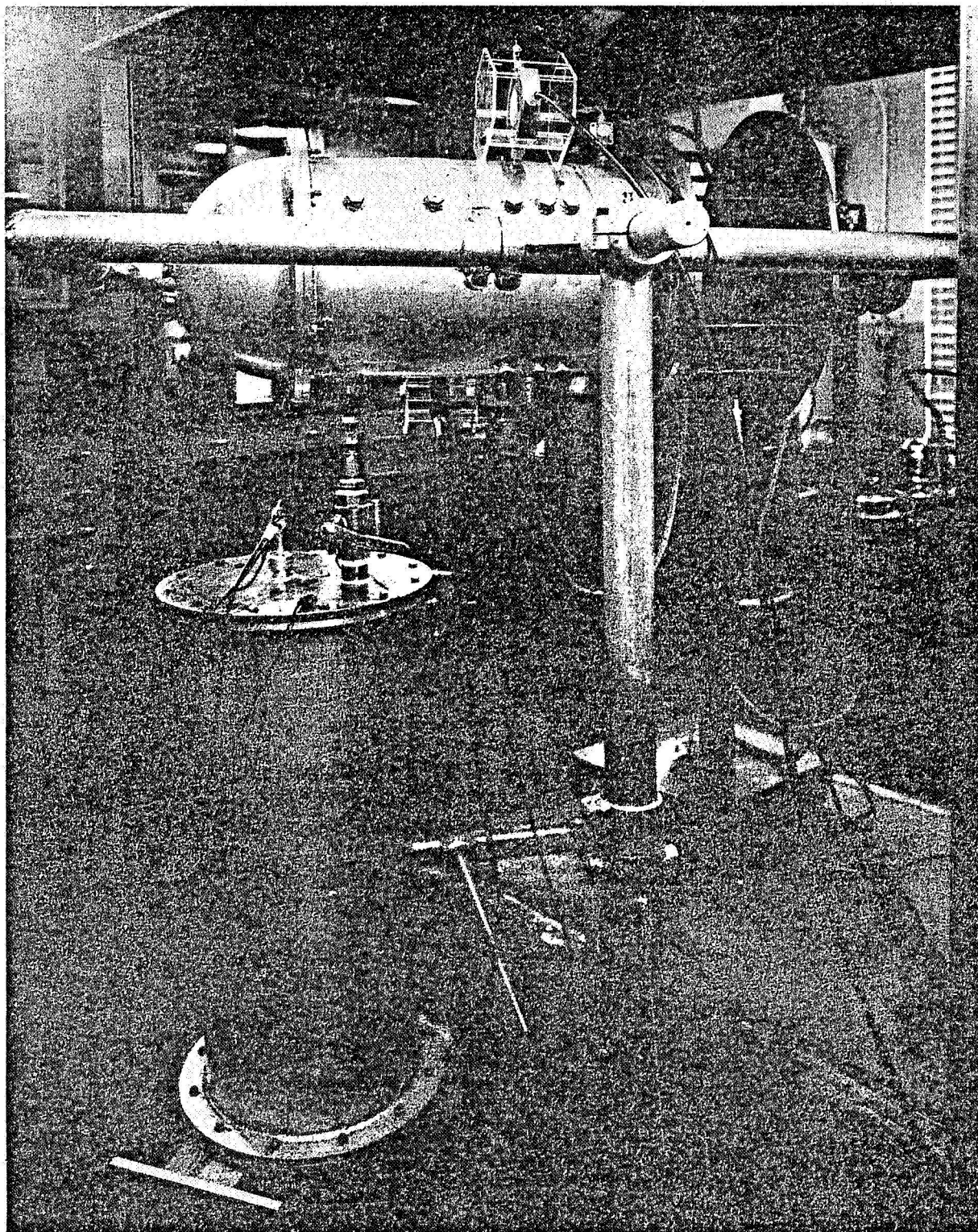
FRACTIONAL FILLING	RESONANCE COUNT					
	1°	2°	3°	4°	5°	AVG.
0.01	237	238	237	239	244	239
0.02	244	244	239	244	237	242

Once the 2/5 scale THERMO tank was matched, a flow test was set up to determine the feasibility of gaging propellants under dynamic flow conditions. The implementation of the flow test required the use of a closed system which consisted of; 1) a reservoir for the simulated propellant, 2) a lever-action control valve and interconnecting plumbing, and 3), associated electronics. Figure 4-27 is a block diagram of the test setup and Figure 4-28 provides a pictorial view of the equipment.

The mechanical hardware used in the flow test allowed for the pressurization of the 2/5 scale THERMO tank so that a constant flow rate could be maintained. The use of a lever-action control valve coupled to a micro-switch made the synchronization of resonant count to mass content of the THERMO tank possible. Two kinds of data were needed to complete the information needed to verify dynamic flow response; 1) the instantaneous mass content of the THERMO tank, and 2), the resonant count that was related to the mass content.

In order to provide a measure of mass content, a level detector (capacitance probe) was placed in the reservoir. The capacitance probe in conjunction with a Bendix Universal Capacitance Gaging Servo provided an analog output (0 to 10 volts) that was directly proportional to the liquid level in the reservoir.

The number of resonances were determined by the use of an electronic resonance counter similar to the one described in Phase A report. The electronic resonance counter differentiates the video signal from the crystal detector, detects a zero crossing and shapes the signal to a pulse that can be counted. The number of pulses resonances per unit RF sweep period are accumulated in a counter. The operation of the entire system can be explained as follows. The THERMO tank is initially pressurized. The control valve is thrown, starting the flow and RF sweep generator simultaneously. The resonance count information is fed to a digital printer that is activated by a print command which is dependent on a reset pulse from the sweep generator. The counter has the capacity of counting down the print command to



DYNAMIC FLOW TEST SETUP

FIGURE 4-28

reset-event ratio in multiples of 10. This is desirable in that it allows an averaging capability. By averaging the resonant count over 10 to 100 periods, spurious events, such as resonance variations, are eliminated.

By recording the print command event and the capacitance analog signal on two different channels of a strip chart recorder, synchronized data on propellant mass and the resonance count can be obtained.

The basic criteria in determining the feasibility of RF gaging under dynamic conditions is whether or not a linear loading dependence is retained within the system accuracy. The loading dependence was linear within $\pm 3.9\%$ as shown in Figure 4-29. The flow time required to perform this test was 165 seconds which corresponds to a 0.6% volume change/second. The basic accuracy of the electronic resonance detector was checked under static loading conditions and was found to have an error of approximately $\pm 1\%$ in repeatability. Therefore, the results obtained are very encouraging in that:

- 1) the loading dependence was linear
- 2) the data could be repeated.

The fact that the electronic resonant count is not the same as that obtained by the visual hand count method is of no consequence since the visual method has many inaccuracies, because resonance recognition is based on individual discretion and also a human error in counting. But the fact that the electronic resonant count is linear, and repeatable, is very encouraging because it proves the system is operating correctly.

The flow test was repeated for higher flow rates but it was found that the accuracy of the system suffered. The inaccuracy at higher flow rates can be corrected through the use of an improved electronic resonant counter and swept RF oscillator system, such as using an A/D convert or technique for resonant counting and a non-linear RF oscillator. The data obtained is shown in Table 4-8.

TABLE 4-8
FLOW TEST RESULTS, 2/5 SCALE THERMO

RESONANT COUNT DEVIATION (%)	FLOWTIME (SEC)	% VOLUME/TIME
$\pm 3.7\%$	165 sec	0.60%/sec
$\pm 3.9\%$	155 sec	0.65%/sec
$\pm 4.5\%$	137 sec	0.73%/sec
$\pm 4.9\%$	127 sec	0.80%/sec

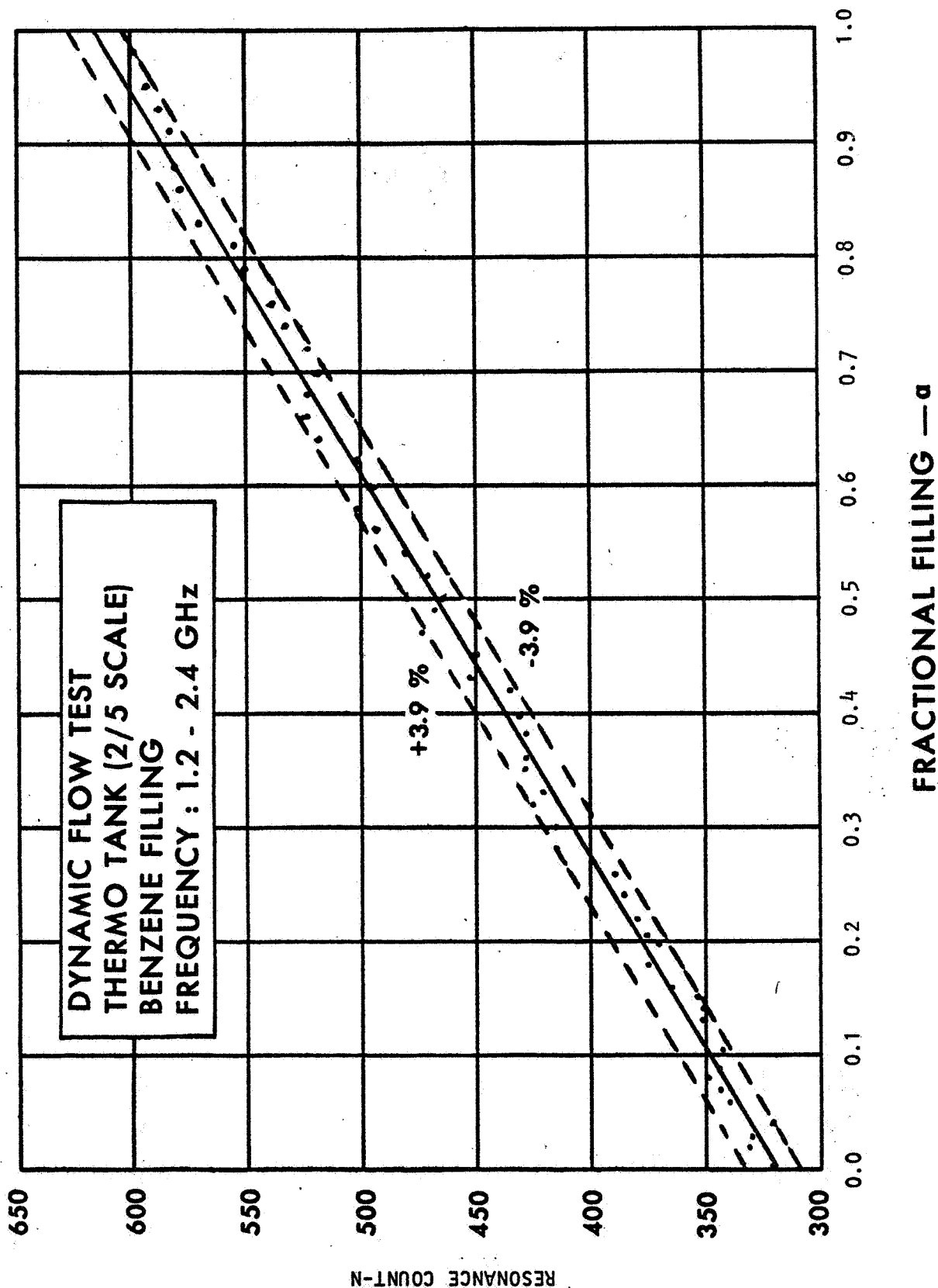


FIGURE 4-29

4.5 THERMO Tank Tests (1/3 Scale Model)

Due to the thermodynamic problems associated with cryogenic liquids, it was decided to use the 1/3 scale THERMO tank for testing the RF system loading response to liquid hydrogen.

A reflected energy technique was used on the 1/3 scale THERMO tank in order to obtain a sufficiently high empty resonant count and to assure a matched condition.

The configuration of the bottom of the tank, as in the 2/5 scale THERMO tank, attenuated the radiated energy and prevented exciting a sufficiently large number of resonances. Therefore, the spacing between the cylinder wall and the bottom dome was filled with plumbers wool in order to attain the tank configuration necessary to prevent attenuation of radiated energy.

An operating frequency range of 2-4 GHz was chosen in order to attain a high enough sensitivity for operation with LN₂ and LH₂. An antenna length of a quarter wave length was chosen (center frequency 3 GHz) and mounted approximately at the center of the cylindrical wall. The tank was assembled in this configuration so that a sufficiently large number of resonances were excited in order to attain a matched condition. Preliminary tests were conducted on the 1/3 scale THERMO tank using Benzene. The static loading tests was conducted with an operating frequency range of 2-4 GHz. The loading response is shown in Figure 4-30. Loadings above 70% were neglected since the number of resonances excited were too concentrated to be detected satisfactorily. As stated previously, this frequency range was selected for operation with LN₂ and LH₂.

The 1/3 scale THERMO tank was retrofitted for operation with LN₂ and LH₂. Ref. Paragraph 4.1. Using the same operating frequency range and antenna length that were used for the Benzene tests, (the tank was left intact) a static loading test was performed using LN₂. The results of the test are shown in Figure 4-31. In the performance of the LN₂ tests, considerable difficulty was encountered in keeping the LN₂ from boiling. Since the resonant count was being obtained through the use of a strip chart recorder, care had to be exercised to assure that the LN₂ was not boiling. A second difficulty encountered was the establishment of a correct correlation between the resonant count and the mass content of the tank. This problem arose due to the tendency of the cryostat to gain weight due to formation of ice on its walls.

The solution of these problems seemed both formidable and prohibitively expensive if the tank were to be used for LH₂ testing. It was decided that a simulated spacecraft tank constructed from a cryogenic dewar would be used for the LH₂ testing.

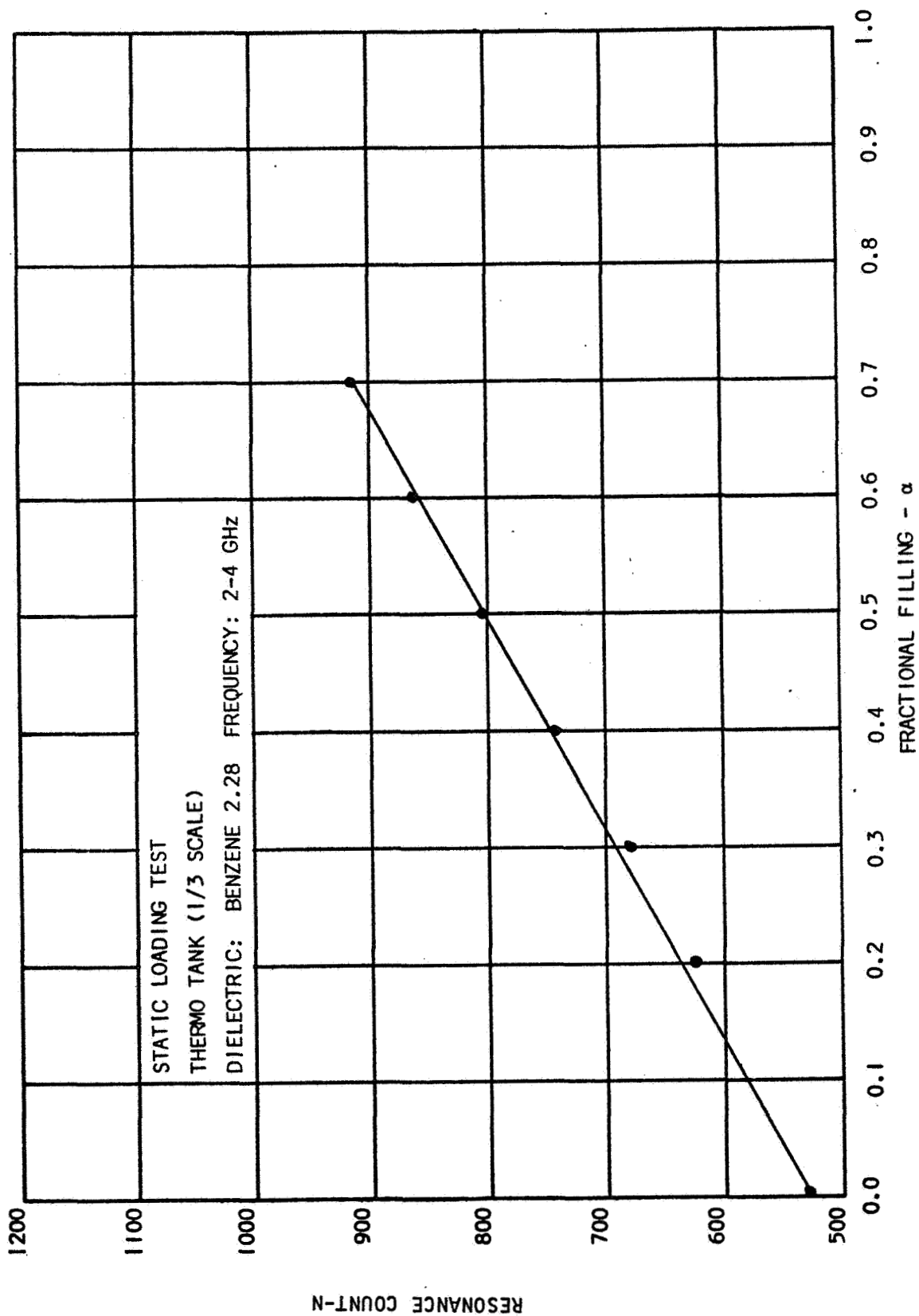


FIGURE 4-30

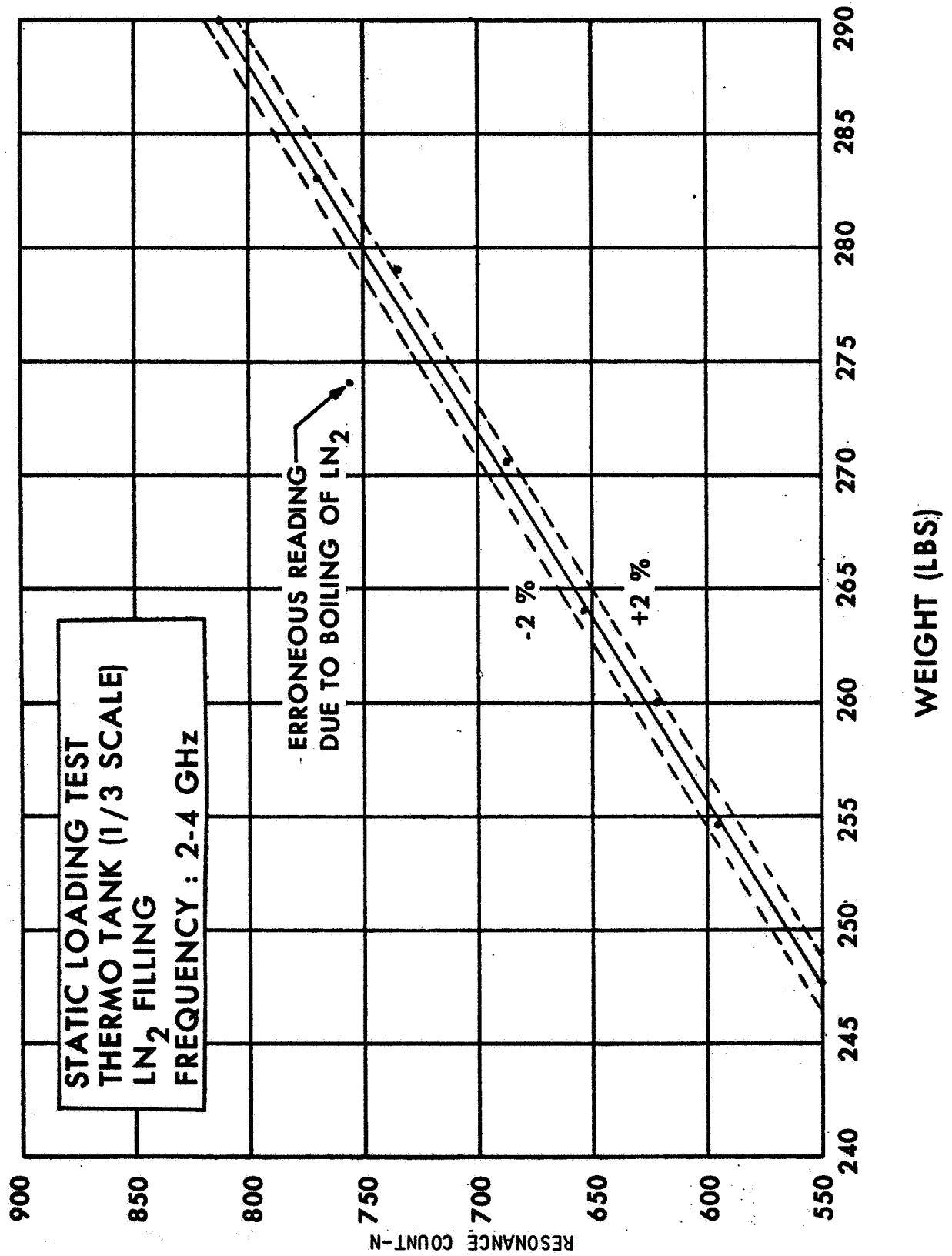
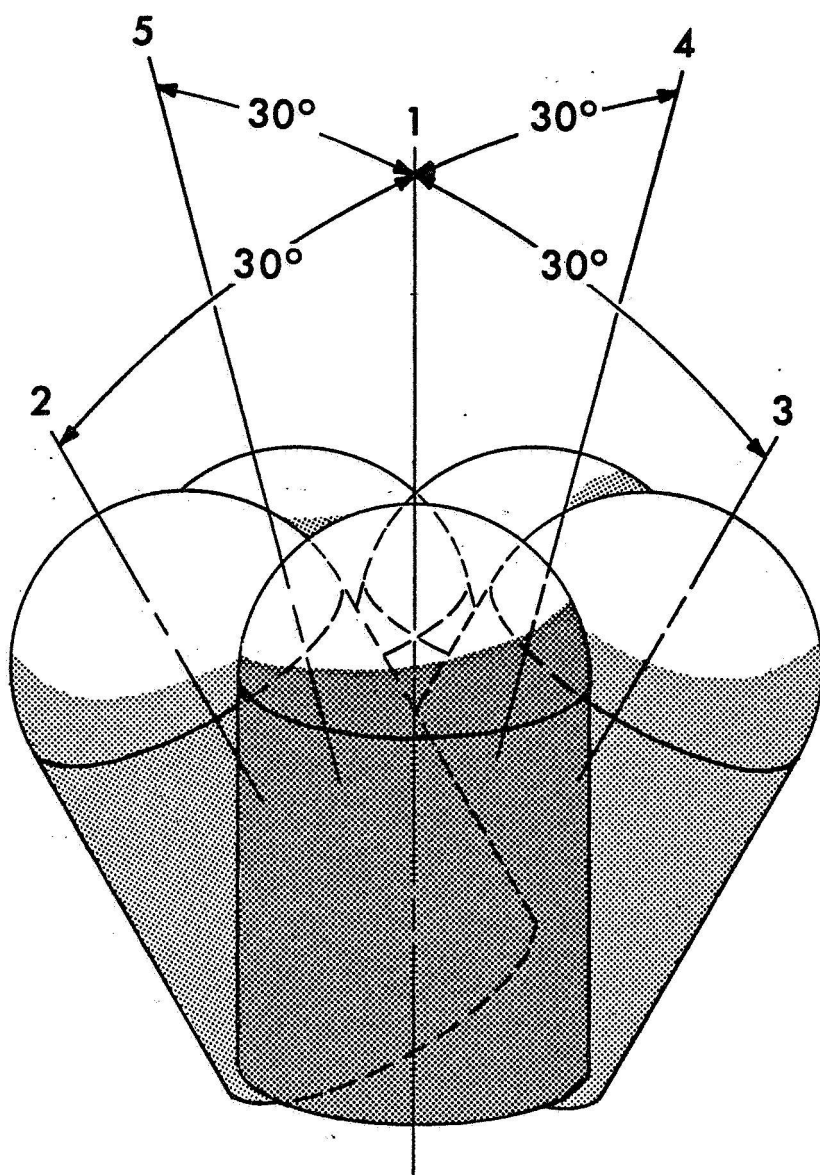


FIGURE 4-31



STATIC ORIENTATIONS SIMULATED SPACECRAFT TANK

FIGURE 4-32

A-3745-67-201A

4.6 Simulated Spacecraft Tank Tests

In order to achieve a sufficiently high sensitivity for the static loading tests with LN_2 and LH_2 , a frequency range from 2.8-4 GHz was selected due to the small size of the simulated spacecraft tank. The simulated spacecraft tank was excited using the reflective energy technique with a quarter wavelength antenna (center frequency 3.4 GHz). The position of the antenna is shown in Figure 4.4.

Verification of the correct selection of operating frequency range was made by determining that the empty resonant count was 90% of the predicted count. A static loading and orientation test was performed with Benzene. Figure 4-32 shows the orientation of the tank. Figure 4-33 and Table 4-9 show the loading dependence.

TABLE 4-9

STATIC ORIENTATION TEST, SIMULATED SPACECRAFT TANK

FRACTIONAL FILLING	RESONANT COUNT				
	1	2	3	4	5
0.0	315	315	315	315	315
0.1	342	350	344	351	350
0.2	383	384	384	376	366
0.4	443	441	440	421	423
0.6	507	495	488	486	484
0.8	539	536	540	556	545

The use of the electronic resonance detector was proposed in the performance of the LH_2 tests. Normal use of the resonance detector requires that the RF sweep oscillator be operated at a 10 millisecond sweep rate. The fast sweep rate makes the RF system independent of liquid sloshing. In the operation of the empty tank at this sweep rate, it was found that a number of resonances would ring. An decrease in the sweep rate would stop the ringing. The ringing was noticed on all tanks when filled with low loss liquids such as LN_2 , LH_2 .

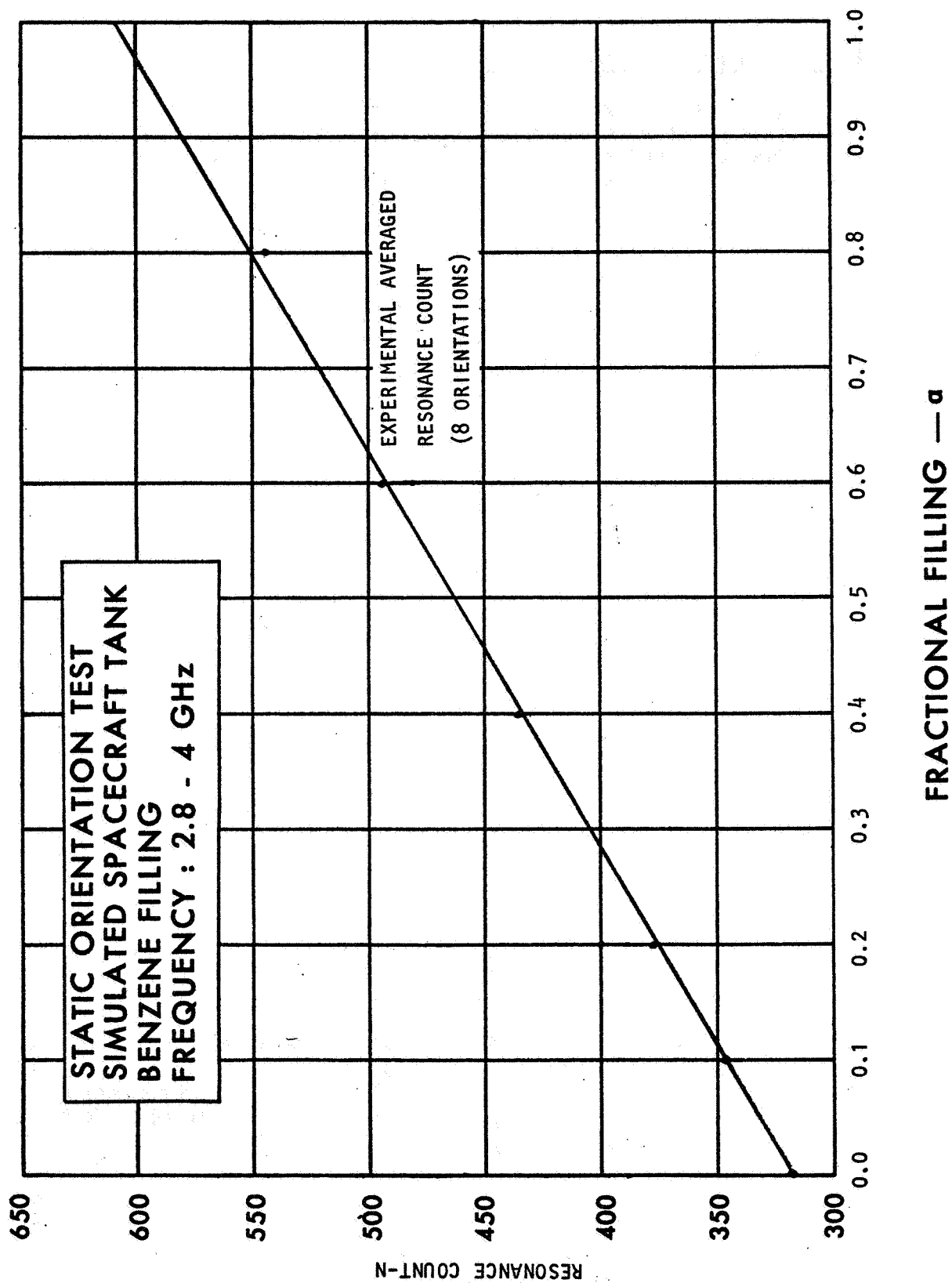
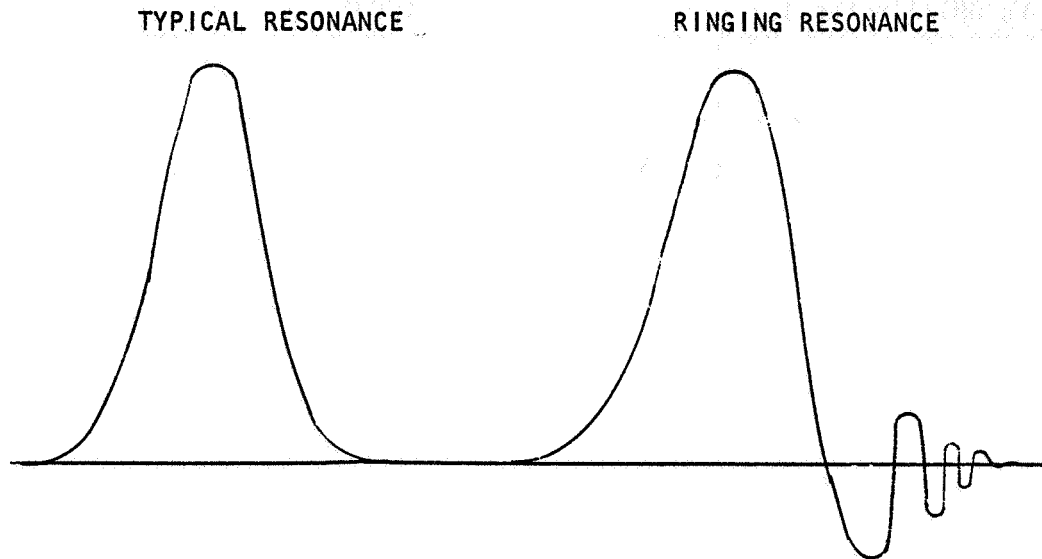


FIGURE 4-33

Figure 4-34 shows a typical resonance compared to a resonance that rings.



RESONANCE RINGING
FIGURE 4-34

The tank ringing was attributed to the high tank "Q" and the inability of the tank to dissipate the stored energy quickly. Since the resonance detector detects the peak of RF energy, the ringing would be counted as resonance. A high loss, paper base, hard phenolic rod was inserted in the spacecraft tank in order to increase the system dissipation. A static loading test was performed using LN_2 . The rod stopped the ringing but at the sacrifice of lowering the system "Q". The initial nonlinearity in the loading response was due to the insertion of the high loss material in the tank.

It was decided to increase the sweep time in order to eliminate the ringing and record the number of resonances by use of a strip chart recorder for the LH_2 test. The LH_2 test was attempted using the high loss rod but the loading dependence was so nonlinear that the rod had to be removed.

A static loading test using LH_2 was performed on the spacecraft tank. The test was repeated three times to insure consistency of data. Table 4-10 and Figure 4-35 show the results of this test. It can be concluded that the basic RF system is operable with LH_2 .

TABLE 4-10
LH₂ STATIC LOADING TEST

WEIGHT (In Lbs.)	RESONANT COUNT		
	1	2	3
62.0 (73%)	362	358	359
61.6	348	351	350
61.4	341	342	340
61.1	333	331	332
60.8	324	323	320
60.5	318	319	317
60.2	312	314	312
59.9	303	305	303
59.6	296	294	295
59.3	289	289	287
59.0	281	281	280
58.8 (Empty)	279	277	278

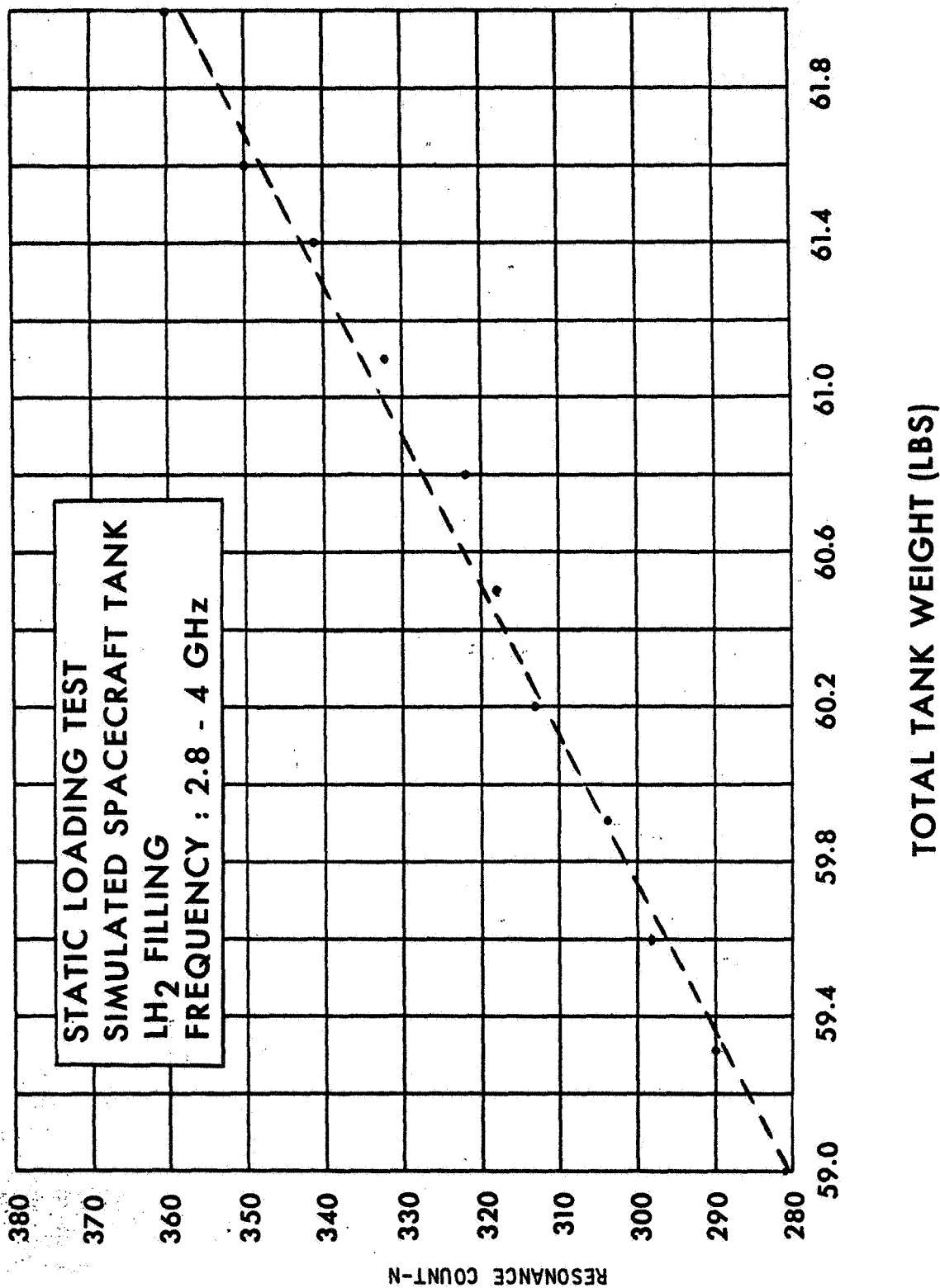


FIGURE 4-35

SECTION V

COMPARISON OF EXPERIMENTAL RESULTS TO THEORETICAL PREDICTIONS

5.1 Introduction

The use of the computer program or the mathematical approximation formula to predict the loading dependence of tanks based on System "Q", operating frequency and dielectric constant can be checked by comparing their results to those obtained from actual experiments. A relative comparison of the results obtained from each prediction technique was previously given in Section III for a cylindrical tank. Some differences existed between the loading dependence predicted by each technique which make it necessary to compare the predictions to experimental data for a number of different tanks and dielectrics to choose most useful technique.

The comparison of the computer program results to experiment is made by the use of equivalent volume tank models of the spacecraft tanks. Equivalent cylindrical tanks were made of the 2/5 scale THERMO tank and the 1/3 scale THERMO tank. Measurement of the external "Q" for the 1/20 scale S-IVB and the 1/3 scale THERMO tank resulted in an average external "Q" of approximately 2500 and 4500 respectively. The average external "Q" for the 2/5 scale THERMO and the SST tank were measured as 2100 and 5100. A cigar-shaped tank used in Phase I had a measured "Q" of 4000, and experimental data is included here for evaluation of the two loading dependence technique. The external "Q" and the dielectric "Q" are sufficient to specify a system "Q".

$$\frac{1}{Q_{\text{System}}} = \frac{1}{Q_{\text{Dielectric}}} + \frac{1}{Q_{\text{External}}}$$

The theory states that if the system "Q" is known, and a solution to the modes of a cavity can be obtained, entry of this data into the statistical computer program is sufficient to determine the loading dependence and operating frequency band. Also, the system "Q" may be entered into the mathematical formula for the loading dependence and the results compared to experiment. This formula does not require the use of equivalent volume cylindrical tanks, and is applied directly to the experimental tanks.

Computations were made of the loading dependence predictions for the computer program for some of the tanks for which experimental data was available for the comparison of theory and experiment. A more complete set of loading dependences was made with the mathematical formula because of the ease of making the computations. A sufficient number of each are given, though, to allow an evaluation of the ability of each to predict experimental loading dependencies.

5.2 Computer Calculated Loading Dependencies Comparisons

5.2.1 1/3 Scale THERMO Tank Comparisons

The 1/3 scale THERMO tank was represented by a cylindrical tank of equal volume for theoretical analysis and a computer program was run to determine the loading dependence of the tank. The tank was analyzed for the following system parameters:

- A. Frequency Range: 1 - 4 GHz
- B. Dielectric: LH₂ 1.23, LN₂ 1.46, Benzene 2.28
- C. System "Q": ∞, 10,000, 6666, 5000, 2500

The system "Q" is calculated as approximately 4,500 for both LH₂ and LN₂ dielectric fillings. The nearest system "Q" value that was run on the computer program is 5,000. Figure 5-1 shows a comparison of the calculated and the experimental loading dependence performed with LN₂. The complete computer analysis for LN₂ can be found in Appendix D, Section 1.

It can be concluded that the static loading response can be accurately predicted. A LH₂ static loading test was not performed on the 1/3 scale THERMO tank, but was performed on the simulated spacecraft tank. Since the external "Q" is the dominant factor in the system "Q" for low loss dielectrics, a direct comparison can be made relating the theoretical response of the 1/3 scale THERMO tank to the experimental response obtained on the simulated spacecraft tank. That is, the slope or sensitivity should remain the same. Figure 5-2 shows the theoretical loading response for the 1/3 scale THERMO tank assuming a system "Q" of 5000. Figure 5-3 is the experimental curve obtained when a static LH₂ loading test was conducted on the simulated spacecraft tank. It can be seen that the ratio $\frac{N_{full}}{N_{empty}}$ is constant.

$$\frac{N_f}{N_e} = 1.46 \text{ (1/3 Scale THERMO Tank - Theoretical)}$$

$$\frac{N_f}{N_e} = 1.44 \text{ (Simulated Spacecraft Tank - Experimental)}$$

If the 1/3 THERMO tank was capable of containing LH₂, a complete comparison could be made of the predicted results and the experimental results. The equivalence of slope, however, suffices; therefore, a complete analysis has been made of the 1/3 scale THERMO tank for static loadings with Benzene, LN₂ and LH₂. The results of the analysis specified the operating frequency range, and the correct loading sensitivity.

5.2.2 2/5 Scale THERMO Tank Comparisons

A computer analysis was made of the 2/5 scale THERMO tank by assuming an equivalent volumetric cylindrical tank (L/D ratio equal to that of the

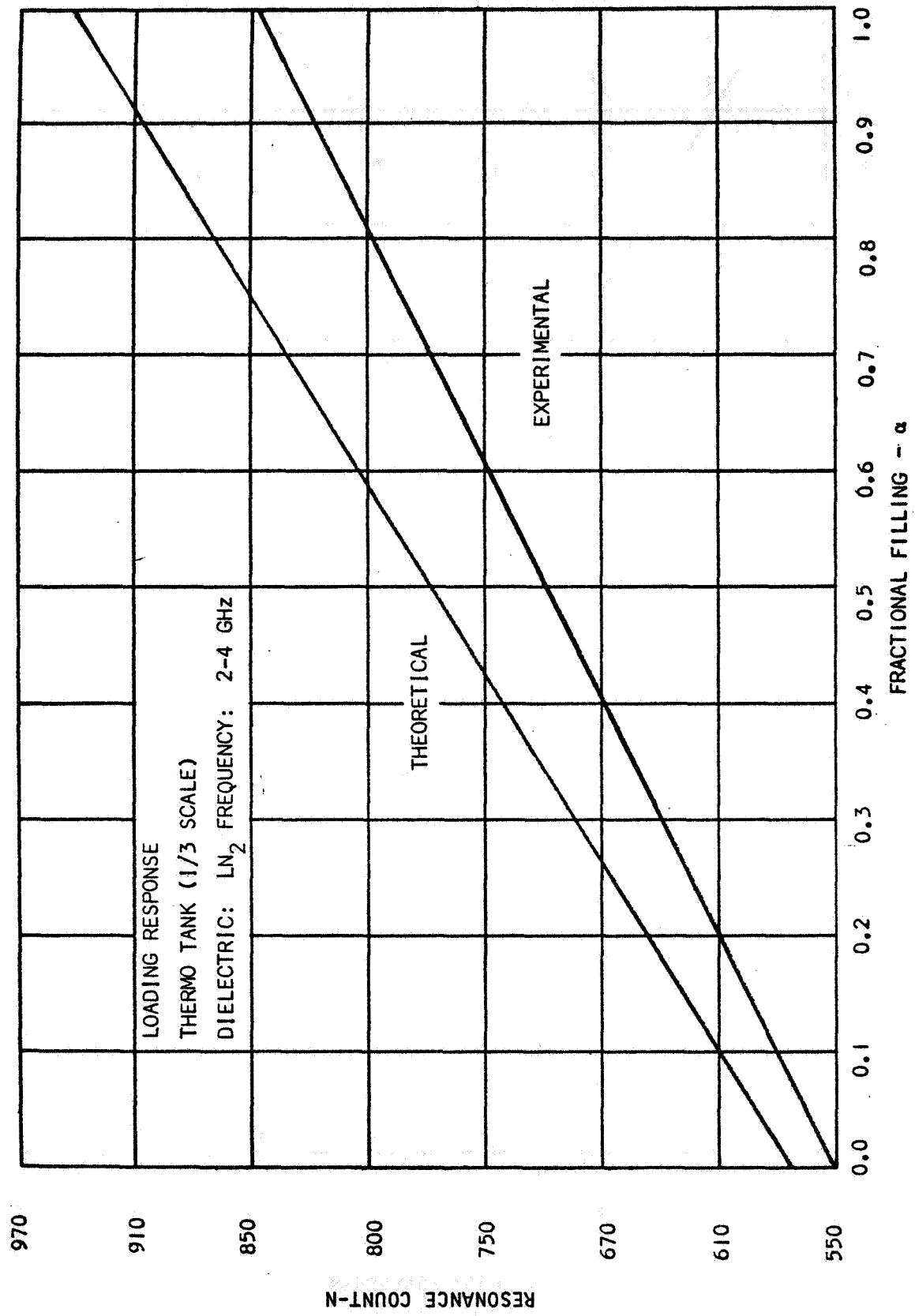


FIGURE 5-1

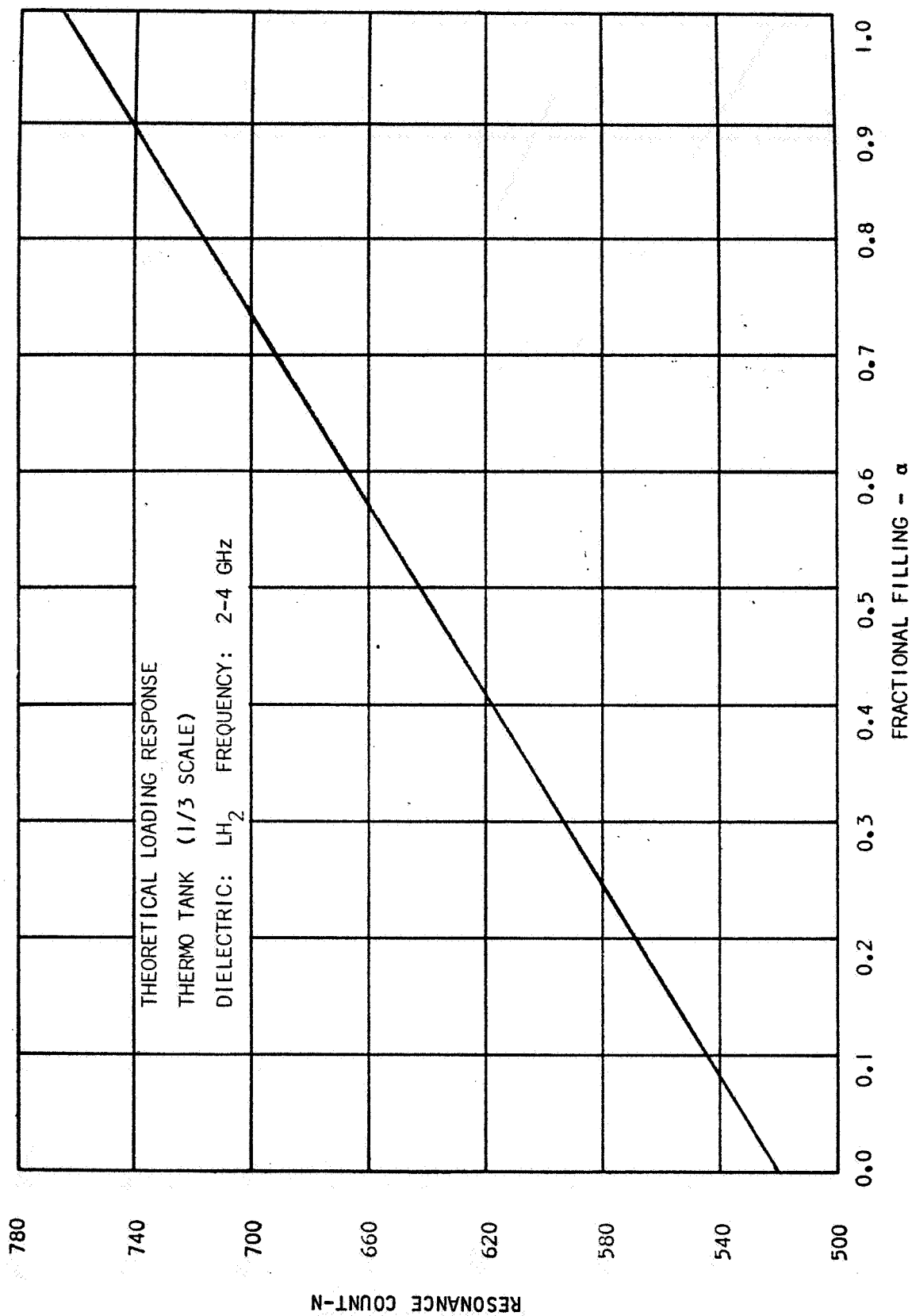


FIGURE 5-2

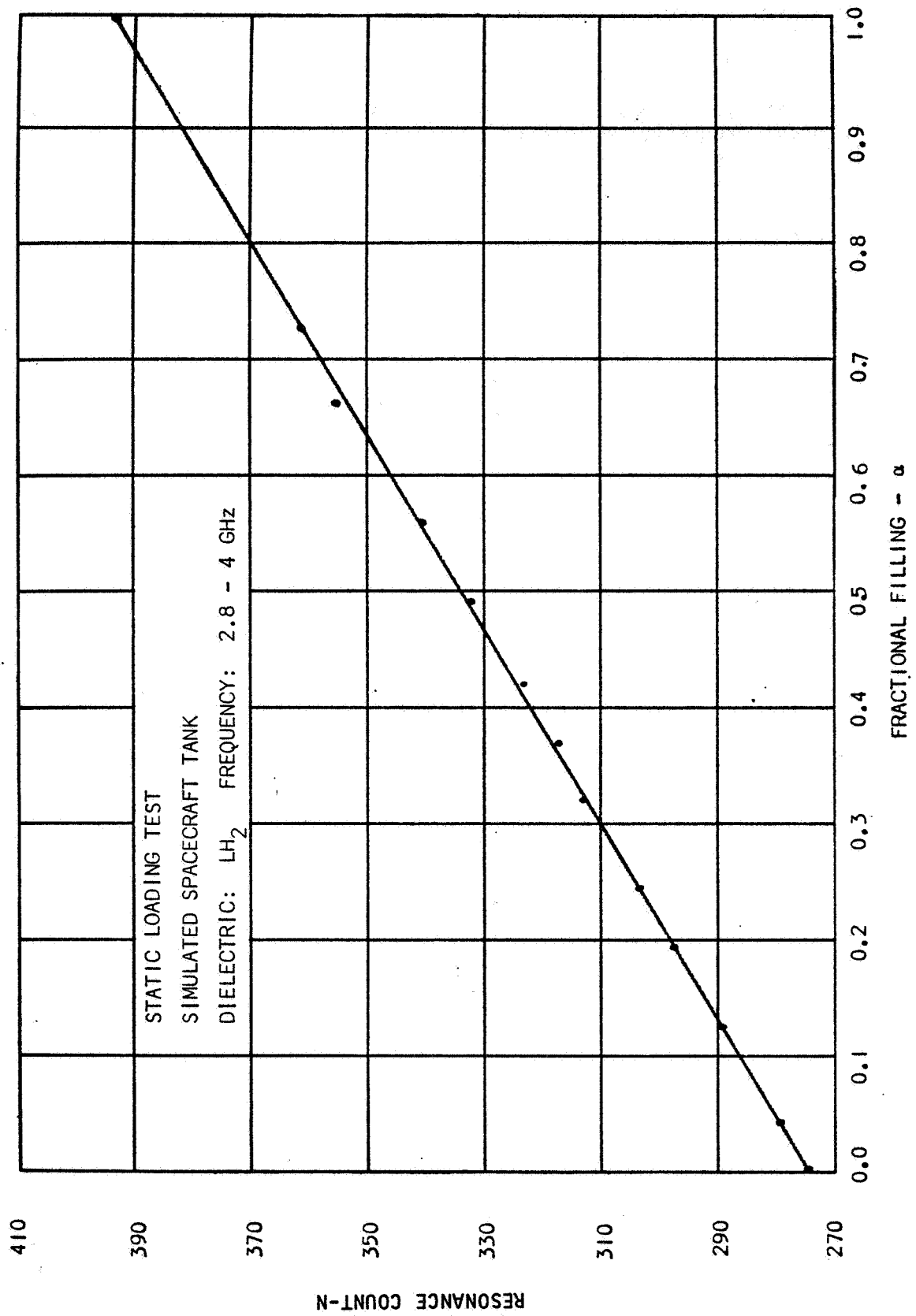


FIGURE 5-3
N-INNOO3

THERMO tank), and solving for the resonant modes of the tank. The dielectric used was Benzene, 2.28.

The analysis was performed for the frequency range 1 - 3 GHz. The upper cutoff frequency was chosen as 2.4 GHz in the experimental section. A comparison of the mode distribution curves can be made to see if the upper cutoff frequency is correct. For static loadings with Benzene, the system "Q" can be calculated as:

$$Q_{\text{system}} = \frac{1}{\frac{1}{4500} + \frac{1}{6500}} \approx 2600$$

Computer runs were made for the following system "Q"'s: ∞ , 20,000, 10,000, 5,000, 2,000, 1,000. The mode distribution curve, Figure 5-4 for a system "Q" of 2,000 and a fractional filling of 0.9, shows that the point of zero slope $d^2N/df^2=0$, is at a frequency of approximately 2.4 GHz.

The predicted static loading response compared to the experimental curve for partial fillings with Benzene is shown in Figure 5-5. Again, the theoretical and experimental loading responses are in agreement.

5.3 Mathematical Formula Loading Dependencies Comparison

5.3.1 S-IVB Tank Comparison

The mathematical formula for loading dependence was applied to the calculation of the response of the 1/20 scale S-IVB model tanks. The tank was analyzed for the following system parameters:

- A. Frequency Range: 2 - 4 GHz
- B. Dielectric: Benzene, $\epsilon_r = 2.28$, $Q = 6500$
- C. External "Q": 2000, 2500, 3000
- D. Tank Volume: 29 Liters

The system "Q" was measured as varying from 1000 to 2500 as reported in Section 4.3. An average "Q" value would fall around 1750 for the tank fully loaded. The "Q" of Benzene is 6500, and the external "Q" is 2500. For the mathematical formula:

$$N = N' \left[1 - \exp\left(\frac{-Q}{3N'}\right) + \frac{Q}{3N'} E_1\left(\frac{Q}{3N'}\right) \right]$$

N is calculated at each end of the frequency band (N_2 and N_1), and the difference found ($N_2 - N_1$) giving the number of detectable resonances in the band. The maximum number of resonances N' is given by:

$$N' = \frac{8\pi}{3} \frac{V}{c^3} f^3 (1 + (\epsilon_r^{3/2} - 1) \alpha)$$

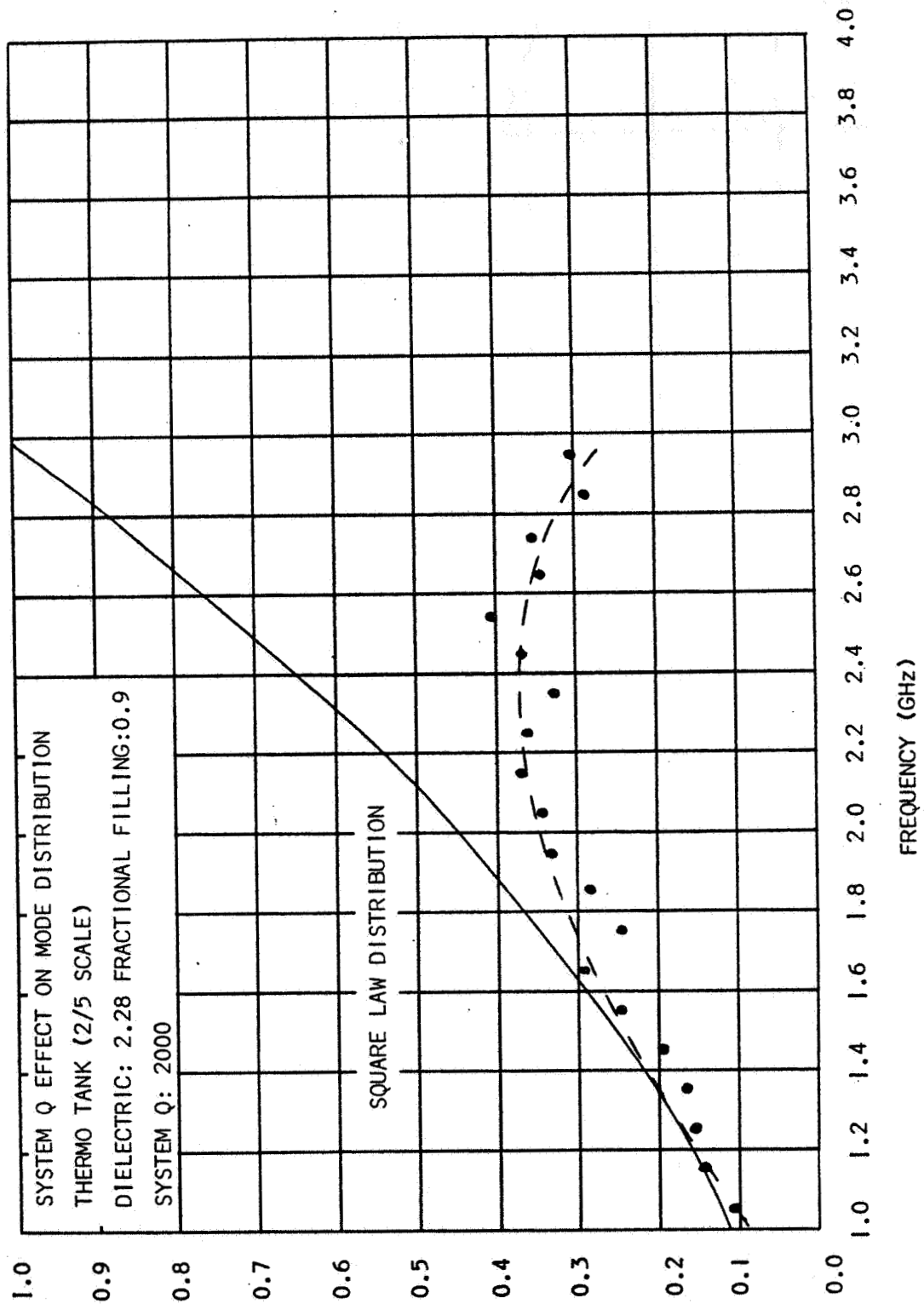


FIGURE 5-4

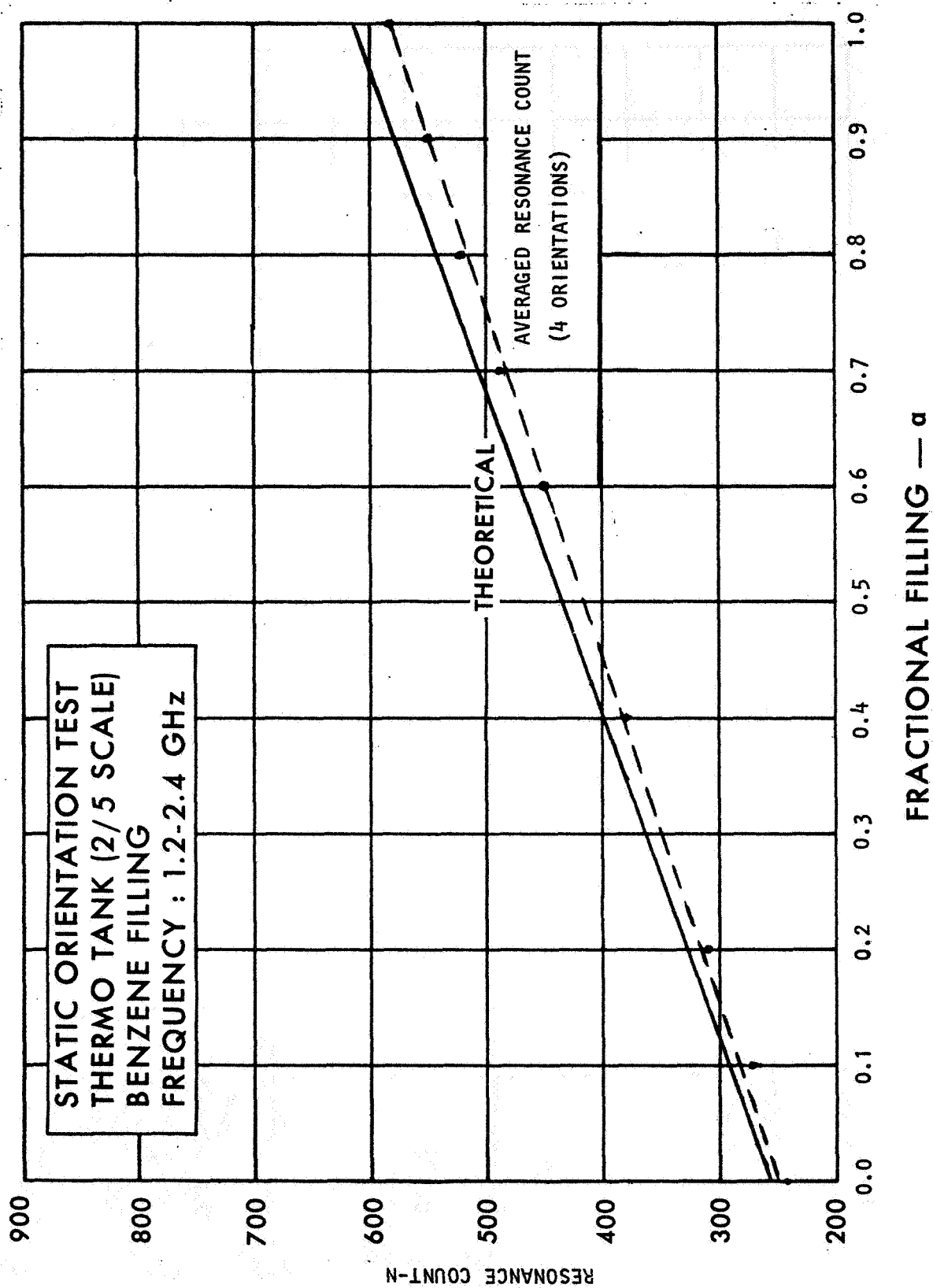


FIGURE 5-5

and

$$Q_{\text{dielectric}} = \frac{\epsilon_1' + (\epsilon_2' - \epsilon_1') \alpha}{\epsilon_1'' + (\epsilon_2'' - \epsilon_1'') \alpha}$$

The dielectric "Q" here is assumed to vary from that for the tank full of gas ($\alpha = 0$) to the tank full of liquid ($\alpha = 1$).

The result of the calculation is shown in Figure 5-6 for empty tank "Q"'s of 2000, 2500 and 3000. The calculated response is bowed, while the experimental response is linear. The bow in the calculated response is due to the way the average "Q" is assumed to vary with tank content, and the loading response with lower or higher "Q" dielectrics must be looked at to see if the predicted response fits these situations better.

5.3.2 Loading Response Spacecraft Tank

To check the predicted loading response for lower "Q" dielectrics or other tank external "Q" values, a cigar-shaped model spacecraft tank was analyzed. Experimental data was available for this tank from the Phase A studies. The tank was analyzed for the following parameters.

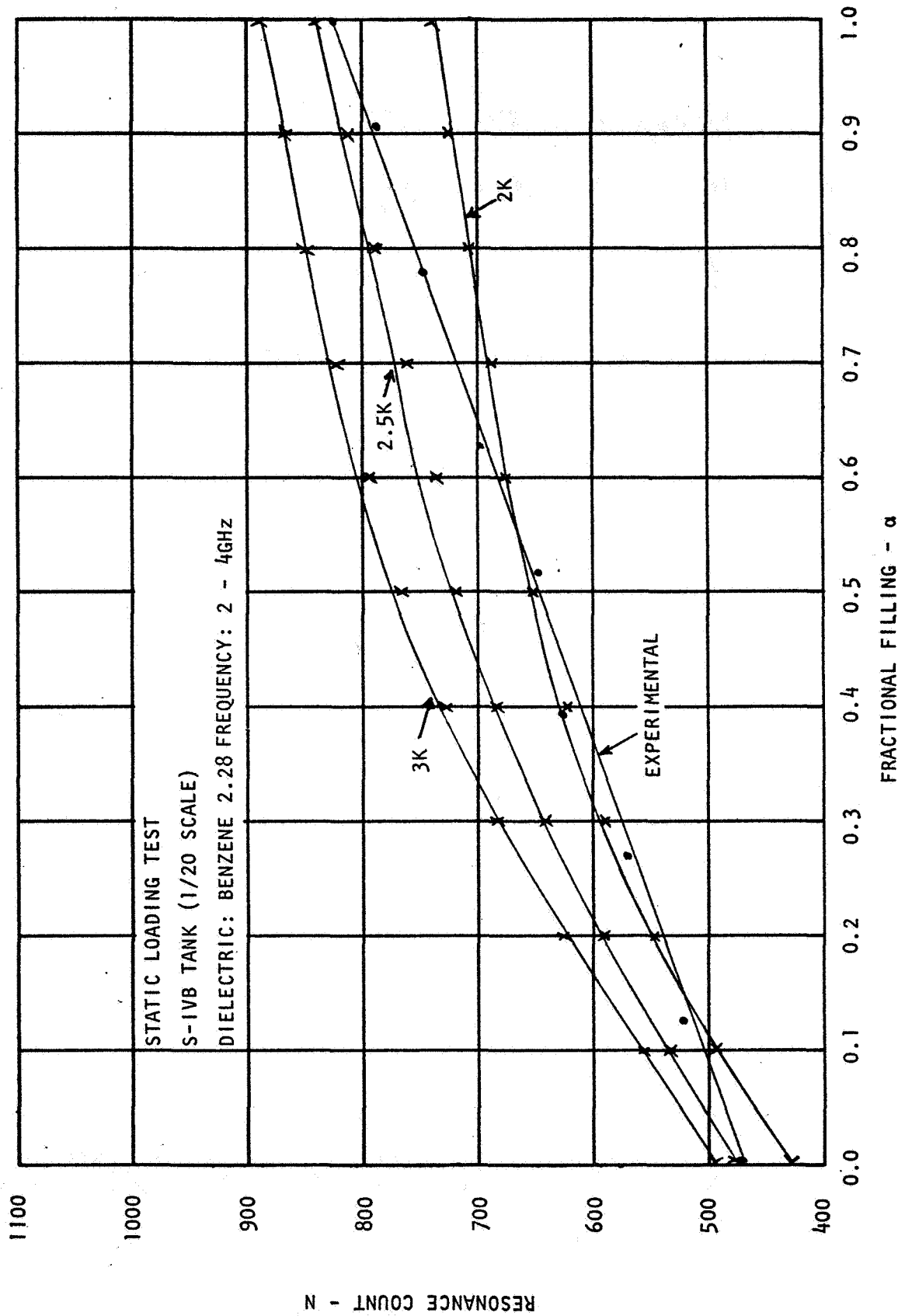
- A. Frequency Range: 2 - 4 GHz
- B. Dielectrics:
 - Benzene $\epsilon_r = 2.28$, $Q = 6500$
 - Freon $\epsilon_r = 2.425$, $Q = 87$
 - Polystyrene $\epsilon_r = 1.925$, $Q = 240$
- C. External "Q": 4000
- D. Tank Volume: 59 Liters

The comparison of the predicted and experimental response for these dielectrics is shown in Figures 5-7 to 5-10. The comparison for the loading shows a predicted response somewhat higher and more bowed than the experimental data. It is thought, that the experimental excitation method used (transmission type) achieved only fair resonance detectability, and thus, the experimental response would be below the predicted response. For the Freon and Polystyrene dielectric loadings, the form of the predicted response is similar to the experimental and somewhat higher. Again, this could be due to poor resonance detection for the transmission excitation method.

5.3.3 Loading Response 1/3 Scale THERMO

A tank of a different shape than the previous two, and having a different external "Q", was the 1/3 scale THERMO tank. The tank was analyzed for the following parameters:

- A. Frequency Range: 2 - 4 GHz
- B. Dielectric:
 - LH₂ $\epsilon_r = 1.23$, $Q = 1 \times 10^7$
 - LN₂ $\epsilon_r = 1.428$, $Q = 2.34 \times 10^4$
 - Benzene $\epsilon_r = 2.28$, $Q = 6500$



FM-40

FIGURE 5-6

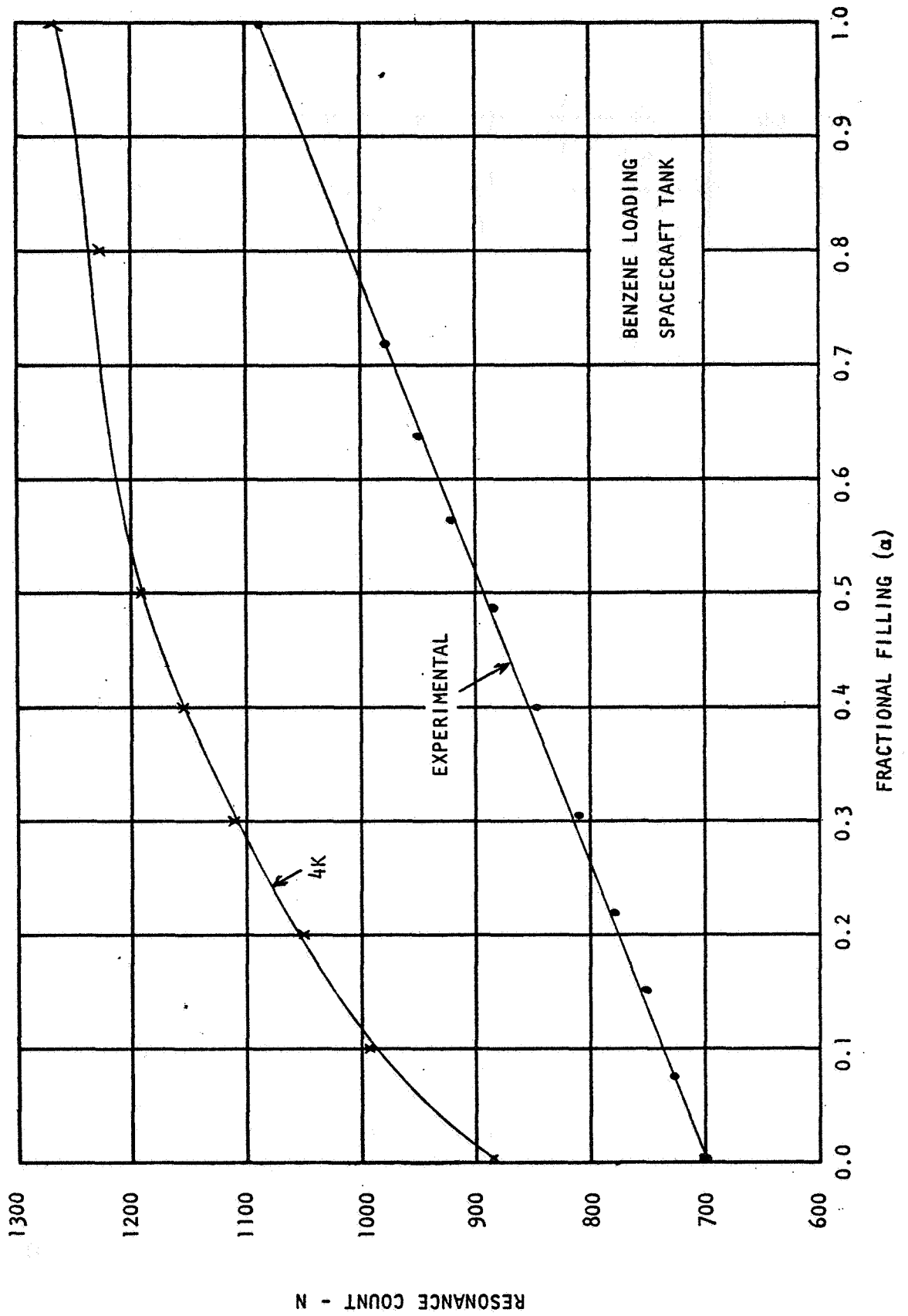
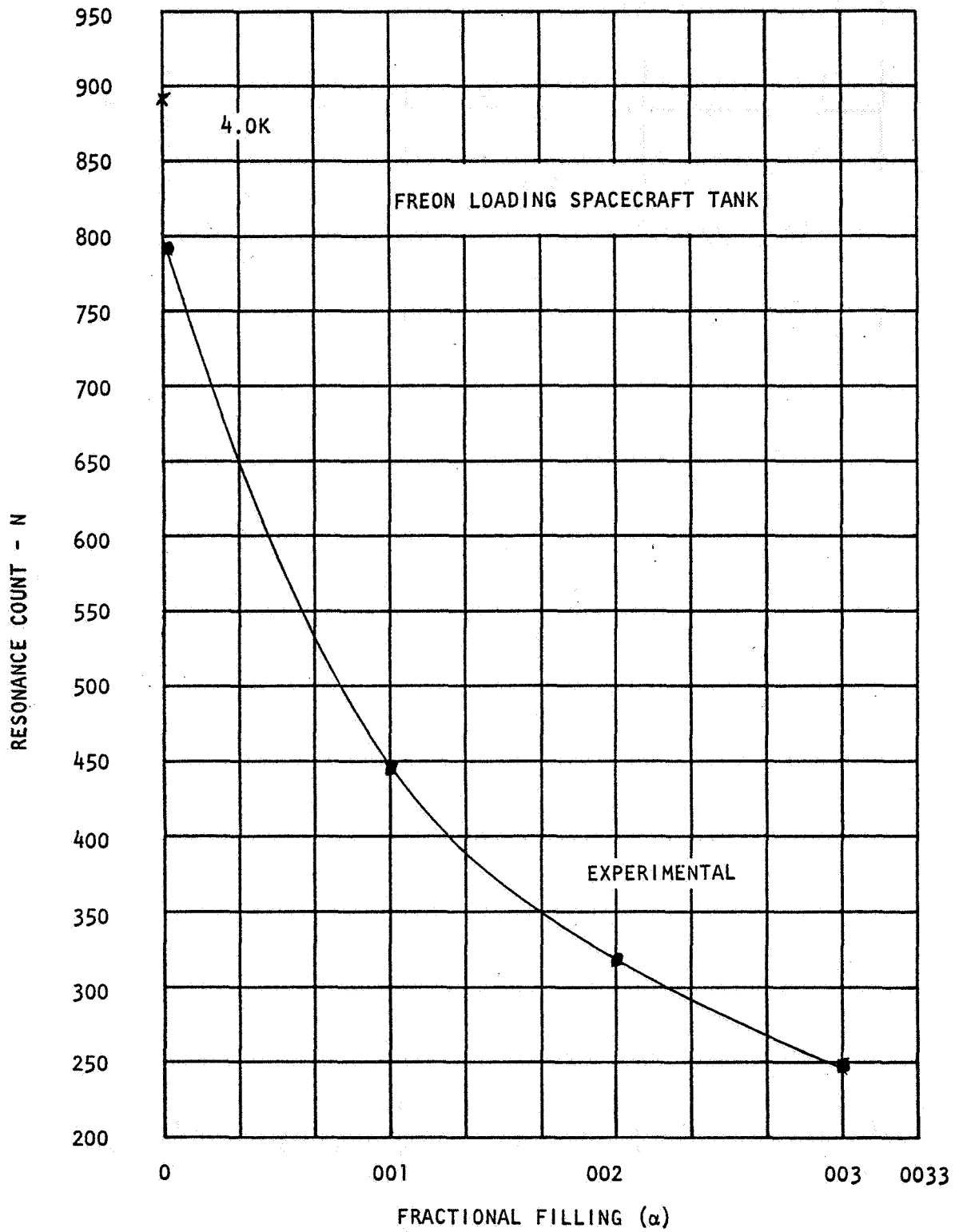
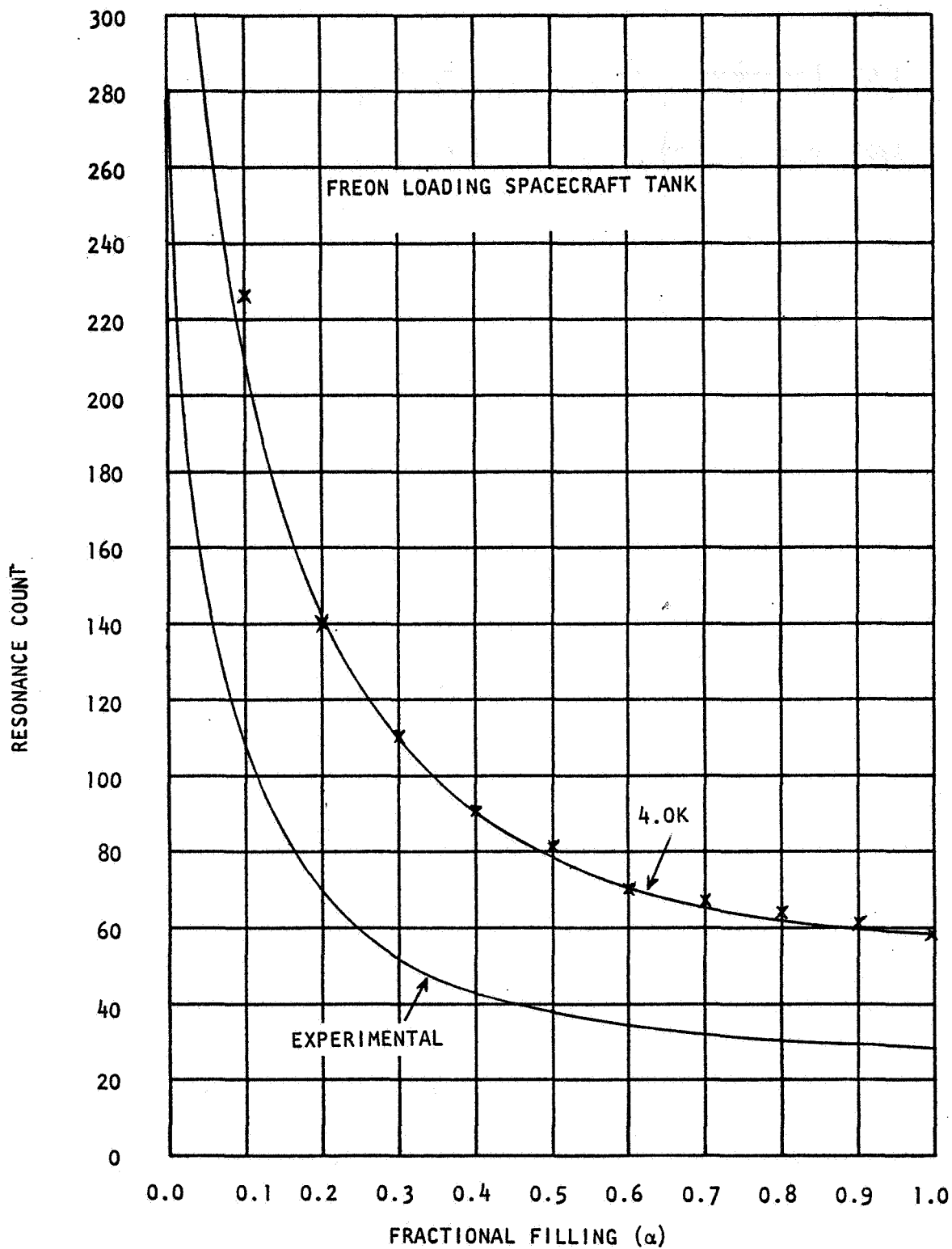


FIGURE 5-7



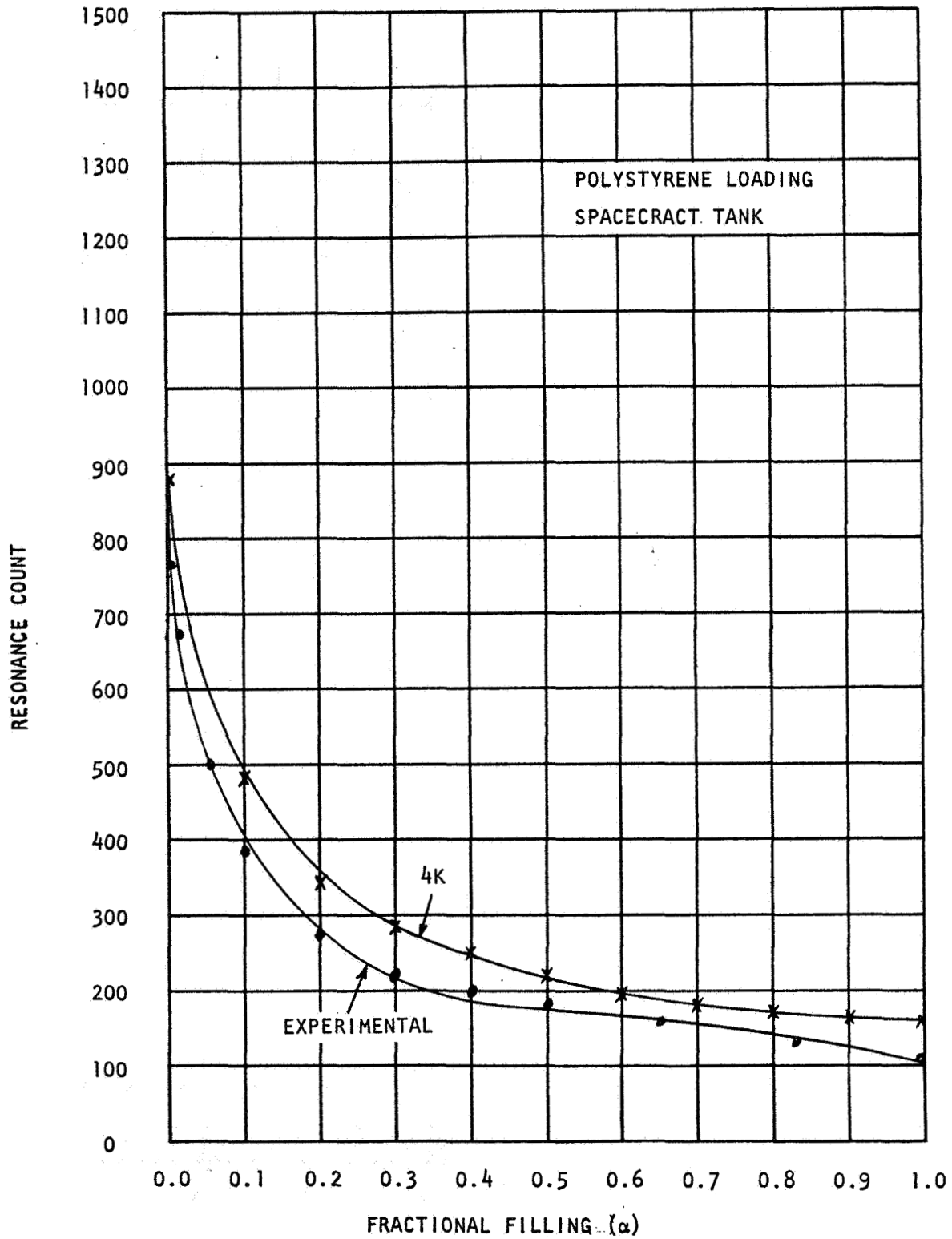
FM-42

FIGURE 5-8



FM-43

FIGURE 5-9



FM-44

FIGURE 5-10

- C. External "Q": 4500
- D. Tank Volume: 37.4 Liter

A comparison was made between the computer prediction and the mathematical prediction for LH_2 as no experimental data was available for LH_2 in this tank (Figure 5-11). However, the computer prediction for this tank was compared to experimental data for the simulated spacecraft tank (Figure 5-3). It is apparent that a difference does exist in the slopes of the two prediction techniques. Just how much this difference matters for predicting the SST response with LH_2 , must be seen from the application of the mathematical formula to the SST. Of interest here, also, is the fact that the loading response predicted by the mathematical formula is linear in contrast to the bowed response shown for Benzene in other tanks or this tank.

The mathematical prediction for LN_2 in this tank is almost parallel, but bowed in comparison to the experimental response (Figure 5-12). The difference in the number of resonances, is probably due to non-optimum excitation. Usually only about 90% of the predicted response is achieved and this seems to be sufficient to keep the response approximately constant with dielectric relocation in the tank. Again, the mathematical formula response is not as high as that of the computer formula, and tends to parallel the actual data better.

For Benzene loading the "Q" external equal to 4500 does not quite parallel the experimental data, and is bowed (Figure 5-13). The experimental response is lower than the predicted response as has been found for the tanks previously analyzed.

5.3.4 Loading Dependence Of Simulated Spacecraft Tank

The Dewar used to simulate the spacecraft tanks was analyzed for LH_2 and Benzene loading dependencies. The tank parameters were:

- A. Frequency Range: 2.8 - 4.0 GHz
- B. Dielectric: $\text{LH}_2 \quad \epsilon_r = 1.23, Q = 1 \times 10^7$
Benzene $\epsilon_r = 2.28, Q = 6500$
- C. External "Q": 2500, 4000, 4500, 5000
- D. Tank Volume: 27.8 Liter

Several different external "Q" values were used to show the difference in the predicted response with each "Q" value.

The predicted response with LH_2 is shown in Figure 5-14, and is roughly parallel to the experimental response for external "Q" values of 4500 and 5000. The use of an external "Q" of 2500 is too low to agree with the data. In later experiments, the empty tank count was raised to 315 with Benzene. Here the Benzene response moved up roughly parallel to itself, thus, if the LH_2 experimental response is moved up to correspond to a

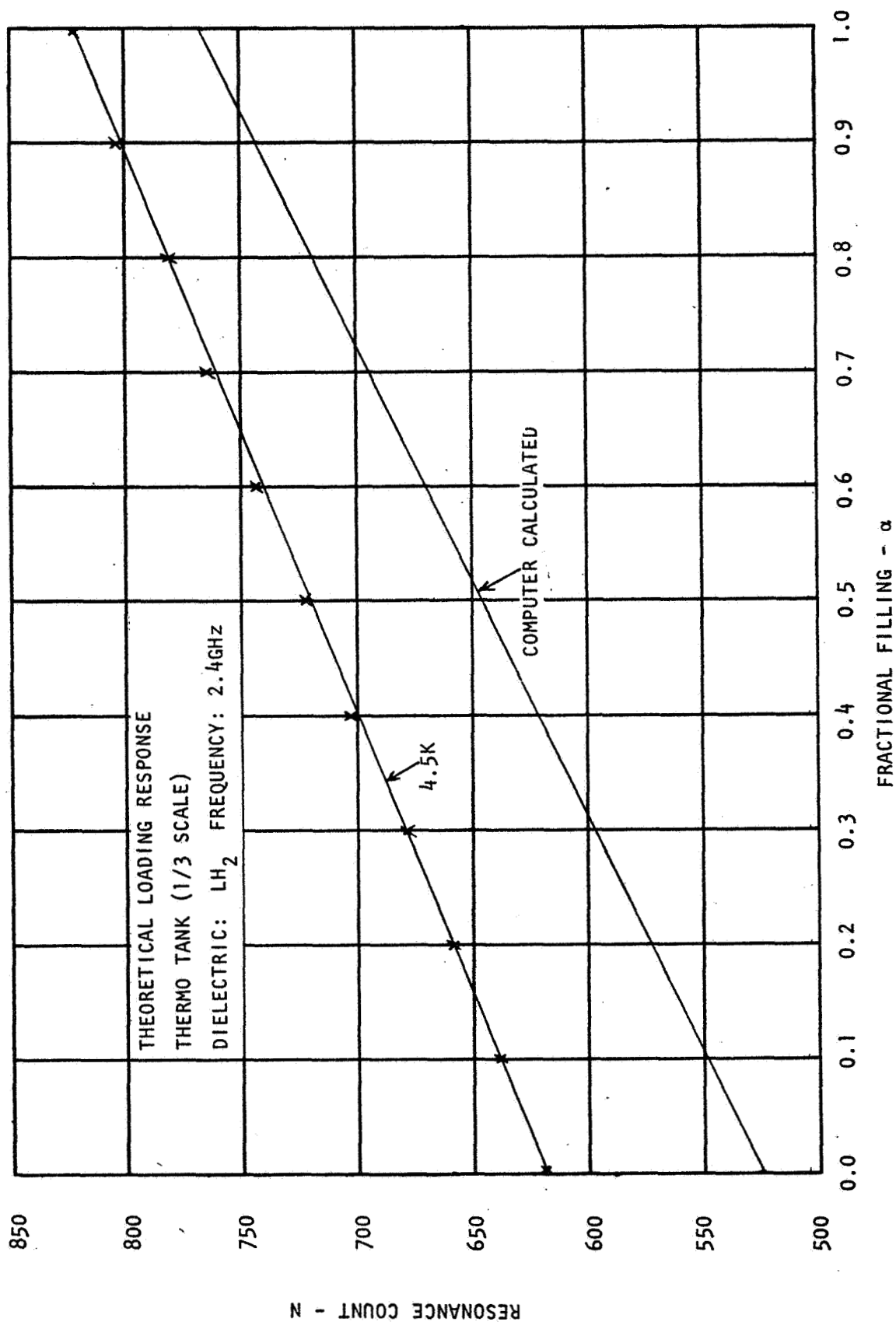
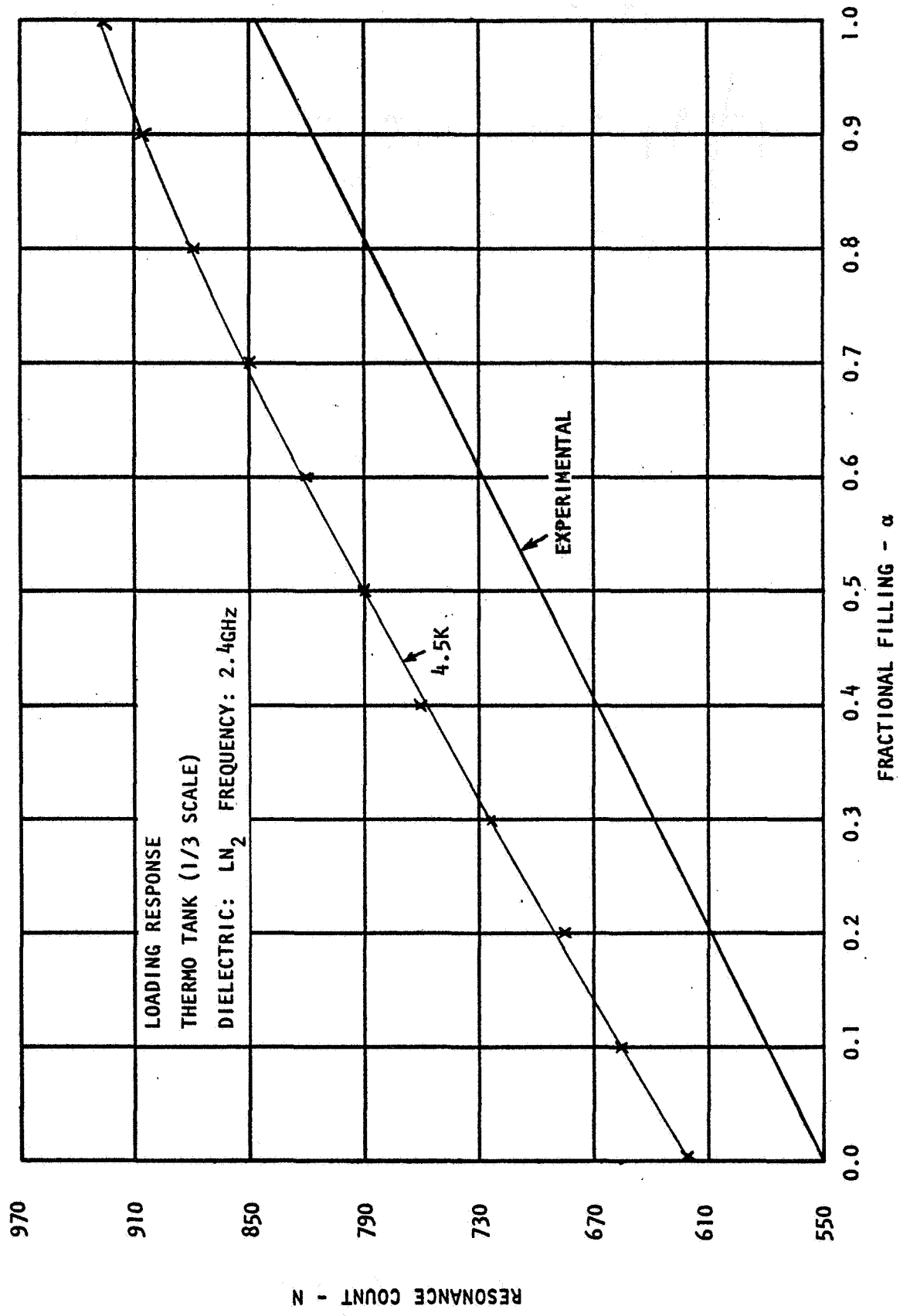


FIGURE 5-11



RESONANCE COUNT - N

FIGURE 5-12

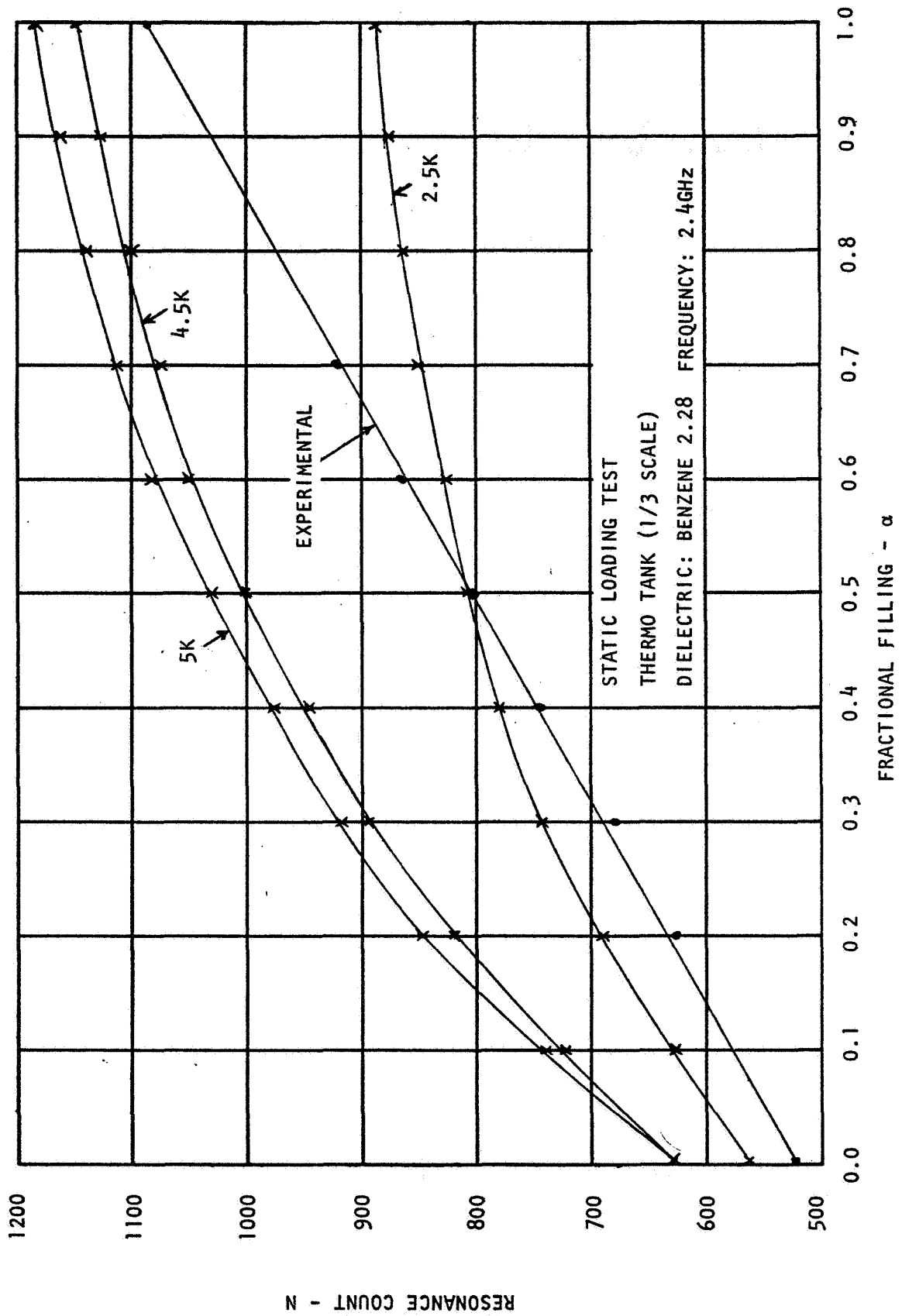


FIGURE 5-13

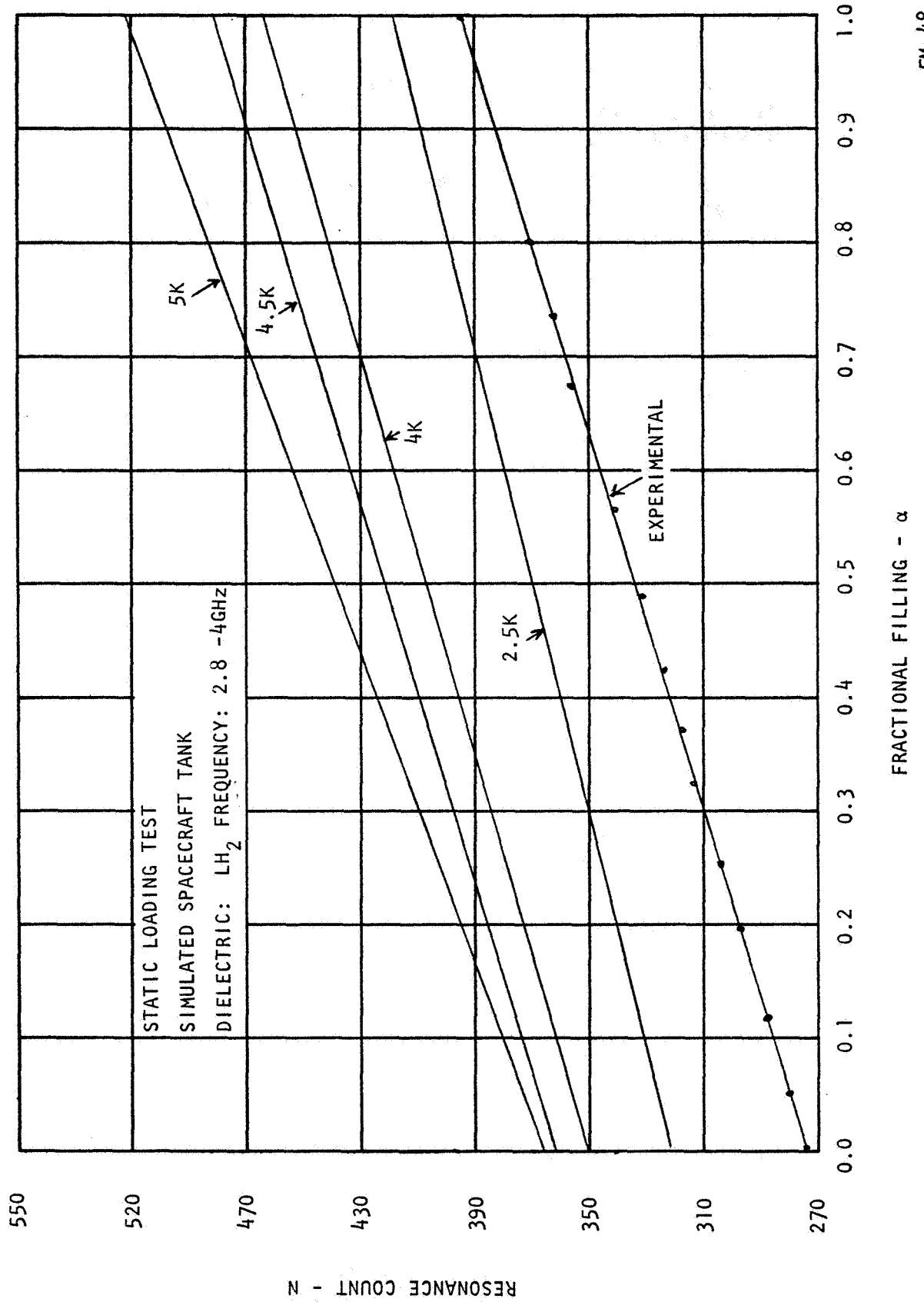


FIGURE 5-14

count of 315 empty, a better agreement is found between the magnitude of the predicted and experimental response. The measured empty tank external "Q" was 5100 which is close to the 4500 and 5000 used for the predicted response curves.

For Benzene loading, the predicted loading response is parallel, but bowed for an external "Q" of 4500 and 5000. The predicted response for "Q" of 2500 is too low to agree with the experimental loading response (Figure 5-15)

5.3.5 Loading Response 2/5 Scale THERMO Tank

A loading response was calculated for the 2/5 scale THERMO tank loaded with Benzene. The tank parameters were as follows:

- A. Frequency Range: 1.0 - 2.4 GHz
1.2 - 2.4 GHz
- B. Dielectric: Benzene $\epsilon_r = 2.28$, $Q = 6500$
- C. External "Q": 2000, 2500, 5000
- D. Tank Volume: 69.5 Liter

A measurement of the external tank "Q" of the empty tank gave an average value of 2100 over the frequency range of interest. The loading response was calculated with different external "Q" values to show the difference in predicted response. These predicted responses with Benzene are shown in Figures 5-16 and 5-17. In each case, the predicted response of the 2000 and 2500 "Q" values lie on either side of the experimental response for a full tank. Thus, it appears that a loading prediction for an external "Q" of 2100 would give a fair agreement with the experimental results. Also, the predicted response for "Q" of 5000 is not parallel to the experimental data emphasizing the better fit of the lower "Q" value.

5.4 Conclusion

While a great number of comparisons of the computer calculation and the mathematical formula to experimental data have not been presented, there are a sufficient number available to make preliminary conclusions.

The loading response of the mathematical formula parallels the experimental data better than the computer calculation. Some bowing exists in the predicted loading response of the mathematical formula, which is not present in the experimental response. This formula, however, is felt to be more realistic in taking into account the variation in the average system "Q" between the empty and full tank case than the computer calculation fits which were made for constant system "Q" values. The cases where either the dielectric "Q" or external "Q" largely determine the system "Q", give better correspondence between the mathematical formula and the experimental data than the case where both factors must be considered. However, in the latter case, where upward bowing occurs, if a straight line were drawn between the empty tank and full tank predicted response, a good correspondence would exist between the form of the predicted and experimental loading response.

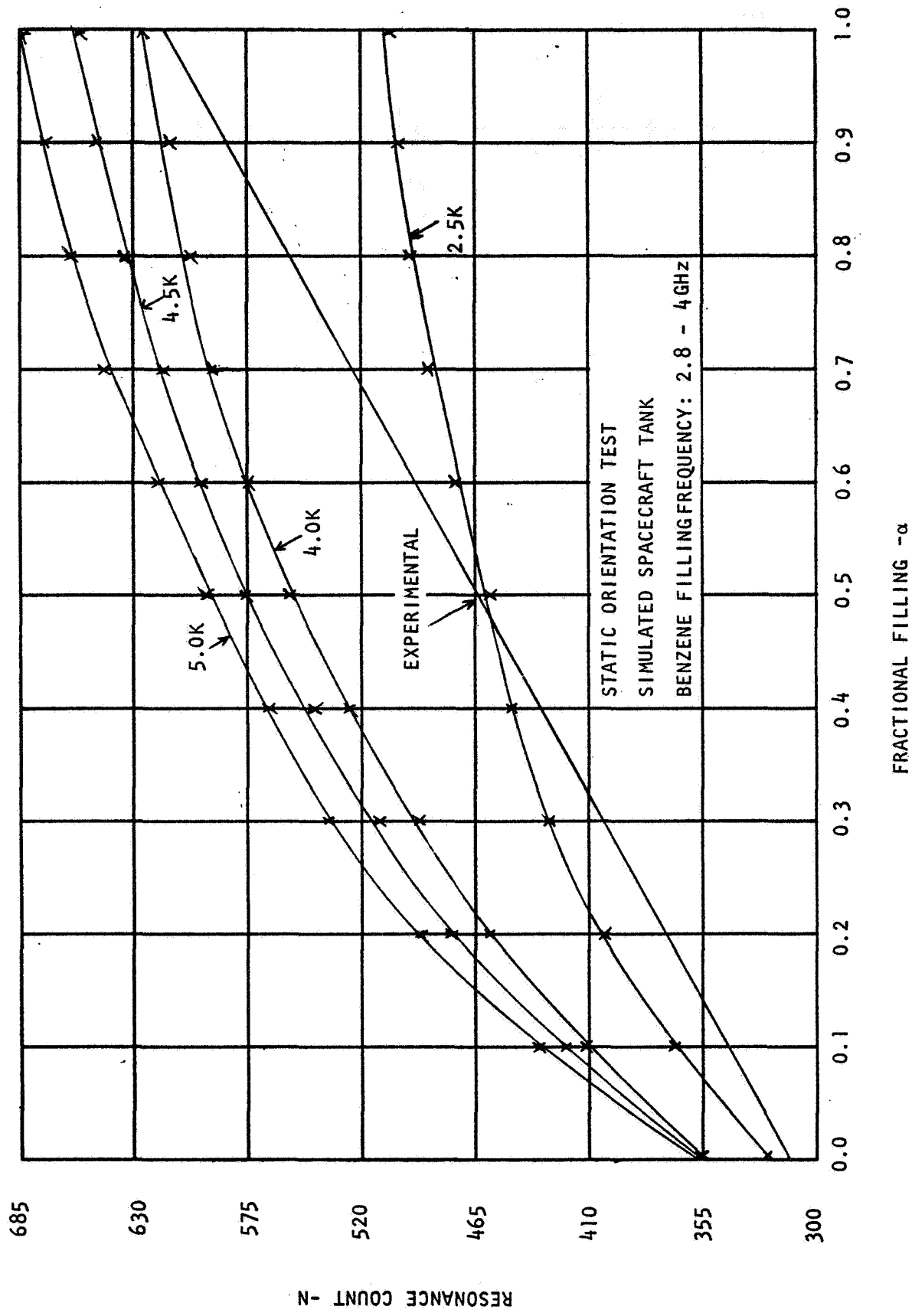


FIGURE 5-15

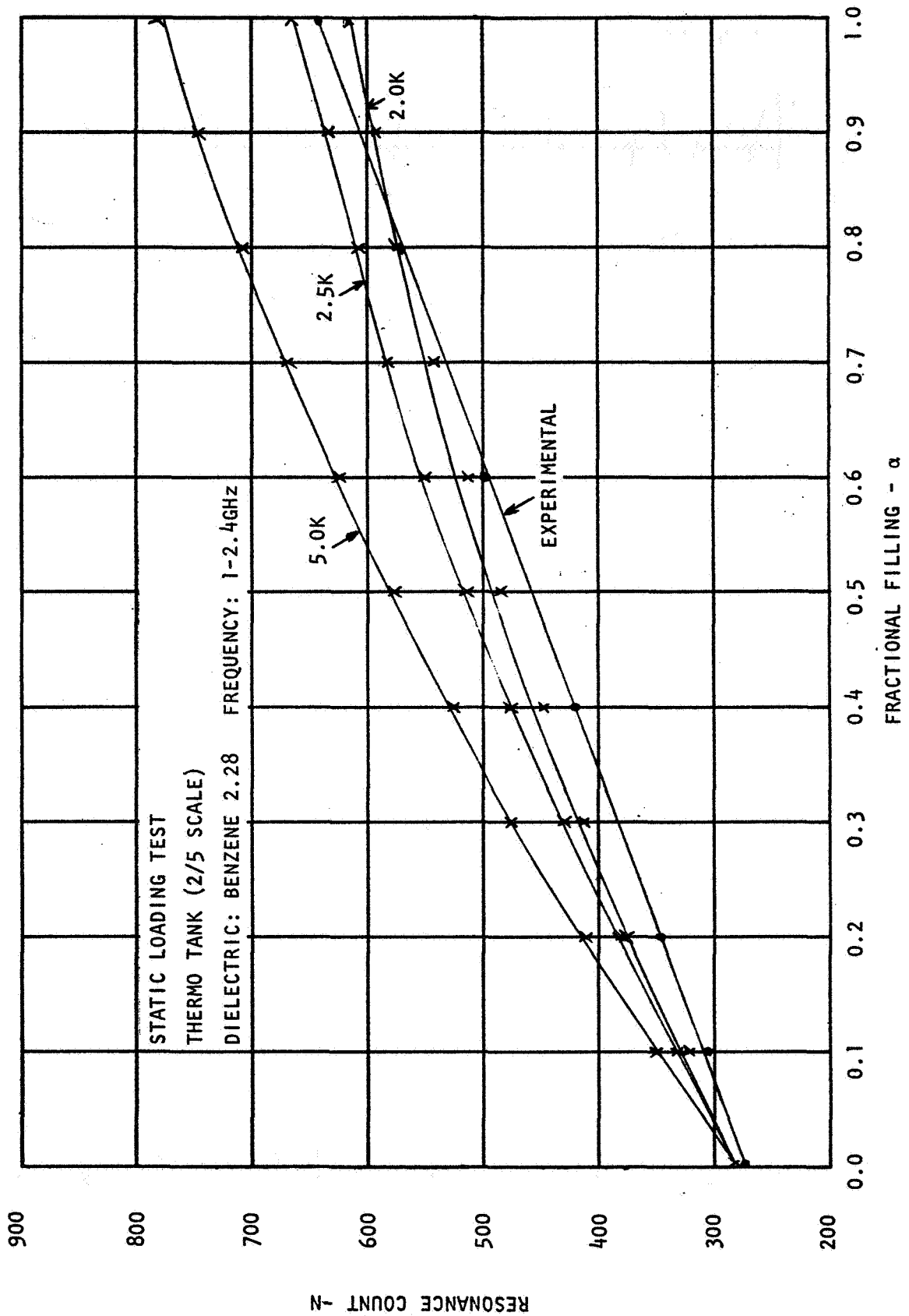


FIGURE 5-16

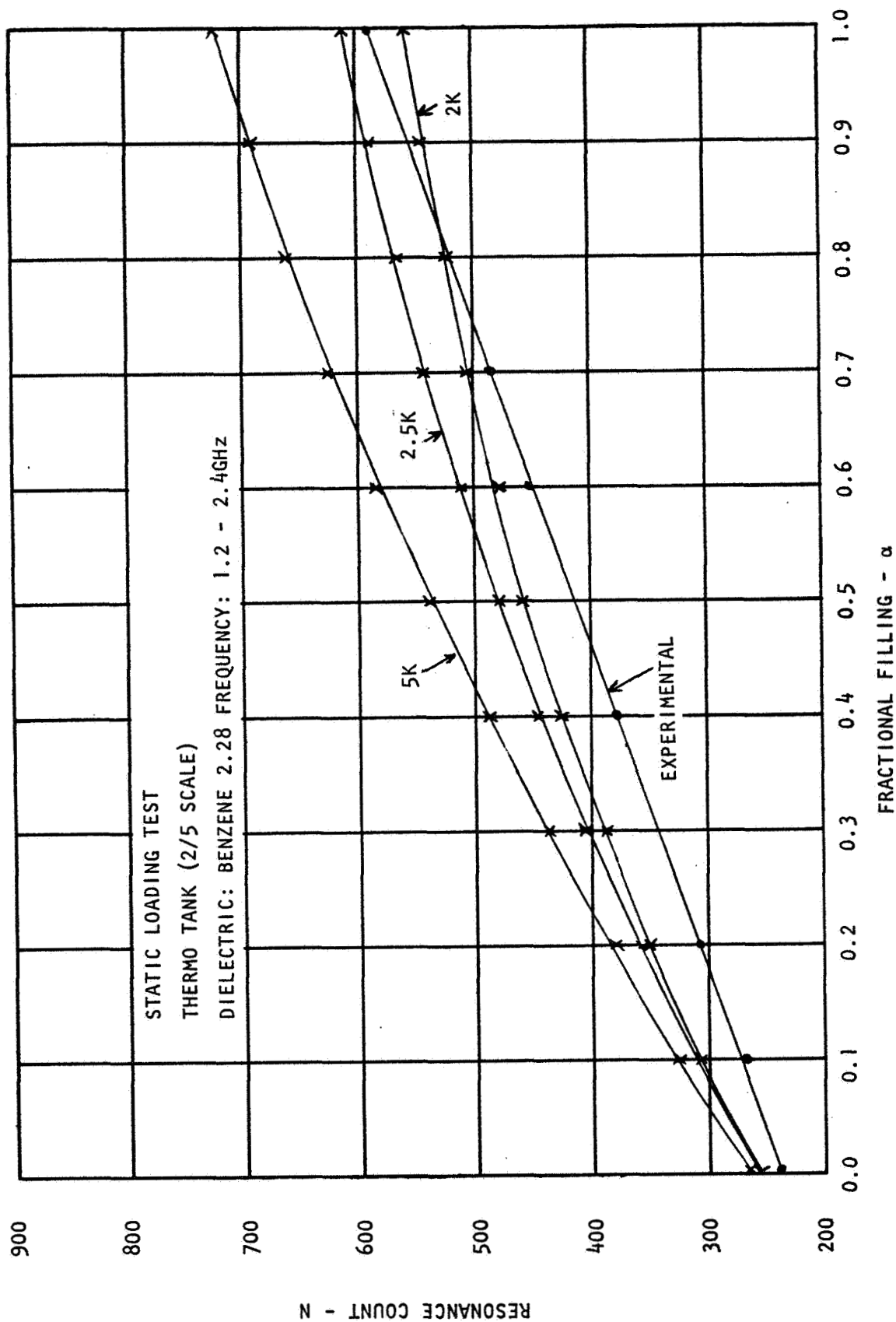


FIGURE 5-17

In conclusion, it appears that the mathematical formula for the prediction of tank loading response can be used in place of the computer calculation. In addition, much time and labor can be saved in using the mathematical formula in place of the computer calculation, because of its compact form and general applicability.

SECTION VI

GENERALIZED RF GAGING HANDBOOK

The purpose of the Phase B study program can be summarized as the development of system parameters and specifications that specify the use and limitations of a Radio Frequency Gaging System for generalized tank configurations.

The basic theory developed in Phase B permits the solution of the modes that exist in the following tank geometries:

- a) rectangular tank
- b) cylindrical tank
- c) spherical tank
- d) tanks that are volumes of revolution

The theory outlines mode solutions for all generalized spacecraft tanks, including tanks with re-entrant sections such as the S-IVB and THERMO tanks. The use of the statistical program allows for the inclusion of the physical effect of system "Q", and provides a means of determining optimum frequency band of operation as well as loading dependence. The simulation of the S-IVB and THERMO tanks by the use of equivalent cylindrical tanks (volume and L/D ratio), provides a simple means of solving for the number of resonances within the tanks.

The experimental work coupled with the theoretical work developed in Phase B permits the formulation of design parameters that specify the use and limitations of the R.F. Gaging System.

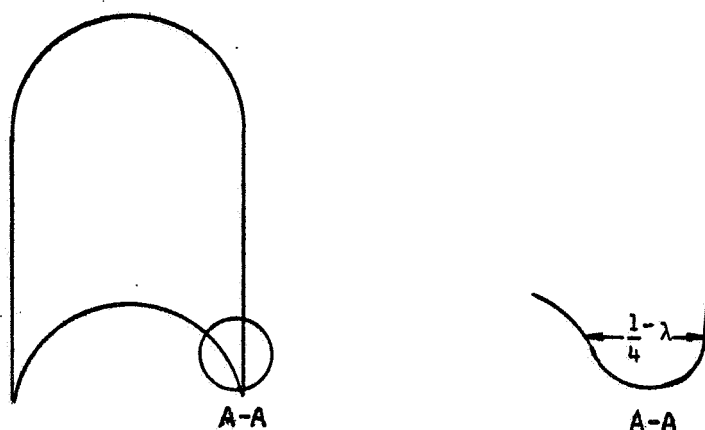
A. Tank Configurations

The R.F. Gaging System can be used to gage the following tanks under zero gravity conditions if the tank can be properly illuminated (dependent upon configuration and use of re-entrant sections) with R.F. energy i.e., 90% of the theoretical maximum empty tank resonance count is obtainable:

- a) rectangular tanks
- b) cylindrical tanks
- c) spherical tanks
- d) cylindrical tank with one hemisphere
- e) cylindrical tank with two hemispheres
- f) tanks that are volumes of revolution
- g) S-IVB tanks
- h) THERMO tank

Tanks that have reentrant sections should be analyzed using the volumes of revolution theory to insure that none of the RF energy is dissipated in the reentrant section. In general, if the reentrant section is concaved outward, the RF energy can be reflected and a matched condition achieved.

A good design rule is that the reentrant section should be at least a quarter wavelength of the center frequency of the tank's operating frequency band across the base of the section. A quarter wavelength (λ) at f_c was chosen since it is at this frequency that a large number of resonances are statistically orientated. It was found that a lower frequency is too restrictive. Figure 6-1 illustrates the results developed over a statistical value of many experiments.



DETAIL OF REENTRANT SECTION

FIGURE 6-1

Internal metallic perturbations tend to assist the operation of the mass gage because they split mode degeneracies the computer programmer reveals exist in symmetrical sections. The use of stand pipes, wall spheres, vents, and temperature probes will not affect the RF system. Materials that have high losses (low Q's) including tank walls must be taken into consideration however. The low Q will modify the loading dependence and can be taken into account through use of the statistical computer program.

The basic volumes that can be gaged are dependent on the ability to completely illuminate the tank with RF energy and the frequency range of the RF oscillators available. The minimum volume that can be gaged is dependent on the availability of RF solid state sweep oscillators. With present state-of-the-art oscillators (1.5 to 3.6 GHz) a volume as small as 4,000 cubic inches can be gaged with ease. The maximum volume that can be gaged is dependent of the ability to uniformly illuminate the entire tank with RF energy. Experience leads Bendix to believe that tanks having volumes of approximately 25,000 cubic feet can be gaged using RF techniques.

B. Propellant Characteristics

Propellants having low loss tangents are ideally suited to be gaged using R.F. resonance counting techniques. The cryogenic propellants are in this class. Propellants having a high loss tangent can be gaged, but at a sacrifice of sensitivity once a 25 to 30% loading has been obtained. See Volume 1. The upper limit of loss tangent is approximately 10×10^{-4} therefore, the following propellants can be gaged satisfactorily:

MATERIAL	DIELECTRIC CONSTANT (ϵ)	LOSS TANGENT (δ)
Liquid Hydrogen	1.23	1×10^{-7}
Liquid Nitrogen	1.428	3×10^{-5}
Liquid Fluorine	1.52	3.5×10^{-5} *
Liquid Oxygen	1.510	9×10^{-4}

* Estimated

Again, other propellants can be gaged satisfactorily, using a multiple resonance counting technique if the propellant loss tangent is less than 10×10^{-4}

C. Loading Dependence

For a given tank and fluids, the R.F. parameters f_2 , f_1 , $N_{1,2}$ (empty), $N_{1,2}$ (full) can be determined as shown in Figures 6-2 and 6-3.

Using:

$$N' = \frac{8\pi}{3} \frac{V}{c^3} f^3 (1 + (\epsilon_r^{3/2} - 1) \alpha)$$

The intersection of this N' for $\alpha=1$ with $N'=Q/3$ is found. The Q used, is calculated from:

$$Q^{-1} = Q_{\text{external}}^{-1} + Q_{\text{dielectric}}^{-1}$$

$$= \frac{S\delta}{V} + \frac{\epsilon_1'' + (\epsilon_2'' - \epsilon_1'') \alpha}{\epsilon_1' + (\epsilon_2' - \epsilon_1') \alpha}$$

Where: V = Interior Tank Volume

S = Interior Tank Area

$\delta = e^{-1}$ Depth of Field Penetration Into Interior Wall

$$= \sqrt{\frac{2}{\sigma\mu\omega}}$$

σ = Wall Conductivity In MKS Units

μ = Wall Permeability In MKS Units

ω = Frequency In Radians

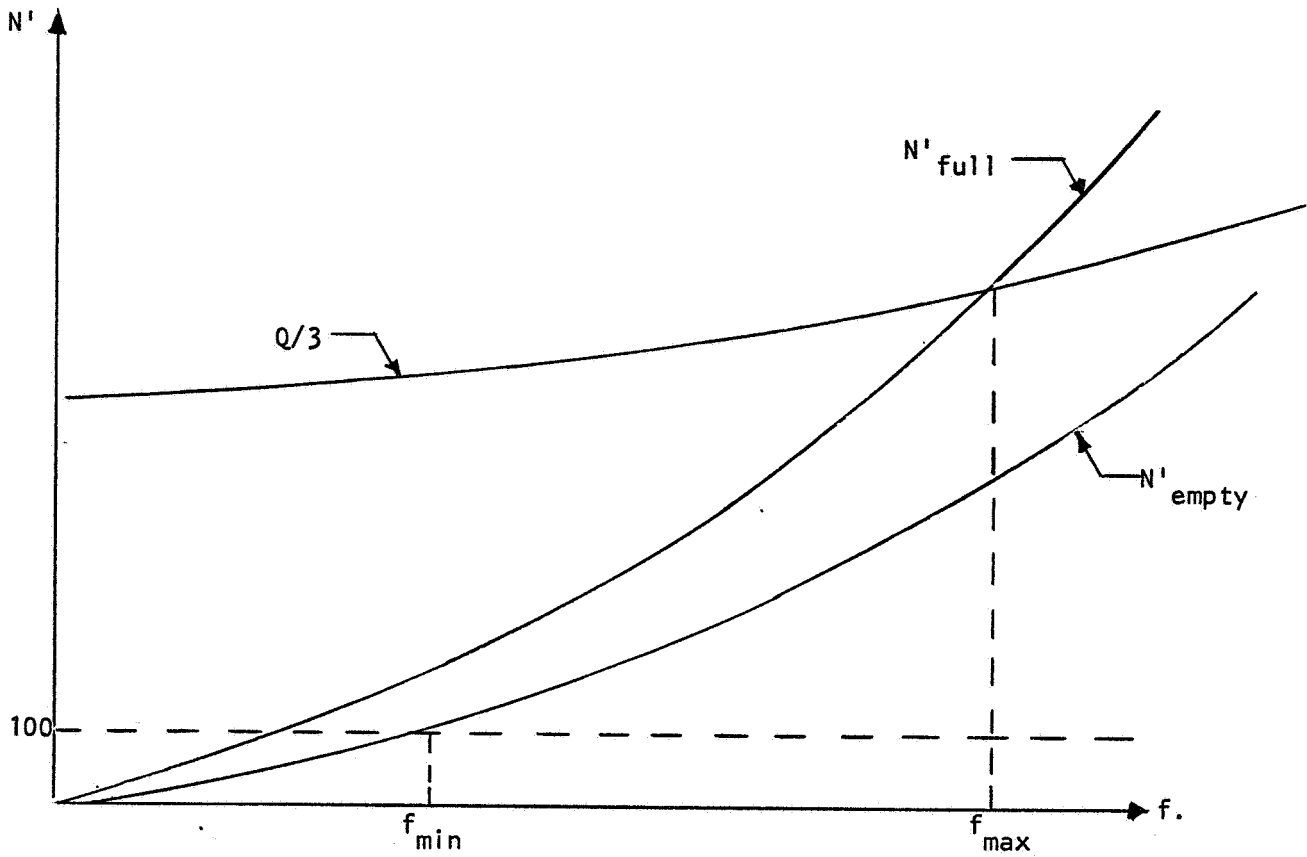


Figure 6-2 Illustration of f_{min} and f_{max} determination

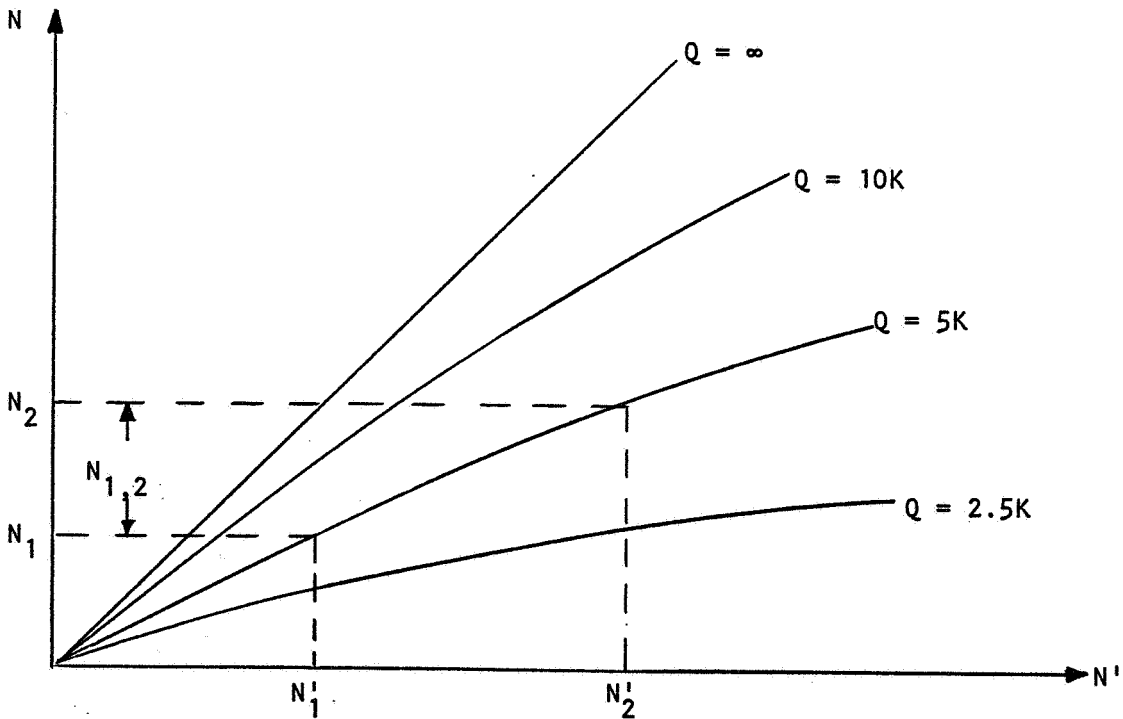


Figure 6-3 Determination of resonance count

$\epsilon_1', \epsilon_1''$ = Dielectric Constant And Dielectric Loss Factor of Gas

$\epsilon_2', \epsilon_2''$ = Dielectric Constant And Dielectric Loss Factor of Liquid

or known from measurements on the tank of interest in a filled condition. This determines the maximum desirable value of the upper frequency f_2 . Next the minimum desirable frequency f_1 , is calculated by setting $N' = 100$ with $\alpha = 0$. The difference between N_2' and N_1' should be at least 500 for the empty tank for a $\pm 2\%$ system accuracy. If it is not, f_2 should be increased until this number is reached.

Next, the loading characteristic for the tank is computed by allowing α to vary and using:

$$N = N' (1 - \exp(-x) + x E_1(x))$$

Where: $E(x) = -\gamma - \ln x - \sum_{n=1}^{\infty} \frac{(-1)^n x^n}{n! n}$

= Exponential Integral

γ = Euler's constant

= 0.5772

$x = Q/3N'$

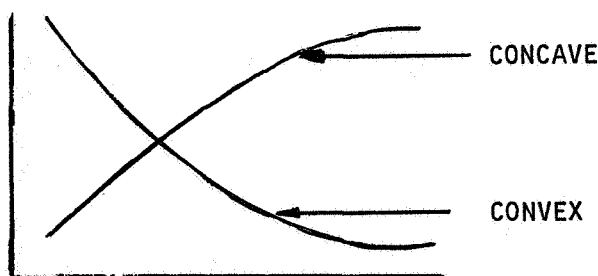
Here ω is chosen in the center of the frequency band for convenience in calculating Q_{external} . In this way:

$$N_{1,2} = N_2 - N_1$$

Where: $N_2 = N$ Calculated at f_2

$N_1 = N$ Calculated at f_1

may be calculated for the empty and full tank and the detectable resonance count difference between empty ($\alpha = 0$), and full ($\alpha = 1$) loading determined. This gives a quick calculation of the expected system resonance count sensitivity to propellant in the tanks. For low external tank Q and/or medium loss liquids such as LOX, the loading dependence will show a decreasing $N_{1,2}$ with α . This loading response curve of $N_{1,2}$ versus α is convex (Figure 6-4) with respect to the α axis. This predicted response is to be used as is. For a tank having a high external Q , and loaded with low loss liquids (LH_2 , LN_2 , LF_2) the plot of $N_{1,2}$ versus α is concave (Figure 6-4) with respect to the α axis.



LOADING RESPONSE $N_{1,2}$ CONCAVE AND CONVEX w.r.t. α AXIS

FIGURE 6-4

For this latter case, the concave curve is replaced by a straight line between the $N_{1,2}$ value at empty and full tank conditions.

For a great number of calculations of loading dependencies, a computer calculation may be made, using the previous mathematical formula for N versus N' at various Q values expected in practice. This may be plotted as shown in Figure 6-3 to obtain a universal curve for ready determination of the expected loading dependence of a tank and fuel.

SECTION VII CONCLUSIONS

From the theoretical analysis of the tanks studied and the experimental results of the tests conducted to verify the theoretical analysis, the following conclusions can be made:

- 1) The R.F. Gaging System is independent of propellant location within the tank to a degree sufficient to meet the basic sensitivity and accuracy design goals of $\pm 2\%$ of full tank mass content.
- 2) The R.F. Gaging System can be applied to a variety of tank and cryogenic propellant combinations. The tanks may have many different sizes.
- 3) Complex tanks such as the S-IVB and THERMO tanks can be simulated by the use of equivalent volumetric cylindrical tanks having similar "L/D" ratios for system optimization. Computer programs have been written that provide a means of determining an optimum frequency band and the loading dependence for the generalized tanks. These programs include the effect of the physical parameters on system "Q". An alternate and shorter computational procedure has been formulated which provides equivalent results by use of a mathematical formula.
- 4) The "no loss" loading dependence for tanks filled with a dielectric material is approximated by the mathematical formula:

$$a) \quad N = \frac{8\pi V}{3c^3} (f_2^3 - f_1^3) \left(1 + (\epsilon_r^{3/2} - 1) \alpha \right)$$

The loading dependence for tanks with "loss" is approximated by the mathematical formula:

$$b) \quad N = N_2 - N_1$$

$$\text{Where: } N_i = N_i' \left(1 - \exp\left(-\frac{Q}{3N_i'}\right) + \frac{Q}{3N_i'} \times E_1\left(\frac{Q}{3N_i'}\right) \right)$$

$$N_i' = \frac{8\pi}{3} \frac{V}{c} f_i^3 \left(1 + (\epsilon_r^{3/2} - 1) \alpha \right)$$

Q = Average system quality factor

E_1 = Exponential Integral

These approximation become better as the number of resonances excitable (N_i') for a given tank is increased.

- 5) The sampling time of the system will meet the desired response time of less than 0.5 seconds.
- 6) The implementation of the Radio Frequency Zero "G" Gaging System for space applications using present state-of-the-art components is feasible.

The basic objective of determining the feasibility of using a R.F. resonance counting technique to measure the propellant mass aboard an orbiting space vehicle has been proven. The R.F. Gaging System that was defined during the study will meet the design specifications.

SECTION VIII

RECOMMENDATIONS

During the performance of both Phase A and Phase B of the feasibility study, the need for the development of some state-of-the-art electronic hardware became necessary. The use of RF Gaging subsystems for test purposes during the feasibility study has emphasized the effort needed to produce a complete RF Gaging System suitable for space applications. While feasibility has been proven using laboratory equipment, the implementation of a complete RF Gaging System has not been accomplished. The Bendix Corporation recommends that in order to assure that a physically realizable RF Gaging System can be fabricated, a complete breadboard prototype system should be constructed. The necessity for development of a breadboard system can be justified on the basis of:

- 1) the technical hardware problems generated during the feasibility study, and
- 2) fabrication and testing of the entire system will completely specify the definition of a flight prototype system.

The proposed breadboard system is shown in Figure 8-1. It is recommended that a system consisting of these subassemblies should be fabricated and tested with a scale model tank in order to reinforce the system specifications developed in Volume I, Appendix C. It is proposed that the breadboard system be implemented in a period of 3 months. This work will be broken down into the following three tasks:

1. Fabricate basic system.
2. Test subassemblies.
3. Test basic system.

The effort accomplished in this program will be used to prepare a report describing the characteristics of an RF Gaging System. Included in this report will be a new indication of any problem area which can be experienced in the implementation of a flight type prototype RF Gaging System.

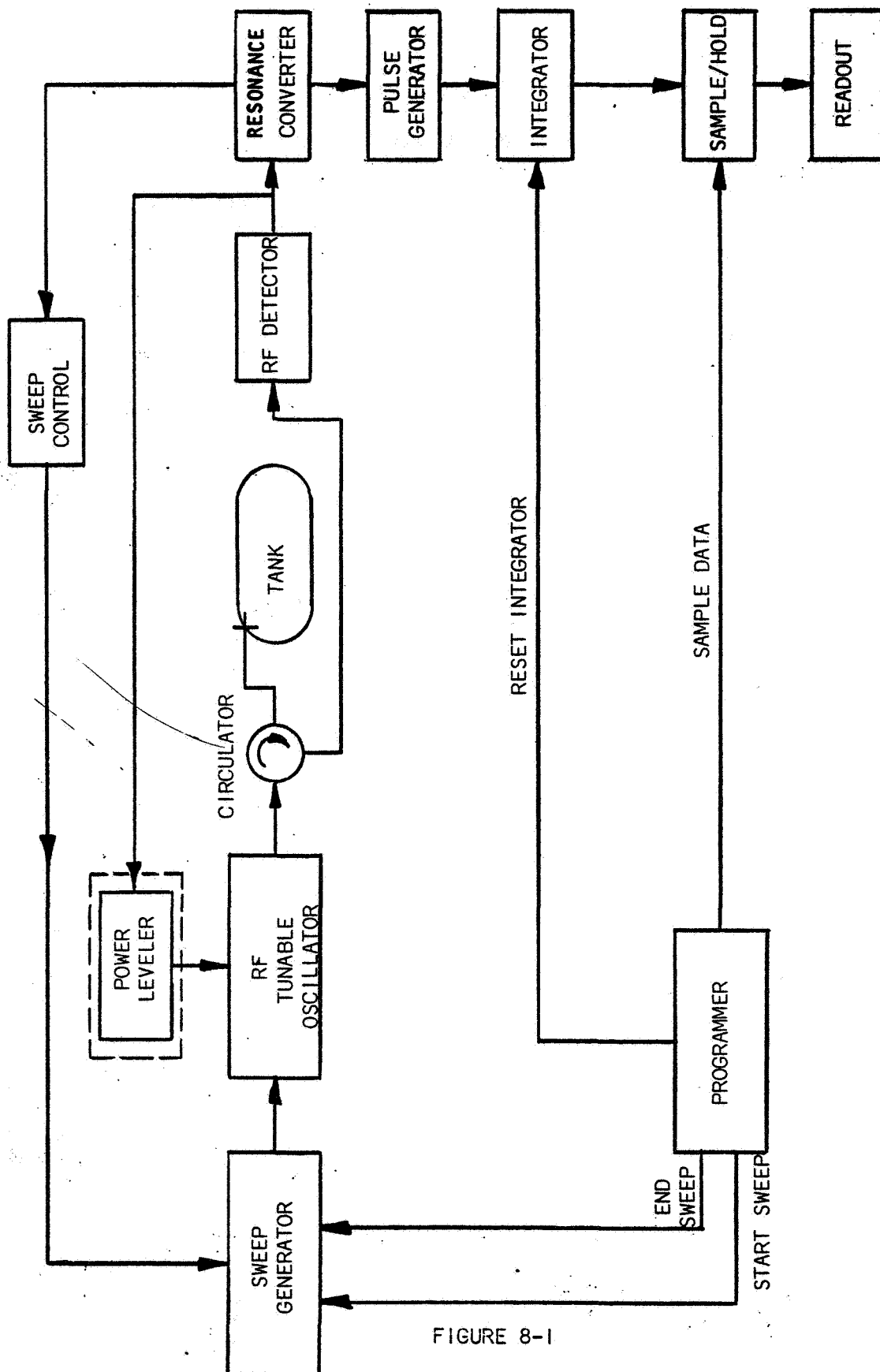


FIGURE 8-1

DETAILED BLOCK DIAGRAM OF RF SYSTEM

SECTION IX

REFERENCES

1. Harrington, R.F., Time-Harmonic Electromagnetic Fields, McGraw-Hill Book Co., New York, New York, 1961.
2. Roe, Glenn M., Frequency Distribution of Normal Modes, Volume 13, Number 1, The Journal of The Acoustical Society of America.
3. Jackson, Curtis C., Field and Wave Electrodynamics, McGraw-Hill Book Co., New York, New York, 1961.
4. Roder, H. M.; Webber, L. A.; Goodwin, R. D., The Thermodynamic Functions of Parahydrogen from the Triple Point to 100° K at Pressure up to 340 Atm., NBS Report 7639, January, 1963.
5. Moreno, T., Microwave Transmission Design Data, pp. 215, Dover Publications, New York, New York, 1958.
6. Technique of Microwave Measurements, Volume 11, pp. 662, MIT Radiation Laboratory Series, Boston Technical Publishers, Inc., Lexington, Massachusetts.
7. Waveguide Handbook, Volume 10, pp. 66, MIT Radiation Laboratory Series, Boston Technical Publishers, Inc., Lexington, Massachusetts, 1964.
8. Jahnke, Eugene; Emde, Fritz, Tables of Functions, pp. 143, Dover Publications, New York, New York, 1945.

APPENDIX A

THEORETICAL ANALYSIS OF CAVITIES

APPENDIX A

INTRODUCTION

This appendix consists of the theoretical analysis of the resonances for partially filled cavities. The analysis has been directed toward rectangular, cylindrical, and spherical cavities. The analysis provides the basic equations of resonance which may be solved to determine the number of resonances in any frequency band for any partial filling.

SECTION I THEORETICAL ANALYSIS OF A RECTANGULAR CAVITY

MICROWAVE THEORY BEHIND RECTANGULAR CAVITY

The theory is essentially that of R. F. Harrington's, adapted from waveguide to cavity. The important difference is the region where standing waves in the liquid are supported by exponential type solutions in the free space part of the cavity. For the computer program, all the variables must be real. Consequently, there are generally two cases to consider. The first is the simpler case of standing waves in both the liquid and air, and second, the case of standing waves in the liquid only.

Case 1. Resonances Having Standing Waves In Both The Liquid And Air

Here, using Harrington's notation, we assume ψ solutions for TM to x resonances as follows:

$$\psi_1 = C_1 \cos K_{x1} x \sin \frac{n\pi y}{b} \sin \frac{p\pi z}{c}$$

$$\psi_2 = C_2 \cos K_{x2} (a-x) \sin \frac{n\pi y}{b} \sin \frac{p\pi z}{c}$$

The wave equation gives:

$$K_{x1}^2 + \left(\frac{n\pi}{b}\right)^2 + \left(\frac{p\pi}{c}\right)^2 = \epsilon_r \left(\frac{\omega}{c}\right)^2 \quad (1a)$$

$$K_{x2}^2 + \left(\frac{n\pi}{b}\right)^2 + \left(\frac{p\pi}{c}\right)^2 = \left(\frac{\omega}{c}\right)^2 \quad (1b)$$

And the field components of interest are:

$$E_{y1} = \frac{-i}{j\omega\epsilon_1} C_1 K_{x1} \frac{n\pi}{b} \sin K_{x1} x \cos \frac{n\pi y}{b} \sin \frac{p\pi z}{c}$$

$$E_{z1} = \frac{-i}{j\omega\epsilon_1} C_1 K_{x1} \frac{p\pi}{c} \sin K_{x1} x \sin \frac{n\pi y}{b} \cos \frac{p\pi z}{c}$$

$$H_{y1} = \frac{p\pi}{c} C_1 \cos K_{x1} \sin \frac{n\pi y}{b} \cos \frac{p\pi z}{c}$$

$$H_{z1} = \frac{-n\pi}{c} C_1 \cos K_{x1} \cos \frac{n\pi y}{b} \sin \frac{p\pi z}{c}$$

$$E_{y2} = \frac{i}{j\omega\epsilon_0} C_2 K_{x2} \frac{n\pi}{b} \sin K_{x2} (a-x) \cos \frac{n\pi y}{b} \sin \frac{p\pi z}{c}$$

$$E_{z2} = \frac{i}{j\omega\epsilon_0} C_2 K_{x2} \frac{p\pi}{c} \sin K_{x2} (a-x) \sin \frac{n\pi y}{b} \cos \frac{p\pi z}{c}$$

$$H_{y2} = \frac{p\pi}{c} C_2 \cos K_{x2} (a-x) \sin \frac{n\pi y}{b} \cos \frac{p\pi z}{c}$$

$$H_{z2} = -\frac{n\pi}{b} C_2 \cos K_{x2} (a-x) \cos \frac{n\pi y}{b} \sin \frac{p\pi z}{c}$$

Continuity of E_y and E_z at $x=d$ gives:

$$\frac{-K_{x1}}{\epsilon_1} C_1 \sin K_{x1} d = \frac{K_{x2}}{\epsilon_0} C_2 \sin K_{x2} (a-d)$$

Continuity of H_y and H_z at $x=d$ gives:

$$C_1 \cos K_{x1} d = C_2 \cos K_{x2} (a-d)$$

Dividing these last two equations gives:

$$-K_{x1} \tan K_{x1} d = \epsilon_r K_{x2} \tan K_{x2} (a-d)$$

or

$$K_{x1} \sin K_{x1} d \cos K_{x2} (a-d) + \epsilon_r K_{x2} \cos K_{x1} d \sin K_{x2} (a-d) = 0 \quad (1c)$$

For Resonances TE to the x axis we assume:

$$\psi_1 = C_1 \sin K_{x1} x \cos \frac{n\pi y}{b} \cos \frac{p\pi z}{c}$$

$$\psi_2 = C_2 \sin K_{x2} (a-x) \cos \frac{n\pi y}{b} \cos \frac{p\pi z}{c}$$

The wave equation gives;

$$K_{x1}^2 + \left(\frac{n\pi}{b}\right)^2 + \left(\frac{p\pi}{c}\right)^2 = \epsilon_r \left(\frac{\omega}{c}\right)^2 \quad (2a)$$

$$K_{x2}^2 + \left(\frac{n\pi}{b}\right)^2 + \left(\frac{p\pi}{c}\right)^2 = \left(\frac{\omega}{c}\right)^2 \quad (2b)$$

and the field components become:

$$E_{y1} = \frac{p\pi}{c} C_1 \sin K_{x1} x \cos \frac{n\pi y}{b} \sin \frac{p\pi z}{c}$$

$$E_{z1} = -\frac{n\pi}{b} C_1 \sin K_{x1} x \sin \frac{n\pi y}{b} \cos \frac{p\pi z}{c}$$

$$H_{y1} = \frac{-1}{j\omega\mu_1} C_1 K_{x1} \frac{n\pi}{b} \cos K_{x1} x \sin \frac{n\pi y}{b} \cos \frac{p\pi z}{c}$$

$$H_{z1} = \frac{-1}{j\omega\mu_1} C_1 K_{x1} \frac{p\pi}{c} \cos K_{x1} x \cos \frac{n\pi y}{b} \sin \frac{p\pi z}{c}$$

$$E_{y2} = \frac{p\pi}{c} C_2 \sin K_{x2} (a-x) \cos \frac{n\pi y}{b} \sin \frac{p\pi z}{c}$$

$$E_{z2} = \frac{-n\pi}{b} C_2 \sin K_{x2} (a-x) \sin \frac{n\pi y}{b} \cos \frac{p\pi z}{c}$$

$$H_{y2} = \frac{1}{j\omega\mu_0} C_2 K_{x2} \frac{n\pi}{b} \cos K_{x2} (a-x) \sin \frac{n\pi y}{b} \cos \frac{p\pi z}{c}$$

$$H_{z2} = \frac{1}{j\omega\mu_0} C_2 K_{x2} \frac{p\pi}{c} \cos K_{x2} (a-x) \cos \frac{n\pi y}{b} \sin \frac{p\pi z}{c}$$

Continuity of E_y and E_z at $x=d$ gives:

$$C_1 \sin K_{x1} d = C_2 \sin K_{x2} (a-d)$$

Continuity of H_y and H_z at $x=d$ gives:

$$\frac{-C_1 K_{x1}}{\mu_1} \cos K_{x1} d = \frac{C_2 K_{x2}}{\mu_0} \cos K_{x2} (a-d)$$

Dividing these and putting $\mu_1 = \mu_0$ gives:

$$-K_{x1} \cot K_{x1} d = K_{x2} \cot K_{x2} (a-d)$$

or

$$K_{x1} \cos K_{x1} d \sin K_{x2} (a-d) + K_{x2} \sin K_{x1} d \cos K_{x2} (a-d) = 0 \quad (2c)$$

Thus, to get the TM Resonances, we solve equations (1a), (1b) and

(1c); for the TE Resonances we solve equations (2a), (2b) and (2c).

Case 2. Resonances Having Standing Waves In The Liquid Only.

Here, using Harrington's notation, we assume ψ solutions for TM to x resonances as follows:

$$\psi_1 = C_1 \cos K_{x1} x \sin \frac{n\pi y}{b} \sin \frac{p\pi z}{c}$$

$$\psi_2 = C_2 \cosh K_{x2} (a-x) \sin \frac{n\pi y}{b} \sin \frac{p\pi z}{c}$$

The wave equation now gives:

$$K_{x1}^2 + \left(\frac{n\pi}{b}\right)^2 + \left(\frac{p\pi}{c}\right)^2 = \epsilon_r \left(\frac{\omega}{c}\right)^2 \quad (3a)$$

$$-K_{x2}^2 + \left(\frac{n\pi}{b}\right)^2 + \left(\frac{p\pi}{c}\right)^2 = \left(\frac{\omega}{c}\right)^2 \quad (3b)$$

And the field components of interest are:

$$E_{y1} = \frac{-1}{j\omega\epsilon_1} C_1 K_{x1} \frac{n\pi}{b} \sin K_{x1} x \cos \frac{n\pi y}{b} \sin \frac{p\pi z}{c}$$

$$E_{z1} = \frac{-1}{j\omega\epsilon_1} C_1 K_{x1} \frac{p\pi}{c} \sin K_{x1} x \sin \frac{n\pi y}{b} \cos \frac{p\pi z}{c}$$

$$H_{y1} = \frac{p\pi}{c} C_1 \cos K_{x1} x \sin \frac{n\pi y}{b} \cos \frac{p\pi z}{c}$$

$$H_{z1} = \frac{-n\pi}{b} C_1 \cos K_{x1} x \cos \frac{n\pi y}{b} \sin \frac{p\pi z}{c}$$

$$E_{y2} = \frac{-1}{j\omega\epsilon_0} C_2 K_{x2} \frac{n\pi}{b} \sinh K_{x2} (a-x) \cos \frac{n\pi y}{b} \sin \frac{p\pi z}{c}$$

$$E_{z2} = \frac{-1}{j\omega\epsilon_0} C_2 K_{x2} \frac{p\pi}{c} \sinh K_{x2} (a-x) \sin \frac{n\pi y}{b} \cos \frac{p\pi z}{c}$$

$$H_{y2} = \frac{p\pi}{c} C_2 \cosh K_{x2} (a-x) \sin \frac{n\pi y}{b} \cos \frac{p\pi z}{c}$$

$$H_{z2} = \frac{-n\pi}{b} C_2 \cosh K_{x2} (a-x) \cos \frac{n\pi y}{b} \sin \frac{p\pi z}{c}$$

Continuity of E_y and E_z at $x=d$ gives:

$$\frac{C_1 K_{x1}}{\epsilon_1} \sin K_{x1} d = \frac{C_2 K_{x2}}{\epsilon_0} \sinh K_{x2} (a-d)$$

Continuity of H_y and H_z at $x=d$ gives:

$$C_1 \cos K_{x1} d = C_2 \cosh K_{x2} (a-d)$$

Dividing these gives:

$$\frac{K_{x1}}{\epsilon_1} \tan K_{x1} d = \frac{K_{x2}}{\epsilon_0} \tanh K_{x2} (a-d)$$

or

$$K_{x1} \sin K_{x1} d \cosh K_{x2} (a-d) - \epsilon_r K_{x2} \cos K_{x1} d \sinh K_{x2} (a-d) = 0 \quad (3c)$$

For resonances TE to the x axis we assume:

$$\psi_1 = C_1 \sin K_{x1} x \cos \frac{n\pi y}{b} \cos \frac{p\pi z}{c}$$

$$\psi_2 = C_2 \sinh K_{x2} (a-x) \cos \frac{n\pi y}{b} \cos \frac{p\pi z}{c}$$

The wave equation gives,

$$K_{x1}^2 + \left(\frac{n\pi}{b}\right)^2 + \left(\frac{p\pi}{c}\right)^2 = \epsilon_r \left(\frac{\omega}{c}\right)^2 \quad (4a)$$

$$-K_{x2}^2 + \left(\frac{n\pi}{b}\right)^2 + \left(\frac{p\pi}{c}\right)^2 = \left(\frac{\omega}{c}\right)^2 \quad (4b)$$

and the field components become:

$$E_y = \frac{p\pi}{c} C_1 \sin K_{x1} x \cos \frac{n\pi y}{b} \sin \frac{p\pi z}{c}$$

$$E_z = \frac{n\pi}{b} C_1 \sin K_{x1} x \sin \frac{n\pi y}{b} \cos \frac{p\pi z}{c}$$

$$H_y = \frac{-1}{j\omega\mu_1} C_1 K_{x1} \frac{n\pi}{b} \cos K_{x1} x \sin \frac{n\pi y}{b} \cos \frac{p\pi z}{c}$$

$$H_z = \frac{-1}{j\omega\mu_1} C_1 K_{x1} \frac{p\pi}{c} \cos K_{x1} x \cos \frac{n\pi y}{b} \sin \frac{p\pi z}{c}$$

$$E_{y2} = \frac{p\pi}{c} C_2 \sinh K_{x2} (a-x) \cos \frac{n\pi y}{b} \sin \frac{p\pi z}{c}$$

$$E_{z2} = \frac{-n\pi}{b} C_2 \sinh K_{x2} (a-x) \sin \frac{n\pi y}{b} \cos \frac{p\pi z}{c}$$

$$H_{y2} = \frac{1}{j\omega\mu_0} \frac{n\pi}{b} K_{x2} C_2 \cosh K_{x2} (a-x) \sin \frac{n\pi y}{b} \cos \frac{p\pi z}{c}$$

$$H_{z2} = \frac{1}{j\omega\mu_0} \frac{p\pi}{c} K_{x2} C_2 \cosh K_{x2} (a-x) \sin \frac{n\pi y}{b} \cos \frac{p\pi z}{c}$$

Continuity of E_y and E_z at $x=d$ gives:

$$C_1 \sin K_{x1} d = C_2 \sinh K_{x2} (a-d)$$

Continuity of H_y and H_z at $x=d$ gives:

$$-C_1 \frac{K_{x1}}{\mu_1} \cos K_{x1} d = \frac{C_2 K_{x2}}{\mu_0} \cosh K_{x2} (a-d)$$

Dividing these and putting $\mu_1 = \mu_0$ gives:

$$-K_{x1} \cot K_{x1} d = K_{x2} \coth K_{x2} (a-d)$$

or

$$K_{x1} \cos K_{x1} d \sinh K_{x2} (a-d) + K_{x2} \sin K_{x1} d \cosh K_{x2} (a-d) = 0 \quad (4c)$$

Thus, to get the TM resonances, we solve equations (3a), (3b) and (3c), and to get the TE resonances, we solve equations (4a), (4b) and (4c).

SUMMARY OF EQUATIONS TO SOLVE, AND METHOD OF SOLUTION

For TM resonances in Case I, we solve:

$$K_{x1}^2 + \left(\frac{n\pi}{b}\right)^2 + \left(\frac{p\pi}{c}\right)^2 = \epsilon_r \left(\frac{\omega}{c}\right)^2 \quad (1a)$$

$$K_{x2}^2 + \left(\frac{n\pi}{b}\right)^2 + \left(\frac{p\pi}{c}\right)^2 = \left(\frac{\omega}{c}\right)^2 \quad (1b)$$

$$K_{x1} \sin K_{x1} d \cos K_{x2} (a-d) + \epsilon_r K_{x2} \cos K_{x1} d \sin K_{x2} (a-d) = 0 \quad (1c)$$

For TE resonances in Case I, we solve:

$$K_{x1}^2 + \left(\frac{n\pi}{b}\right)^2 + \left(\frac{p\pi}{c}\right)^2 = \epsilon_r \left(\frac{\omega}{c}\right)^2 \quad (2a)$$

$$K_{x2}^2 + \left(\frac{n\pi}{b}\right)^2 + \left(\frac{p\pi}{c}\right)^2 = \left(\frac{\omega}{c}\right)^2 \quad (2b)$$

$$K_{x1} \cos K_{x1} d \sin K_{x2} (a-d) + K_{x2} \sin K_{x1} d \cos K_{x2} (a-d) = 0 \quad (2c)$$

For TM Resonances in Case 2 we solve:

$$K_{x1}^2 + \left(\frac{n\pi}{b}\right)^2 + \left(\frac{p\pi}{c}\right)^2 = \epsilon_r \left(\frac{\omega}{c}\right)^2 \quad (3a)$$

$$-k_{x2}^2 + \left(\frac{n\pi}{b}\right)^2 + \left(\frac{p\pi}{c}\right)^2 = \left(\frac{\omega}{c}\right)^2 \quad (3b)$$

$$K_{x1} \sin K_{x1} d \cosh K_{x2} (a-d) - \epsilon_r K_{x2} \cos K_{x1} d \sinh K_{x2} (a-d) = 0 \quad (3c)$$

For TE Resonances in Case 2 we solve:

$$K_{x1}^2 + \left(\frac{n\pi}{b}\right)^2 + \left(\frac{p\pi}{c}\right)^2 = \epsilon_r \left(\frac{\omega}{c}\right)^2 \quad (4a)$$

$$K_{x1}^2 + \left(\frac{n\pi}{b}\right)^2 + \left(\frac{p\pi}{c}\right)^2 = \left(\frac{\omega}{c}\right)^2 \quad (4b)$$

$$K_{x1} \cos K_{x1} d \sinh K_{x2} (a-d) + K_{x2} \sin K_{x1} d \cosh K_{x2} (a-d) = 0 \quad (4c)$$

By the assumption of this type of solution, we have in all cases, taken K_{x1} , and K_{x2} real. Also, K_{x1} has the same meaning in both Case 1 and Case 2, since it refers to standing waves. However, K_{x2} in Case 1 refers to a standing wave, and K_{x2} in Case 2 refers to a decaying wave. Thus K_{x2} has two different meanings.

Consider the set of resonances having constant n and p values. Then, as ω is varied K_{x1} , by equations (1a), (2a), (3a) and (4a), will have a lower bound of zero, and an infinite upper bound. Thus, we may say that there is a cutoff frequency ω_{x1} given by:

$$\left(\frac{n\pi}{b}\right)^2 + \left(\frac{p\pi}{c}\right)^2 = \epsilon_r \left(\frac{\omega_{x1}}{c}\right)^2 \quad (5a)$$

And this will be the frequency with K_{x1} equal to zero.

Now for Case 1, K_{x2} will have a lower bound of zero at a cutoff frequency ω_{x2} given by (from equation (1b) and (2b):

$$\left(\frac{n\pi}{b}\right)^2 + \left(\frac{p\pi}{c}\right)^2 = \left(\frac{\omega_{x2}}{c}\right)^2 \quad (5b)$$

In Case 2, K_{x2} will have an upper bound of zero at a cutoff frequency ω_{x2} (from equation (3b) and (4b)) which again is given by equation (5b).

From equation (5a) and (5b) we immediately see:

$$\omega_{x1} < \omega_{x2}$$

because $\epsilon_r > 1$

Thus, we may consider three different regions. First, we say that if $\omega < \omega_{x1}$, no solutions exist at all to the equations, and hence no resonances. For $\omega_{x1} < \omega < \omega_{x2}$, we have the situation in Case 2. The frequency is above the cutoff frequency in the liquid, but below the cutoff frequency in the air. For $\omega > \omega_{x2}$, we have the situation in Case 1, where standing waves exist in both the liquid and the air.

Suppose we wish to find the number of resonances between two frequencies f_1 and f_2 ($f_1 < f_2$). We first choose n and p (not both zero, or the boundary conditions cannot be satisfied). From equations (5a) and (5b), we calculate ω_{x1} and ω_{x2} . We call the frequencies corresponding to these f_4 and f_3 respectively. Hence, $f_4 < f_3$. Thus, for this (n, p) pair we have two frequency ranges. The first is the frequency range in which we want the resonances f_1 to f_2 . The second is the frequency range f_4 to f_3 . Below f_4 , there are no resonances. Between f_4 and f_3 , there may be resonances which must be solved by equations (3a), (3b), (3c), (4a), (4b) and (4c). Above f_3 , there may be resonances which must be solved by equations (1a), (1b), (1c), (2a), (2b), and (2c). Thus, the initial part of the problem will come in deciding the relationship between the f_1, f_2 range and the f_4, f_3 range. When this has been done, and the equations to be solved for the given partial frequency range decided upon, then ω is taken to be the independent variable. A value of ω at one end of the frequency range is chosen, and the corresponding K_{x1} and K_{x2} are calculated from the appropriate equation. These values are then put into the third equation of the group, and the value of the function on the lefthand side of the equals sign is calculated. An improvement is then added to ω , and the function is recalculated. This new value of the function is then compared to the old value, and if a change of sign has taken place, then it is known that there is a resonance between the old and new values of ω . Since we do not want to know the accurate resonant frequencies, but simply whether there is one there, the approximate frequency ω is printed out, and the value of ω is again increased to see if there are any more modes. When ω reaches the upper limit of the frequency range, the next range is chosen and the process repeated. When all the resonances have been found for a given (n, p) pair, then a different pair is chosen and the new resonances found. Eventually, when n and p get too big, all the resonances fall above the required frequency range, and here the program is terminated.

SECTION II

THEORETICAL ANALYSIS OF A CYLINDRICAL CAVITY (EXACT)

MICROWAVE THEORY BEHIND CYLINDRICAL CAVITY

The idea is exactly that of the rectangular cavity applied to cylindrical coordinates. As in the rectangular cavity, there are two cases. The first case is for resonances having standing waves in both the liquid and the air, and the second case is for resonances having standing waves in the liquid being supported by exponential type waves in the air side.

Case I. Resonances Having Standing Waves In Both The Liquid And The Air

Here, using Harrington's notation, we assume ψ solutions for TM to z modes as follows:

$$\psi_1 = C_1 J_n \left(\frac{x_{np}}{a} \right) \begin{bmatrix} \sin n \phi \\ \cos n \phi \end{bmatrix} \cos K_1 (d-z)$$

$$\psi_2 = C_2 J_n \left(\frac{x_{np}}{a} \right) \begin{bmatrix} \sin n \phi \\ \cos n \phi \end{bmatrix} \cos K_2 z$$

The wave equation gives:

$$K_1^2 + \left(\frac{x_{np}}{a} \right)^2 = \left(\frac{\omega}{c} \right)^2 \quad (1a)$$

$$K_2^2 + \left(\frac{x_{np}}{a} \right)^2 = \epsilon_r \left(\frac{\omega}{c} \right)^2 \quad (1b)$$

and the field components of interest are:

$$E_{\rho 1} = \frac{C_1}{j\omega\epsilon_0} \frac{x_{np}}{a} K_1 J'_n \left(\frac{x_{np}}{a} \right) \begin{bmatrix} \sin n \phi \\ \cos n \phi \end{bmatrix} \sin K_1 (d-z)$$

$$E_{\phi 1} = \frac{C_1}{j\omega\epsilon_0} n K_1 J_n \left(\frac{x_{np}}{a} \right) \begin{bmatrix} \cos n \phi \\ -\sin n \phi \end{bmatrix} \sin K_1 (d-z)$$

$$H_{\rho 1} = \frac{C_1}{\rho} n J_n \left(\frac{x_{np}}{a} \right) \begin{bmatrix} \cos n \phi \\ -\sin n \phi \end{bmatrix} \cos K_1 (d-z)$$

$$H_{\phi 1} = -C_1 \frac{x_{np}}{a} J'_n \left(\frac{x_{np}}{a} \right) \begin{bmatrix} \sin n \phi \\ \cos n \phi \end{bmatrix} \cos K_1 (d-z)$$

$$E_{\rho 2} = \frac{-C_2}{j\omega\epsilon_1} \frac{x_{np}}{a} K_2 J'_n \left(\frac{x_{np}}{a} \right) \begin{bmatrix} \sin n \phi \\ \cos n \phi \end{bmatrix} \sin K_2 z$$

$$E_{\phi 2} = \frac{-C_2}{j\omega\epsilon_1\rho} n K_2 J_n \left(\frac{x_{np}\rho}{a} \right) \begin{bmatrix} \cos n\phi \\ -\sin n\phi \end{bmatrix} \sin K_2 z$$

$$H_{\rho 2} = \frac{C_2}{\rho} n J_n \left(\frac{x_{np}\rho}{a} \right) \begin{bmatrix} \cos n\phi \\ -\sin n\phi \end{bmatrix} \cos K_2 z$$

$$H_{\phi 2} = -C_2 \frac{x_{np}}{a} J_n \left(\frac{x_{np}\rho}{a} \right) \begin{bmatrix} \sin n\phi \\ \cos n\phi \end{bmatrix} \cos K_2 z$$

Continuity of E_y and E_z at $x=c$ gives:

$$\frac{C_1}{\epsilon_0} K_1 \sin K_1 (d-c) = \frac{-C_2}{\epsilon_1} K_2 \sin K_2 c$$

Putting $d-c = b$ and $\frac{\epsilon_1}{\epsilon_0} = \epsilon_r$ gives:

$$\epsilon_r C_1 K_1 \sin K_1 b = -C_2 K_2 \sin K_2 c$$

Continuity of H_y and H_z at $x = c$ gives:

$$C_1 \cos K_1 b = C_2 \cos K_2 c$$

Dividing these equations gives:

$$\epsilon_r K_1 \tan K_1 b + K_2 \tan K_2 c = 0$$

or

$$K_2 \sin K_2 c \cos K_1 b + \epsilon_r K_1 \cos K_2 c \sin K_1 b = 0 \quad (1c)$$

For modes TE to the z axis we assume:

$$\psi_1 = C_1 J_n \left(\frac{x'_{np}\rho}{a} \right) \begin{bmatrix} \sin n\phi \\ \cos n\phi \end{bmatrix} \sin K_1 (d-z)$$

$$\psi_2 = C_2 J_n \left(\frac{x'_{np}\rho}{a} \right) \begin{bmatrix} \sin n\phi \\ \cos n\phi \end{bmatrix} \sin K_2 z$$

The wave equation gives:

$$K_1^2 + \left(\frac{x'_{np}}{a}\right)^2 = \left(\frac{\omega}{c}\right)^2 \quad (2a)$$

$$K_2^2 + \left(\frac{x'_{np}}{a}\right)^2 = \epsilon_r \left(\frac{\omega}{c}\right)^2 \quad (2b)$$

and the field components become:

$$E_{\rho 1} = \frac{-C_1}{\rho} n J_n' \left(\frac{x'_{np}}{a}\right) \begin{bmatrix} \cos n \phi \\ -\sin n \phi \end{bmatrix} \sin K_1 (d-z)$$

$$E_{\phi 1} = C_1 \frac{x'_{np}}{a} J_n' \left(\frac{x'_{np}}{a}\right) \begin{bmatrix} \sin n \phi \\ \cos n \phi \end{bmatrix} \sin K_1 (d-z)$$

$$H_{\rho 1} = \frac{-C_1}{j\omega\mu_0} K_1 \left(\frac{x'_{np}}{a}\right) J_n' \left(\frac{x'_{np}}{a}\right) \begin{bmatrix} \sin n \phi \\ \cos n \phi \end{bmatrix} \cos K_1 (d-z)$$

$$H_{\phi 1} = \frac{-C_1}{j\omega\mu_0 \rho} K_1 n J_n \left(\frac{x'_{np}}{a}\right) \begin{bmatrix} \cos n \phi \\ -\sin n \phi \end{bmatrix} \cos K_1 (d-z)$$

$$E_{\rho 2} = \frac{-C_2}{\rho} n J_n \left(\frac{x'_{np}}{a}\right) \begin{bmatrix} \cos n \phi \\ -\sin n \phi \end{bmatrix} \sin K_2 z$$

$$E_{\phi 2} = C_2 \frac{x'_{np}}{a} J_n' \left(\frac{x'_{np}}{a}\right) \begin{bmatrix} \sin n \phi \\ \cos n \phi \end{bmatrix} \sin K_2 z$$

$$H_{\rho 2} = \frac{C_2}{j\omega\mu_1} K_2 \frac{x'_{np}}{a} J_n' \left(\frac{x'_{np}}{a}\right) \begin{bmatrix} \sin n \phi \\ \cos n \phi \end{bmatrix} \cos K_2 z$$

$$H_{\phi 2} = \frac{C_2}{j\omega\mu_1 \rho} K_2 n J_n' \left(\frac{x'_{np}}{a}\right) \begin{bmatrix} \sin n \phi \\ \cos n \phi \end{bmatrix} \cos K_2 z$$

Continuity of E_ρ and E_ϕ at $x = c$ gives:

$$C_1 \sin K_1 b = C_2 \sin K_2 c$$

Continuity of H_ρ and H_ϕ at $x = c$ gives:

$$-C_1 K_1 \cos K_1 b = C_2 K_2 \cos K_2 c$$

Dividing these gives:

$$K_1 \cot K_1 b + K_2 \cot K_2 c = 0 \quad (2c)$$

or

$$K_2 \cos K_2 c \sin K_1 b + K_1 \sin K_2 c \cos K_1 b = 0 \quad (2c)$$

Thus, to get the TM modes, we solve equation (1a), (1b) and (1c), while for the TE modes we solve equation (2a), (2b) and (2c).

Case 2. Resonances Having Standing Waves In Liquid Only

Here using Harrington's notation, we assume ψ solutions for TM to z modes as follows:

$$\psi_1 = C_1 J_n \left(\frac{x_{np}}{a} \right) \begin{bmatrix} \sin n \phi \\ \cos n \phi \end{bmatrix} \cosh K_1 (d-z)$$

$$\psi_2 = C_2 J_n \left(\frac{x_{np}}{a} \right) \begin{bmatrix} \sin n \phi \\ \cos n \phi \end{bmatrix} \cos K_2 z$$

The wave equation now gives:

$$-K_1^2 + \left(\frac{x_{np}}{a} \right)^2 = \left(\frac{\omega}{c} \right)^2 \quad (3a)$$

and

$$K_2^2 + \left(\frac{x_{np}}{a} \right)^2 = \epsilon_r \left(\frac{\omega}{c} \right)^2 \quad (3b)$$

and the field components of interest are:

$$E_{\rho 1} = \frac{-C_1}{j\omega\epsilon_0} \frac{x_{np}}{a} K_1 J_n' \left(\frac{x_{np}}{a} \right) \begin{bmatrix} \sin n \phi \\ \cos n \phi \end{bmatrix} \sinh K_1 (d-z)$$

$$E_{\phi 1} = \frac{-C_1}{j\omega\epsilon_0} n K_1 J_n' \left(\frac{x_{np}}{a} \right) \begin{bmatrix} \cos n \phi \\ -\sin n \phi \end{bmatrix} \sinh K_1 (d-z)$$

$$H_{\rho 1} = \frac{C_1}{\rho} n J_n \left(\frac{x_{np}}{a} \right) \begin{bmatrix} \cos n \phi \\ -\sin n \phi \end{bmatrix} \cosh K_1 (d-z)$$

$$H_{\phi 1} = C_1 \left(\frac{x_{np}}{a} \right) J_n \left(\frac{x_{np}}{a} \right) \begin{bmatrix} \sin n \phi \\ \cos n \phi \end{bmatrix} \cosh K_1 (d-z)$$

$$E_{\rho 2} = \frac{-C_2}{j\omega\epsilon_1} \frac{x_{np}}{a} K_2 J_n' \left(\frac{x_{np}}{a} \right) \begin{bmatrix} \sin n \phi \\ \cos n \phi \end{bmatrix} \sin K_2 z$$

$$E_{\phi 2} = \frac{-C_2}{j\omega\epsilon_1 \rho} n K_2 J_n \left(\frac{x_{np}}{a} \right) \begin{bmatrix} \cos n \phi \\ -\sin n \phi \end{bmatrix} \sin K_2 z$$

$$H_{\rho 2} = \frac{C_2}{\rho} n J_n \left(\frac{x_{np} \rho}{a} \right) \begin{bmatrix} \cos n \phi \\ -\sin n \phi \end{bmatrix} \cos K_2 z$$

$$H_{\phi 2} = -C_2 \frac{x_{np}}{a} J_n' \left(\frac{x_{np} \rho}{a} \right) \begin{bmatrix} \sin n \phi \\ \cos n \phi \end{bmatrix} \cos K_2 z$$

Continuity of E_ρ and E_ϕ at $x = c$ gives:

$$\frac{C_1}{\epsilon_0} K_1 \sinh K_1 b = \frac{C_2}{\epsilon_1} K_2 \sin K_2 c$$

Continuity of H_ρ and H_ϕ at $x = c$ gives:

$$C_1 \cosh K_1 b = C_2 \sinh K_2 c$$

Dividing gives:

$$\epsilon_r K_1 \tanh K_1 b = K_2 \tan K_2 c$$

or

$$K_2 \sin K_2 c \cosh K_1 b - \epsilon_r K_1 \cos K_2 c \sinh K_1 b = 0 \quad (3c)$$

For modes TE to the x axis we assume:

$$\psi_1 = C_1 J_n \left(\frac{x_{np} \rho}{a} \right) \begin{bmatrix} \sin n \phi \\ \cos n \phi \end{bmatrix} \sinh K_1 (d-z)$$

$$\psi_2 = C_2 J_n \left(\frac{x_{np} \rho}{a} \right) \begin{bmatrix} \sin n \phi \\ \cos n \phi \end{bmatrix} \sin K_2 z$$

The wave equation gives:

$$\left(-K_1 \right)^2 + \left(\frac{x_{np}}{a} \right)^2 = \left(\frac{\omega}{c} \right)^2 \quad (4a)$$

$$\left(K_2 \right)^2 + \left(\frac{x_{np}}{a} \right)^2 = \epsilon_r \left(\frac{\omega}{c} \right)^2 \quad (4b)$$

the field components become:

$$E_{\rho 1} = \frac{-C_1}{\rho} n J_n \left(\frac{x'_{np}\rho}{a} \right) \begin{bmatrix} \cos n \phi \\ -\sin n \phi \end{bmatrix} \sinh K_1 (d-z)$$

$$E_{\phi 1} = C_1 \frac{x'_{np}}{a} J_n \left(\frac{x'_{np}\rho}{a} \right) \begin{bmatrix} \sin n \phi \\ \cos n \phi \end{bmatrix} \sinh K_1 (d-z)$$

$$H_{\rho 1} = \frac{-C_1}{j\omega\mu_0} K_1 \frac{x'_{np}}{a} J'_n \left(\frac{x'_{np}\rho}{a} \right) \begin{bmatrix} \sin n \phi \\ \cos n \phi \end{bmatrix} \cosh K_1 (d-z)$$

$$H_{\phi 1} = \frac{-C_1}{j\omega\mu_0} K_1 n J_n \left(\frac{x'_{np}\rho}{a} \right) \begin{bmatrix} \sin n \phi \\ \cos n \phi \end{bmatrix} \cosh K_1 (d-z)$$

$$E_{\rho 2} = \frac{-C_2}{\rho} n J_n \left(\frac{x'_{np}\rho}{a} \right) \begin{bmatrix} \cos n \phi \\ -\sin n \phi \end{bmatrix} \sin K_2 z$$

$$E_{\phi 2} = C_2 \frac{x'_{np}}{a} J'_n \left(\frac{x'_{np}\rho}{a} \right) \begin{bmatrix} \sin n \phi \\ \cos n \phi \end{bmatrix} \sin K_2 z$$

$$H_{\rho 2} = \frac{-C_2}{j\omega\mu_1} K_2 \frac{x'_{np}}{a} J'_n \left(\frac{x'_{np}\rho}{a} \right) \begin{bmatrix} \sin n \phi \\ \cos n \phi \end{bmatrix} \cos K_2 z$$

$$H_{\phi 2} = \frac{-C_2}{j\omega\mu_1 \rho} K_2 n J_n \left(\frac{x'_{np}\rho}{a} \right) \begin{bmatrix} \sin n \phi \\ \cos n \phi \end{bmatrix} \cos K_2 z$$

Continuity of E_ρ and E_ϕ at $x = c$ gives:

$$C_1 \sinh K_1 b = C_2 \sin K_2 c$$

Continuity of H_ρ and H_ϕ at $x = c$ gives:

$$-K_1 C_1 \cosh K_1 b = K_2 C_2 \cos K_2 c$$

Dividing these gives:

$$-K_1 \coth K_1 b = K_2 \cot K_2 c$$

or

$$K_2 \cos K_2 c \sinh K_1 b + K_1 \sin K_2 c \cosh K_1 b = 0 \quad (4c)$$

Thus to get the TM modes we solve equations (1), (2) and (3) and to get the TE modes we solve equation (1), (2) and (4), with x'_{np} replacing x_{np} in equations (1) and (2).

Summary Of Equations To Solve:

For TM modes in Case 1, we solve:

$$\left(K_1\right)^2 + \left(\frac{x_{np}}{a}\right)^2 = \left(\frac{\omega}{c}\right)^2 \quad (1a)$$

$$\left(K_2\right)^2 + \left(\frac{x_{np}}{a}\right)^2 = \epsilon_r \left(\frac{\omega}{c}\right)^2 \quad (1b)$$

$$K_2 \sin K_2 c \cos K_1 b + \epsilon_r K_1 \cos K_2 c \sin K_1 b = 0 \quad (1c)$$

For TE modes in Case 1 we solve:

$$\left(K_1\right)^2 + \left(\frac{x_{np}}{a}\right)^2 = \left(\frac{\omega}{c}\right)^2 \quad (2a)$$

$$\left(K_2\right)^2 + \left(\frac{x_{np}}{a}\right)^2 = \epsilon_r \left(\frac{\omega}{c}\right)^2 \quad (2b)$$

$$K_2 \cos K_2 c \sin K_1 b + K_1 \sin K_2 c \cos K_1 b = 0 \quad (2c)$$

For TM modes in Case 2, we solve:

$$\left(-K_1\right)^2 + \left(\frac{x'_{np}}{a}\right)^2 = \left(\frac{\omega}{c}\right)^2 \quad (3a)$$

$$\left(K_2\right)^2 + \left(\frac{x'_{np}}{a}\right)^2 = \epsilon_r \left(\frac{\omega}{c}\right)^2 \quad (3b)$$

$$K_2 \sin K_2 c \cosh K_1 b - \epsilon_r K_1 \cos K_2 c \sinh K_1 b = 0 \quad (3c)$$

For TE modes in Case 2, we solve:

$$\left(-K_1\right)^2 + \left(\frac{x'_{np}}{a}\right)^2 = \left(\frac{\omega}{c}\right)^2 \quad (4a)$$

$$\left(K_2\right)^2 + \left(\frac{x'_{np}}{a}\right)^2 = \epsilon_r \left(\frac{\omega}{c}\right)^2 \quad (4b)$$

$$K_2 \cos K_2 c \sinh K_1 b + K_1 \sin K_2 c \cosh K_1 b = 0 \quad (4c)$$



As in the rectangular case, K_1 and K_2 are, by nature of the type of solution chosen, real. The difference between this case and the rectangular case is that here the liquid is assumed to be in medium 2, whereas, in the previous case it was assumed to be in medium 1.

The method of solution of the equation is similar to that of the rectangular program, in that values of the transcendental function are noted as the frequency is changed. The main difference is that the frequency increment variation is more sophisticated, and thus, the resonant frequency solutions are more accurate. Also, the approach is slightly different, in that the values of the transcendental function are stored in the computer and then looked at to see if there are any zeros. In the rectangular program only, the zeros are stored.

SECTION III

THEORETICAL ANALYSIS OF A SPHERICAL CAVITY (EXACT)

MICROWAVE THEORY BEHIND PARTIALLY FILLED SPHERICAL CAVITY

The following is an analysis of the resonant frequencies of a spherical cavity partially filled with a dielectric. The cavity to be considered is shown in Figure A-1 with a dielectric ϵ_1, μ_1 occupying region 1 and a dielectric of ϵ_2, μ_2 in Region 2.

For modes TE_r^r and TM_r^r , we need solutions ψ to the scalar Helmholtz (Wave) equation denoted as F_r, A_r of the form:

$$C_n \hat{J}_n(Kr) P_n^m(\cos \theta) \begin{bmatrix} \cos m \phi \\ \sin m \phi \end{bmatrix}$$

in the dielectric and:

$$[A_n \hat{J}_n(Kr) + B_n \hat{N}_n(Kr)] P_n^m(\cos \theta) \begin{bmatrix} \cos m \phi \\ \sin m \phi \end{bmatrix}$$

between the inner dielectric interface and the conductor.

The above forms for the ψ (A_r or F_r) are chosen for the following reasons:

- (1) Use $\hat{J}_n(Kr)$ only, in the center as the fields must be finite at $r = 0$.
- (2) Use $m = \text{integer}$ as $\psi(\phi) = \psi(\phi + 2\pi)$ is required (i.e. ψ must be single-valued).
- (3) Use P_n^m with n integer as we want fields finite in θ at $\theta = 0, \pi$.
- (4) Use $P_n^m(\cos \theta)$ in each region to facilitate a match of the fields at the dielectric boundary.
- (5) Use $\begin{bmatrix} \cos m \phi \\ \sin m \phi \end{bmatrix}$ to give simplest form of $e^{\pm jm\phi}$

The propagation constant K is defined as:

$$K = \omega\sqrt{\mu\epsilon} \text{ and } K_1 = \omega\sqrt{\mu_1\epsilon_1} \text{ and } K_2 = \omega\sqrt{\mu_2\epsilon_2}$$

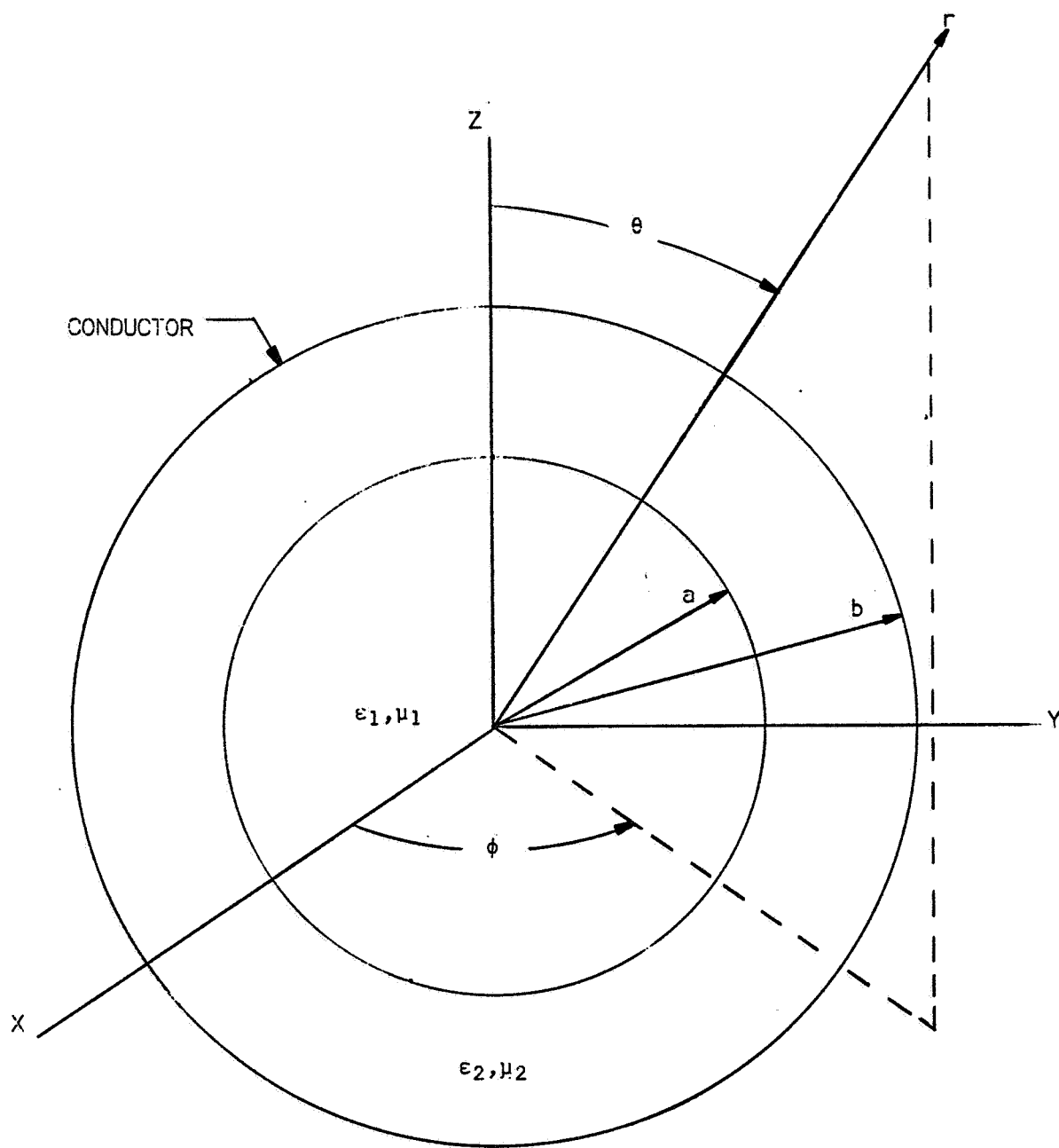
Now for the $\begin{pmatrix} TE_r^r \\ TM_r^r \end{pmatrix}$ modes in Region 2, we can say:

$$F_r = A_n \hat{J}_n(K_2 r) + B_n \hat{N}_n(K_2 r) P_n^m(\cos \theta) \begin{bmatrix} \cos m \phi \\ \sin m \phi \end{bmatrix}$$

$$A = A \hat{J}_n(K_2 r) = B \hat{N}_n(K_2 r) P_n^m(\cos \theta) \begin{bmatrix} \cos m \phi \\ \sin m \phi \end{bmatrix}$$

The boundary conditions of tangential \underline{E} at $r = b$ are:

$$E_\theta = E_\phi = 0$$



SPHERICAL CAVITY PARTIALLY FILLED WITH DIELECTRIC

FIGURE A-1

For modes TE^r , the following field components exist:

$$E_\theta = \frac{-1}{r \sin \theta} \frac{\partial F_r}{\partial \phi} \quad (\text{for } TE^r \text{ modes})$$

$$= \frac{1}{r} \frac{\partial^2 A_r}{\partial r \partial \theta}$$

$$E_\phi = \frac{1}{r} \frac{\partial F_r}{\partial \theta} \quad (\text{for } TM^r \text{ modes})$$

$$= \frac{1}{r \sin \theta} \frac{\partial^2 A_r}{\partial r \partial \phi}$$

In order to satisfy the boundary condition on E_θ , E_ϕ at $r = b$, we need:

$$A_n \hat{J}_n(K_2 b) + B_n \hat{N}_n(K_2 b) = 0 \quad (\text{for } TE^r \text{ modes})$$

Or letting $A_n = \hat{N}_n(K_2 b)$ and $B_n = -\hat{J}_n(K_2 b)$, we can say:

$$F_r = [\hat{N}_n(K_2 b) \hat{J}_n(K_2 r) - \hat{J}_n(K_2 b) \hat{N}_n(K_2 r)] P_n^m(\cos \theta) \begin{bmatrix} \cos m \phi \\ \sin m \phi \end{bmatrix}$$

To meet the same boundary condition for A_r , we need:

$$A_n \hat{J}_n'(K_2 b) + B_n \hat{N}_n'(K_2 b) = 0$$

letting: $A_n = \hat{N}_n'(K_2 b)$, $B_n = -\hat{J}_n'(K_2 b)$ we have:

$$A_r = [\hat{N}_n'(K_2 b) \hat{J}_n(K_2 r) - \hat{J}_n'(K_2 b) \hat{N}_n(K_2 r)] P_n^m(\cos \theta) \begin{bmatrix} \cos m \phi \\ \sin m \phi \end{bmatrix}$$

Now to meet the boundary conditions on the dielectric interface, we must match tangential E and H components:

$$E_{\theta 1} = E_{\theta 2}; E_{\phi 1} = E_{\phi 2}; H_{\phi 1} = H_{\phi 2}; H_{\theta 1} = H_{\theta 2}$$

For modes TM^r and TE^r , the following field components exist:

$$H = \frac{1}{r \sin \theta} \frac{\partial A_r}{\partial \phi}; \quad = \frac{1}{2r} \frac{\partial^2 F_r}{\partial r \partial \theta}$$

$$H = \frac{1}{r} \frac{\partial A_r}{\partial \theta}; \quad = \frac{1}{2r \sin \theta} \frac{\partial^2 F_r}{\partial r \partial \phi}$$

Considering TE^r modes for E_θ , E_ϕ , H_θ , H_ϕ , or $Z = \frac{E_\phi}{H_\theta}$ to match at $r = a$, the following characteristic equations must be satisfied:

$$\frac{\eta_1 \hat{J}_n(K_1 a)}{\eta_2 \hat{J}'_n(K_1 a)} = \frac{\hat{N}_n(K_2 b) \hat{J}_n(K_2 a) - \hat{J}_n(K_2 b) \hat{N}_n(K_2 a)}{\hat{N}'_n(K_2 b) \hat{J}'_n(K_2 a) - \hat{J}'_n(K_2 b) \hat{N}'_n(K_2 a)}$$

Where:

$$\begin{aligned} K_1 &= \omega \sqrt{\epsilon_1 \mu_1} & \text{and} & & K_2 &= \omega \sqrt{\epsilon_2 \mu_2} \\ \eta_1 &= \sqrt{\frac{\mu_1}{\epsilon_1}} & \text{and} & & \eta_2 &= \sqrt{\frac{\mu_2}{\epsilon_2}} \end{aligned}$$

Considering TM^r modes for E_θ , E_ϕ , H_θ , H_ϕ , or $Z = -E_\phi/H_\theta$, to match the following characteristic equation applies:

$$\frac{\eta_1 \hat{J}_n(K_1 a)}{\eta_2 \hat{J}'_n(K_1 a)} = \frac{\hat{N}_n(K_2 b) \hat{J}_n(K_2 a) - \hat{J}_n(K_2 b) \hat{N}_n(K_2 a)}{\hat{N}'_n(K_2 b) \hat{J}'_n(K_2 a) - \hat{J}'_n(K_2 b) \hat{N}'_n(K_2 a)}$$

Now $M = 0, 1, 2, 3$; $N = 1, 2, 3$ are the integer values the M & N may take. There are $2n+1$, n values, as $m \leq n$ and has a cosine, sine degeneracy for $m > 0$. The $2n+1$, m values also give the same resonant frequencies as they do not enter into the characteristic equations for K_1 and K_2 . Thus, to find the number of ω values for a particular n and an excitation range $\omega_1 \rightarrow \omega_2$ the following computation could be used:

- (1) Let $n = 1$ and define $\epsilon_1, \mu_1, \epsilon_2, \mu_2, a, b$.
- (2) Find the number of ω between ω_1 and ω_2 which satisfy the TE^r and TM^r characteristic equations. Then multiply this number by $2n+1$ (the number of degeneracies).
- (3) Raise n by one, and repeat 2. Add the new number of ω values to that of previous n , and call the total N .
- (4) Keep repeating 2 and 3 till no ω can be found less than ω_2 .

The number N is now the exact number of resonant modes which exist for this cavity with the given set of parameters.

The \hat{J}_n and \hat{N}_n are the Schelkunoff spherical Bessel functions. They are defined By:

$$\hat{J}_n(x) = C_n(x) \sin \left(x - \frac{n\pi}{2} \right) + D_n(x) \cos \left(x - \frac{n\pi}{2} \right)$$

$$\hat{N}_n(x) = D_n(x) \sin \left(x - \frac{n\pi}{2} \right) - C_n(x) \cos \left(x - \frac{n\pi}{2} \right)$$

$$C_n(x) = \sum_{m=0}^{2m \leq n} \frac{(-1)^m (n+2m)!}{(2m)!(n-2m)!} (2x)^{-2m}$$

$$D_n(x) = \sum_{m=0}^{2m \leq n-1} \frac{(-1)^m (n+2m+1)!}{(2m+1)!(n-2m-1)!} (2x)^{-2m+1}$$

APPENDIX B
COMPUTER PROGRAMS

APPENDIX B

INTRODUCTION

The theoretical analysis outlined in Appendix A were used to obtain computer programs for partially filled cavities. The programs were used to evaluate all the modes present in the cavities, for a number of 'Q' or quality factors.

The programs in this Appendix are for the configurations analysed in Appendix A.

SECTION I

PROGRAM FOR PARTIALLY FILLED RECTANGULAR CAVITY

1.0 Definition And Analysis Of Problem

The object of this program is to calculate the number of resonances in a rectangular metal cavity with sides 'a', 'b' and 'c', which is partially filled with a loss-less liquid whose surface is always parallel to the 'b', 'c' plane. The number of resonances is calculated between two limits 'f₁' and 'f₂', and degenerate resonances are counted in their multiplicity.

The program counts one resonance for each frequency within the range which satisfies any of the following four sets of simultaneous equations.

$$\left. \begin{aligned} K_{x1}^2 + \left(\frac{n\pi}{b}\right)^2 + \left(\frac{p\pi}{c}\right)^2 &= \epsilon \left(\frac{\omega}{c_1}\right)^2 \\ K_{x2}^2 + \left(\frac{n\pi}{b}\right)^2 + \left(\frac{p\pi}{c}\right)^2 &= \left(\frac{\omega}{c_1}\right)^2 \end{aligned} \right\} \quad (1)$$

$$K_{x1} \sin K_{x1} d \cos K_{x2} (a-d) + \epsilon K_{x2} \cos K_{x1} d \sin K_{x2} (a-d) = 0$$

$$\left. \begin{aligned} K_{x1}^2 + \left(\frac{n\pi}{b}\right)^2 + \left(\frac{p\pi}{c}\right)^2 &= \epsilon \left(\frac{\omega}{c_1}\right)^2 \\ K_{x2}^2 + \left(\frac{n\pi}{b}\right)^2 + \left(\frac{p\pi}{c}\right)^2 &= \left(\frac{\omega}{c_1}\right)^2 \end{aligned} \right\} \quad (2)$$

$$K_{x1} \cos K_{x1} d \sin K_{x2} (a-d) + K_{x2} \sin K_{x1} d \cos K_{x2} (a-d) = 0$$

$$\left. \begin{aligned} K_{x1}^2 + \left(\frac{n\pi}{b}\right)^2 + \left(\frac{p\pi}{c}\right)^2 &= \epsilon \left(\frac{\omega}{c_1}\right)^2 \\ -K_{x2}^2 + \left(\frac{n\pi}{b}\right)^2 + \left(\frac{p\pi}{c}\right)^2 &= \left(\frac{\omega}{c_1}\right)^2 \end{aligned} \right\} \quad (3)$$

$$K_{x1} \sin K_{x1} d \cosh K_{x2} (a-d) - \epsilon K_{x2} \cos K_{x1} d \sinh K_{x2} (a-d) = 0$$

$$\left. \begin{aligned} K_{x1}^2 + \left(\frac{n\pi}{b}\right)^2 + \left(\frac{p\pi}{c}\right)^2 &= \epsilon \left(\frac{\omega}{c^1}\right)^2 \\ -K_{x2}^2 + \left(\frac{n\pi}{b}\right)^2 + \left(\frac{p\pi}{c}\right)^2 &= \left(\frac{\omega}{c^1}\right)^2 \end{aligned} \right\} \quad (4)$$

$$K_{x1} \cos K_{x1} d \sinh K_{x2} (a-d) + K_{x2} \sin K_{x1} d \cosh K_{x2} (a-d) = 0$$

In these equations:

d = Height of liquid up the 'a' side.

ω = Radian, Frequency.

ϵ = Dielectric constant of liquid.

c^1 = Velocity of light.

K_{x1} , K_{x2} are real numbers,

'n', 'p' are positive integers, not both zero.

2.0 Method of Solution

Each of the sets of simultaneous equations is solved by feeding in a frequency and then calculating the value of the function on the lefthand side of the equals sign in the third equation of the set. The frequency is increased in increments, and each time the function changes sign, it is known that a solution has been passed through. The method is repeated for all values of 'n' and 'p', which gives solutions in the given frequency range.

3.0 Program Capabilities, Logical Techniques And Options

The program can be run for different sizes of tanks, different liquids, and different fractional fillings.

4.0 Limitations And Accuracy

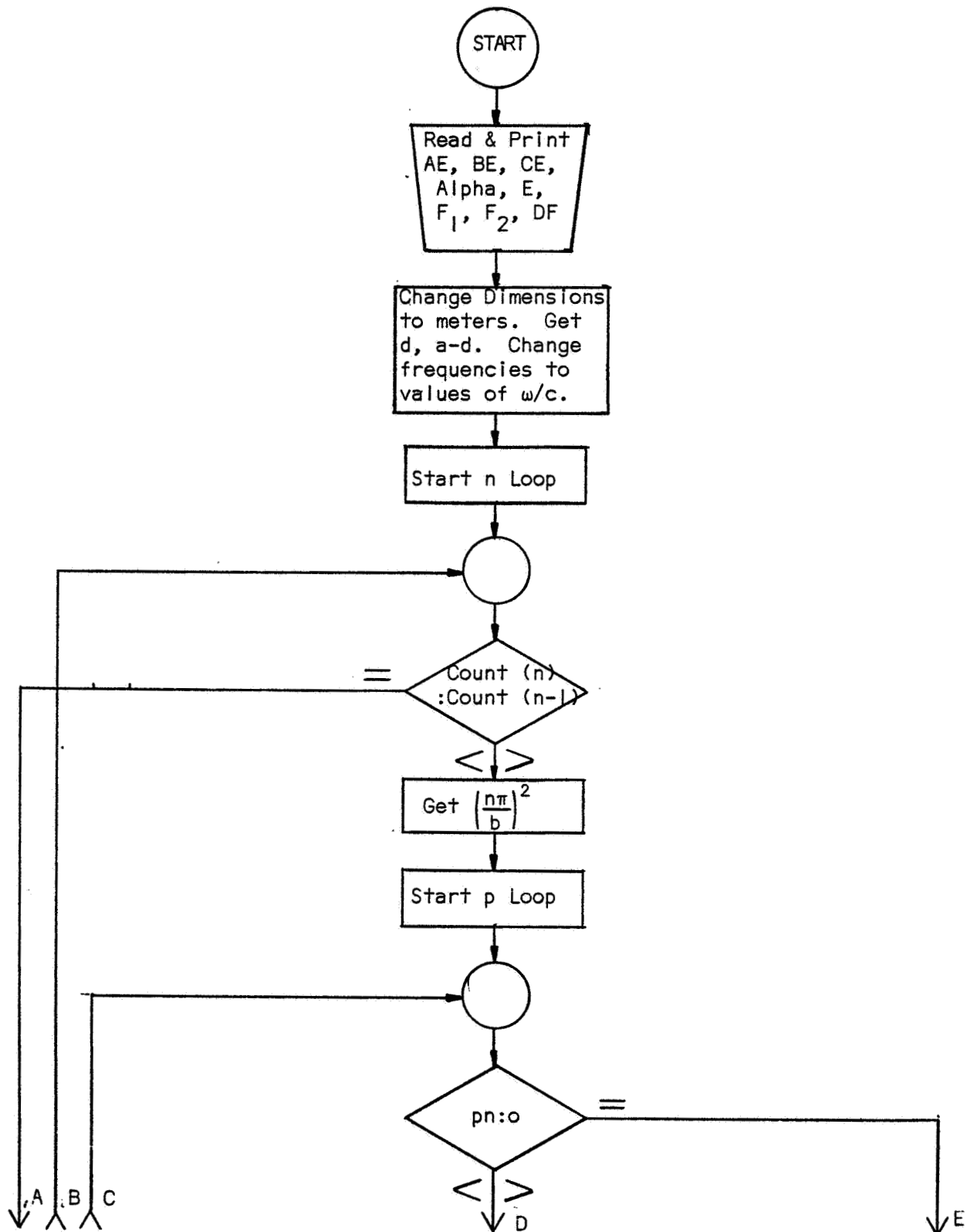
Accuracy of the program is to 4 places. The main limitation of the program is at present in the input format. More variations of parameters could be allowed for by changing the input format.

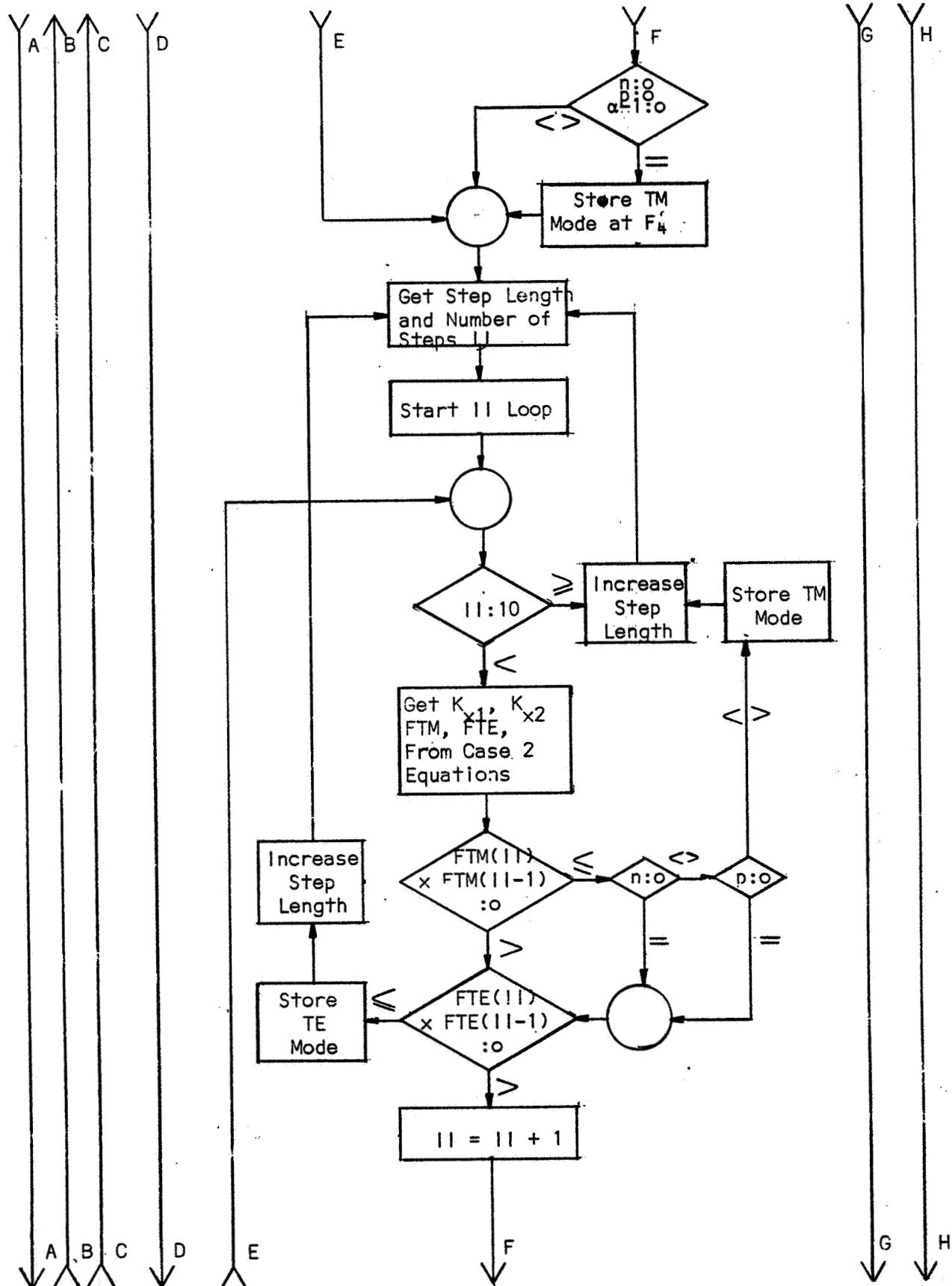
5.0 Input And Output Parameters

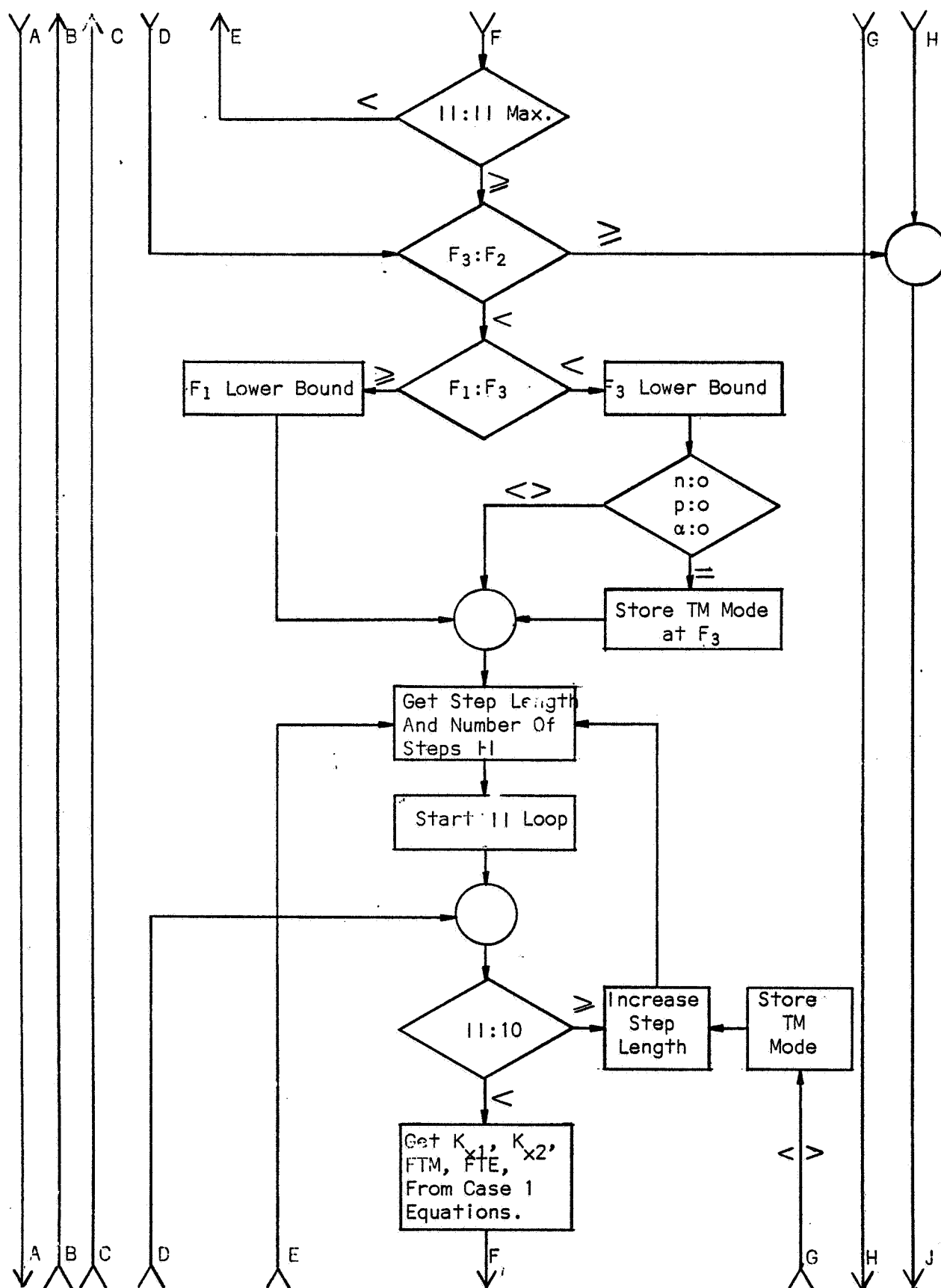
The input data consists of the following:

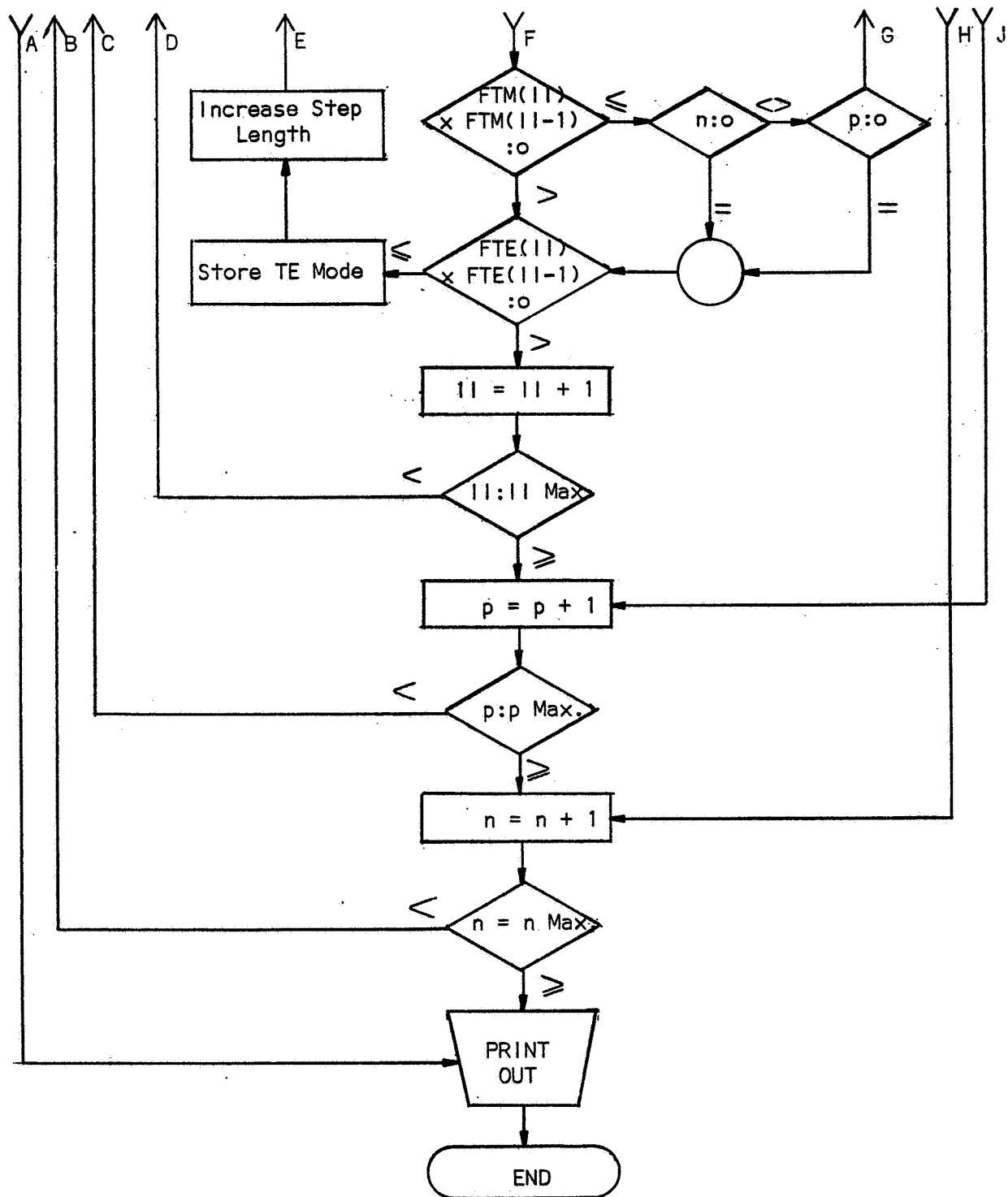
The box dimensions, 'a', 'b' and 'c', are read in in inches followed by the fractional filling constant ' α '. Next, the dielectric constant ' ϵ ' of the liquid, and the lower and upper frequency limits (in GHz) are read in. Finally, the incremental frequency ' ΔF ' is fed in GHz. This input data is also printed out, under appropriate headings, on the output document. The output data consists of the (n, p) pair, then two frequencies, which are relevant to the types of equations to solve, and then the resonant frequencies for the given (n, p) pair. The total number of resonances is printed at the end.

6.0 Flow Chart For Partial Fill Rectangular Programs









SECTION II

PROGRAM FOR PARTIALLY FILLED CYLINDRICAL CAVITY (VARIATIONAL TECHNIQUE)

1.0 Definition and Analysis of Problem

The object of this program is to give all of the modes (TE and TM) that exist in a cylindrical tank for a frequency band and a percentage dielectric fill. In addition, the 'Q' or quality factor is calculated for each mode utilizing the conductivity of the tank material. The 'Q' found is only the tank 'Q' and doesn't take into consideration the loss tangent of the dielectric or 'Q' of external circuitry.

1.1 TM Equation⁽¹⁾

Equation 1

$$FRM = \frac{\epsilon}{2\pi} \left\{ \left(\frac{P\pi}{L} \right)^2 \left[1 + \left(1 - \frac{1}{\epsilon_r} \right) \left(\frac{1}{2P\pi} \sin(2P\pi\alpha) - \alpha \right) \right] + \left(\frac{X_{mn}}{R} \right)^2 \left[1 + \left(\frac{1}{\epsilon_r} - 1 \right) \left(\alpha + \frac{1}{2P\pi} \sin(2P\pi\alpha) \right) \right] \right\}^{1/2}$$

FRM \triangleq Resonant frequency of TM mode.

Where: C = Speed of light in cm/sec
 P = Number of half-wavelength variations of the mode along the axis of the tank
 L = Tank height in cm
 ϵ_r = Relative permittivity of the dielectric in the tank
 α = Filling factor (full = 1.0, 10% full = 0.1)
 X_{mn} = mn order Bessel zero for TM modes

Equation 2

$$QM = \frac{377 \cdot (S)^{1/2} (10)^7 \left\{ (X_{mn})^2 + \left(\frac{P\pi R}{L} \right)^2 \right\}^{1/2}}{4 (\pi) (M_{2r}) (FRM)^{1/2} \left[\alpha (\epsilon_r - 1) + 1 \right]^{1/2} \left(1 + 2 \frac{R}{L} \right)}$$

Where: S = Conductivity of tank wall in mhos/meter
 μ_{2r} = Relative permeability of tank wall in henries/meter

- (1) Frequency and 'Q' equations derived from equations taken from Harrington's "Time-Harmonic Electromagnetic Fields", McGraw-Hill.

When $P = 0$:

Equation 3

$$FRO = \frac{C}{2\pi} \left(\frac{X_{mn}}{R} \right) \left[1 - \alpha \left(1 - \frac{1}{\epsilon_r} \right) \right]^{1/2}$$

$QM \triangleq$ Tank 'Q'

Equation 4

$$QMO = \frac{377 \cdot (X_{mn}) (S)^{1/2} (10)^7}{4 \pi (FRO)^{1/2} \left[\alpha (\epsilon_r - 1) + 1 \right]^{1/2} \left(1 + \frac{R}{L} \right)}$$

1.2 TE Equations

$FRE \triangleq$ Resonant Frequency of TE mode

$QE \triangleq$ 'Q' associated with the TE mode

Equation 5

$$FRE = \frac{C \left\{ \left(\frac{X'_{mn}}{R} \right)^2 + \left(\frac{P\pi}{L} \right)^2 \right\}^{1/2}}{2\pi \left\{ 1 + (\epsilon_r - 1) \alpha \left(1 - \frac{\sin(2P\pi\alpha)}{2P\pi\alpha} \right) \right\}^{1/2}}$$

Equation 6

$$QE = \frac{377 \cdot \left[(X'_{mn})^2 + (P\pi R/L)^2 \right]^{3/2} \left[(X'_{mn})^2 - m^2 \right] (S)^{1/2} + 10^7}{4\pi (FRE)^{1/2} \left[\left(\frac{MP\pi R}{L} \right)^2 + (X'_{mn})^4 + 2 \left(\frac{R}{L} \right) \left(\frac{P\pi R}{L} \right)^2 (X'_{mn})^2 - m^2 \right] \left[1 + \alpha (\epsilon_r - 1) \right]^{1/2}}$$

Where: $X'_{mn} \triangleq$ Bessel zero associated with the TE mode

2.0 Method of Solution

To place limitations on the 'DO LOOP' in the program, the frequency equations were solved for 'P UPPER'.

$$\left(\frac{P\pi}{L} \right)^2 = \frac{\overbrace{\left(\frac{2\pi FR}{C} \right) - \left(\frac{X_{mn}}{R} \right)^2 \left[1 - \left(1 - \frac{1}{\epsilon_r} \right) \alpha \left(1 + \frac{\sin(2P\pi\alpha)}{2P\pi\alpha} \right) \right]}^A}{\underbrace{\left[1 - \left(1 - \frac{1}{\epsilon_r} \right) \alpha \left(1 - \frac{\sin 2P\pi\alpha}{2P\pi\alpha} \right) \right]}_B}$$

It is necessary to find maximum and minimum value of A and B with respect to filling factor, α .

For A:

$$\frac{d \left[\left(1 - \frac{1}{\epsilon_r}\right) \alpha \left(1 + \frac{\sin 2P\pi\alpha}{2P\pi\alpha}\right) \right]}{d\alpha} = \left(1 - \frac{1}{\epsilon_r}\right) + \frac{\sin 2P\pi\alpha}{2P\pi\alpha} + \frac{(2P\pi\alpha)^2 \cos(2P\pi\alpha) - 2P\pi\alpha [\sin(2P\pi\alpha)]}{(2P\pi\alpha)^2}$$

$$= \cos 2P\pi\alpha + 1$$

$$= 0$$

for $P = 1$, $\alpha = \frac{1}{2}$

$$A = \frac{1}{2} \left(1 + \frac{1}{\epsilon_r}\right) \text{ MIN}$$

for $\alpha = 0$

$$A = 1 \text{ MAX}$$

For B:

$$\frac{d \left[1 - \left(1 - \frac{1}{\epsilon_r}\right) \left(1 - \frac{\sin 2P\pi\alpha}{2P\pi\alpha}\right) \right]}{d\alpha} = \cos(2P\pi\alpha) - 1$$

$$= 0$$

for $\alpha = 1$

$$B = \frac{1}{\epsilon_r} \text{ MIN}$$

for $\alpha = 0$

$$B = 1 \text{ MAX}$$

Then $(P \text{ UPPER})^2 = PU2$

$$PU2 = \left(\frac{L}{\pi}\right)^2 \left[\left(\frac{2\pi FU}{C}\right)^2 - \left(\frac{X_{mn}}{R}\right)^2 (A \text{ min}) \right] / (B \text{ min})$$

$$PU2 = \frac{4L^2 (FU)^2 \epsilon_r}{C^2} - \left(\frac{X_{mn}}{R}\right)^2 \left(\frac{L}{\pi}\right)^2 \left(\frac{1}{2}\right) (\epsilon_r + 1)$$

Now solve for X_{mn} so that a means of starting and stopping the

computation can be devised.

$$\left(\frac{X_{mn}}{R}\right)^2 = \frac{\left(\frac{2\pi(FR)}{C}\right)^2 - \left(\frac{P\pi}{L}\right)^2 \left[1 - \left(1 - \frac{1}{\epsilon_r}\right)\alpha \left(1 - \frac{\sin(2P\pi\alpha)}{2P\pi\alpha}\right)\right]}{\left[1 - \left(1 - \frac{1}{\epsilon_r}\right)\alpha \left(1 + \frac{\sin 2P\pi\alpha}{2P\pi\alpha}\right)\right]}$$

Smallest case exists @ $\omega = \omega_L$, $P = P_{UPPER}$, $\alpha = 0$, $B_{max.}$, and $A_{max.}$

$$(X_{mn})^2 \geq R^2 \underbrace{\left[\left(\frac{2\pi(FL)}{C}\right)^2 - (P_U)^2 \left(\frac{\pi}{L}\right)^2\right]}_{A14}$$

This will determine the starting point when used in an 'IF' statement form.

IF $((X_{mn})^2 - A14)$; READ ANOTHER X_{mn} (-),
CONTINUE (0), CONTINUE (+);

Largest case exists at $F = F_U$, $P = 0$, $B_{min.}$, $A_{min.}$

$$(X_{mn})^2 \leq \underbrace{\left(\frac{R2\pi(F_U)}{C}\right)^2}_{A12} \epsilon_r$$

This will determine the stopping point when put in an 'IF' statement.

IF $((X_{mn})^2 - A12)$; CONTINUE (-), CONTINUE (0), STOP (+);

NOTE:

The 'M', 'N', and 'P' found within the equations are integers associated with the 'm', 'n', and 'p' of the TE_{mnp} and TM_{mnp} subscripts. Therefore, the values of P_1 and P_2 are mode integers.

3.0 Program Capabilities, Logical Techniques, and Options

- 3.1 The program can be run for different sizes of tanks, different tank materials, and different filling materials

'AD' is the partial filling code.

If 'AD' is read in as 1, filling of 10% to 100% in 10% increments will be run.

If 'AD' is read in as 0, filling of 1% to 10% in 1% increments will be run.

If 'AD' is read in as 2, filling of 99% to 90% in 1% increments will be run.

- 3.2 'IF' statements are used to give checks on the suitability of a Bessel zero and calculated frequency, the direction of the program to a 'TE' or 'TM' equation and the direction of the program to a 'TM_{mno}' or 'TM_{mnp}' equation. Also the 'IF' statement is used to select different fillings (0 to 10%, 10% to 100%, etc.).
- 3.3 Some of the options lie in the output statements. The output is both punched and printed. This may be changed to tape output if desired. The output can be sorted by machine if punched or by computer if taped. The output may be sorted according to frequency, 'Q', etc. for better readability.

The output formats can be changed to get full eight place accuracy instead of five place as given. However, punching cards may not be practical in that case. (Not enough available columns.) The 'stop' card can be replaced with a 'pause' and 'go to 6' cards if a series of tanks or conditions would like to be run without making the computer recompile.

4.0 Limitations and Accuracy

Five place accuracy can be assured for all output parameters except for the case of $m = 1$. For this case three place accuracy is assured. (Bessel zeros at $m = 1$ are not accurate beyond three places.) The upper frequency limit must not be so high as to allow X_{mn} (last card in data deck) to be less than or equal to

$$[(Fu)^2(2\pi R/\sqrt{\epsilon u})^2 - ((P1)\pi R/L)^2]^{1/2}$$

or the program will not stop automatically. An indication of this happening is the repeating of the last line of printed output. If this case should appear, use the Bessel zero program supplied and generate higher ordered Bessel zeros. (Should not be necessary except in a very extreme case.)

5.0 FORTTRAN Names and Meanings used in Program

Explained in Paragraphs 1.1, 1.2, and 2.

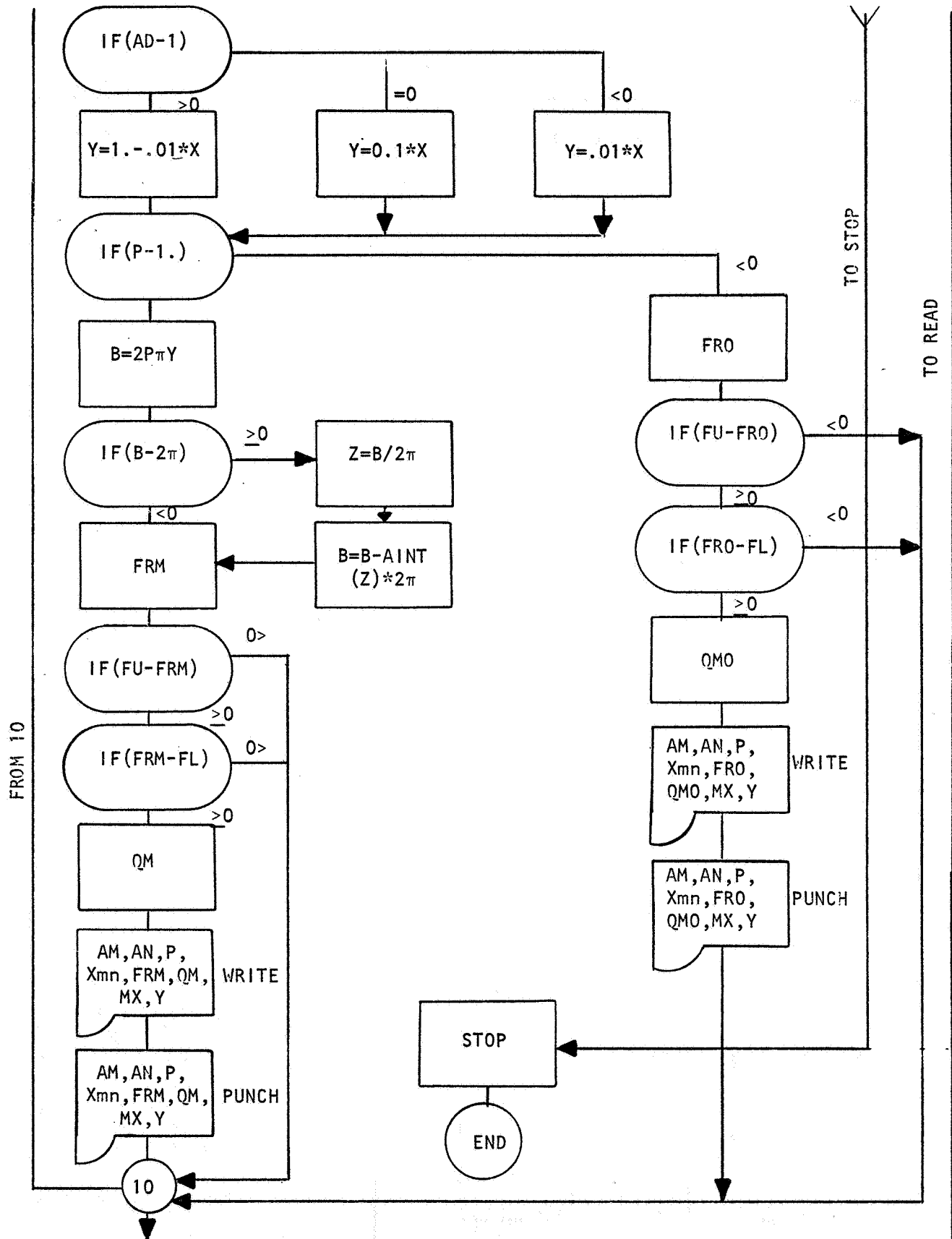
6.0 Input and Output Parameters

6.1 Input

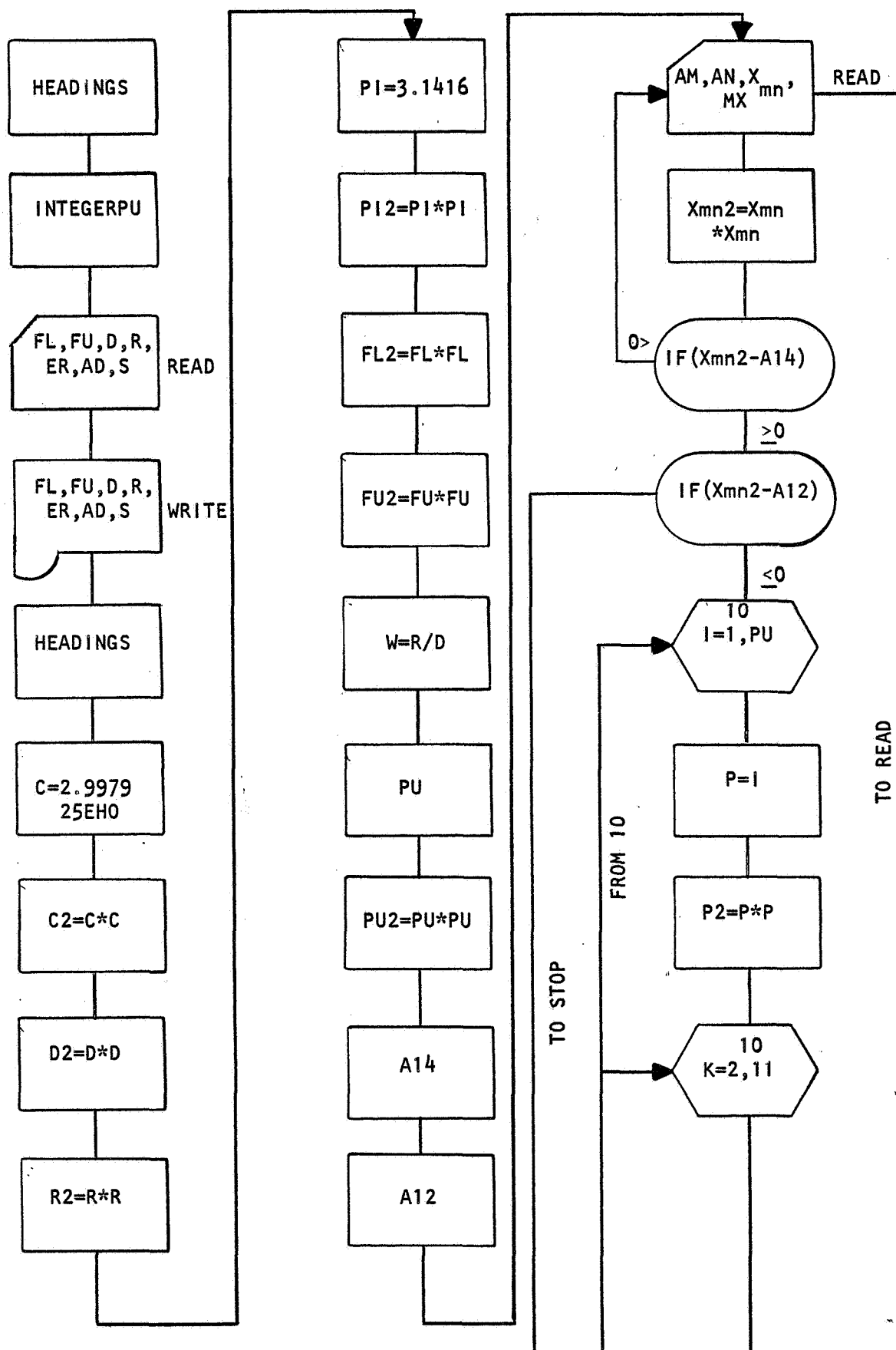
$A1 = M$ (AN integer); E 12.5
 $A2 = N$ (AN integer); E 12.5
 $A3 = X_{mn}$ (A number); E 12.5
 $A4 = FL$ (Hz/sec); E 12.5
 $A5 = F_{\mu}$ (Hz/sec); E 12.5
 $A6 = L$ (ln cm); E 12.5
 $A7 = R$ (ln cm); E 12.5
 $AE = \epsilon_r$ (Dimensionless); E 12.5
 $AD =$ (0, 1, or 2) E 12.5
 $MX =$ Mode TE = 1, 12
 TM = 2;
 $S =$ Conductivity F 8.3
 (mhos/m) $\times 10^{-7}$);

6.2 Output (All of the above with same format plus the following:)

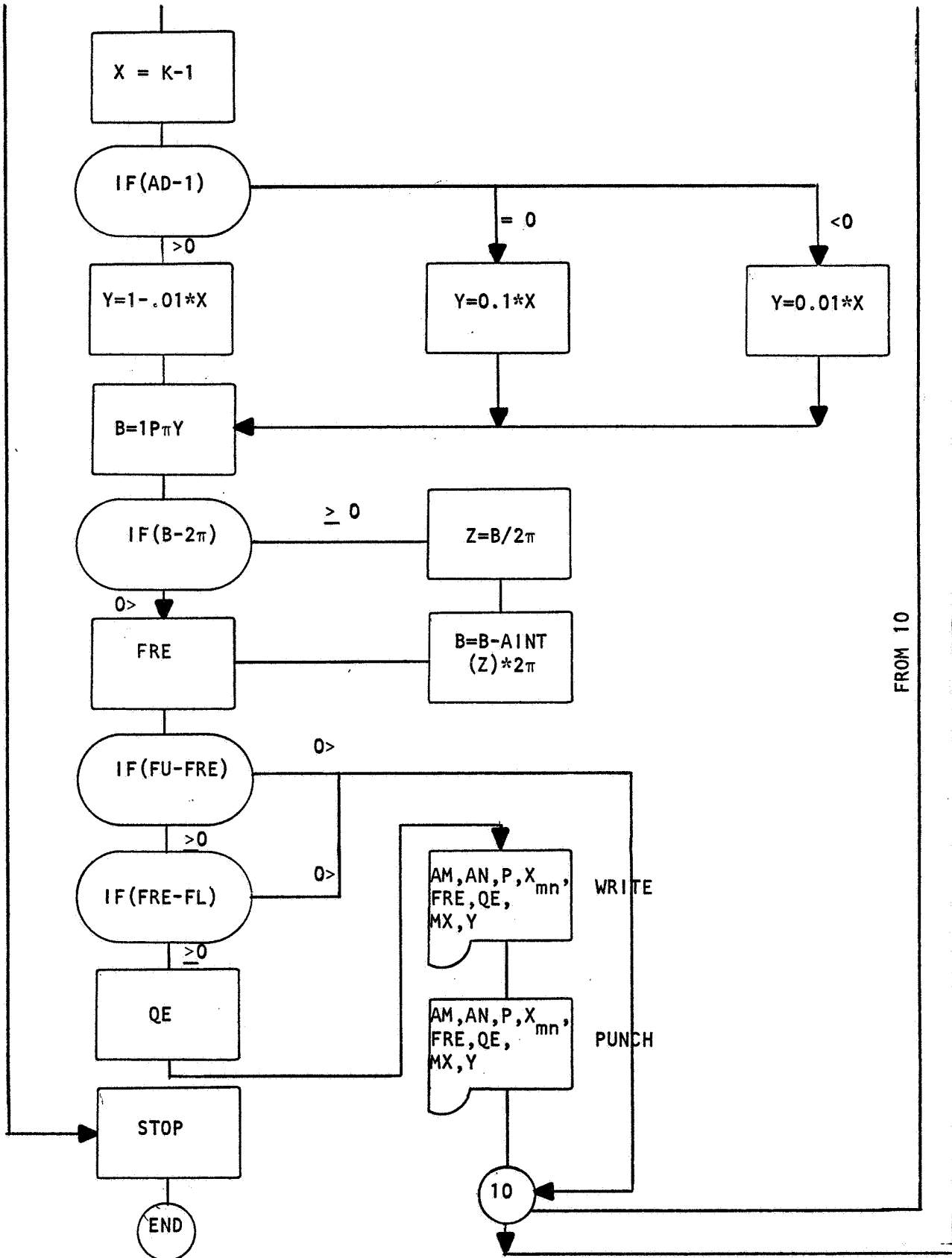
$FRE =$ Resonant frequency of TE Mode (Hz) F 12.0
 $QE =$ Tank 'Q' of TE Mode ($\frac{\text{Energy Stored in 1 cycle}}{\text{Energy dissipated in 1 cycle}}$) F 12.0
 $FRM =$ Resonant frequency of TM Mode (Hz) F 12.0
 $QM =$ Tank 'Q' of TM Mode (A number) F 12.0
 $PF =$ Partial Filling Factor (A number) F 6.3
 $P = P$ (AN integer) E 12.5



B. TE CASE



TO STOP



TO READ

FROM 10

SECTION III

PROGRAM FOR PARTIALLY FILLED CYLINDRICAL CAVITY (EXACT)

1.0 Definition And Analysis Of Problem

The object of the program is to calculate the number of resonances in a cylindrical metal cavity of height 'd', and radius 'a', partially filled with liquid 'ε' up to a height 'c'. The number of resonances 'N' is calculated between two limits 'f₁' and 'f₂', and degenerate resonances are counted in their multiplicity.

The program counts one resonance for each frequency within the range which satisfies any of the following four sets of simultaneous equations:

$$\begin{aligned} K_1^2 + \left(\frac{x_{np}}{a}\right)^2 &= \left(\frac{\omega}{c_1}\right)^2 \\ K_2^2 + \left(\frac{x_{np}}{a}\right)^2 &= \epsilon \left(\frac{\omega}{c_1}\right)^2 \end{aligned} \quad (1)$$

$$K_2 \sin K_2 c \cos K_1 b + \epsilon K_1 \cos K_2 c \sin K_1 b = 0$$

$$\begin{aligned} K_1^2 + \left(\frac{x'_{np}}{a}\right)^2 &= \left(\frac{\omega}{c_1}\right)^2 \\ K_2^2 + \left(\frac{x'_{np}}{a}\right)^2 &= \epsilon \left(\frac{\omega}{c_1}\right)^2 \end{aligned} \quad (2)$$

$$K_2 \cos K_2 c \sin K_1 b + K_1 \sin K_2 c \cos K_1 b = 0$$

$$\begin{aligned} -K_1^2 + \left(\frac{x_{np}}{a}\right)^2 &= \left(\frac{\omega}{c_1}\right)^2 \\ K_2^2 + \left(\frac{x_{np}}{a}\right)^2 &= \epsilon \left(\frac{\omega}{c_1}\right)^2 \end{aligned} \quad (3)$$

$$K_2 \sin K_2 c \cosh K_1 b - \epsilon K_1 \cos K_2 c \sinh K_1 b = 0$$

$$\begin{aligned} -K_1^2 + \left(\frac{x'_{np}}{a}\right)^2 &= \left(\frac{\omega}{c_1}\right)^2 \\ K_2^2 + \left(\frac{x'_{np}}{a}\right)^2 &= \epsilon \left(\frac{\omega}{c_1}\right)^2 \end{aligned} \quad (4)$$

$$K_2 \cos K_2 c \sinh K_1 b + K_1 \sin K_2 c \cosh K_1 b = 0$$

In these equations:

$$b = d - c$$

ω = radian frequency

c^1 = velocity of light

K_1/K_2 are real numbers

x_{np} is a zero of J_n

x'_{np} is a zero of J'_n

n, p are positive integers, $p \neq 0$

2.0 Method Of Solution

Each of the sets of simultaneous equations is solved by feeding in a frequency and then calculating the value of the function on the left-hand side of the equal sign in the third equation of the set. The frequency is increased in increments, and each time the function changes sign, it is known that a solution has been performed. The method is repeated for all values of 'n' and 'p', which give solutions in the given frequency range.

3.0 Program Capabilities, Logical Techniques And Options

The program can be run for different sizes of tanks, different liquids and different fractional fillings.

4.0 Limitations And Accuracy

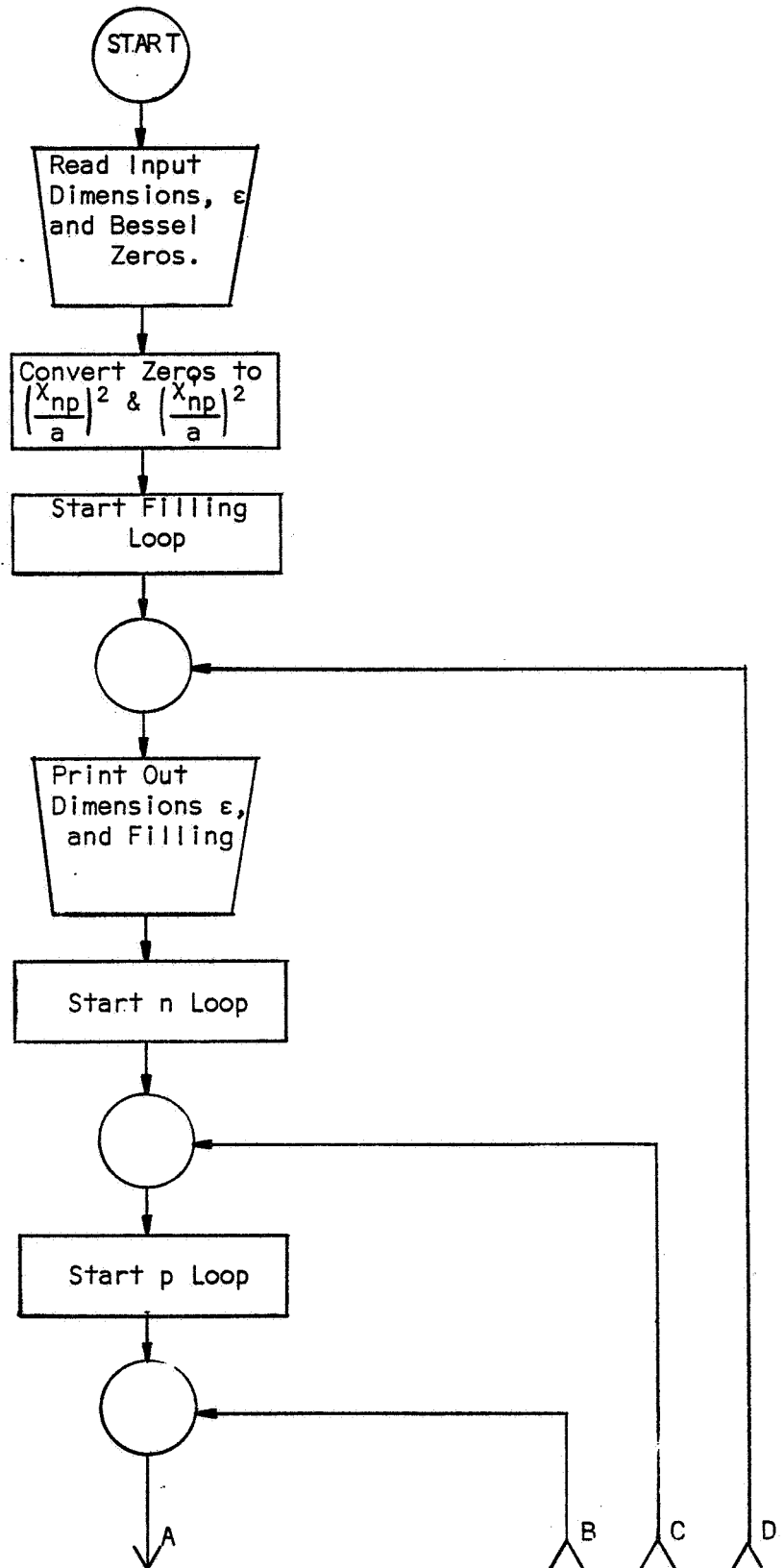
The accuracy of the program is very high, being about 6 or 7 places. At present, the program automatically does 10% to 90% fillings in increments of 10%. This could be changed to other fillings in the 5% to 95% region, but close to the full and empty cases, there may be difficulty with the program. The program also has the disadvantage of finding all the modes below the upper frequency, and consequently, could be expensive when high frequencies are used. Apart from these limitations, the program is quite flexible, although the input data format may have to be changed.

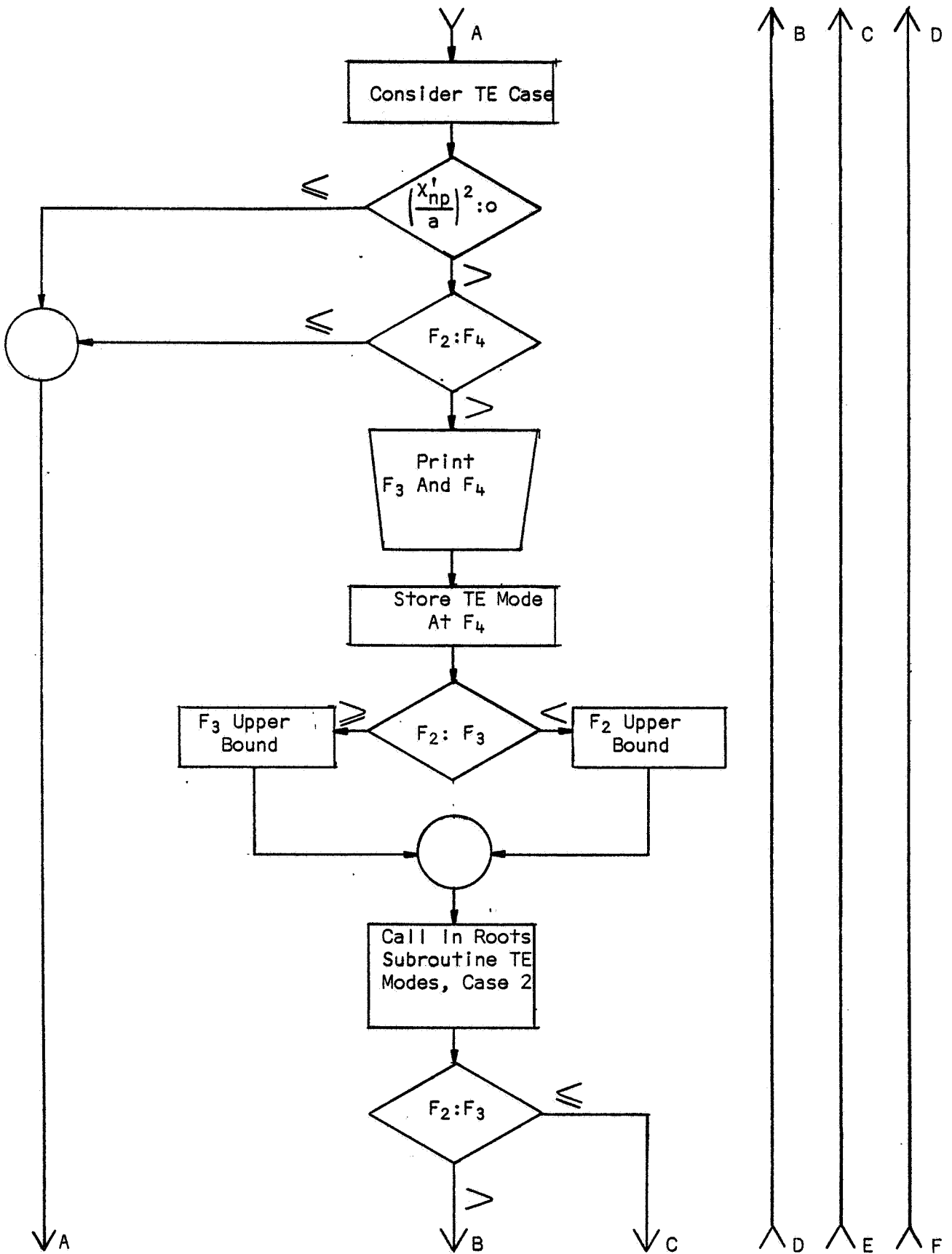
5.0 Input And Output Parameters

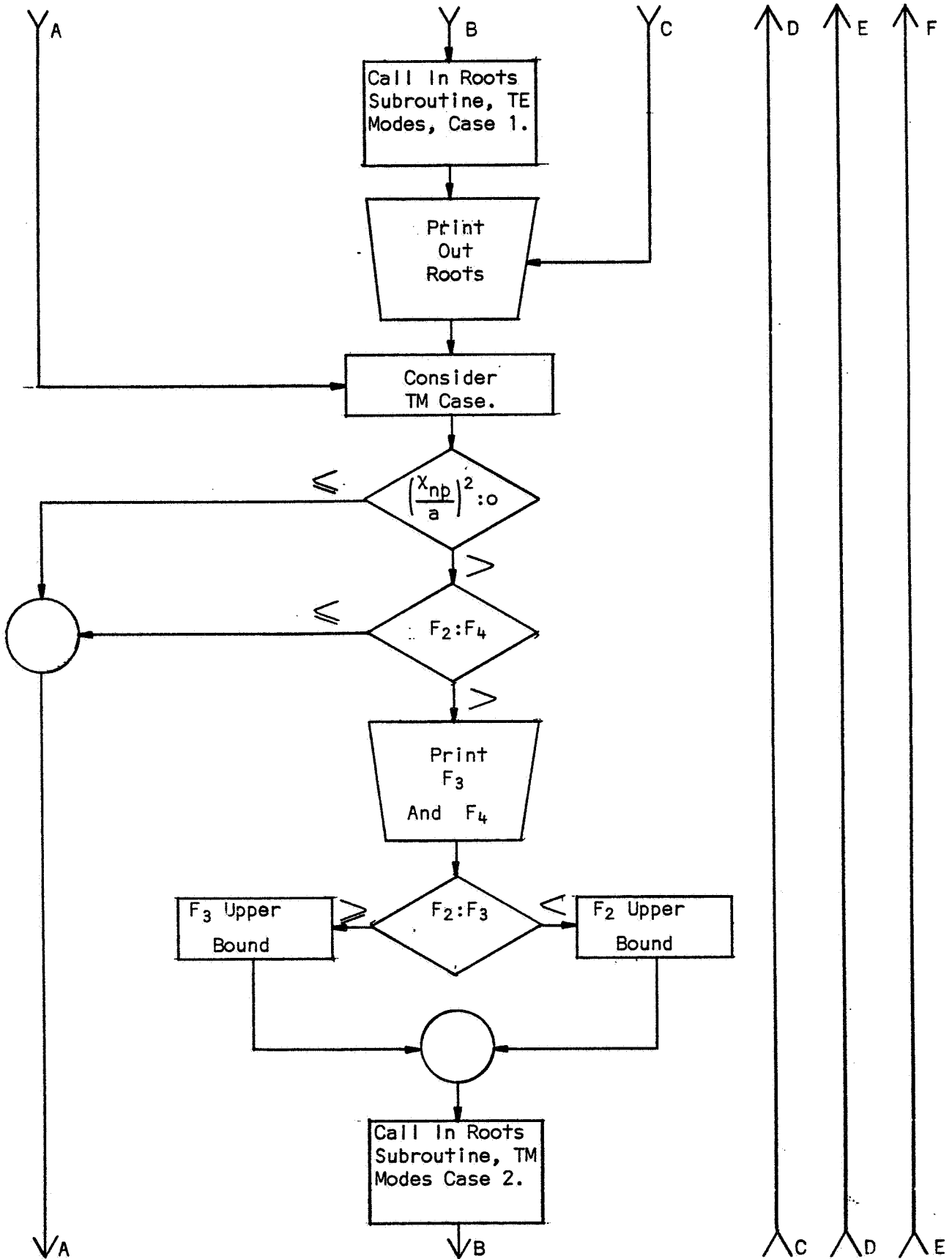
The input data for the program consists of the following: The first card has the radius and the height of the cylinder in meters, the dielectric constant of the liquid, and the lower and upper frequency limits. Next, follows the zeros of the Bessel, x_{np} function with $n = 0$ to 9 and $p = 1$ to 28,

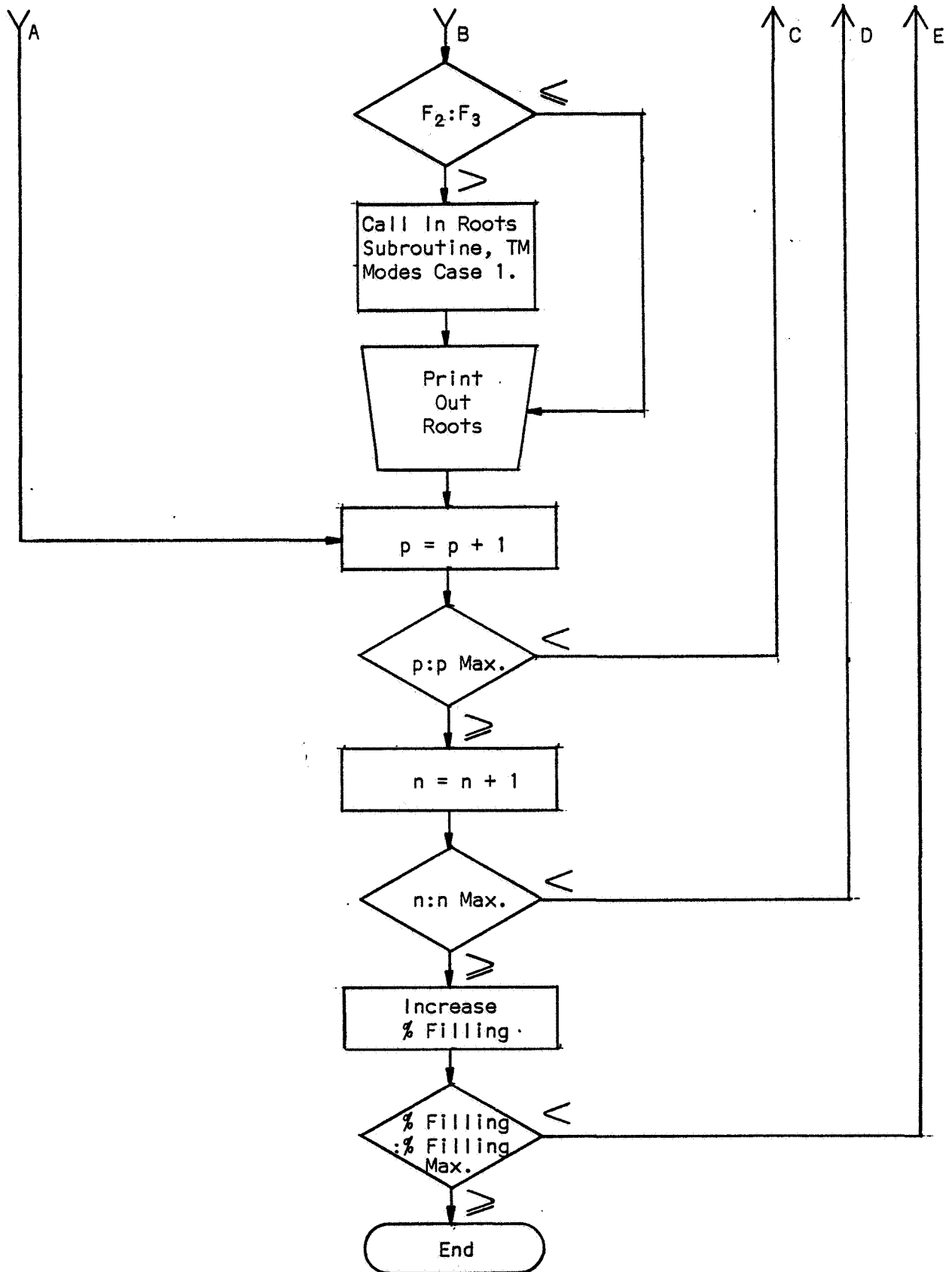
and the same number of zeros of the Bessel x'_{np} function. The output consists of the numbers 'n' and 'p', corresponding Bessel zero, mode ordering number q, the resonant frequency, the 'Q' value of the resonance, a number to show whether the mode is 'TE' or 'TM', the partial filling factor of the cavity, and the total resonance count so far.

6.0 Main Flow Chart For Partial Fill Cylindrical Program

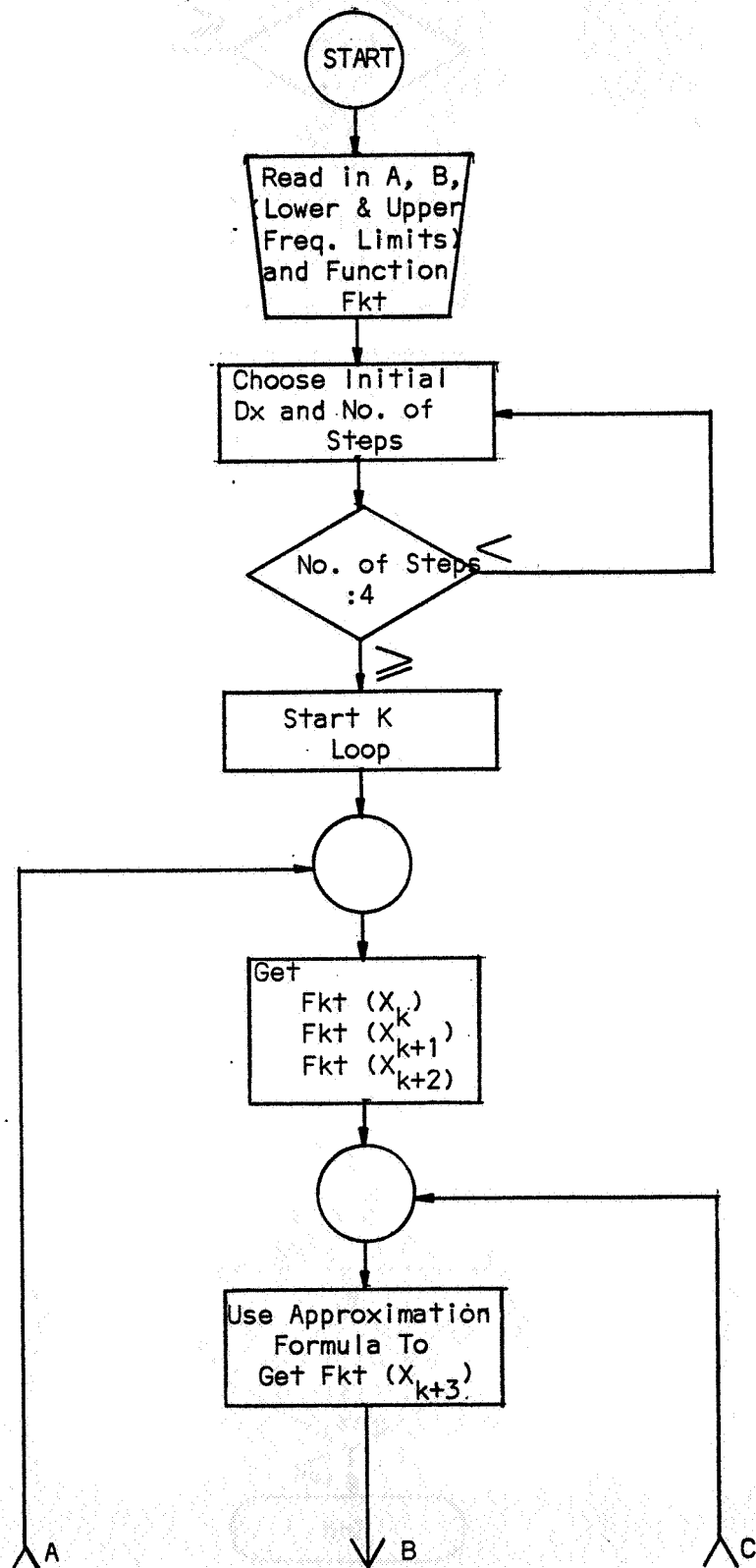


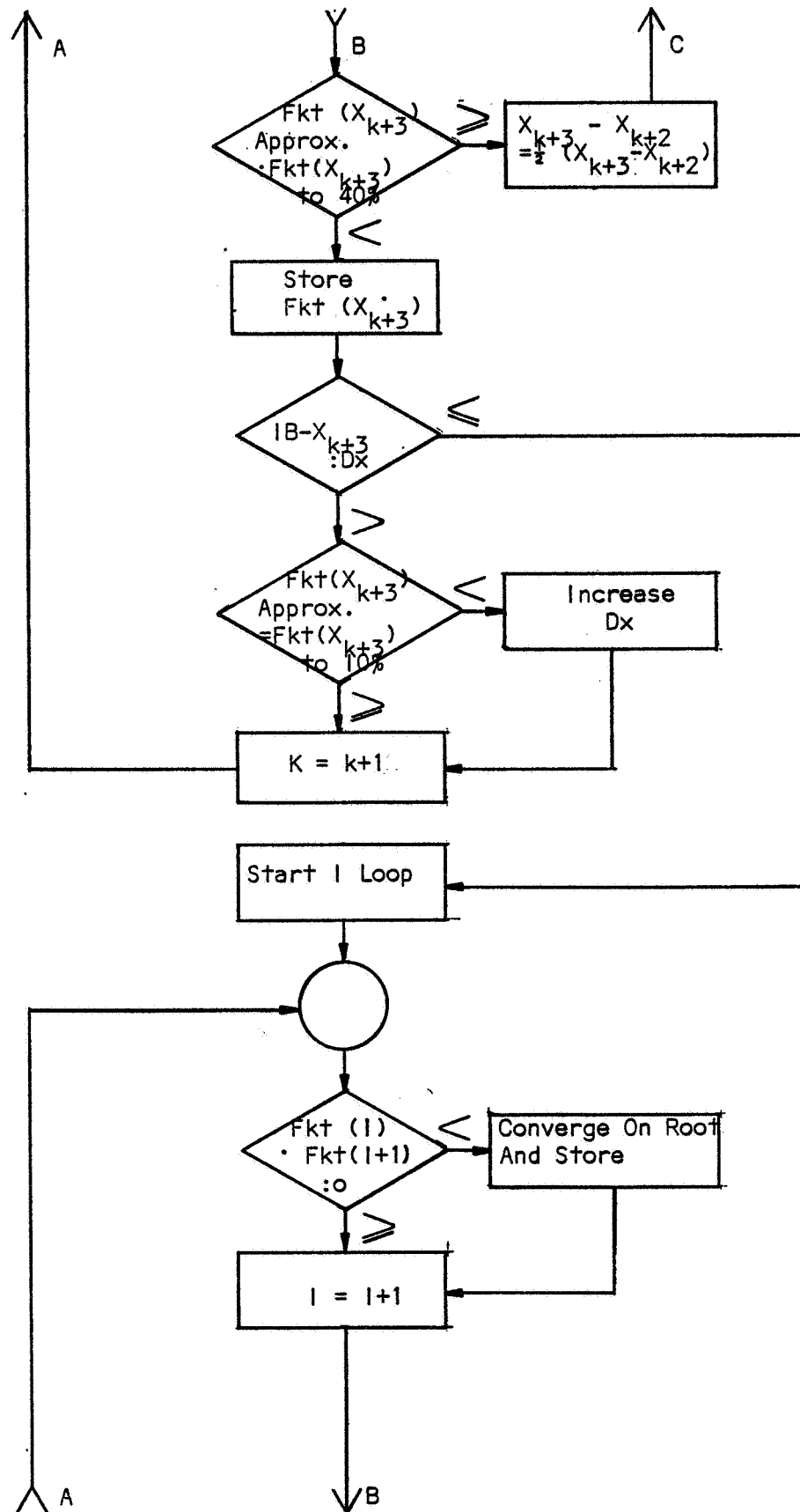


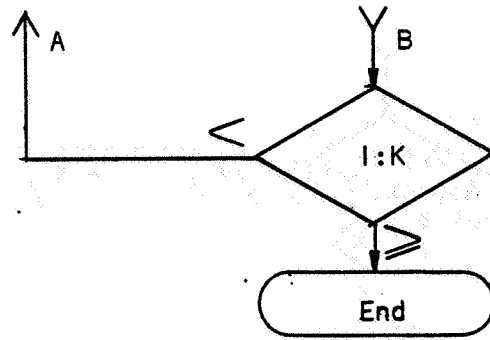




6.1 'Roots' Subroutine Flow Chart For Cylindrical Program







SECTION IV

SPHERICAL CAVITY PROGRAM

1.0 DEFINITION AND ANALYSIS OF PROBLEM

The object of this program is to obtain all of the TE_{mnp} and TM_{mnp} modes that exist in a spherical tank for a frequency band, e.g. (2-4GHz). In addition, the 'Q' or quality factor is calculated for each mode utilizing the conductivity of the tank material. The 'Q' found is only the tank 'Q'.

1.1 TM Equations (1)

Equation 1:

$$FR = \frac{u'_{mn}}{2\pi R \sqrt{\epsilon \mu}}$$

$FR \triangleq$ as the resonant frequency of TM mode.

Where:

u'_{mn} = Bessel zero associated with the derivative of half-order Bessel function (Spherical Bessel function)

R = radius of sphere

$\epsilon = \epsilon_r \epsilon_0$, permittivity of filling material

$\mu = \mu_r \mu_0$, permeability of filling material

Equation 2:

$$QM = \frac{377 \cdot \left(u'_{mn} - \frac{m(n+1)}{u'_{mn}} \right)}{2 \sqrt{\pi (FR) \mu_2 |\epsilon_r|}} \cdot S$$

$Q_m \triangleq$ as the 'Q' associated with 'FR' of 'TM' mode

m = integer quality factor associated with 'm' in u'_{mn} (order of Bessel function)

ϵ_r = relative permittivity of filling material

F_r = Resonant Frequency

$\mu_2 = \mu_{2r} \mu_0$, permeability of cavity wall

S = conductivity of cavity wall

(1) Equations from Harrington's Time-Harmonic Electromagnetic Fields.
McGraw-Hill

1.2 'TE' Equations:

Equation 3:

$$FR = \frac{u_{mn}}{2\pi R \sqrt{\epsilon \mu}}$$

Δ
FR = Resonant frequency of 'TE' mode

Where:

u_{mn} = Bessel zero associated with the half-order Bessel function
(Spherical Bessel function)

Equation 4:

$$QE = \frac{377 \cdot (u_{mn})}{2 \cdot \sqrt{\epsilon_r} \cdot \frac{\sqrt{\pi(FR)\mu_2}}{S}}$$

Δ
QE = as 'Q' or quality factor associated with 'FR' of a 'TE' mode

2.0 METHOD OF SOLUTION

The frequency equation was solved for the Bessel zero.

Equation 5:

$$u_{mn} = (FR)(2)(\pi)(R)\sqrt{(\epsilon)(\mu)}$$

The Bessel zeros are read into the computer as input data, must meet the following conditions:

Equation 6:

$$u_{mn} \geq (FL)(2)(\pi)(R)\sqrt{(\epsilon)(\mu)} = A12$$

Where:

$FL \triangleq$ lower frequency limit

Equation 7:

$$u_{mn} \leq (FU) (2) (\pi) (R) \sqrt{(\epsilon) (\mu)} = A14$$

Where:

$FU \triangleq$ upper frequency limit

In the program the right hand side of Equation 6 is called A12 and the right hand side of Equation 7 is called A14. While u_{mn} is called A3. Two 'IF' Statements determine when computation should start and stop.

IF (A3-A14) go to next 'IF' Statement (-), go to next 'IF' Statement (0), stop (+)

IF (A3-A12) read another u_{mn} (-), go to next statement (0), go to next statement (+)

The number of degenerate modes per Bessel zero is 2 times (M+1), where 'M' is the order of Bessel zero. This number is printed out(D).

The accumulative total is also printed out and is just the running total of 'D'.

3.0 PROGRAM CAPABILITIES, LOGICAL TECHNIQUES, AND OPTIONS

3.1 The program can be run for different sizes of tanks, different tank materials, and different filling materials.

3.2 'IF' statements are used to give checks on the suitability of a Bessel zero and the direction of the program to 'TE' or 'TM' equations as applicable.

3.3 Some of the options lie in the output statements. The output is printed but may be placed on tape if operations are to be performed on the output. The format may be changed for greater accuracy.

4.0 LIMITATIONS AND ACCURACY

4.1 Five place accuracy is assured for all output.

4.2 The upper frequency limit must not be so high as to allow u_{mn} (last card in data deck) to be less than or equal to $A14, (Fu)(2)(\pi)\sqrt{\epsilon\mu}$, or the program will not stop automatically.

5.0 FORTRAN NAMES AND MEANINGS USED IN PROGRAM

Explained in paragraphs 1.1, 1.2, and 2.0

6.0 INPUT AND OUTPUT PARAMETERS

6.1 Input

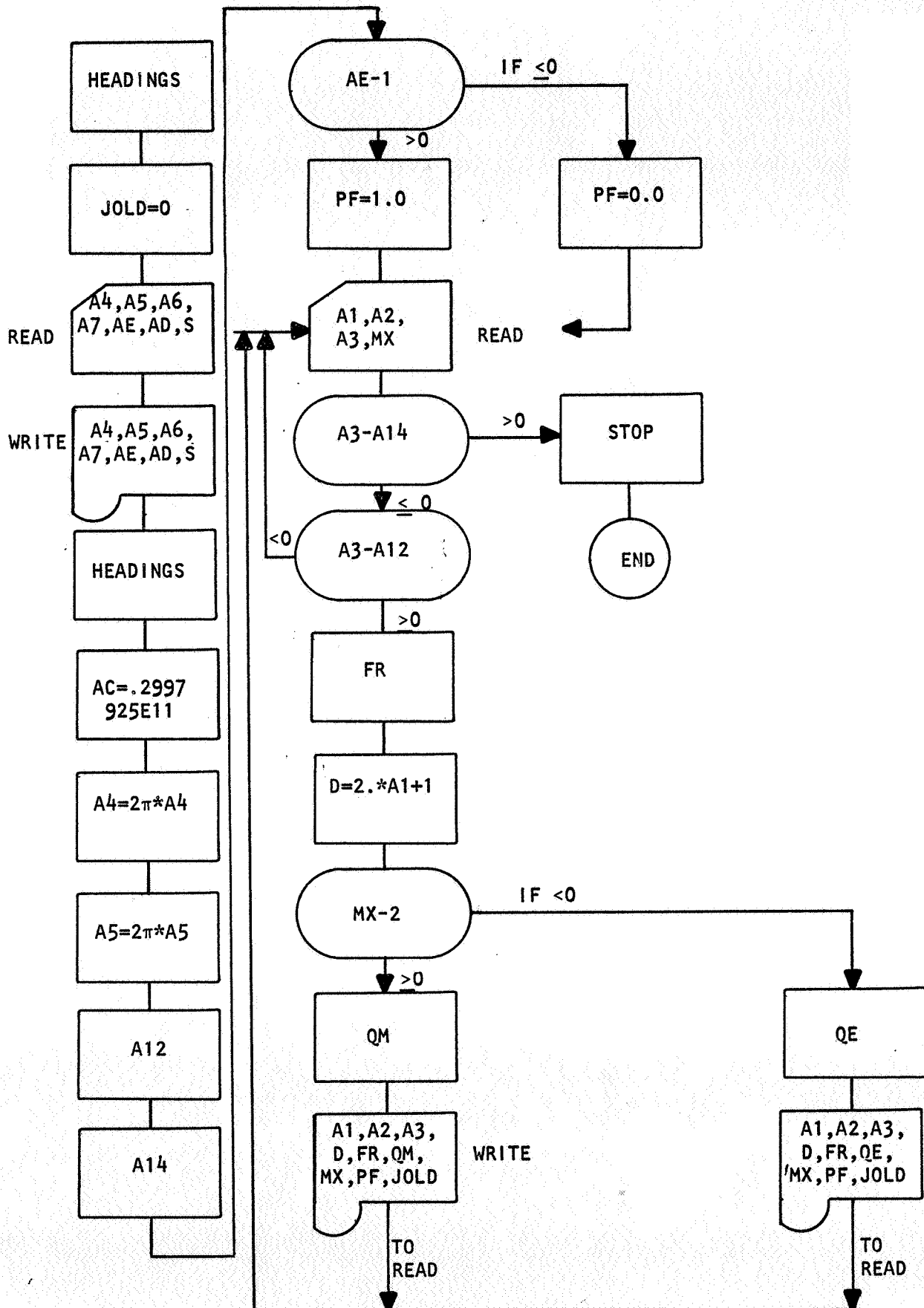
A1 = M (an integer)	E 12.5
A2 = N (an integer)	E 12.5
A3 = X_{mn} (a number)	E 12.5
A4 = FL (Hz)	E 12.5
A5 = F_u (Hz)	E 12.5
A6 = L (cm)	E 12.5
A7 = R (cm)	E 12.5
AE = ϵ_r (Dimensionless)	E 12.5
AD = N/A	E 12.5
MX = Mode TE = 1, TM = 2	I 2
S = Conductivity (mhos/m) $\times 10^{-7}$	F 8.3

6.2 Output

All of the above format except A1 and A2 plus the following:

M = M (an integer)	I 3
N = N (an integer)	I 3
FR = Resonant Frequency of 'TE' or 'TM' mode (Hz)	F 12.0
QE = 'Q' of 'TE' mode (a numerical ratio)	F 12.0
QM = 'Q' of 'TM' mode (a numerical ratio)	F 12.0
J = Number of degeneracies per Bessel zero (an integer)	I 3
JOLD = Accumulative resonance count (a number)	I 6

7.0 DETAILED FLOW DIAGRAM



THIS PAGE INTENTIONALLY LEFT BLANK

SECTION V

STATISTICAL PROGRAM

A. CYLINDRICAL CAVITY - EXACT Q

1.0 Definition and Analysis of Problem

The object of the program is to give all of the TE_{mnp} and TM_{mnp} modes that exist in an empty or full cylindrical tank for a frequency band, e.g. (2.-4. GHz). In addition, the "Q" or quality factor is calculated for each mode utilizing the conductivity of the tank material. The "Q" found is only the tank "Q".

1.1 TM Equations (1)

$FRM \triangleq$ Resonant frequency of TM mode.

$QM \triangleq$ Tank "Q" associated with the TM mode.

Equation 1

$$F \quad FRM = \frac{1}{2\pi R \sqrt{\epsilon \mu}} \sqrt{(X_{mn})^2 + \left(\frac{P\pi R}{L}\right)^2} \quad Hz$$

where: $R \triangleq$ Radius of tank in cm

$\epsilon \triangleq \epsilon_0 \epsilon_r$ farads/cm

$\mu \triangleq \mu_0 \mu_r$ henries/cm

$X_{mn} \triangleq$ Bessel zero

$P \triangleq$ Number of half-wavelength variations of the mode in the axial direction of the tank

$L \triangleq$ Height of the tank in cm

Note: $\epsilon_r \triangleq$ The dielectric constant of the filling material contained in the tank

$\mu_r \triangleq$ The permeability of the filling material contained in the tank.

There are two "Q" equations for TM mode. One is used when $P = 0$, and the other when $P \neq 0$.

When $P = 0$:

Equation 2

$$QM = \frac{\sqrt{\frac{\mu}{\epsilon}} (X_{mn})}{2 \frac{\pi (FRM) M_2}{S} \left(1 + \frac{R_1}{L}\right)}$$

(1) Equations from Harrington's "Time-Harmonic Electromagnetic Fields," McGraw-Hill.



where: S = Conductivity of tank wall in mhos/meter

$\mu_2 = \mu_0 \mu_r$, permeability of tank wall in henries per meter

When $P \neq 0$:

Equation 3

$$QM = \frac{\sqrt{\frac{\mu}{\epsilon}} \left[\left(X_{mn} \right)^2 + \left(\frac{P\pi R}{L} \right)^2 \right]^{1/2}}{2 \sqrt{\frac{\pi (FRm) M_2}{S}} \left(1 + 2 \left(\frac{R}{L} \right) \right)}$$

1.2 TE Equations

FRE \triangleq Resonant frequency of TE mode

QE \triangleq Internal Q Associated with the TE mode

Equation 4

$$FRE = \frac{1}{2\pi R \sqrt{\frac{\epsilon}{\mu}}} \sqrt{\left(X'_{mn} \right)^2 + \left(\frac{P\pi R}{L} \right)^2} \quad H_z$$

Equation 5

$$QE = \frac{\sqrt{\frac{\mu}{\epsilon}} \left[\left(X'_{mn} \right)^2 + \left(\frac{P\pi R}{L} \right)^2 \right]^{3/2} \left[\left(X'_{mn} \right)^2 - m^2 \right]}{2 \sqrt{\frac{\pi (FRE) M_2}{S}} \left\{ \left(\frac{MP\pi R}{L} \right)^2 + \left(X'_{mn} \right)^4 + 2 \left(\frac{R}{L} \right) \left(\frac{P\pi R}{L} \right) \left[\left(X'_{mn} \right)^2 - m^2 \right] \right\}}$$

2.0 Method of Solution

The frequency equations were solved for the Bessel zero (X_{mn}) and P . A maximum and minimum P were found for any Bessel zero which determined the limits of the "DO LOOP"; e.g. (DO 8 K = P1, P2), P1 being P minimum and P2 being P maximum. The Bessel zero equation was solved for maximum and minimum X_{mn} for associated P1, P2, and frequency range. Since the Bessel zeros are read in order of magnitude, a method of determining when the computing should start and end can be determined.

Since FRM and FRE equations are identical except for the value of a Bessel zero; either equation 4 or 5 can be used.

E Equation 6

$$P = \frac{L}{R\pi} \left\{ \left[(FR)^2 (2\pi R \sqrt{\frac{\epsilon}{\mu}})^2 \right] - X_{mn}^2 \right\}^{1/2}$$

Equation 7

$$P2 = P \text{ (UPPER)} = \frac{L}{R\pi} \left\{ \left[(FU)^2 (2\pi R \sqrt{\epsilon\mu})^2 \right] - (X_{mn})^2 \right\}^{1/2}$$

where: FU = Upper frequency limit of the frequency band.

Equation 8

$$P1 = P \text{ (LOWER)} = \frac{L}{R\pi} \left\{ \left[(FL)^2 (2\pi R \sqrt{\epsilon\mu})^2 \right] - (X_{mn})^2 \right\}^{1/2}$$

where: FL = Lower frequency limit of the frequency band.

Equation 9

$$X_{mn} = \left\{ (FR)^2 (2\pi R \sqrt{\epsilon\mu})^2 - \left(\frac{P\pi R}{L} \right)^2 \right\}^{1/2}$$

Equation 10

Now

$$X_{mn} \geq \left\{ (FL)^2 (2\pi R \sqrt{\epsilon\mu})^2 - \left[\frac{(P2)\pi R}{L} \right]^2 \right\}^{1/2}$$

Equation 11

And

$$X_{mn} \leq \left\{ (FU)^2 (2\pi R \sqrt{\epsilon\mu})^2 - \left[\frac{(P1)\pi R}{L} \right]^2 \right\}^{1/2}$$

or the TE_{mnp} or TM_{mnp} will have a frequency outside the band limits.

Note: The "M", "N", and "P" found within the equations are integers associated with the m, n, and p of the TE_{mnp} and TM_{mnp} subscripts.

Therefore, the values of P1 and P2 must be integered. The computer is told to integer each.

3.0 Program Capabilities, Logical Techniques, and Options

- 3.1 The program can be run for different sizes of tanks, different tank materials, and different filling materials.
- 3.2 "IF" statements are used to give checks on the suitability of a Bessel zero, the direction of the program to a TE or TM equation and the direction of the program to a TM_{mno} or TM_{mnp} equation.
- 3.3 Some of the options lie in the output statements. The output is both punched and printed. This may be changed to tape output if desired. The output can be sorted by machine if punched or by computer if taped. The output may be sorted according to frequency, Q, etc. for better readability.

The output formats can be changed to get full eight place accuracy instead of five place as given. However, punching cards may not be practical in that case. (Not enough available columns.) The "stop" card can be replaced with a "pause" and "GO TO 6" cards if a series of tanks or conditions would like to be run without making the computer recompile.

4.0 Limitations and Accuracy

Five place accuracy can be assured for all output parameters except for the case $m = 1$. For this case three place accuracy is assured. (Bessel zeros at $m = 1$ are not accurate beyond three places.) The upper frequency limit must not be so high as to allow X_{mn} (last card in data deck) to be less than or equal to:

$$\left\{ (F_u)^2 (2\pi R \sqrt{\epsilon \mu})^2 - \left[\frac{(P1)\pi R}{L} \right]^2 \right\}^{1/2}$$

or the program will not stop automatically. An indication of this happening is the repeating of the last line of printed output. If this case should appear, use the Bessel zero program supplied and generate higher ordered Bessel zeros. (Should not be necessary except in a very extreme case.)

5.0 FORTTRAN Names and Meanings used in Program

Found on comment cards in the source listing.

6.0 Input and Output Parameters

6.1 Input: A1 = M (An integer); E 12.5

A2 = N (An integer); E 12.5

A3 = X_{mn} (A number); E 12.5

A4 = FL (Hz); E 12.5

A5 = FU (Hz); E 12.5

A6 = L (cm); E 12.5

A7 = R (cm); E 12.5

AE = ϵ_r (Dimensionless); E 12.5

AD = NA; E 12.5

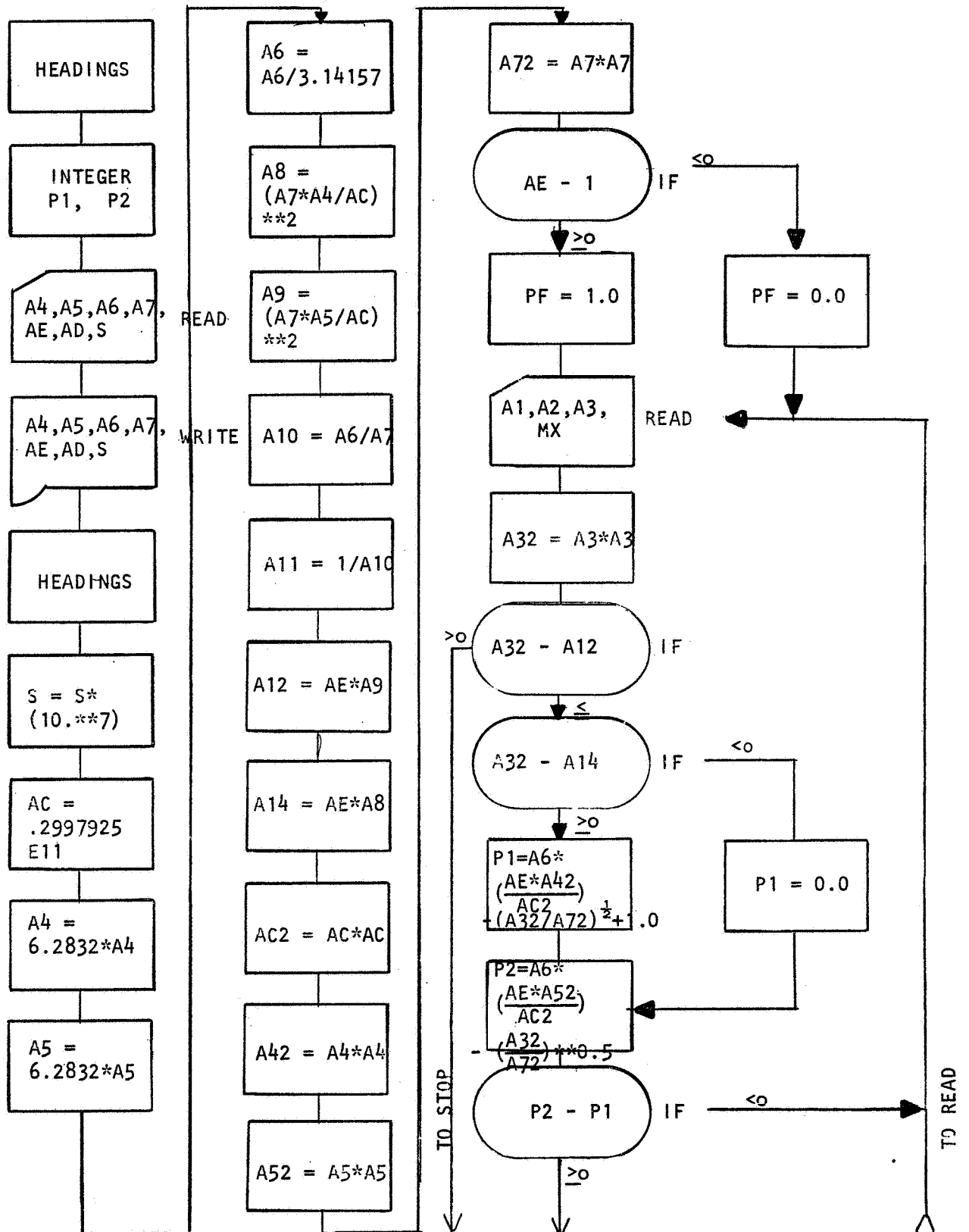
MX = Mode TE = 1, 1 2
TM = 2;

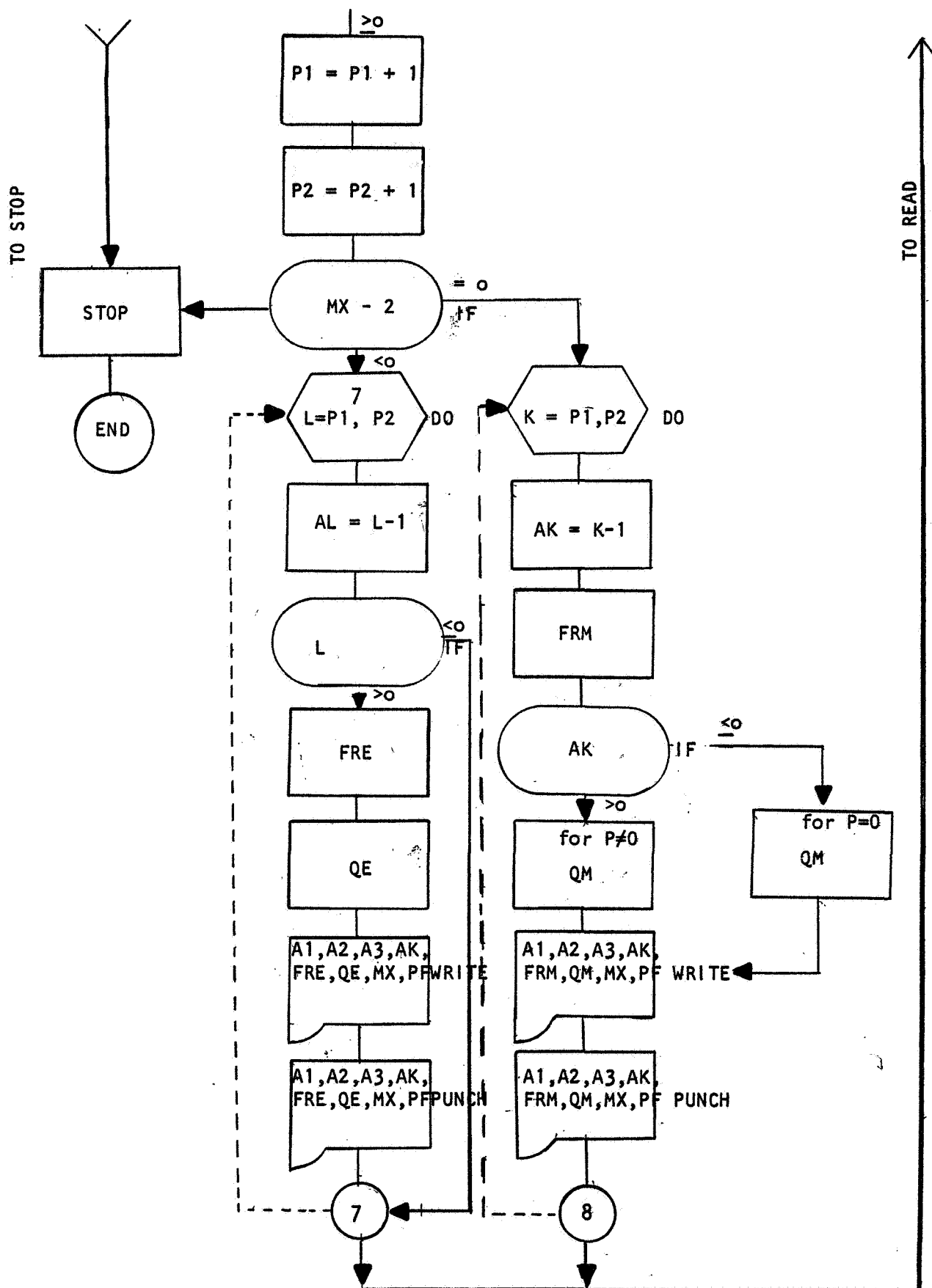
S = Conductivity E 8.3
(mhos/m) x 10^{-7} ;

6.2 Output (All of the above with same format plus the following:)

FRE = Resonant frequency of TE Mode (Hz);	F 12.0
QE = "Q" of TE Mode (A numerical ratio);	F 12.0
FRM = Resonant frequency of TM Mode (Hz);	F 12.0
QM = "Q" of TM Mode (A numerical ratio);	F 12.0
PF = Filling factor for empty or full (A number);	F 6.3
AK = P of TM mode (An integer);	E 12.5
AL = P of TE mode (An integer);	E 12.5

7.0 FLOW DIAGRAM





B. DELTA F PLUS LIST AND COUNT

1.0 Definition and Analysis of Problem

There are two objectives of this program. The first objective is to give a listing and running resonance count of the sorted output of the cylindrical cavity programs. (The outputs of these cavity programs have to be sorted for frequency increases for each filling factor. For example, in sorted form, the frequency might increase in the order from 1 to 4 GHz for a filling factor of 0.1 and the next set of data would have the frequency increasing from 1 to 4 GHz for a filling factor of 0.2.) The second objective is to give the separation of the pulses (modes from a theoretical detection system) for various "Q's" of the filling material plus external circuitry.

1.1 List and Count

For any mode that has a "M" value of zero, it is counted as one mode. If "M" has a value other than zero, it is counted as two modes because of the nature of the fields.

1.2 Delta F (Pulse Readability)

The output from a tank, which has been energized with a band of frequencies, is run through a diode (detected). The result is a series of pulses when viewed on an oscilloscope. The width of these pulses is governed by the frequency and overall "Q" of the system. If the pulse widths of any two adjacent modes are great enough, overlapping will occur. This Delta F Program determines how much overlap or separation of mode pulses occur for various "Q's".

Equation 1a:

$$Q1 = \frac{1}{\frac{1}{QME} + \frac{1}{500}}$$

Equation 1b:

$$Q2 = \frac{1}{\frac{1}{QME} + \frac{1}{1000}}$$

Equation 1c:

$$Q_3 = \frac{1}{\frac{1}{Q_{ME}} + \frac{1}{2000}}$$

Equation 1d:

$$Q_4 = \frac{1}{\frac{1}{Q_{ME}} + \frac{1}{20000}}$$

Where:

Q_{ME} = 'Q' or quality factor of tank only

Q_1, Q_2, Q_3, Q_4 = 'Q' or quality factor of total system

Equation 2:

$$SP = F_2 - F_1$$

$SP \triangleq$ Spacing (Difference between succeeding frequencies in Hz)

Equation 3:

$$DF_1 = F_1/Q$$

$$DF_2 = F_2/Q$$

$DF \triangleq$ 1/2 maximum width of pulse

Equation 4: $DF_4 = SP - \frac{(F_1/Q) + (F_2/Q)}{2}$

$DF_4 \triangleq$ Distance in cycles per second between pulses at half-max. points.

2.0 METHOD OF SOLUTION

Four different 'Q' equations are used to give maximum flexibility to the program. Correspondently, there are four DF_1, DF_2, DF_3 , and DF_4 . Equations used in the program to allow four independent operations to be performed on one mode without having to rewind tape, etc.

3.0 PROGRAM CAPABILITIES, LOGICAL TECHNIQUES, AND OPTIONS

3.1 The program can be run on sorted data (sorted according to frequency for each filling) from Cylindrical Partial Filling, Cylindrical Empty or Full Programs.

3.2 One 'IF' Statement is used to direct the first set of data read to special equations because no mode separation can be determined without a reference.

3.3 The 'Q' equations can be altered for different dielectric loss tangents plus external 'Q's'. Sets of formulas may be removed if less than four cases wish to be computed.

4.0 LIMITATIONS AND ACCURACY

Five place accuracy is guaranteed for all parameters. Eight place accuracy is to be expected for FR, Q, SP, DF₂, DF₃, and DF₄.

NOTE: Put stop card at end of data card deck (-0.10000E+01 in columns 1 through 12 inclusive).

5.0 FORTTRAN NAMES AND MEANINGS USED IN PROGRAM

To be found in paragraphs 1.1 and 1.2.

6.0 INPUT AND OUTPUT PARAMETERS

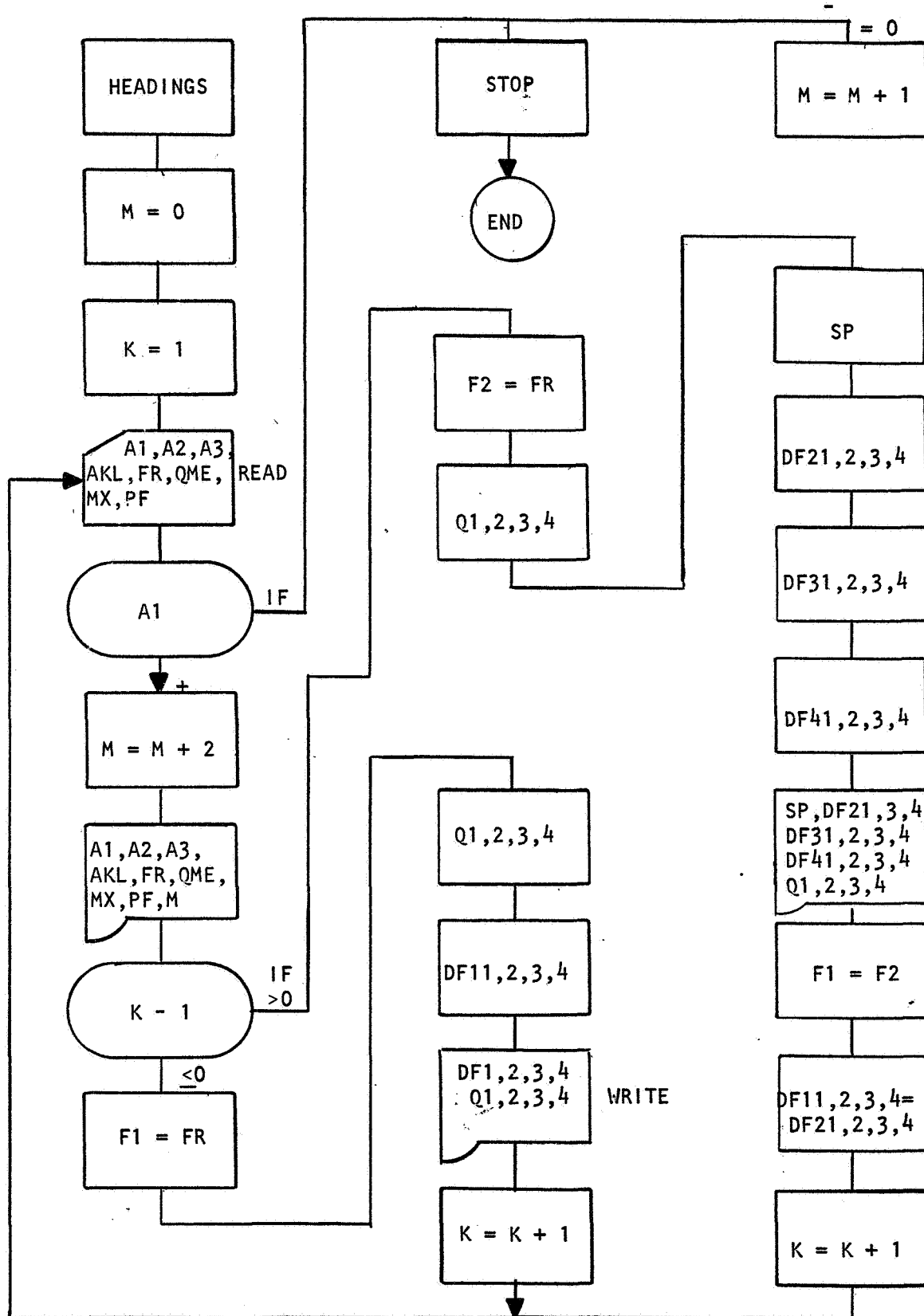
6.1 Input

A1 = M (an integer)	E 12.5
A2 = N (an integer)	E 12.5
A3 = X_{mn} (a number)	E 12.5
AKL = P (an integer)	E 12.5
FR = Resonant frequency of 'TE' or 'TM' mode (Hz)	F 12.0
QME = Tank 'Q' if 'TE' or 'TM' mode (a ratio)	F 12.0
MX = Mode-TE=1, TM=2	I 2
PF = Filling factor (a number)	F 6.3

6.2 Output (all of the above plus)

M = Accumulative mode count (a number)	I 6
DF11	
DF12 = F_1/Q (Hz)	F 12.0
DF13	
DF14	
Q1	
Q2 = System Quality Factor (a ratio)	F 12.0
Q3	
Q4	
DF21	
DF22 = F_2/Q (Hz)	F 12.0
DF23	
DF24	
DF31	
DF32 = $[F_2/Q + F_1/Q]/2$ (Hz)	F 12.0
DF33	
DF34	
DF41	
DF42 = $[SP - DF_3]$ (Hz)	F 12.0
DF43	
DF44	
SP = $[F_2 - F_1]$ (Hz)	F 12.0

7.0 Simplified Flow Diagram



SECTION VI
BESSEL ZERO PROGRAM1.0 DEFINITION AND ANALYSIS OF PROBLEM

The object of this program is to calculate X_{mn} (Bessel zeros) and X'_{mn} (Bessel zeros of J'_m , the derivative of J_m) which cannot be found in existing tables.

1.1 X_{mn} Equations ⁽⁷⁾ (TM)

$$X_{mn} = \frac{A*HPI - B}{FPI*A} - \frac{B*28.*AM*AM - 31}{F8PI*A^3}$$

Where:

$$A = AM + 2*AN - 0.5$$

$$B = 4.*AM*AM - 1.0$$

$$HPI = \pi/2$$

$$FPI = 4\pi$$

$$F8PI = 48.*\pi^3$$

1.2 X'_{mn} Equations ⁽⁸⁾ (TE)

$$X'_{mn} = \frac{C - (D + 3)}{8C} - \frac{7*D^2 + 82.*D - 9}{6.*(4*C)^3} - \frac{83D^3 + 2075D^2 - 3029D + 3537}{15*(4 + C)^5}$$

Where:

for $AM = 0$

$$C = (2*AN + 0.5) * \frac{\pi}{2}$$

for $AM \neq 0$

$$C = (AM + 2*(AN - 1) + 0.5) * \frac{\pi}{2}$$

$$D = 4*AM*AM$$

(⁷) Equation from M.I.T. Radiation Laboratory Series, p. 66, Waveguide Handbook 10.

(⁸) Equations derived from Jahnke & Emde Table of Functions.

2.0 METHOD OF SOLUTION

'AM' corresponds to the order of the Bessel function and 'AN' corresponds to the zero of the Bessel function. Equations in 1.1 and 1.2 are a series representation of the solution of $J_{AM} = 0$ and $J'_{AM} = 0$ respectively. 'DO LOOPS' are used to systematically change the values of 'AM' and 'AN'.

3.0 PROGRAM CAPABILITIES, LOGICAL TECHNIQUES, AND OPTIONS

3.1 The program can generate an unlimited amount of Bessel zeros as the cylindrical cavity program demands.

3.2 'IF' Statements are used to direct the flow to the correct constants. 'GO TO' Statements are used to help the 'IF' Statements in program direction. The 'DO LOOPS' generate 'AM's' and 'AN's'.

3.3 The limits of the 'DO LOOPS' can be changed to give a specific ' X_{mn} ' or a particular group of ' X_{mn} 's'. The output is both written and punched in the format required for reading into the cylindrical cavity programs. Of course, it is necessary to sort according to value of X_{mn} 's (X'_{mn} & X_{mn} together if for cylindrical cavity empty or full program and X'_{mn} and X_{mn} separate for the partial filling cylindrical cavity program.)

Note: X_{mn} = TM mode zero

X'_{mn} = TE mode zero

4.0 LIMITATIONS AND ACCURACY

Five place accuracy is assured for all cases except $AM = 1$, and in the ' X'_{mn} ' case, then three place accuracy is guaranteed. Unfortunately, a series could not be found which better approximated the $AM = 1$ case.

5.0 FORTTRAN NAMES AND MEANINGS USED IN PROGRAM

X_{mn}^{TE} = Bessel zero associated with the 'TE' mode or the ' X_{mn} ' of the derivative of ' J_{AM} ', i.e., (X'_{mn} , J'_{AM}).

X_{mn}^{TM} = Bessel zero associated with the 'TM' mode or the ' X_{mn} ' of ' J_{AM} '.

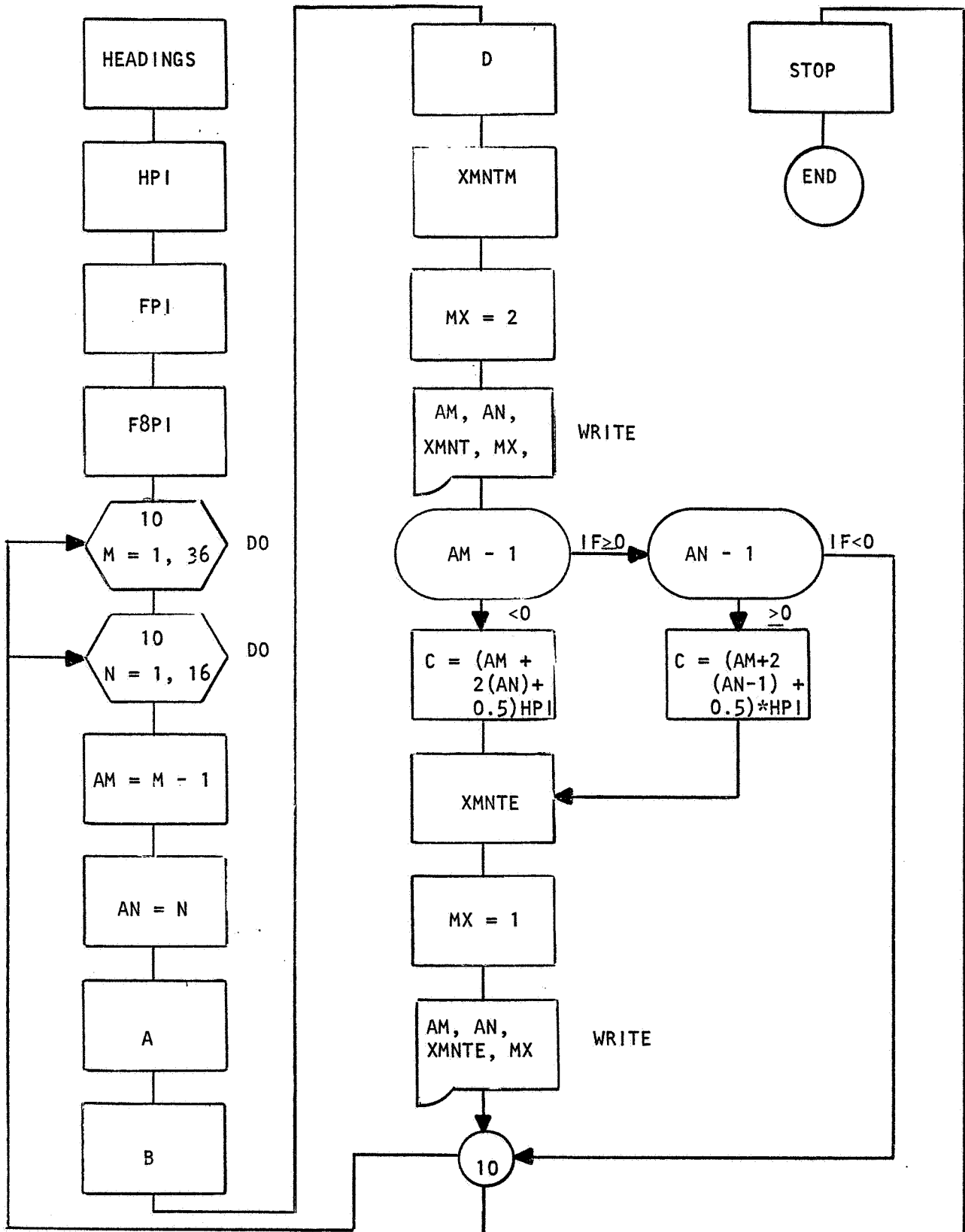
6.0 INPUT AND OUTPUT PARAMETERS

6.1 There is no input.

6.2 Output

$AM = M$ (an integer)	E 12.5
$AN = N$ (an integer)	E 12.5
$X_{mn}^{TE} = X'_{mn}$ (a number)	E 12.5
$X_{mn}^{TM} = X_{mn}$ (a number)	E 12.5
$MX = \text{MODE (TE - 1, TM = 2)}$	I 2

7.0 DETAILED FLOW CHART



APPENDIX C

ANALYTICAL DATA

APPENDIX C.

INTRODUCTION

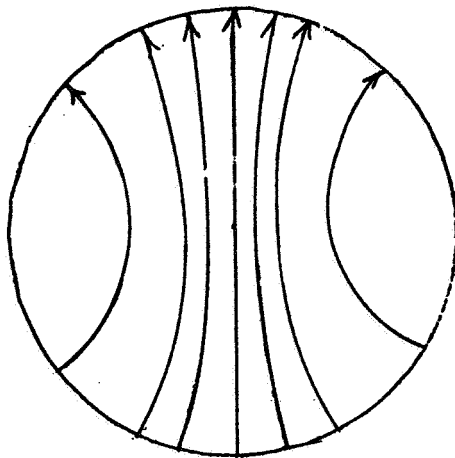
Section I of this appendix describes the field patterns for various TE and TM modes in a cylindrical cavity. A study of these patterns indicates that for a transmitted energy technique of mode detection, the antennas have to be placed in a plane 180° apart.

Section II is a study of the transfer characteristic of adjacent modes. Adjacent modes of various amplitudes and frequencies were considered in order to study the merging of modes. This information was used to obtain the weighing factor for the statistical computer program.

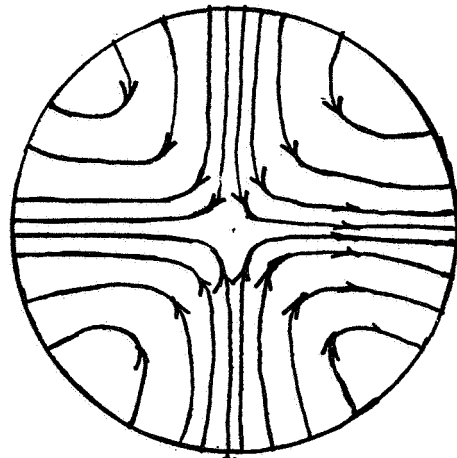
SECTION I

FIELD PATTERNS FOR VARIOUS MODES IN A CYLINDRICAL CAVITY

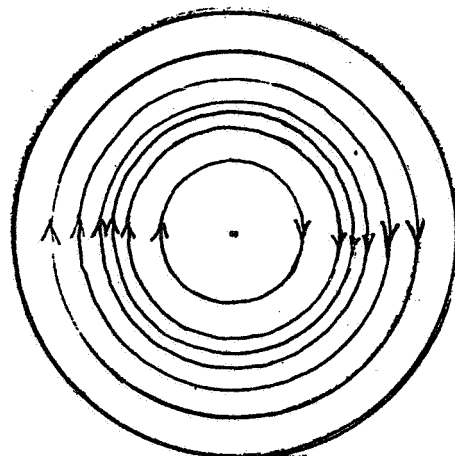
MODE PATTERNS FOR CYLINDRICAL CAVITY
DIAMETER 12" LENGTH 24"
FREQUENCY: 2 - 4 GHz
TRANSVERSE ELECTRICAL MODES



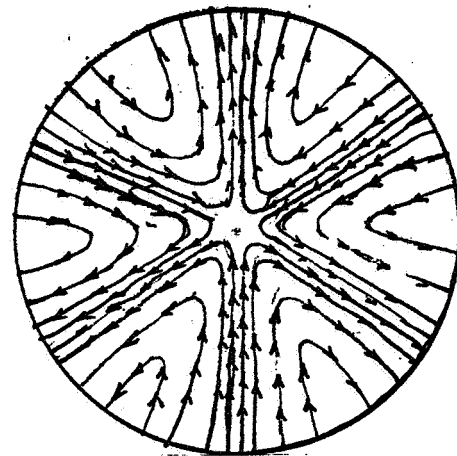
$TE_{1,1}$



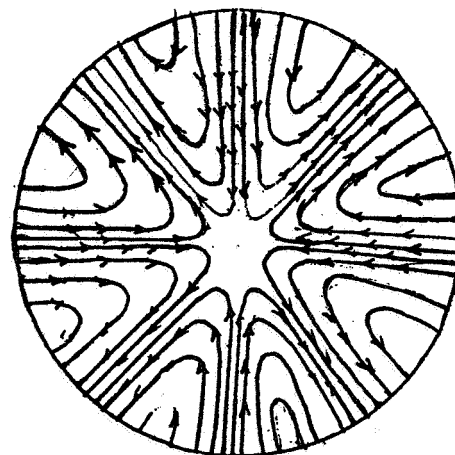
$TE_{2,1}$



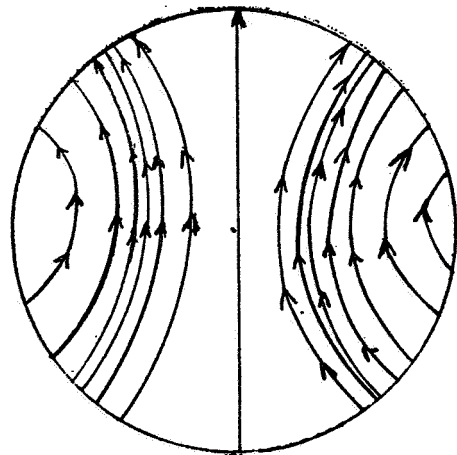
$TE_{0,1}$



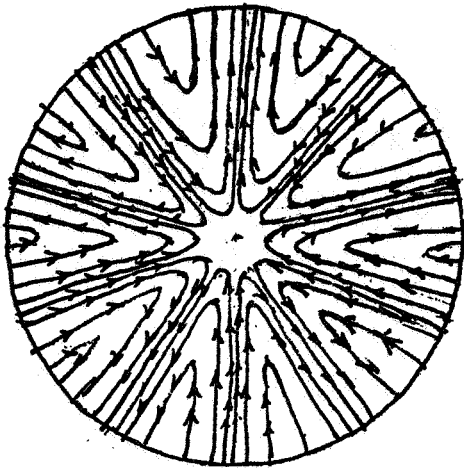
$TE_{3,1}$



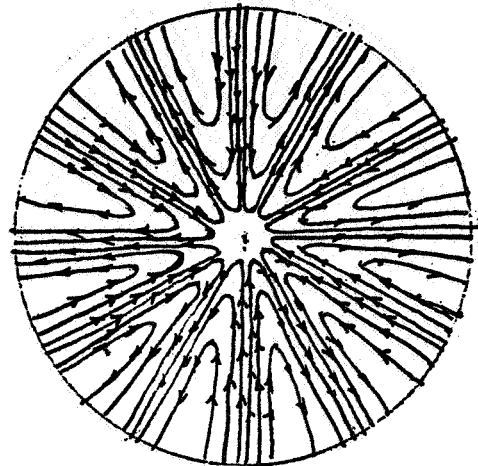
$TE_{4,1}$



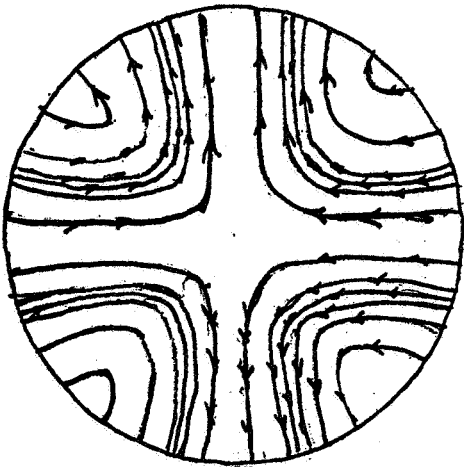
$TE_{1,2}$



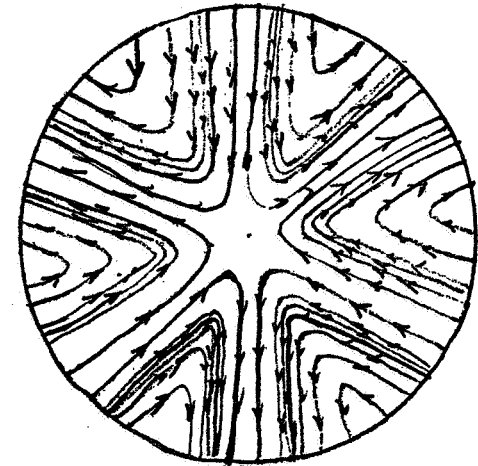
$TE_{5,1}$



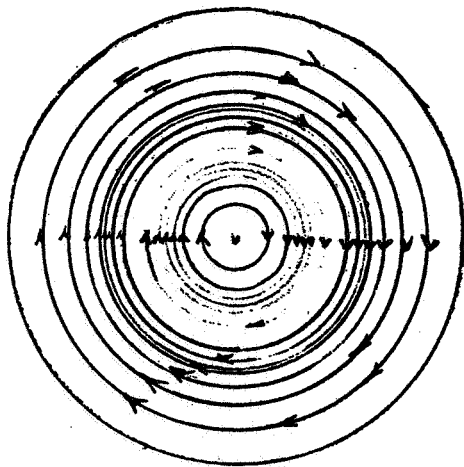
$TE_{6,1}$



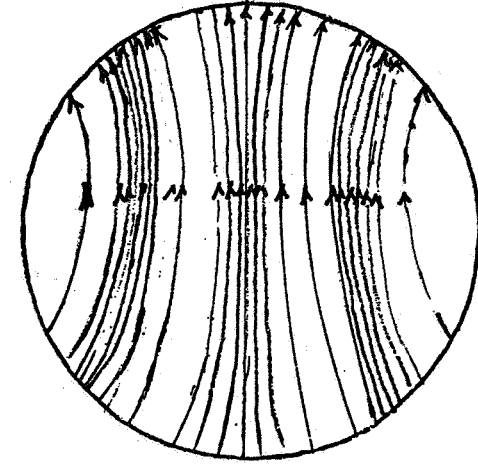
$TE_{2,2}$



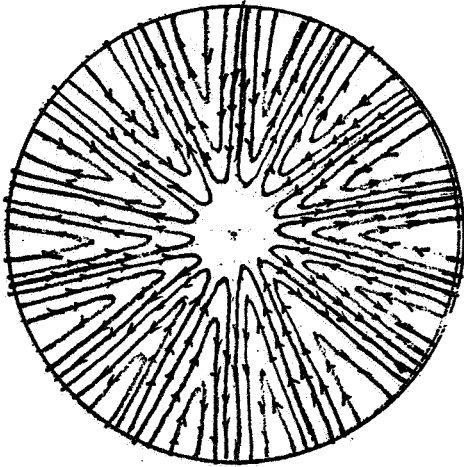
$TE_{3,2}$



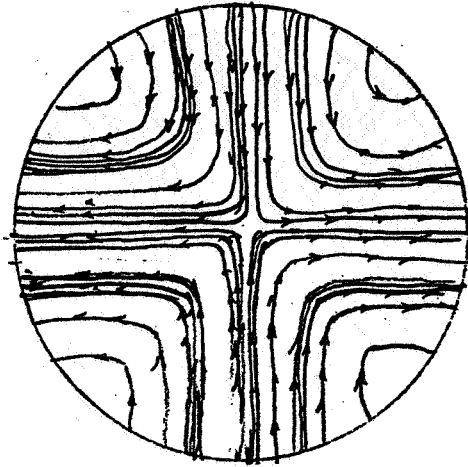
$TE_{0,2}$



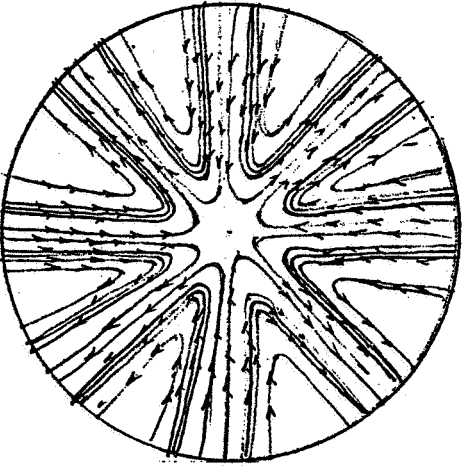
$TE_{1,3}$



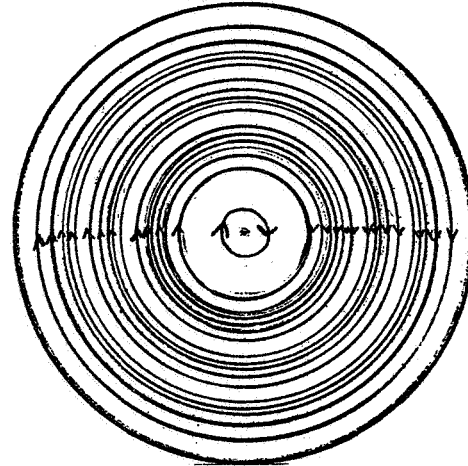
$TE_{7,1}$



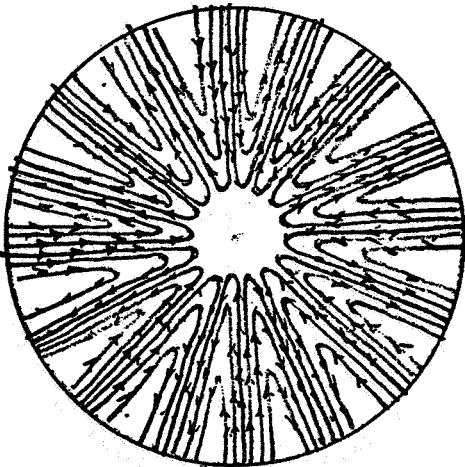
$TE_{2,3}$



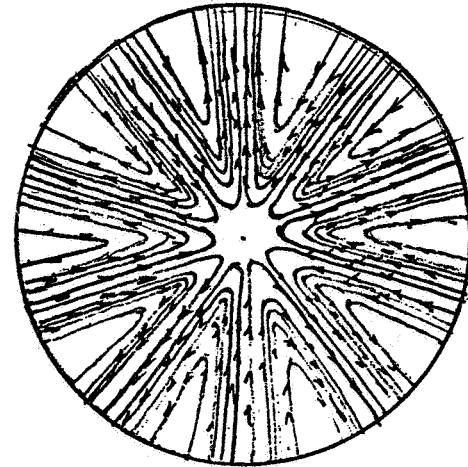
$TE_{4,2}$



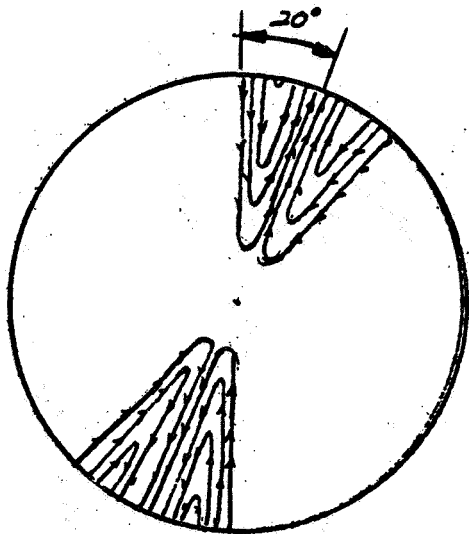
$TE_{0,3}$



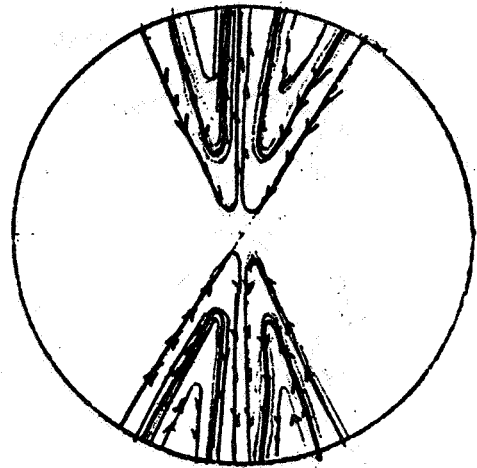
$TE_{8,1}$



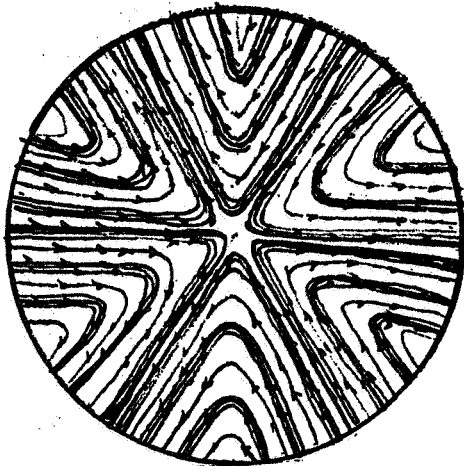
$TE_{5,2}$



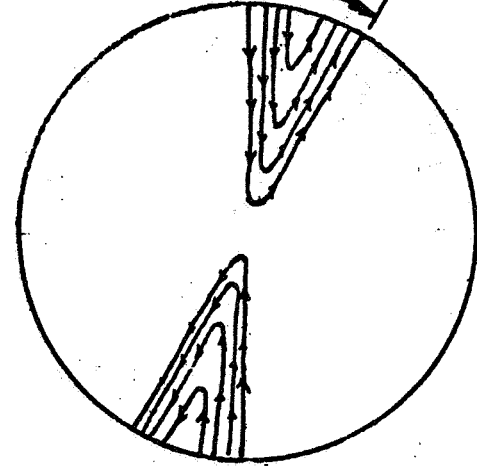
$TE_{9,1}$



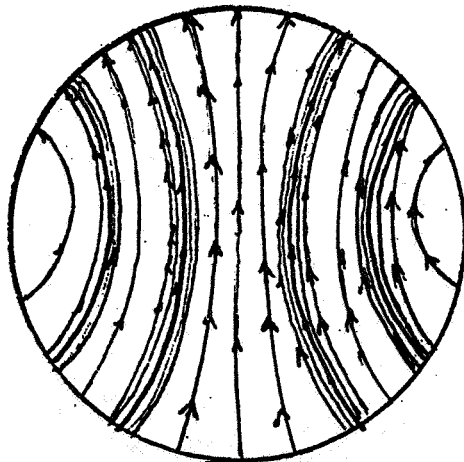
$TE_{6,2}$



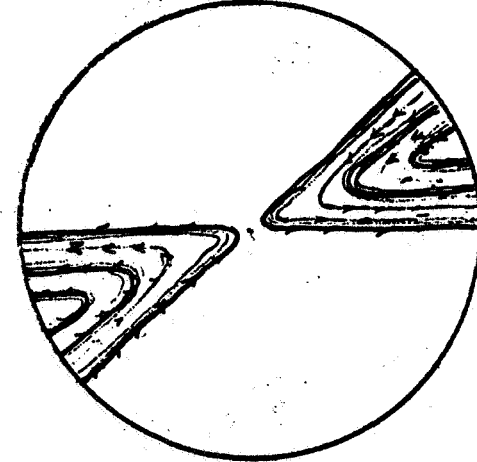
$TE_{3,3}$



$TE_{0,1}$

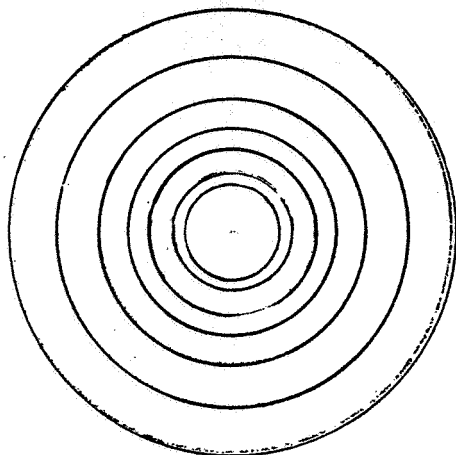


$TE_{1,4}$

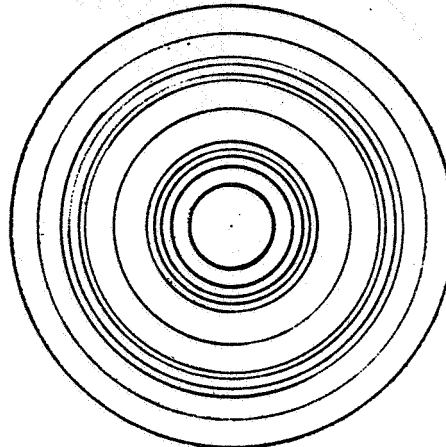


$TE_{4,3}$

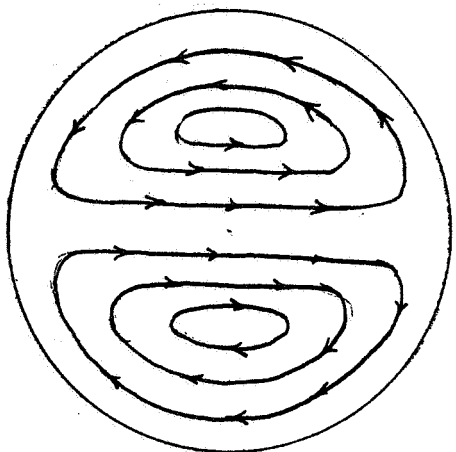
MODE PATTERNS FOR CYLINDRICAL CAVITY
DIAMETER 12" LENGTH 24"
FREQUENCY: 2 - 4 GHz
TRANSVERSE MAGNETIC MODES



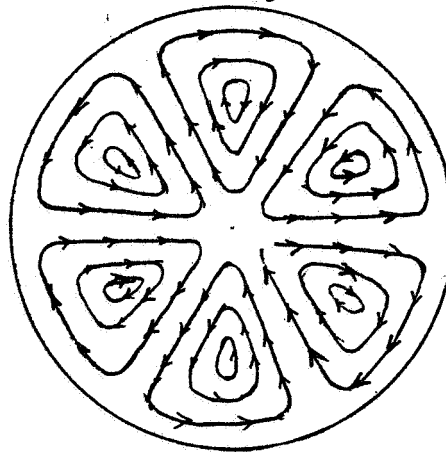
$TM_{0,1}^{15}_8$



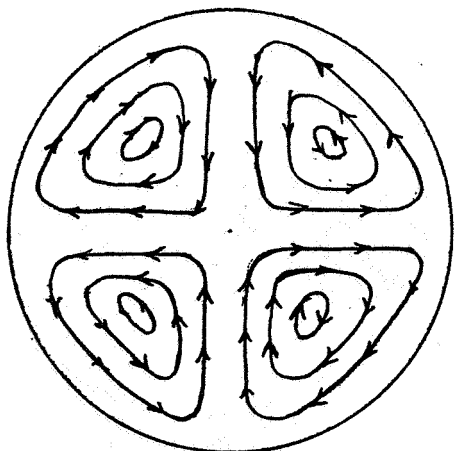
$TM_{0,2}^{14}_5$



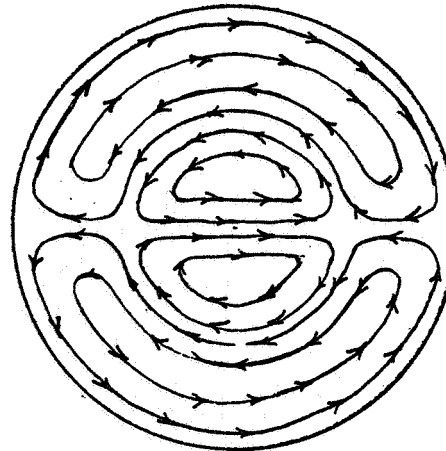
$TM_{1,1}^{15}_7$



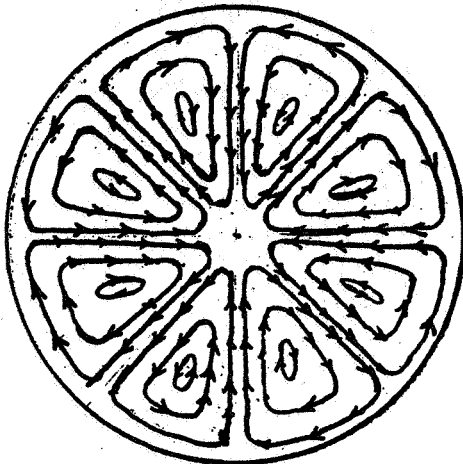
$TM_{3,1}^{14}_1$



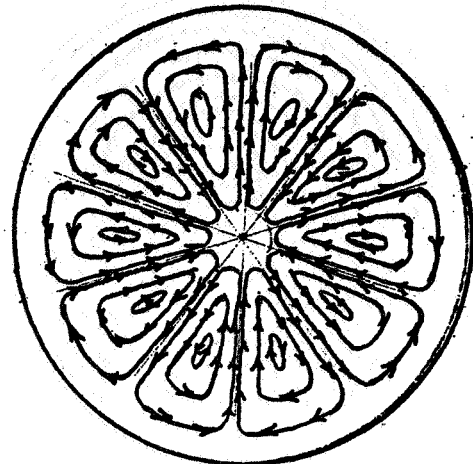
$TM_{2,1}^{14}_5$



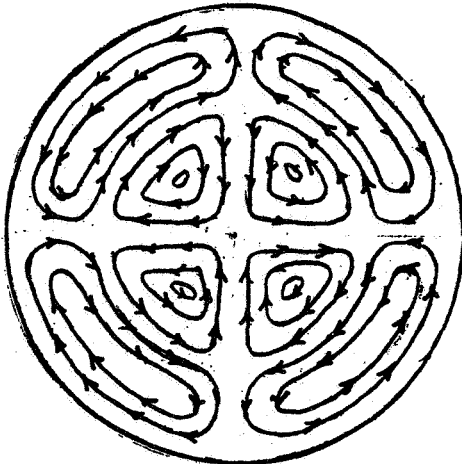
$TM_{1,2}^{13}_0$



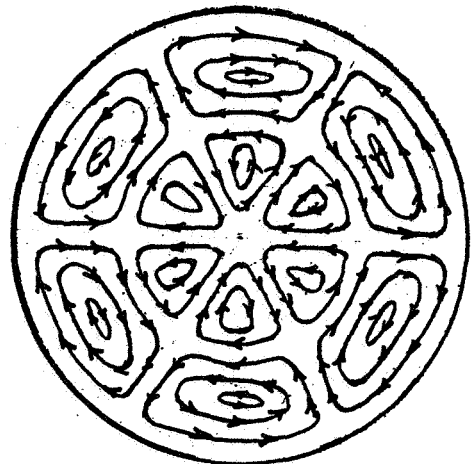
$TM_{4,1}^{13}_0$



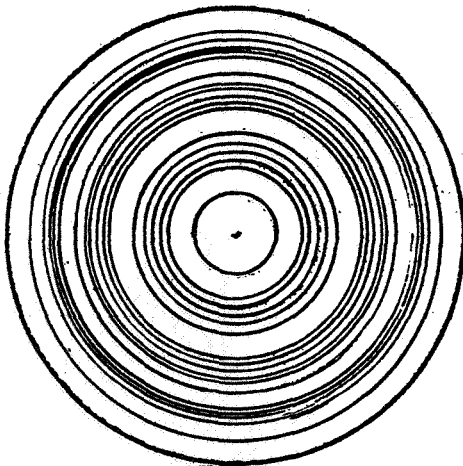
$TM_{5,1}^{11}_0$



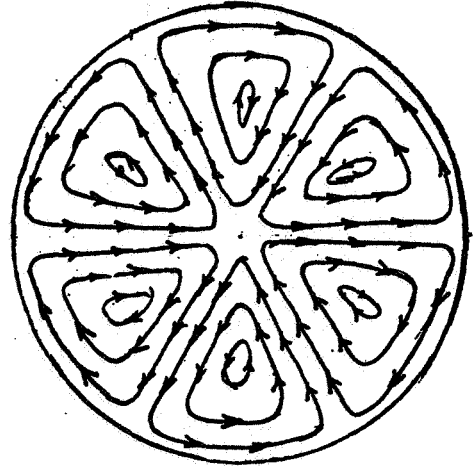
$TM_{2,2}^{12}_0$



$TM_{3,2}^{10}_0$



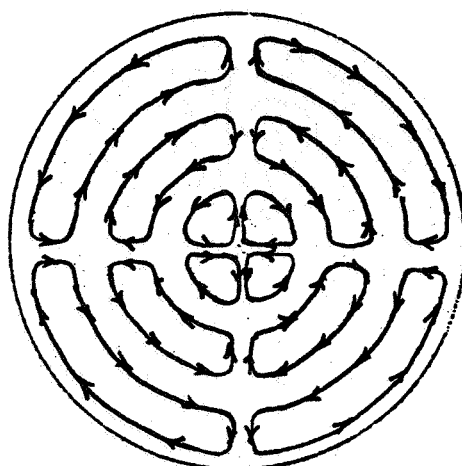
$TM_{0,3}^{11}_0$



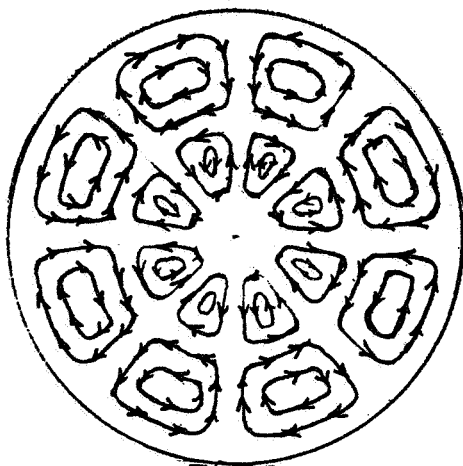
$TM_{6,1}^{10}_0$



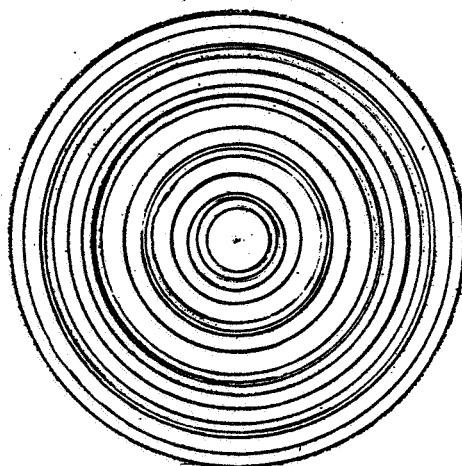
TM_{1,30}⁹



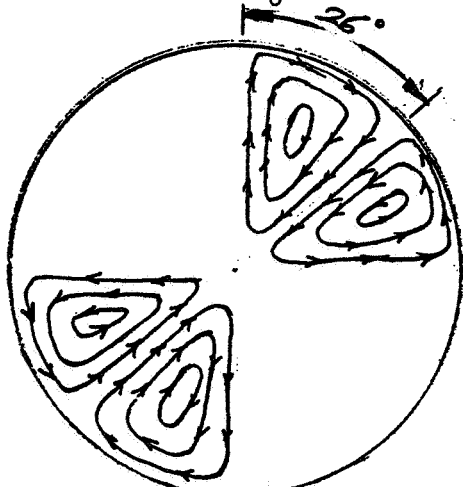
TM_{2,30}⁶



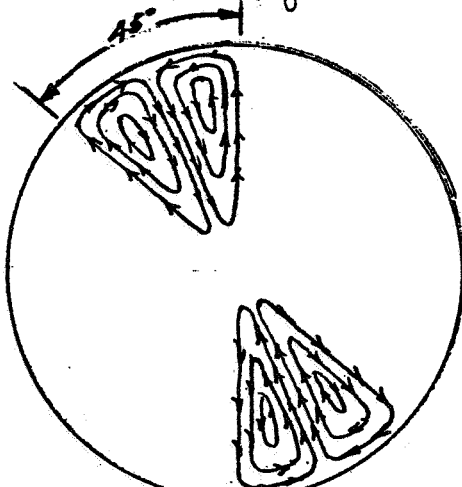
TM_{4,20}⁸



TM_{0,40}⁶



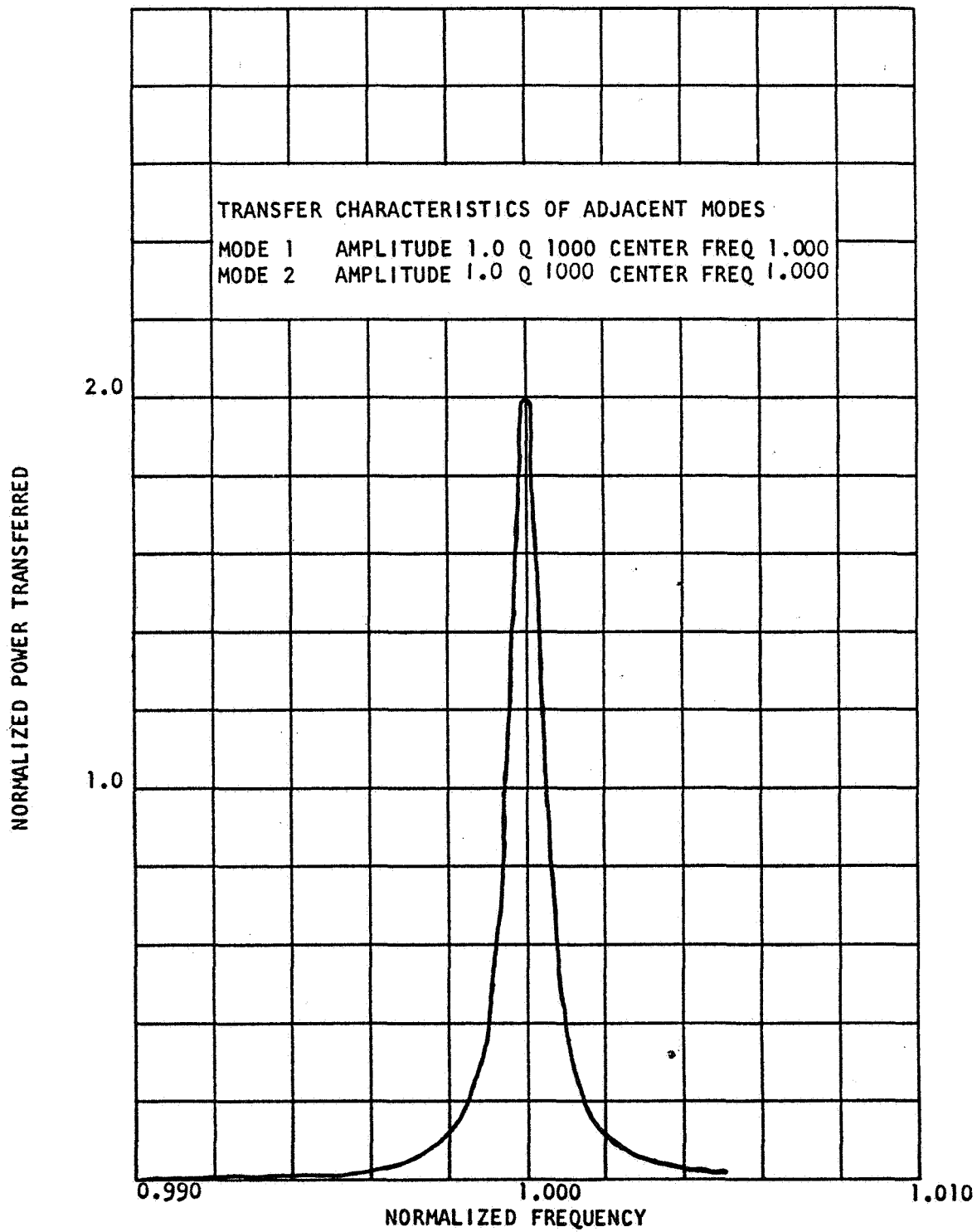
TM_{7,10}⁸

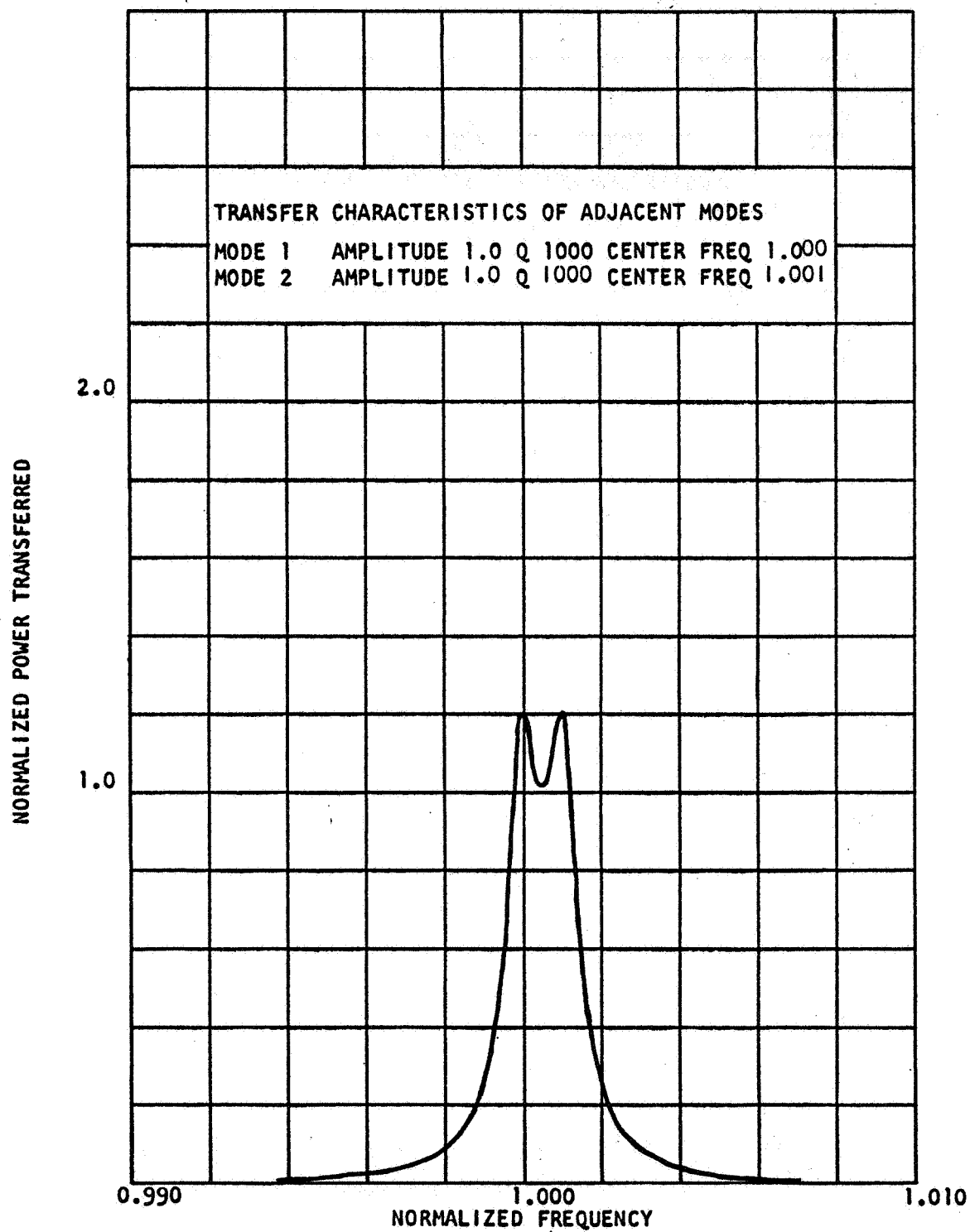


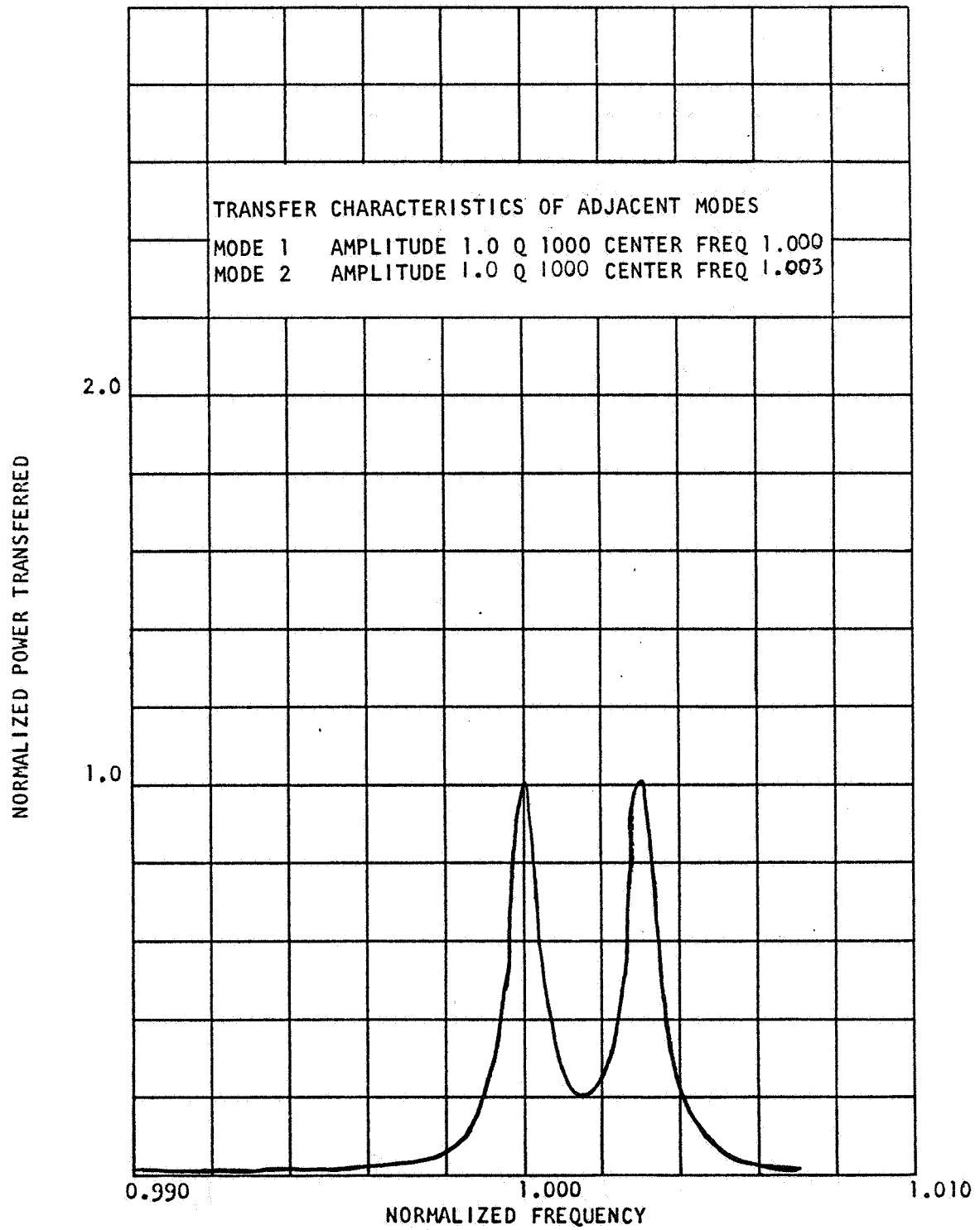
TM_{8,10}⁴

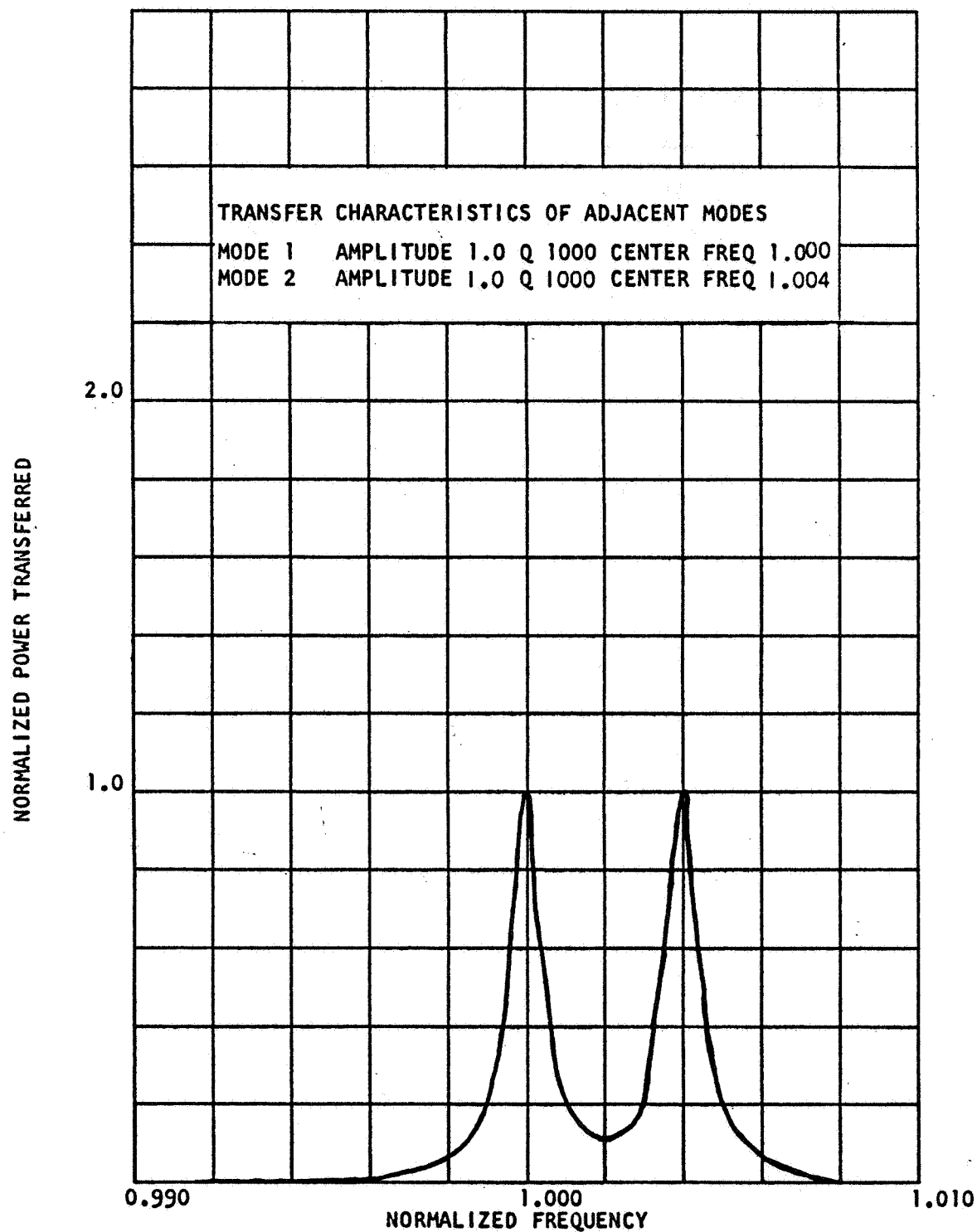
SECTION II

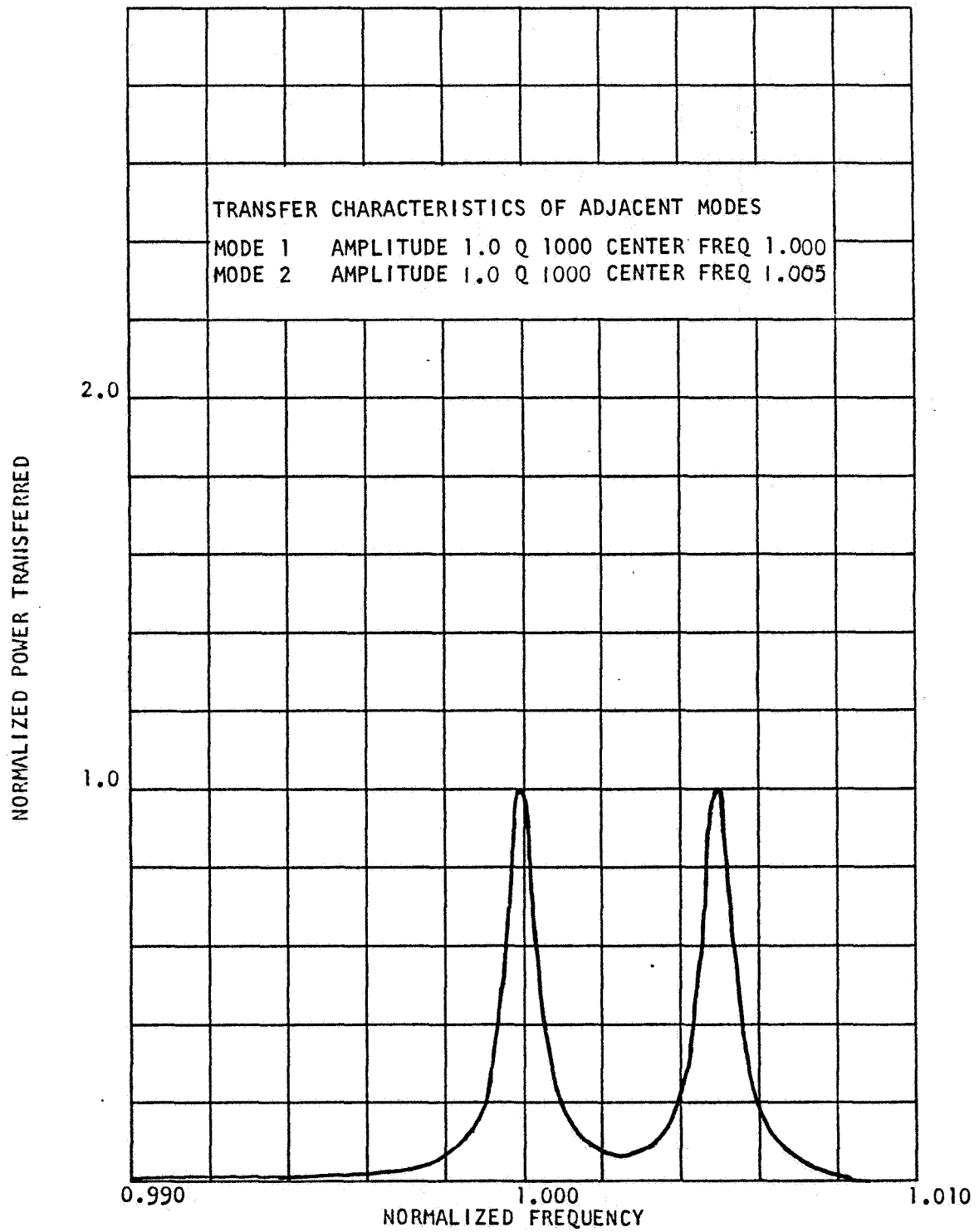
TRANSFER CHARACTERISTICS OF ADJACENT MODES

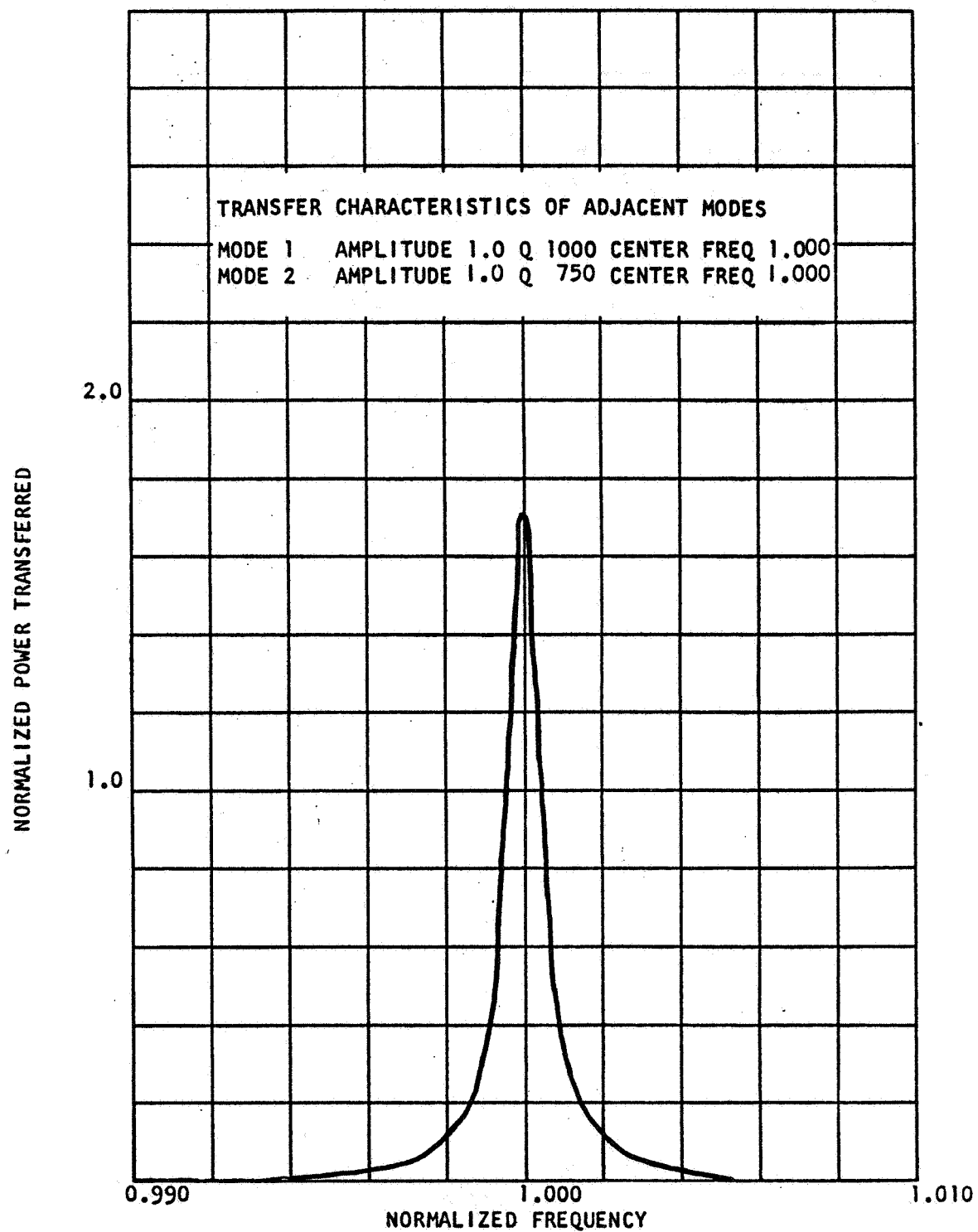


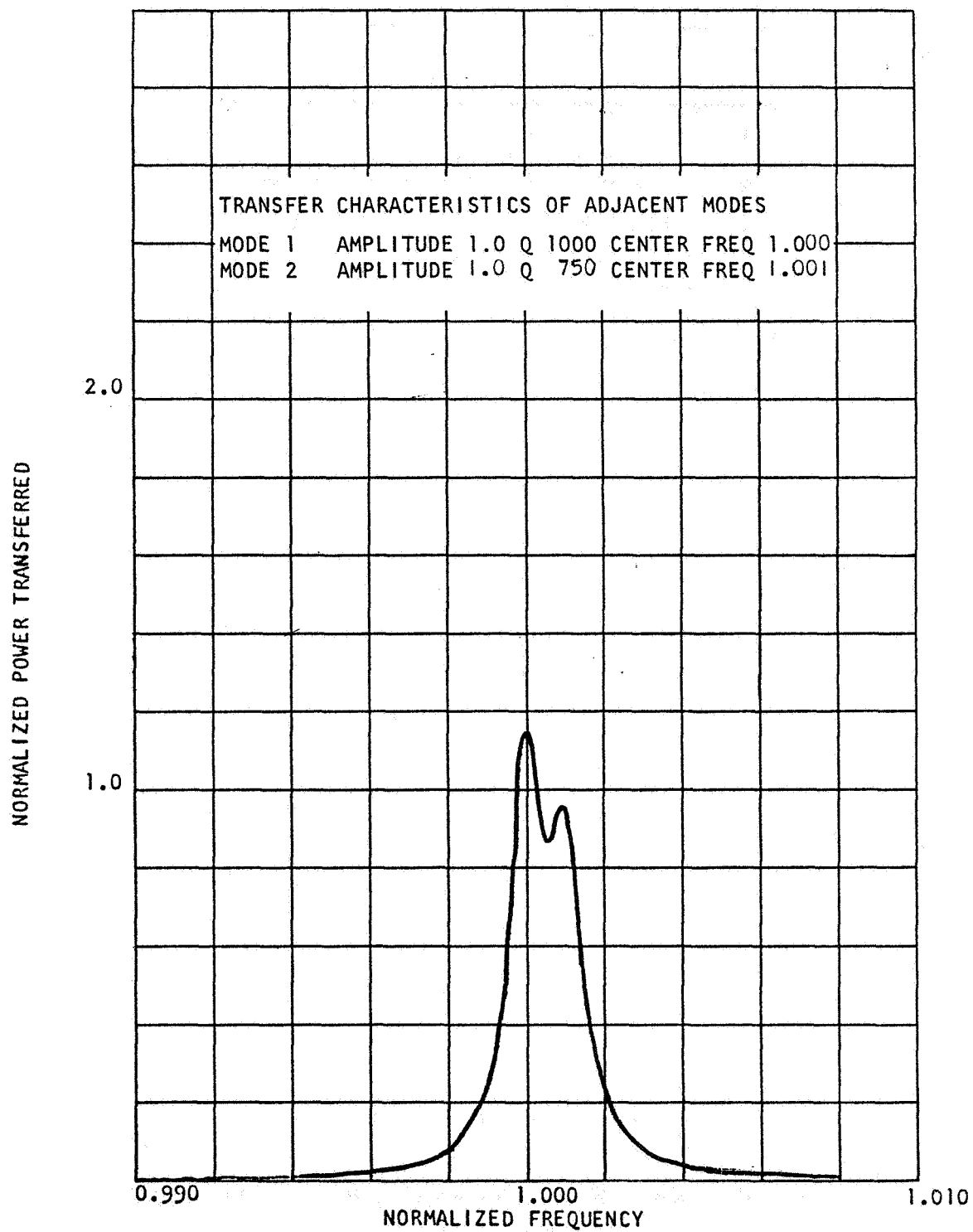


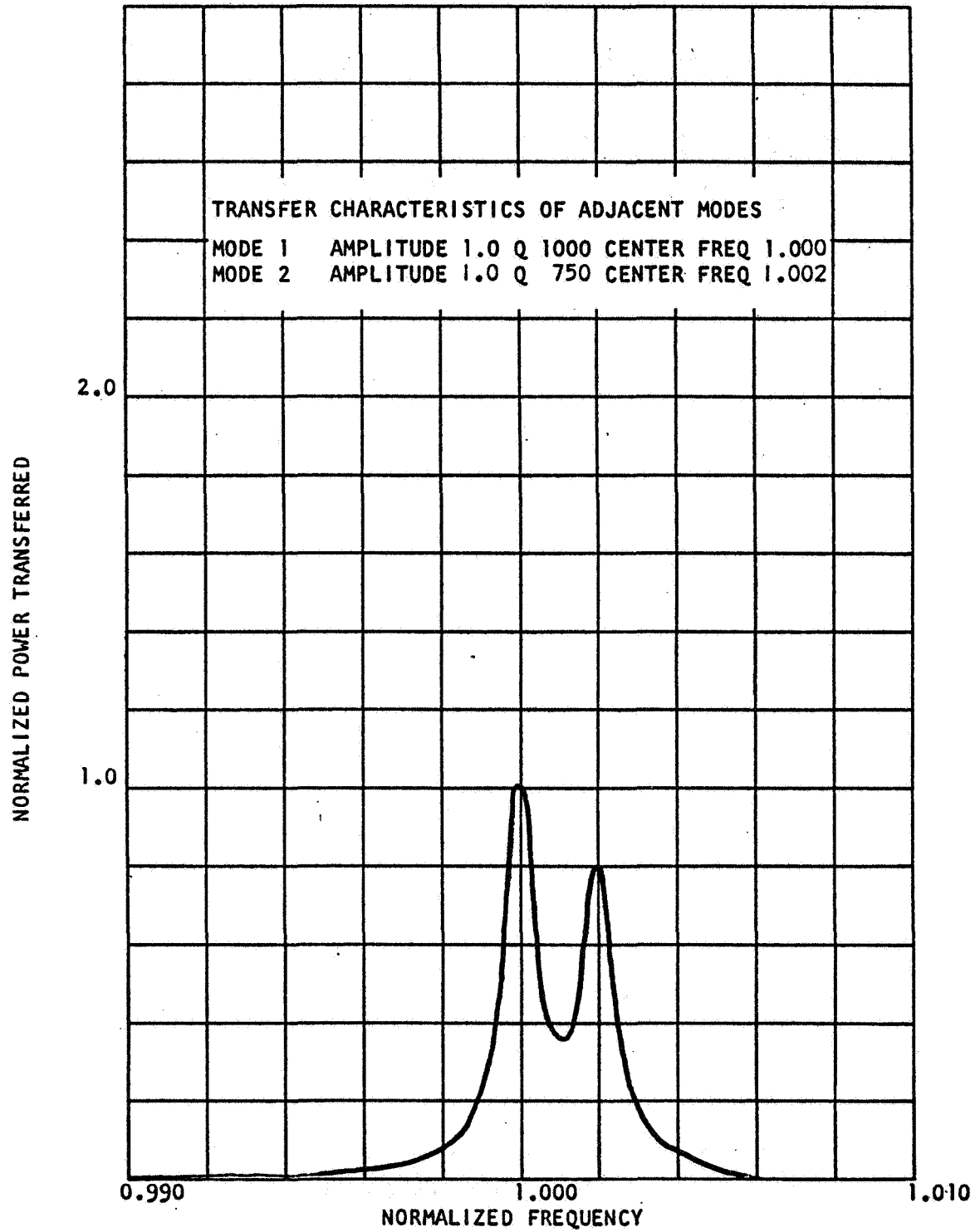


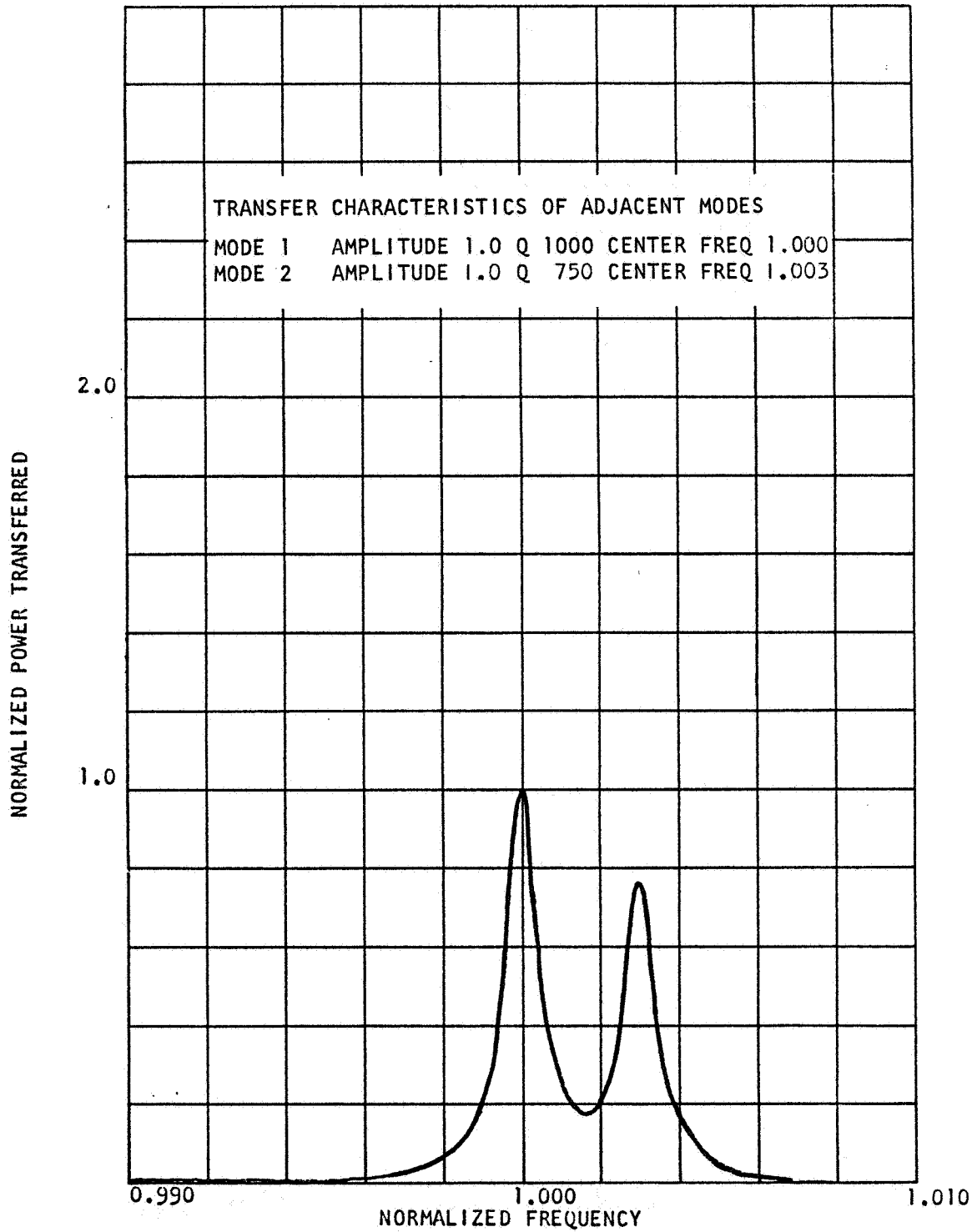


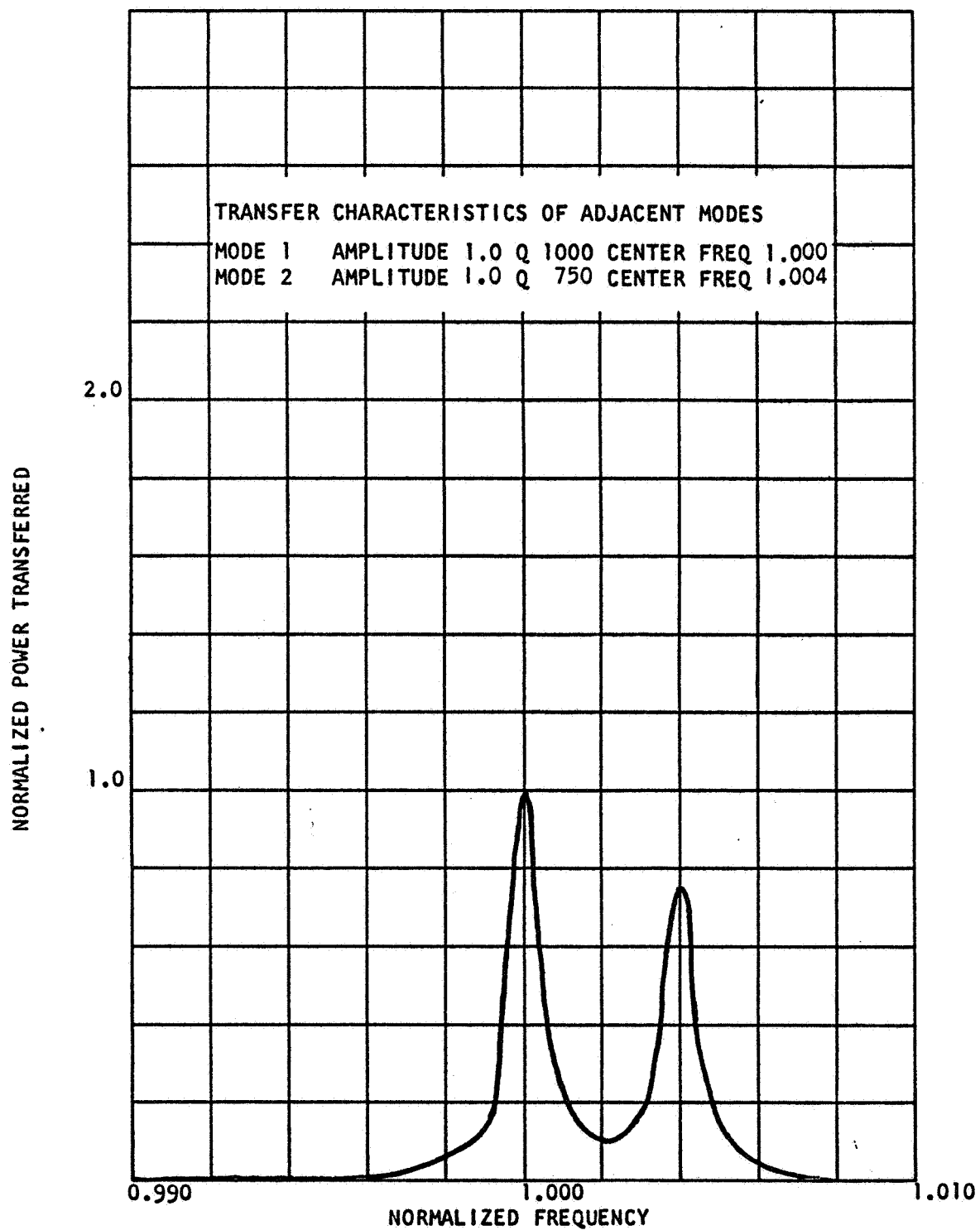


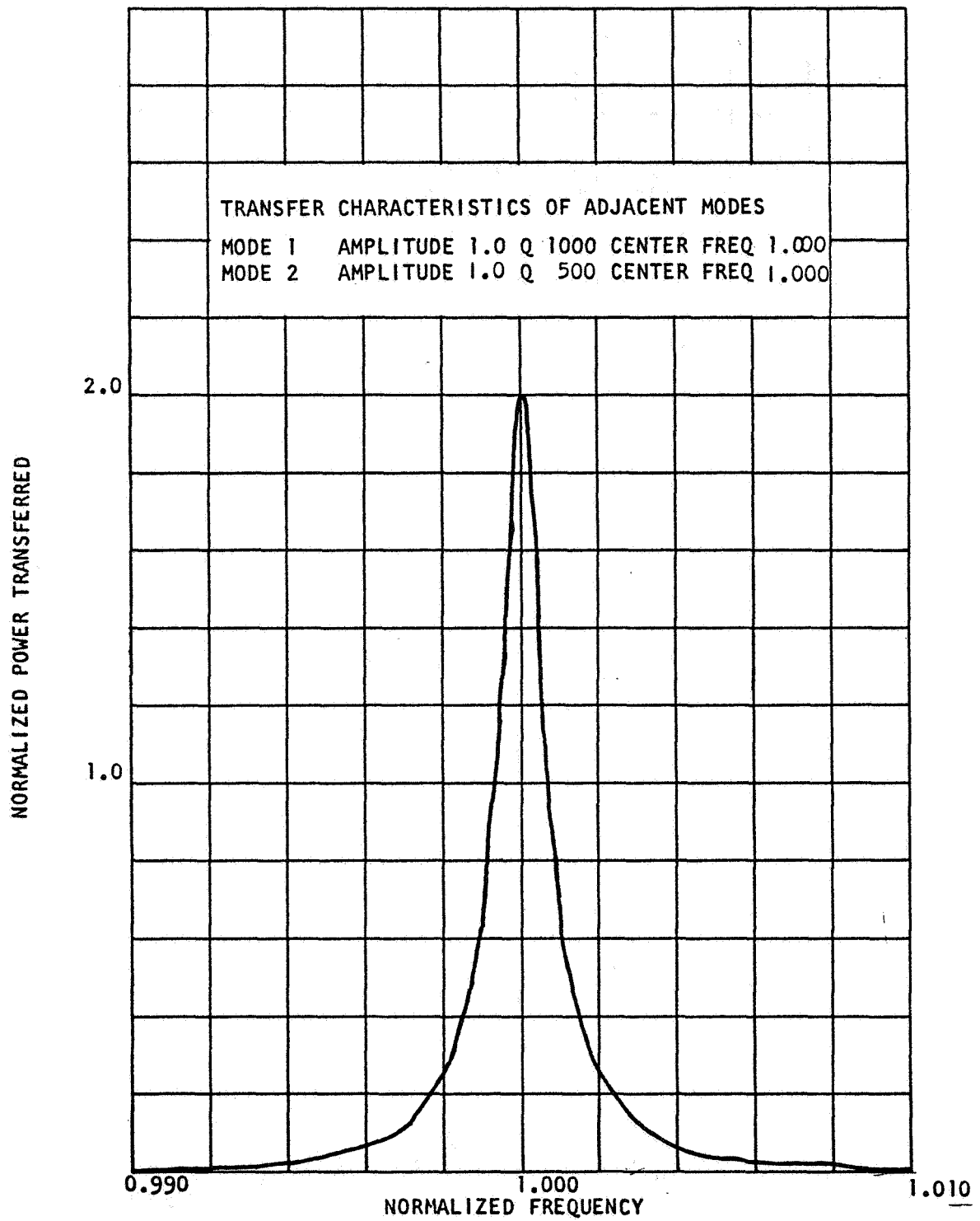


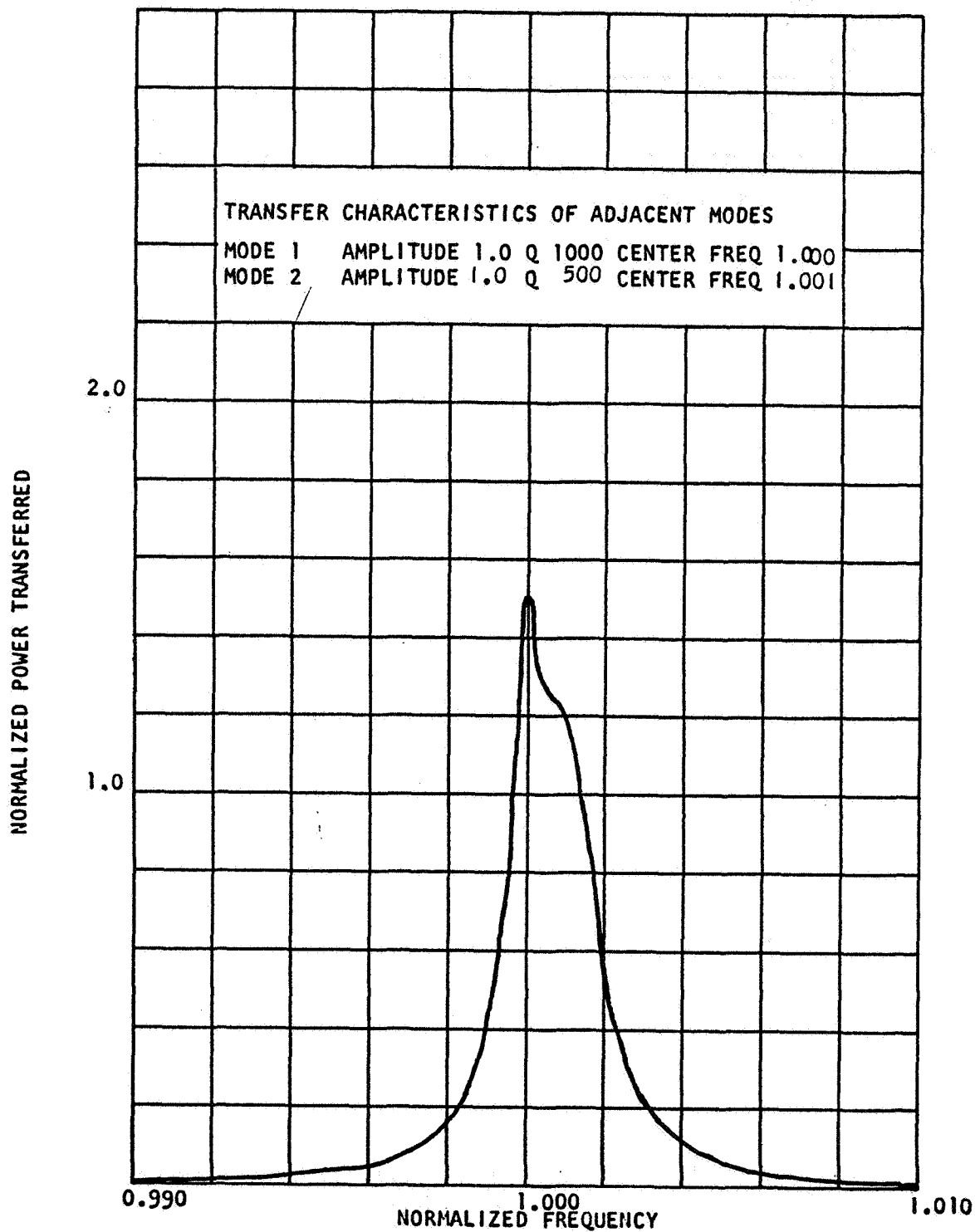


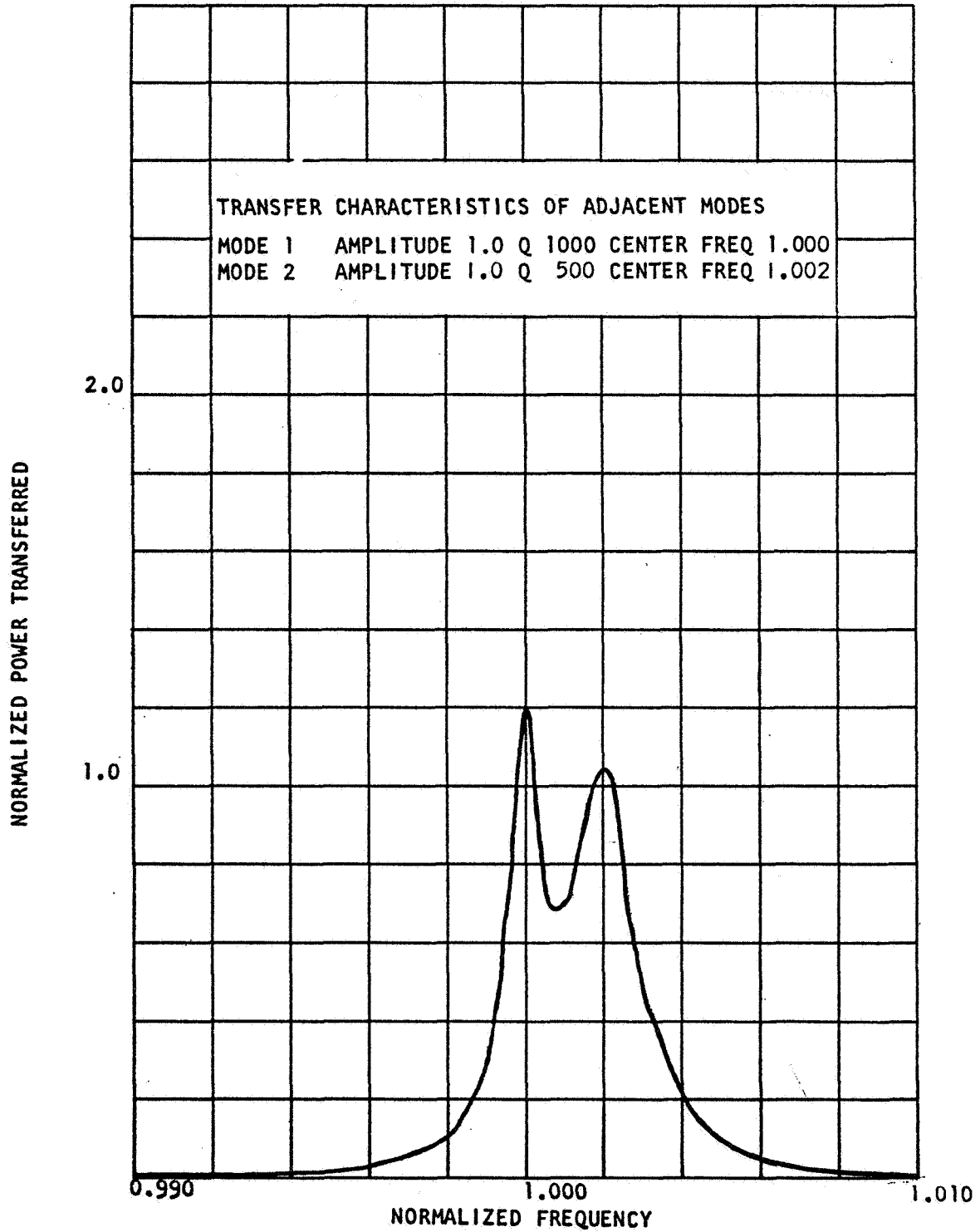


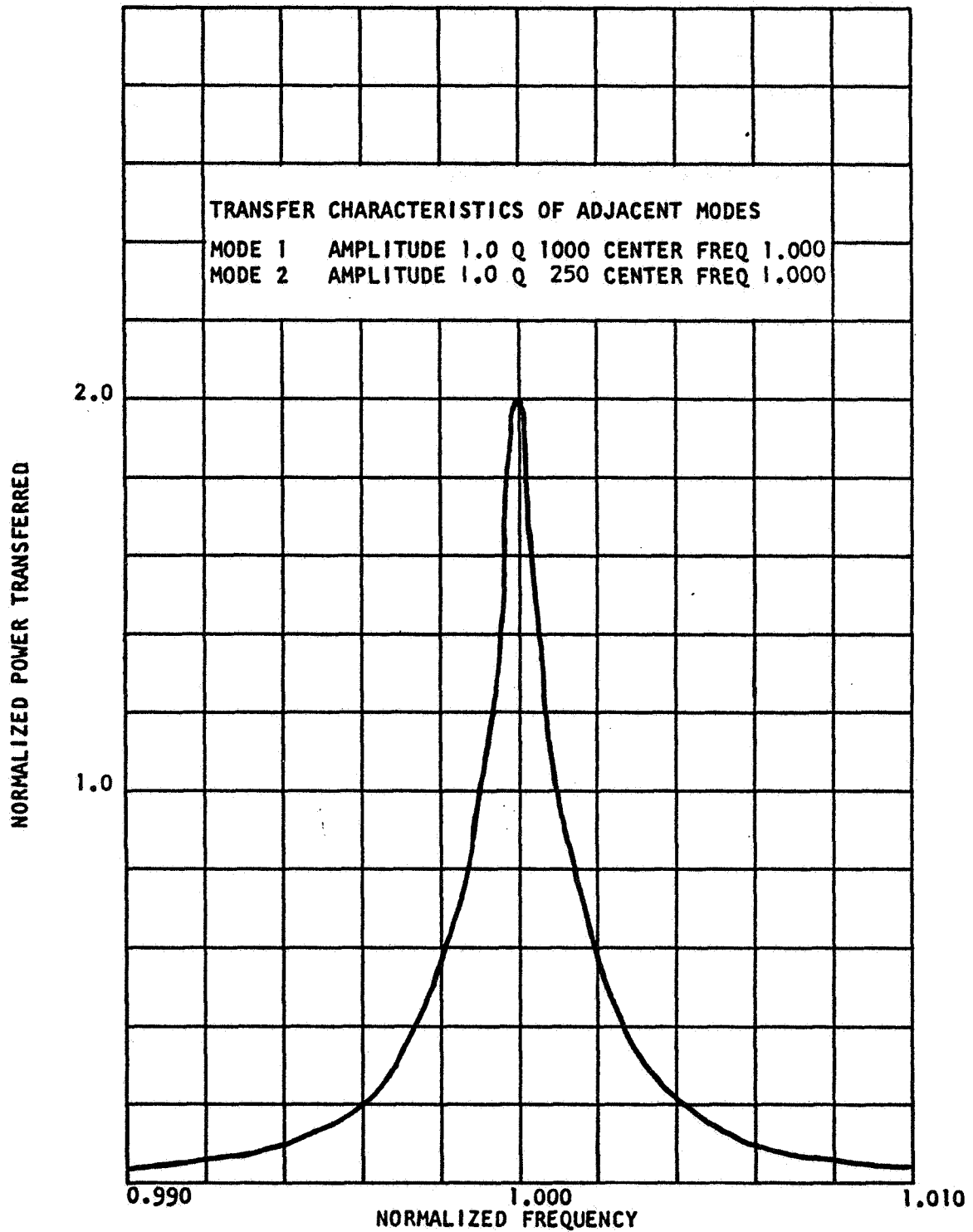


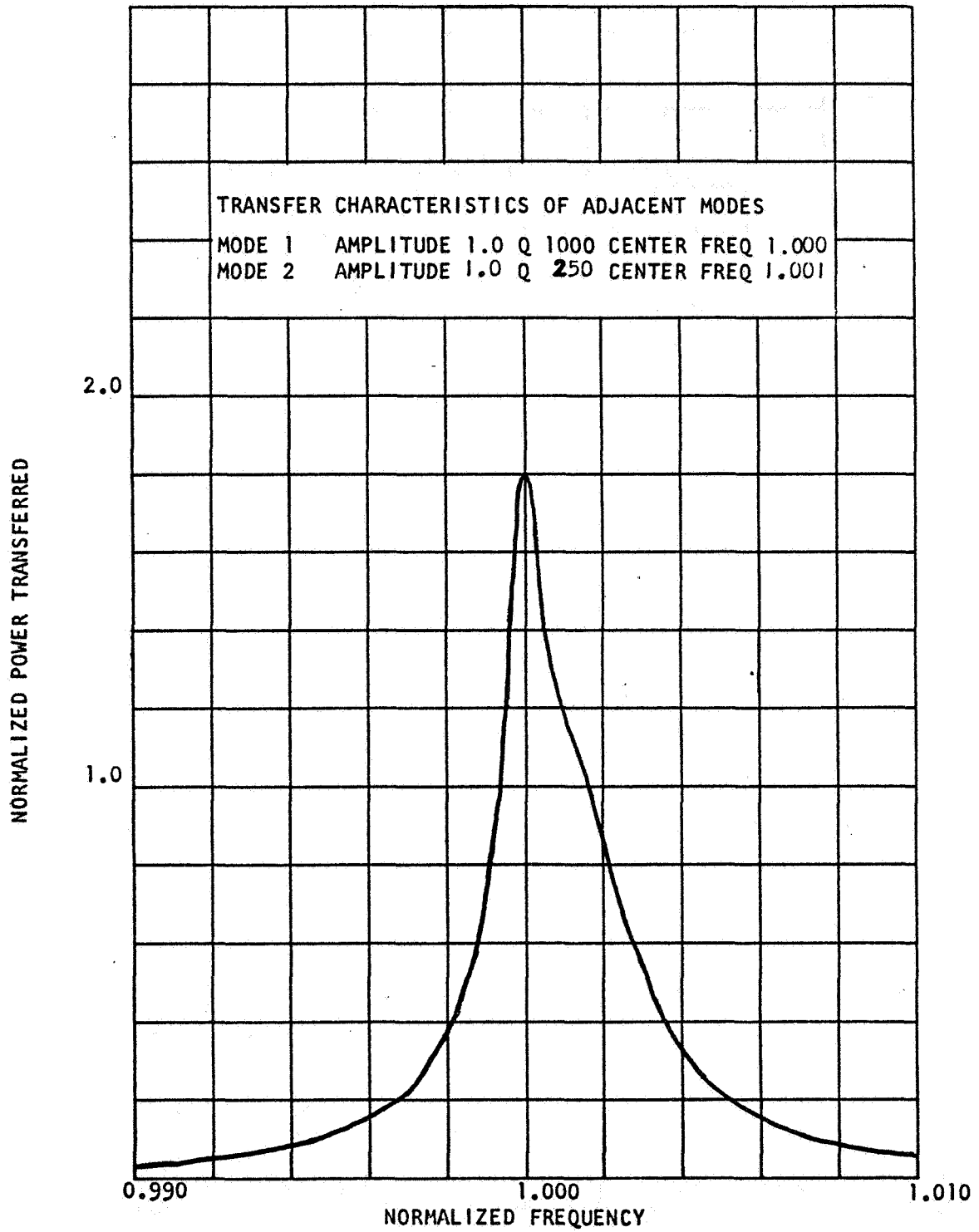


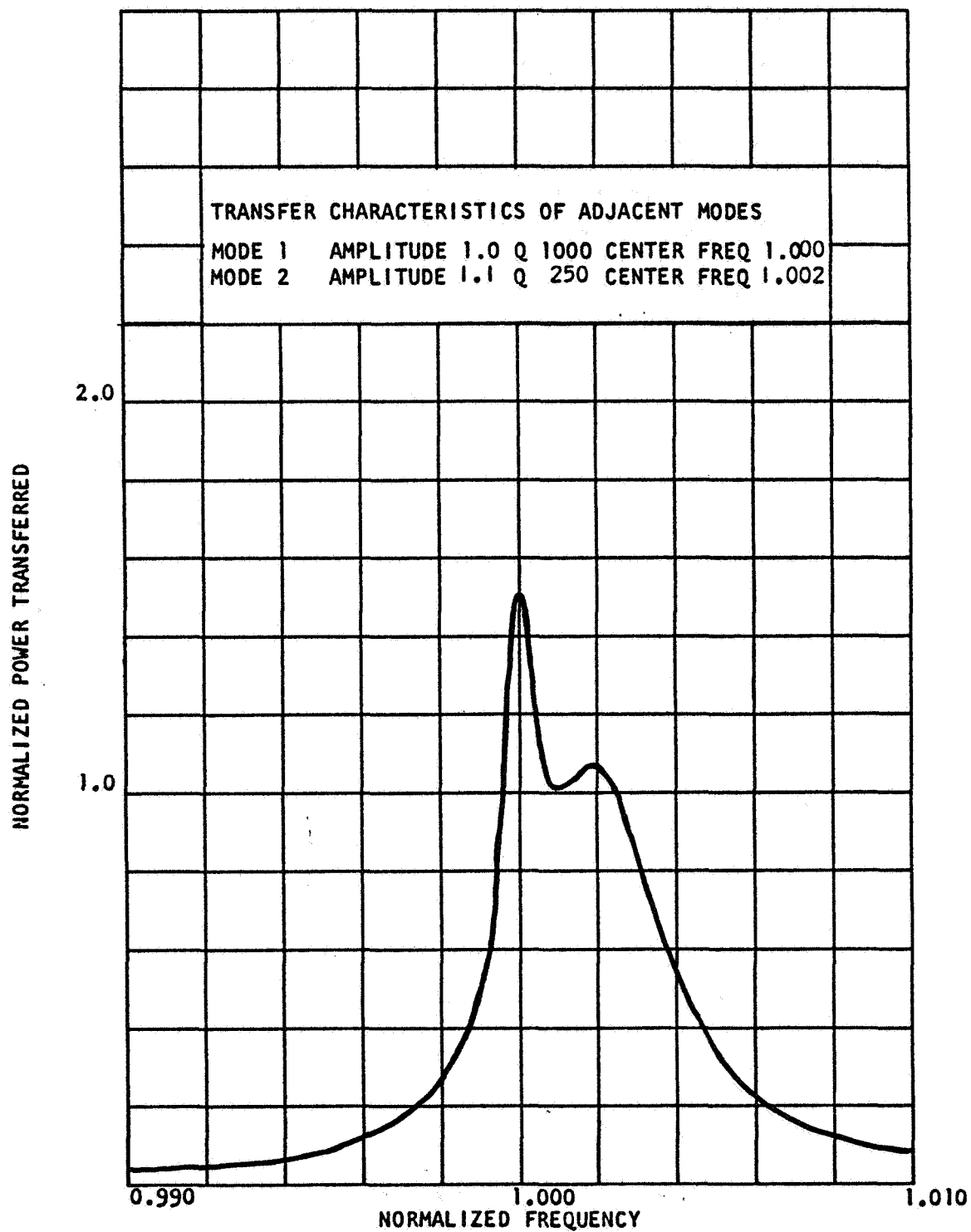


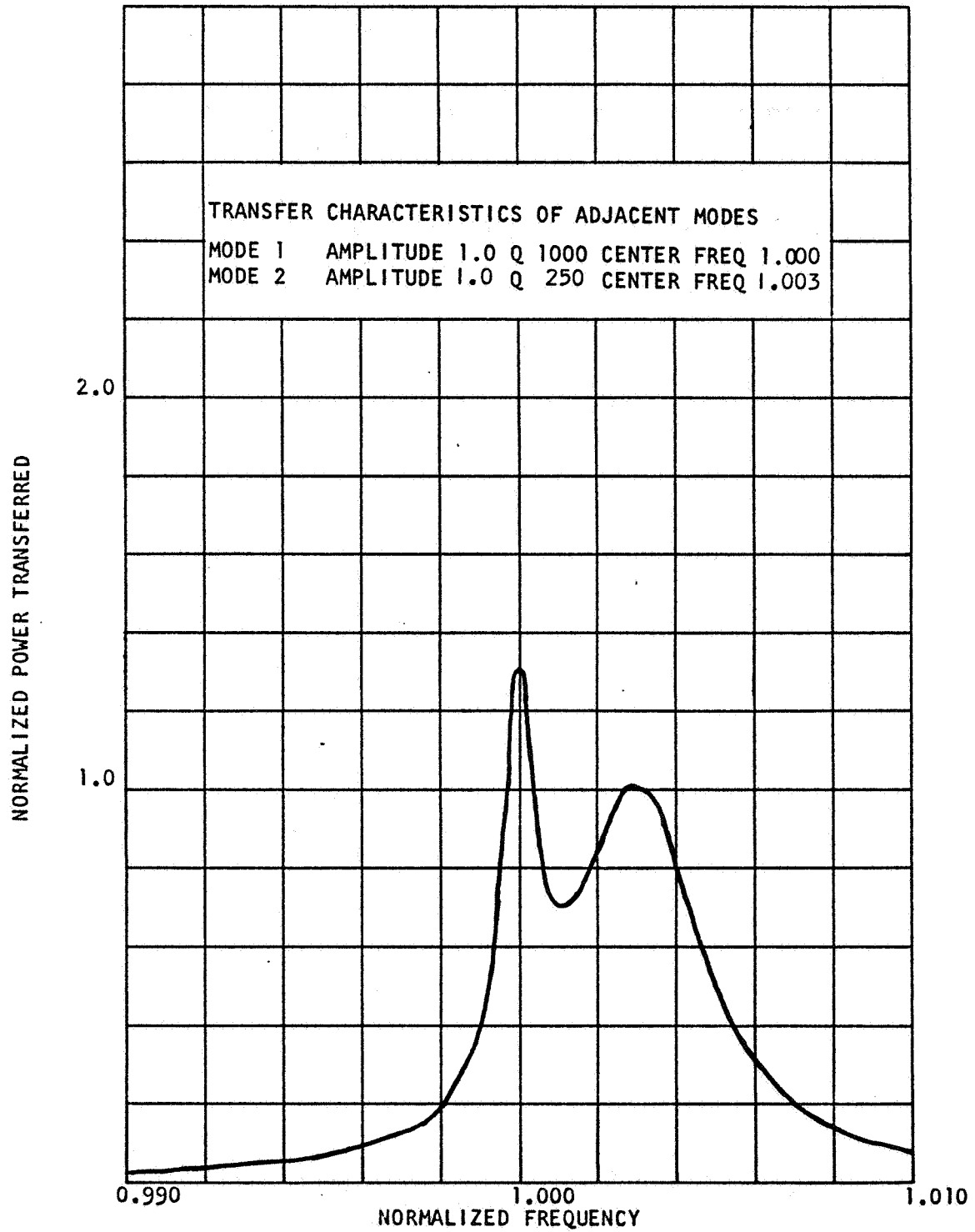


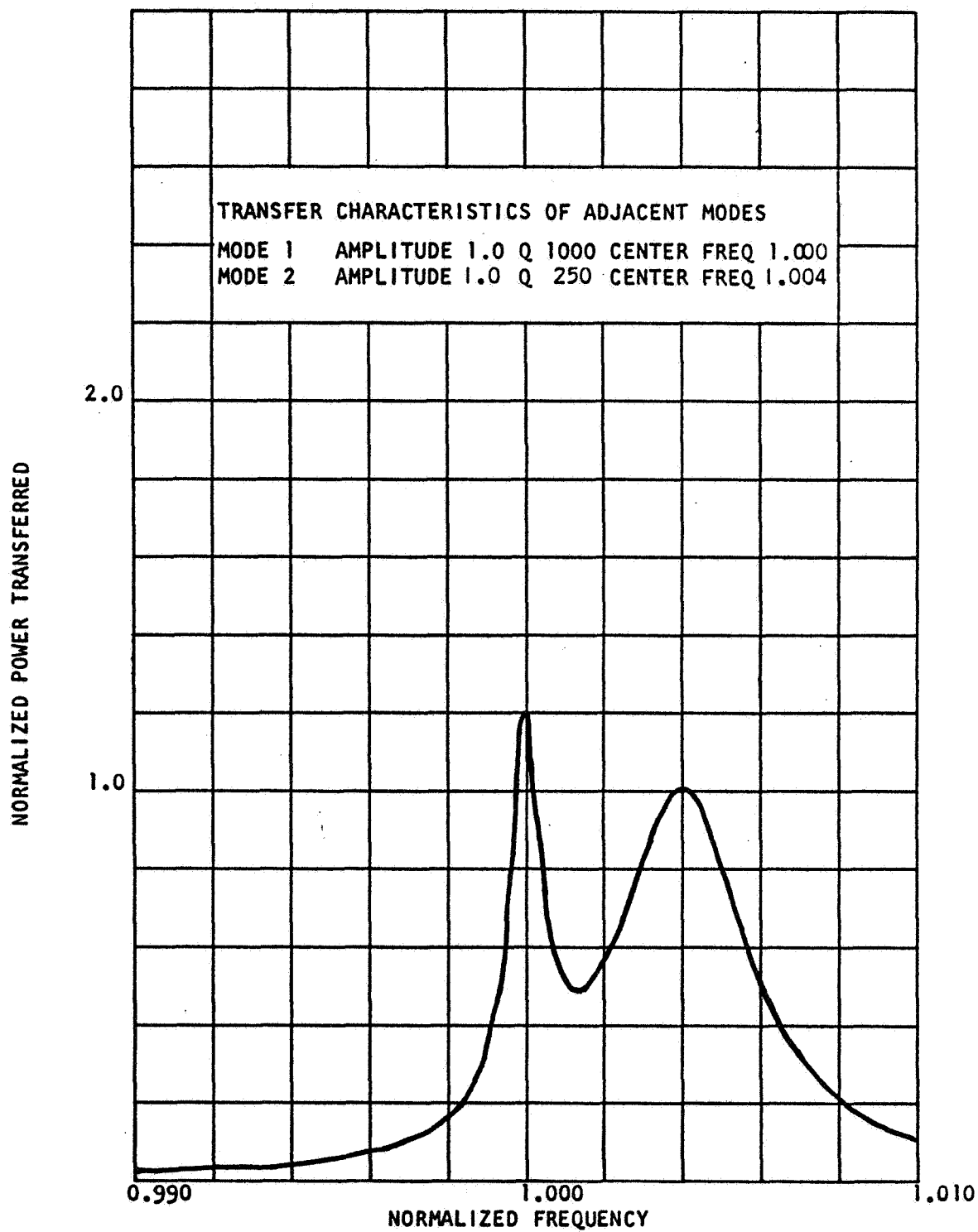


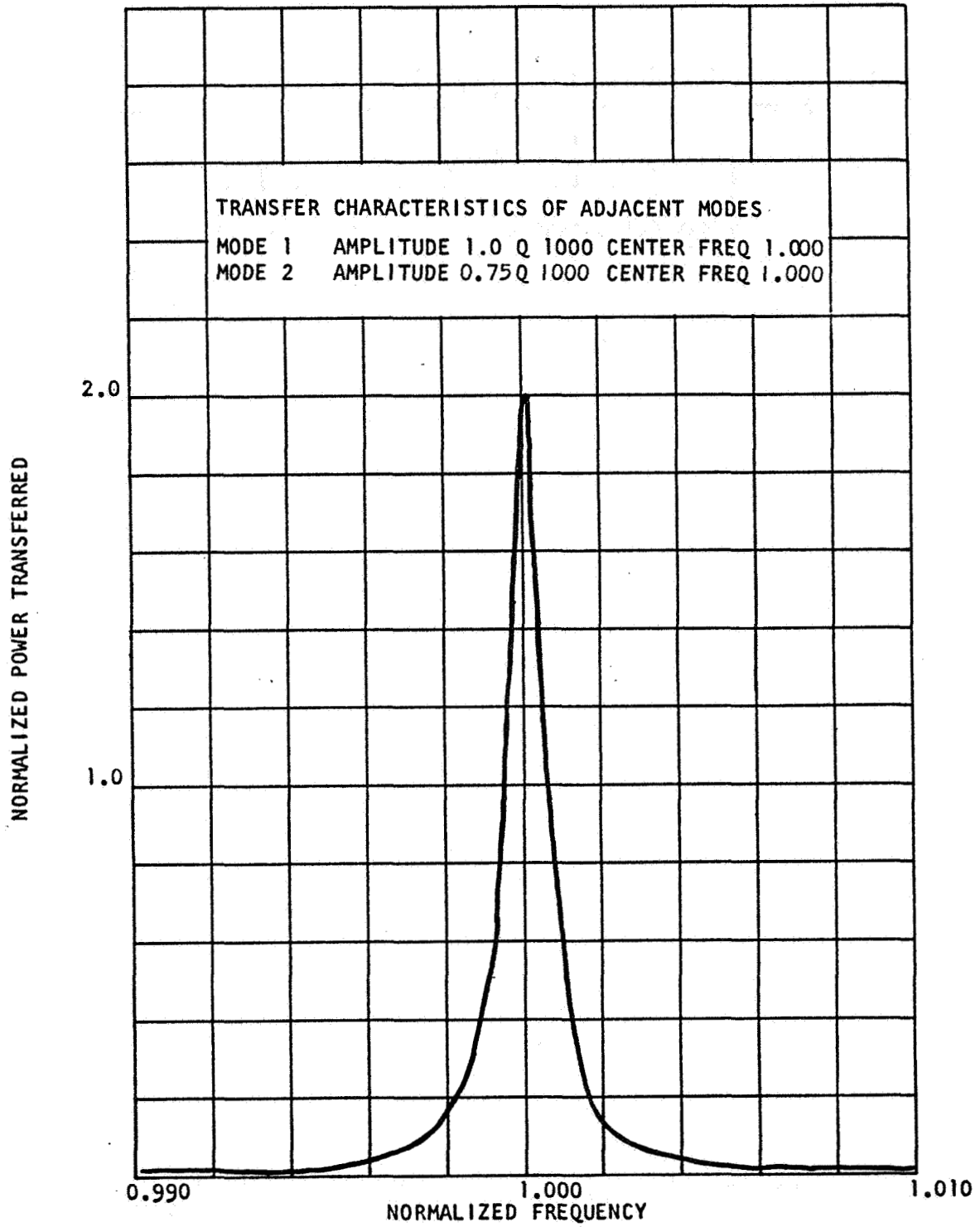


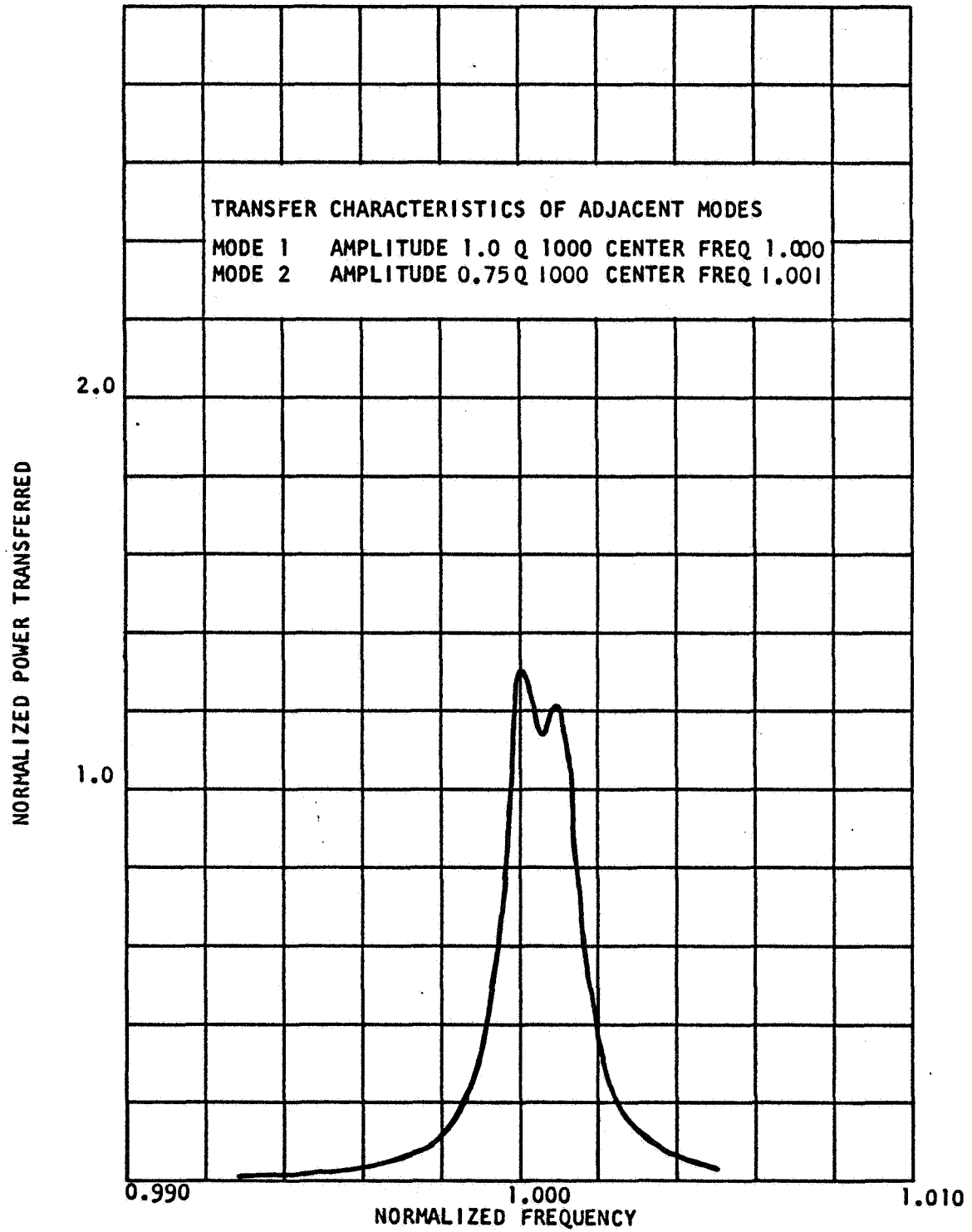


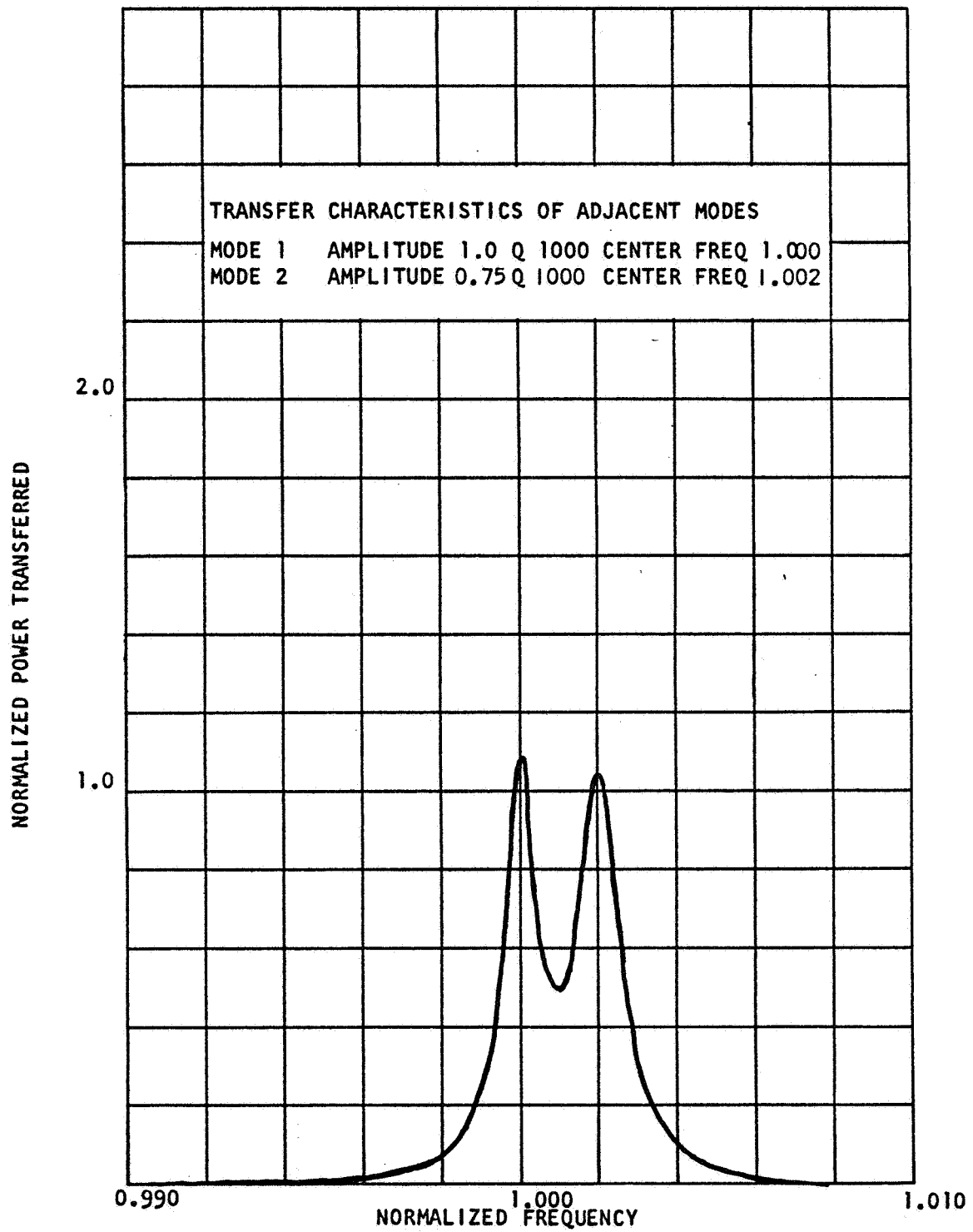


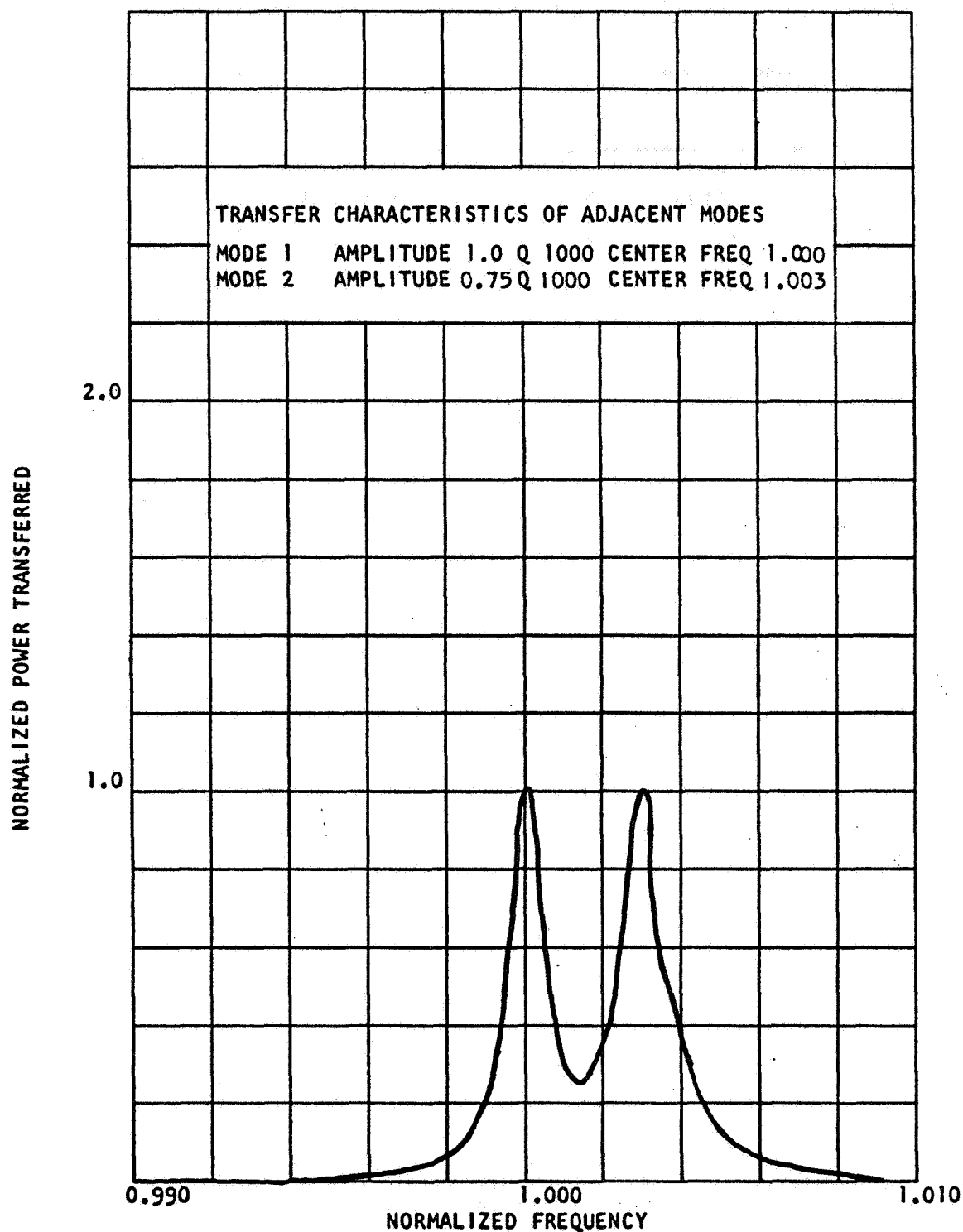


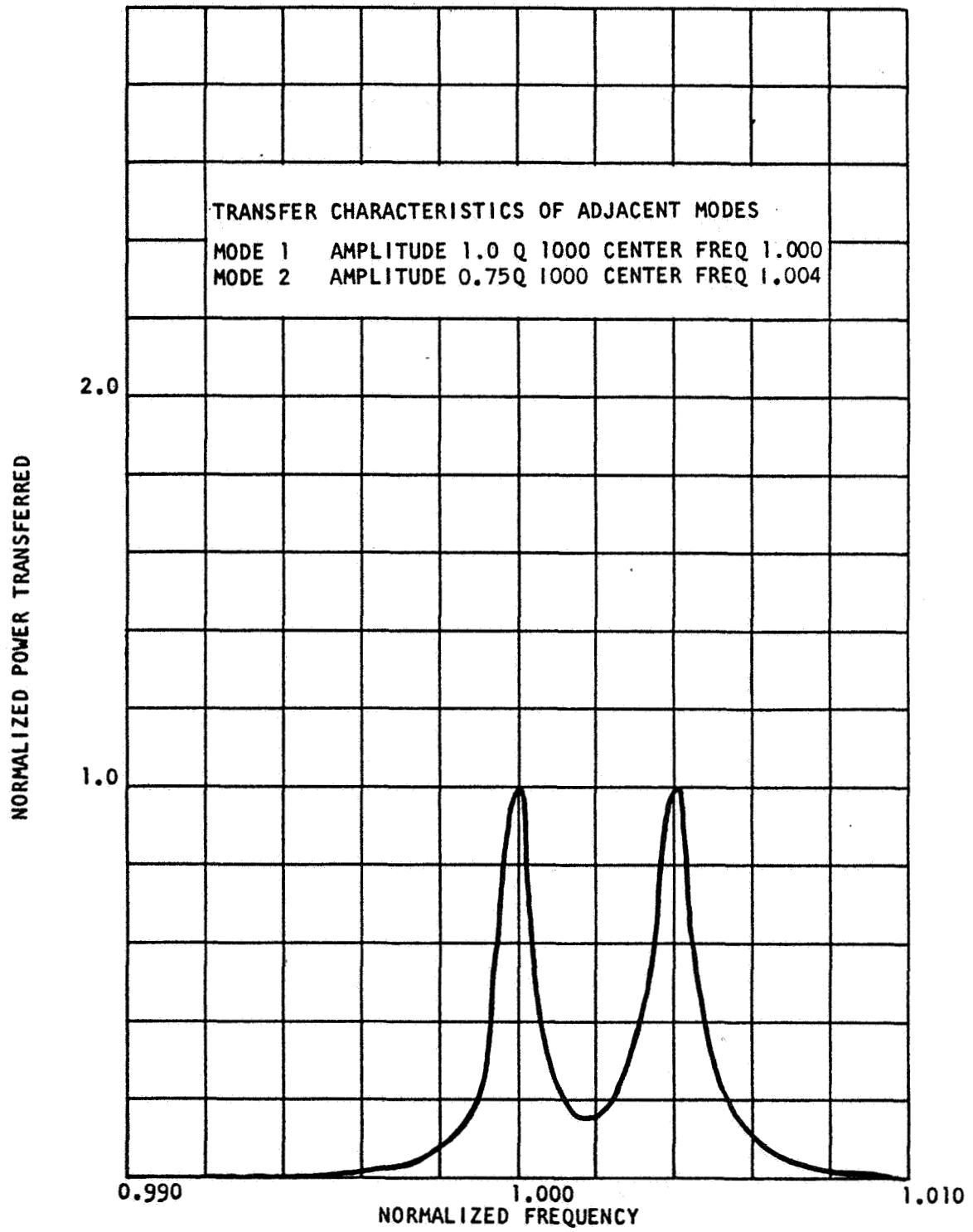


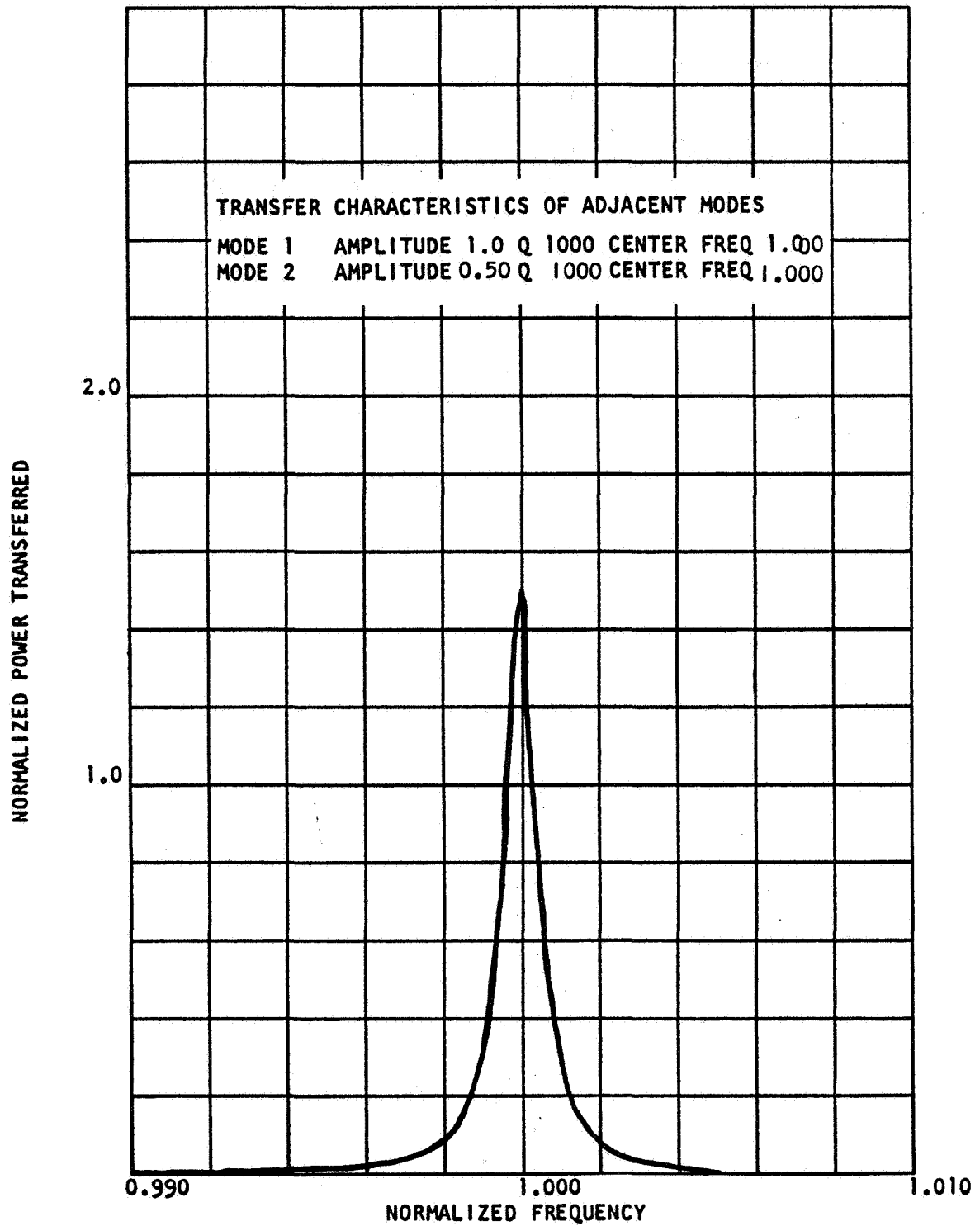


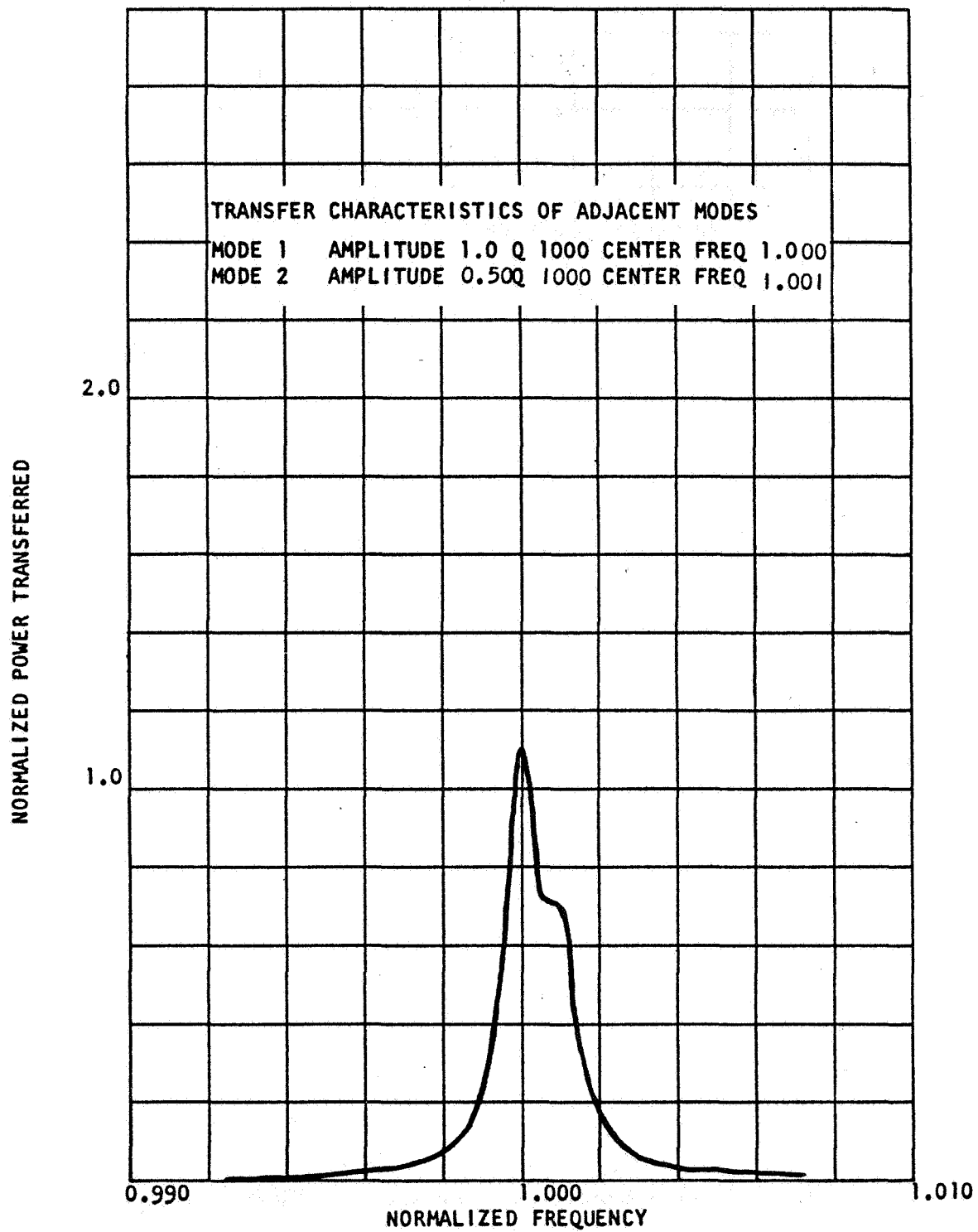


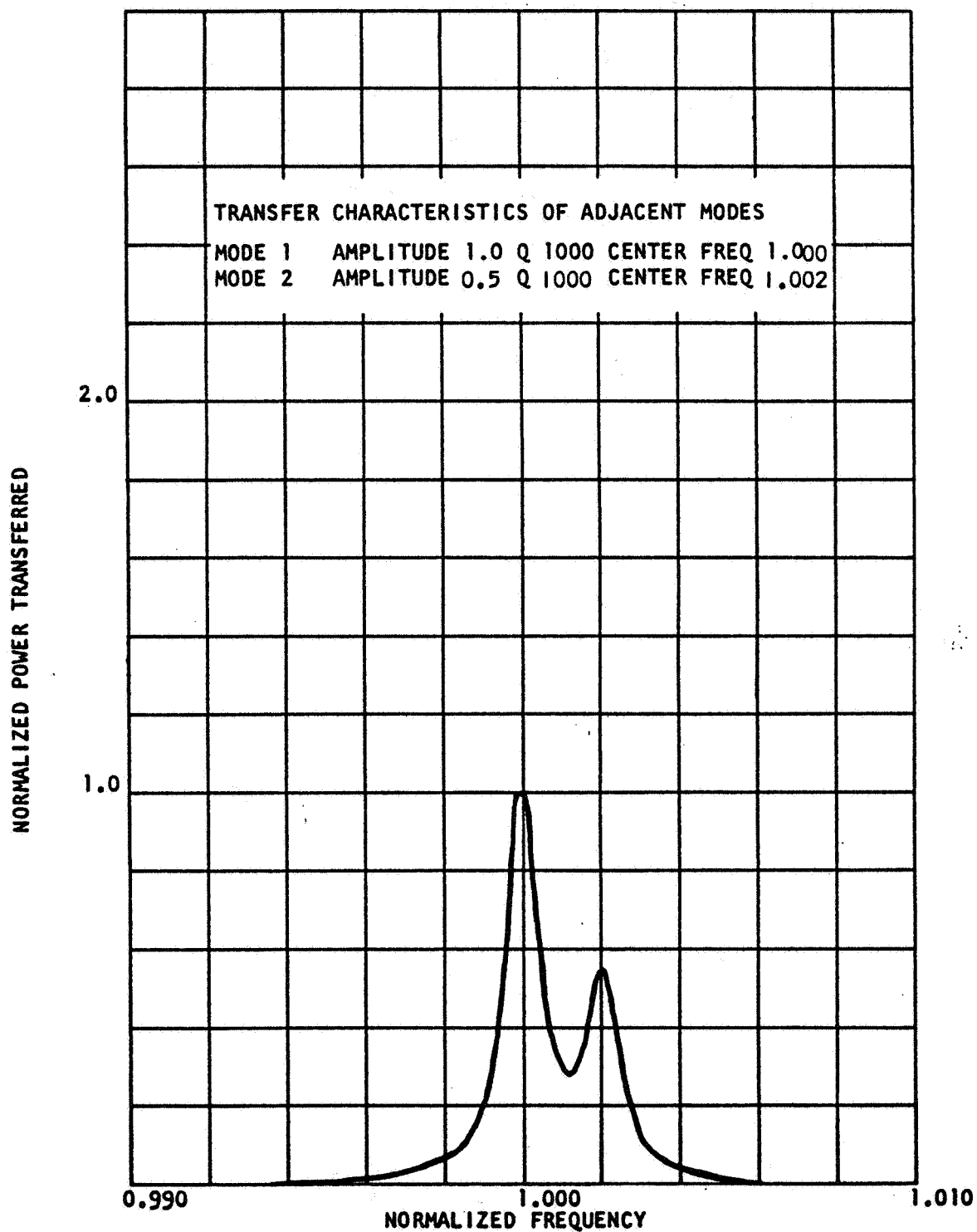


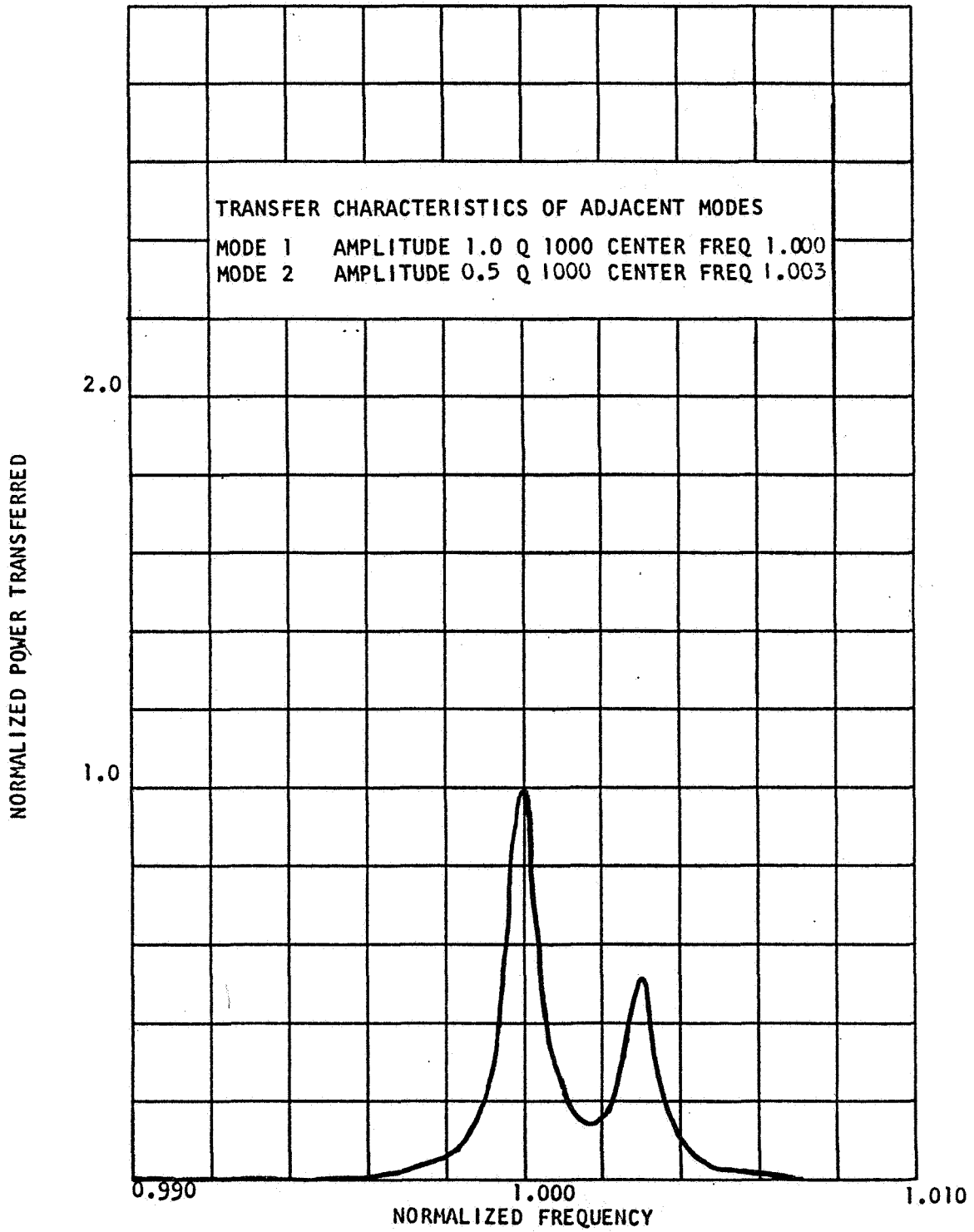


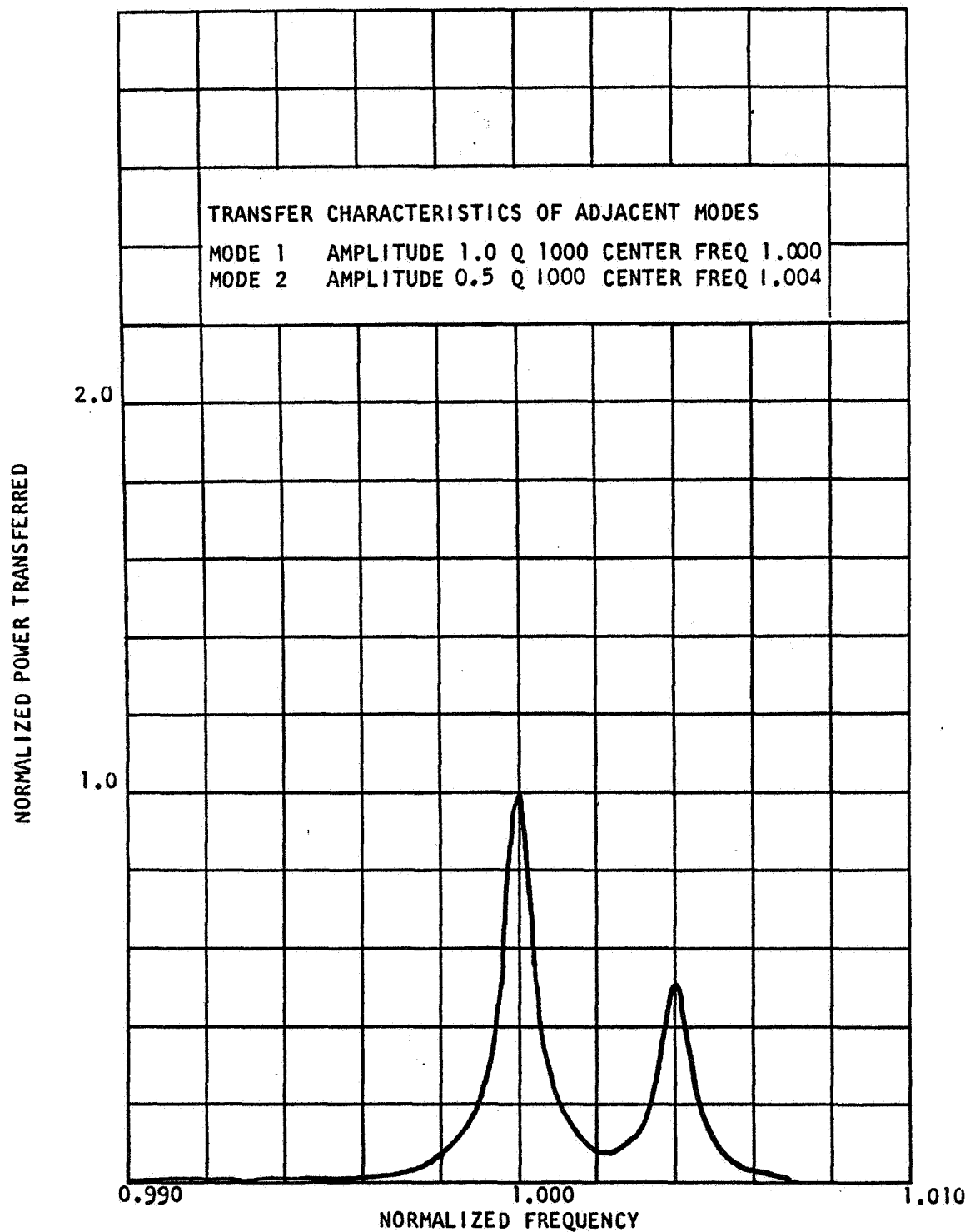


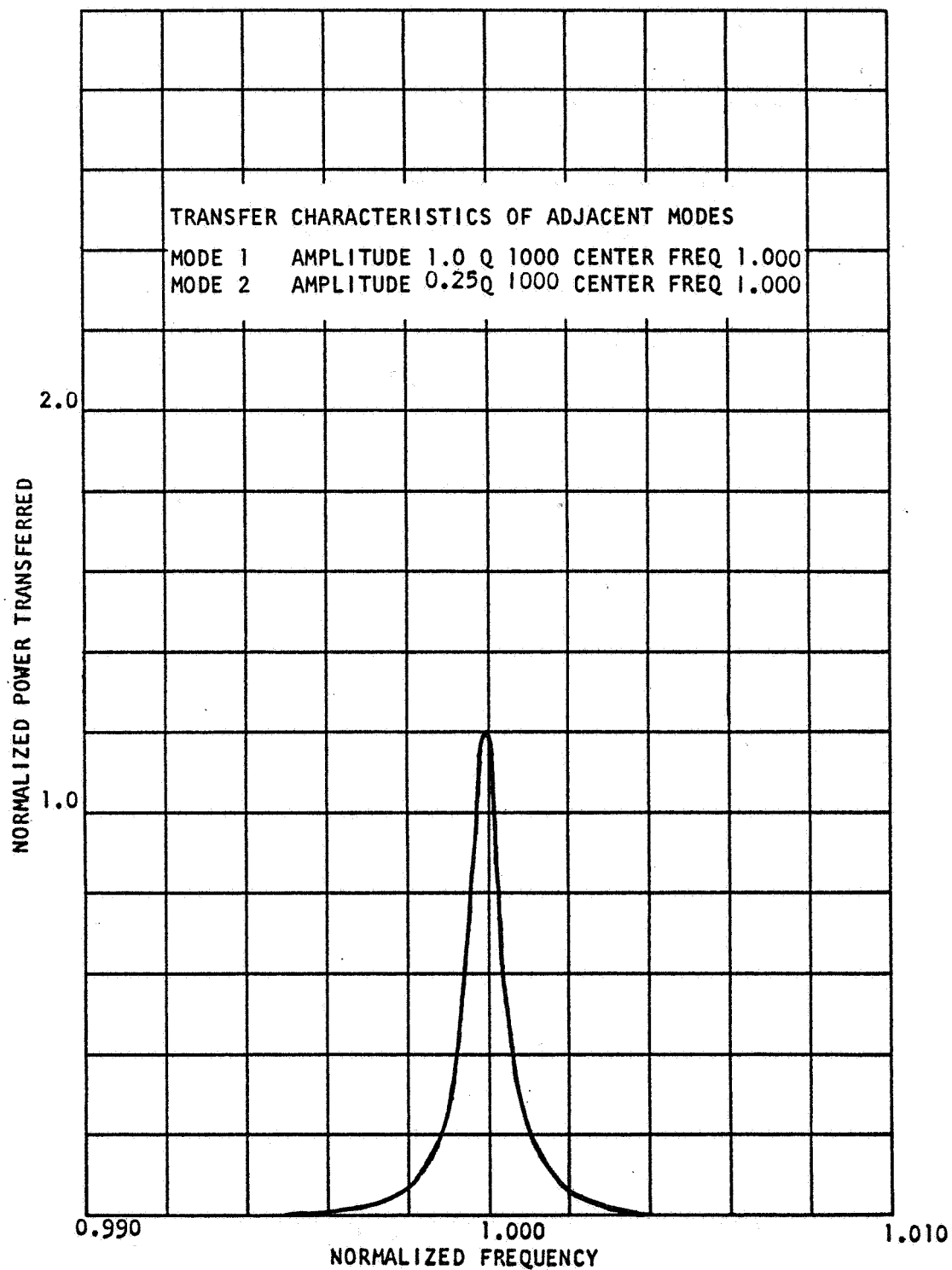


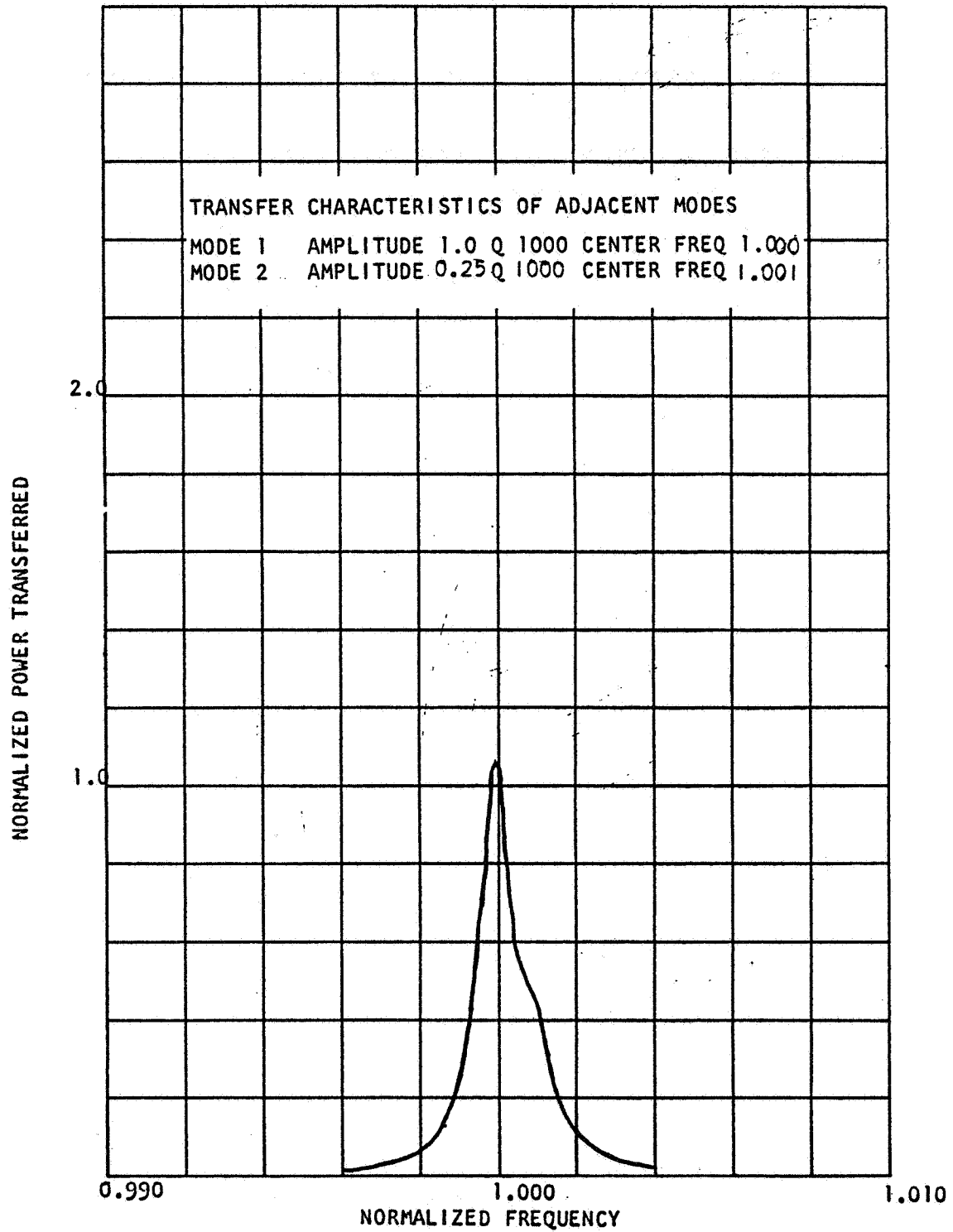


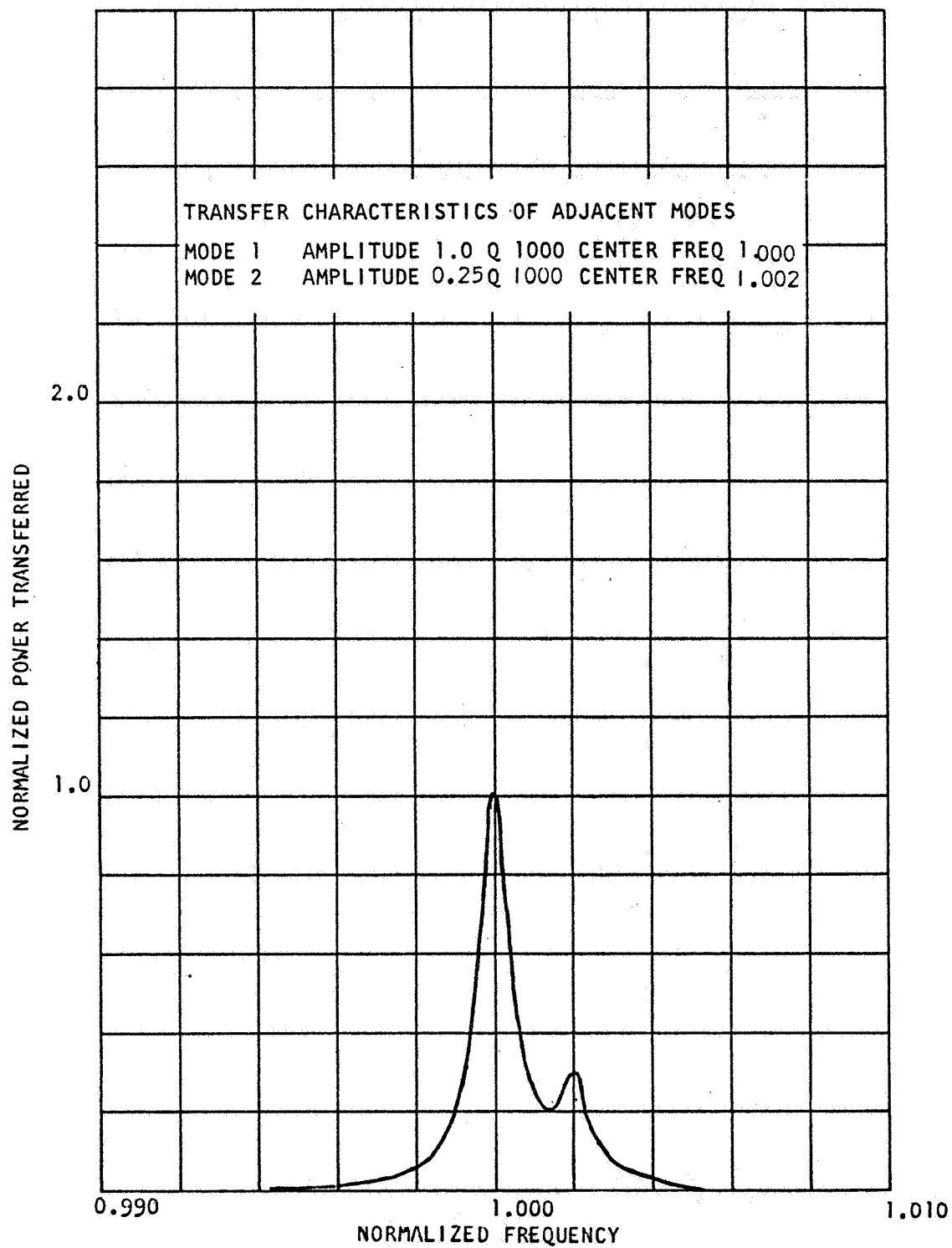


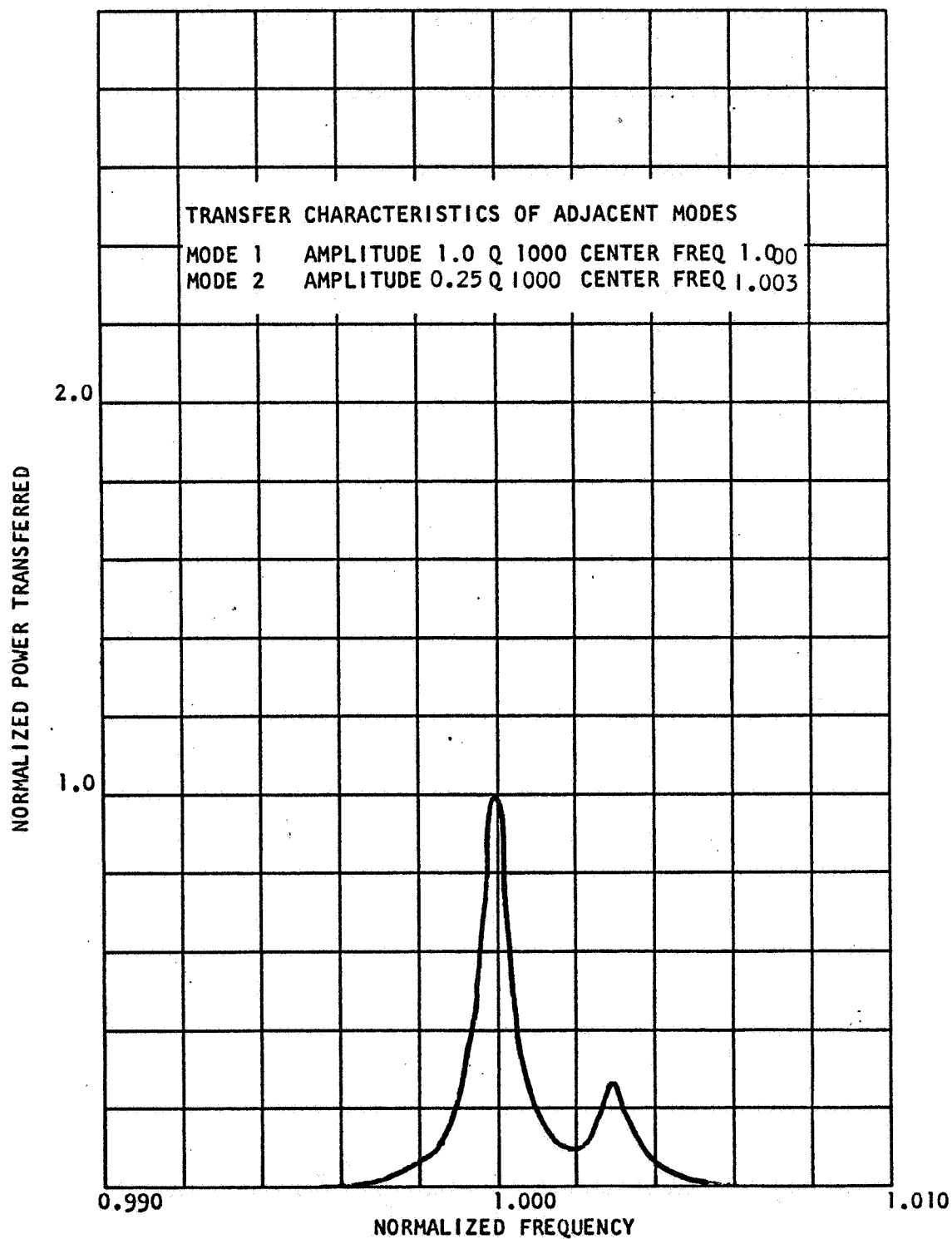


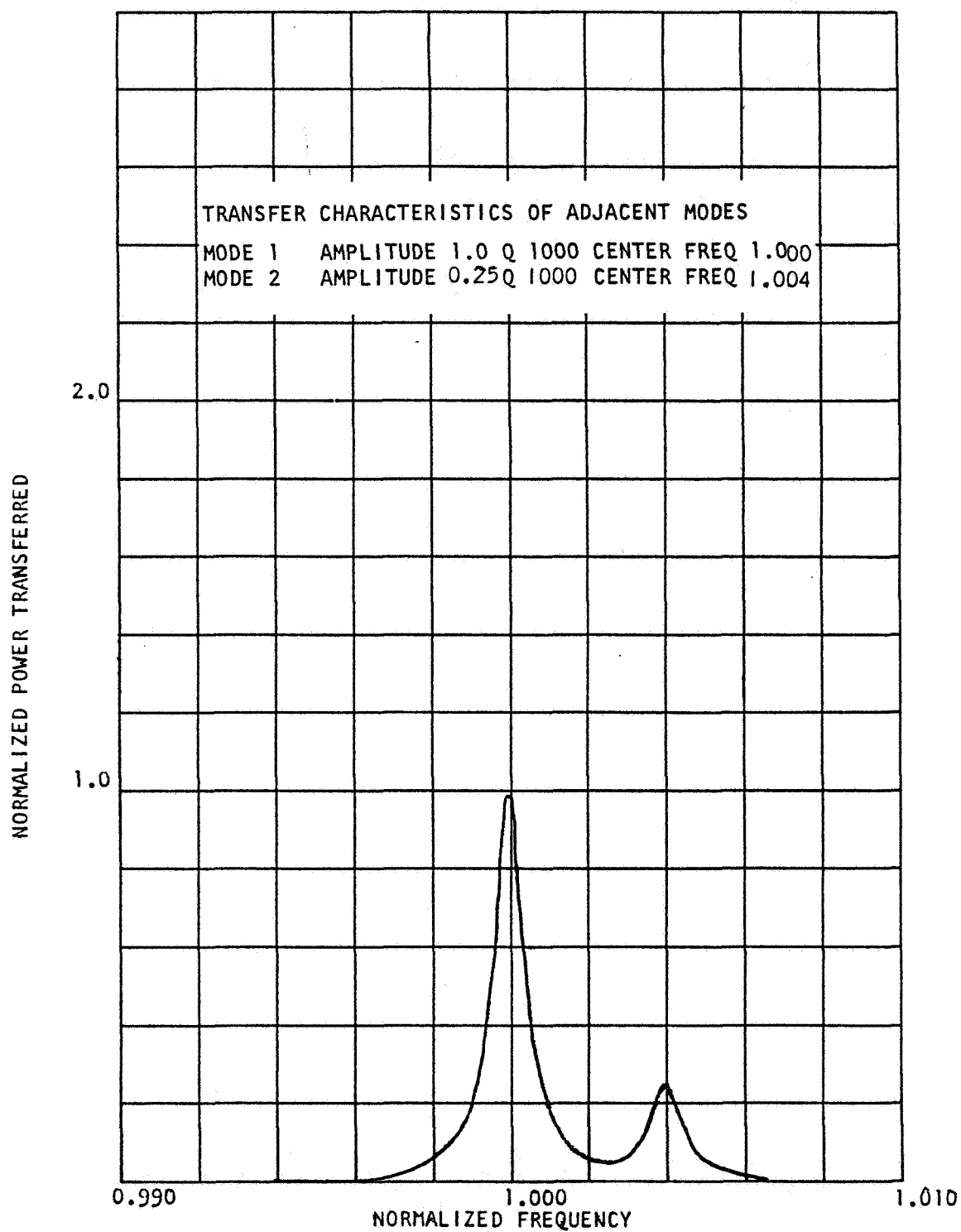












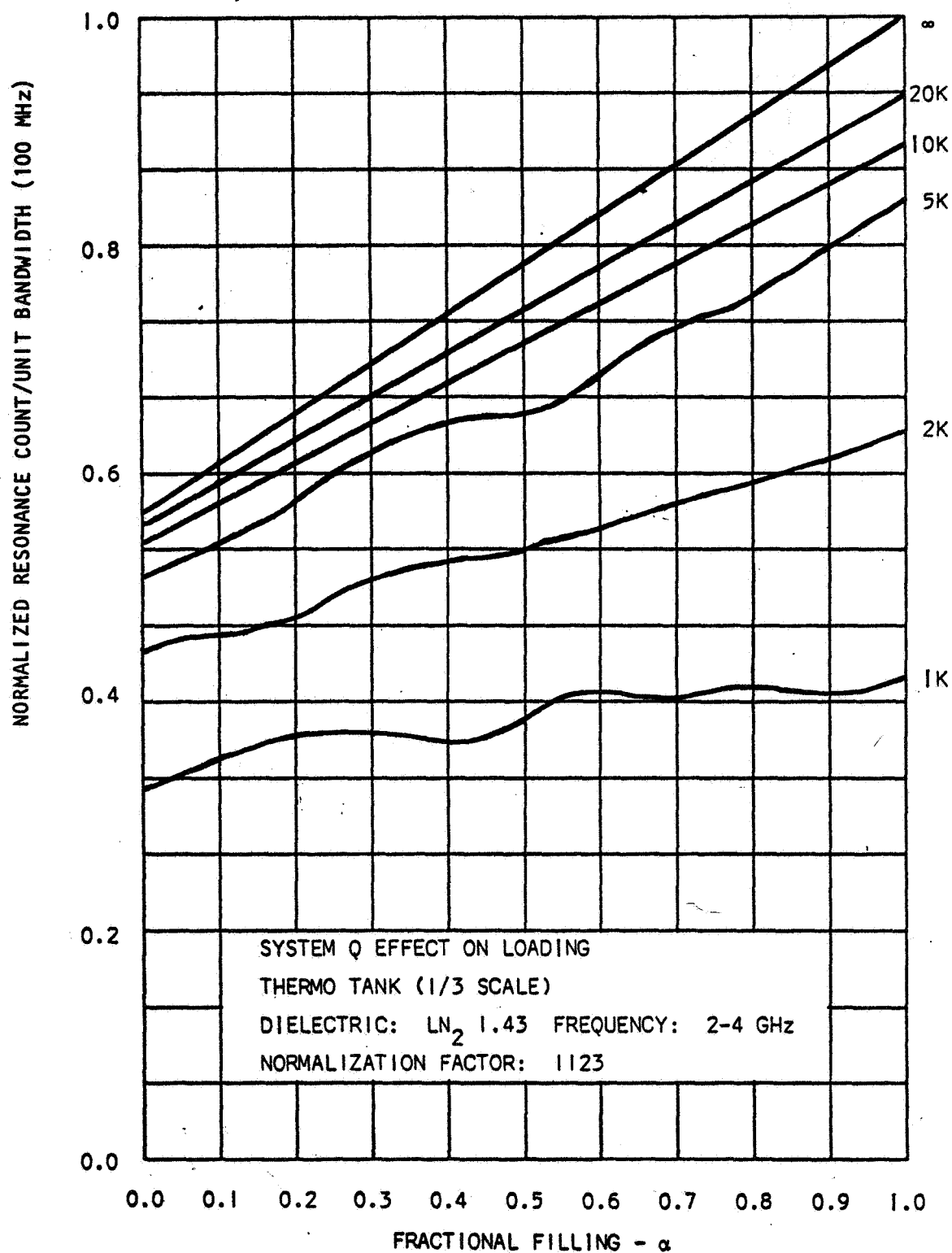
APPENDIX D

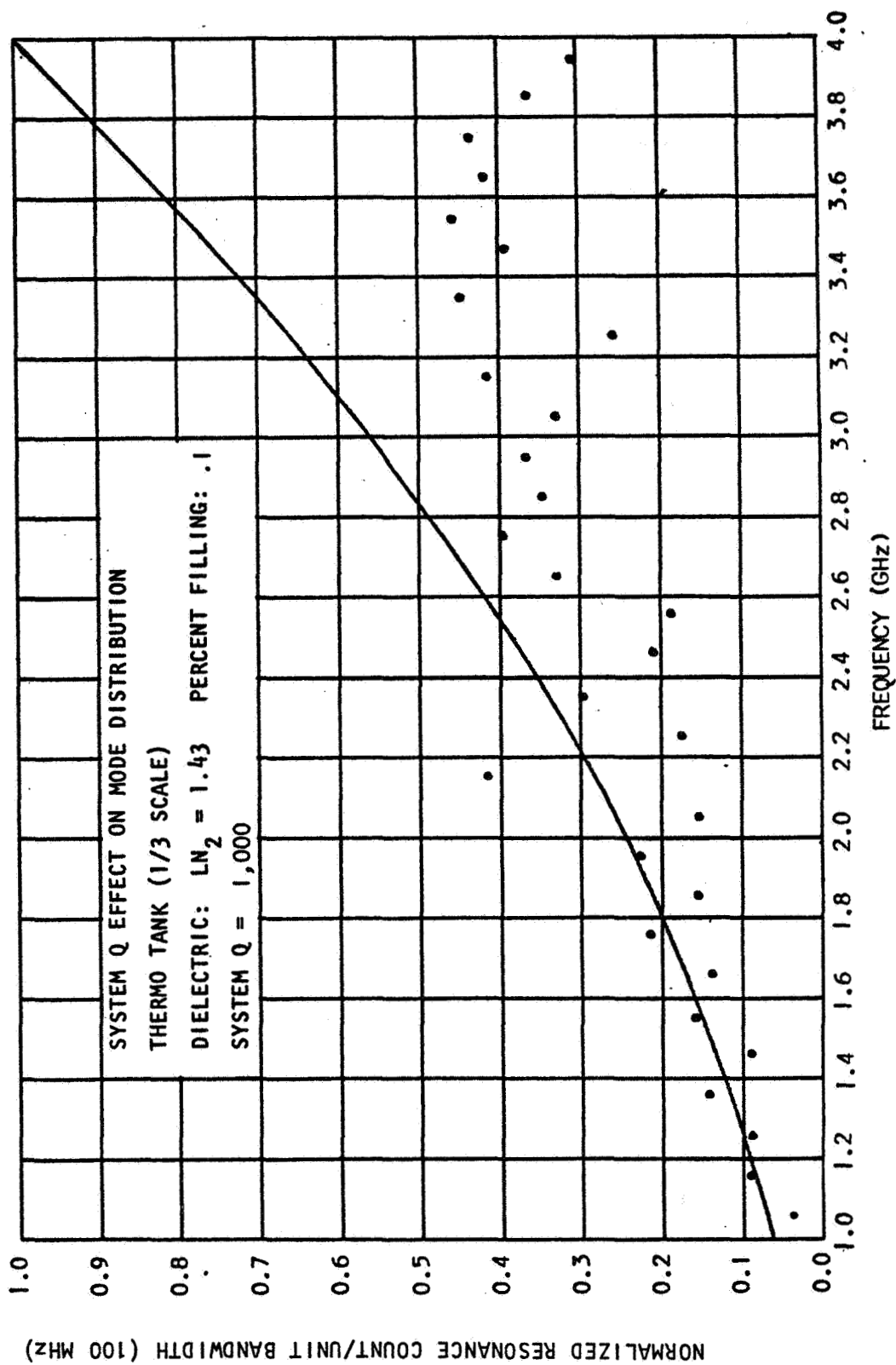
STATISTICAL PROGRAM ANALYSIS

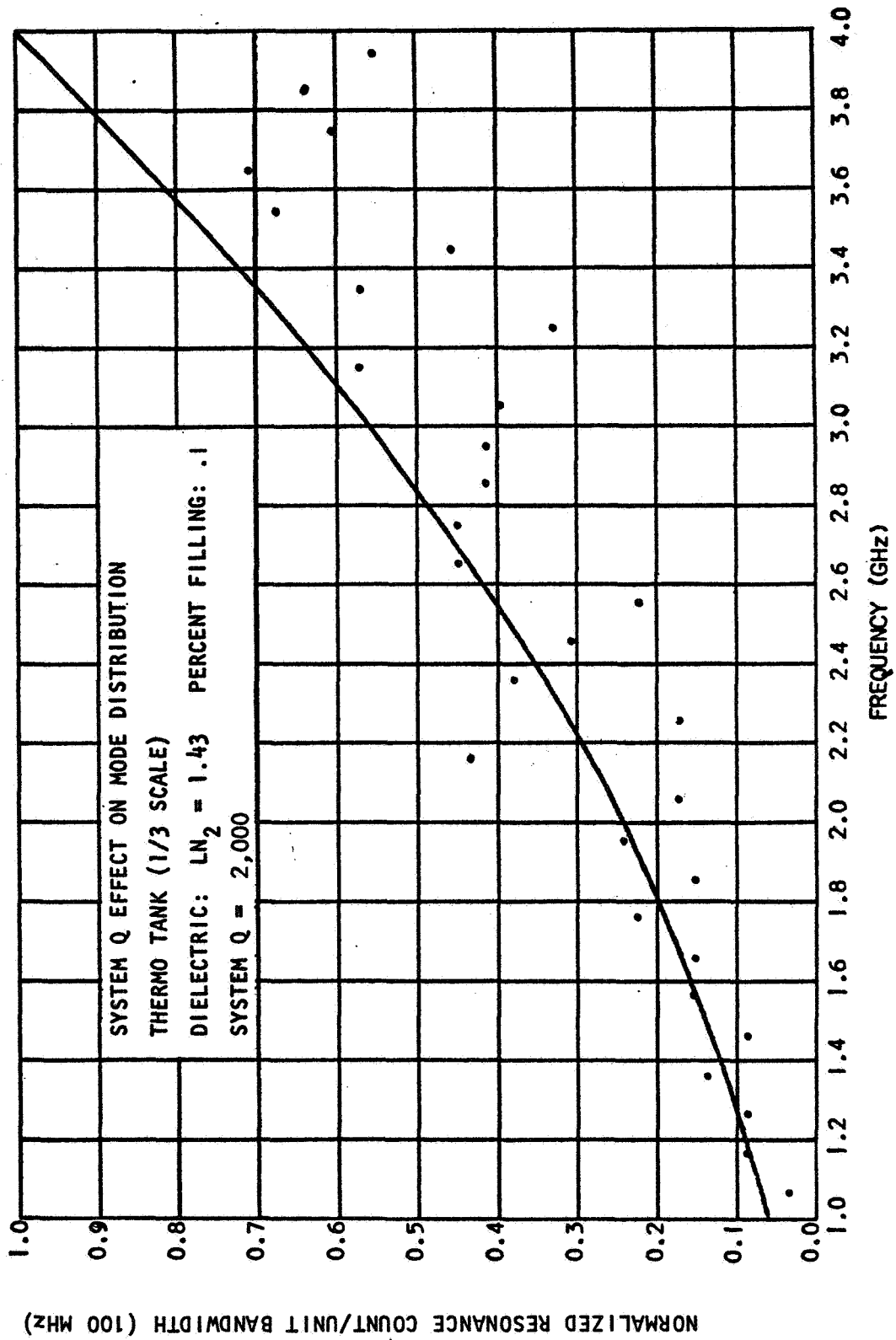
APPENDIX D

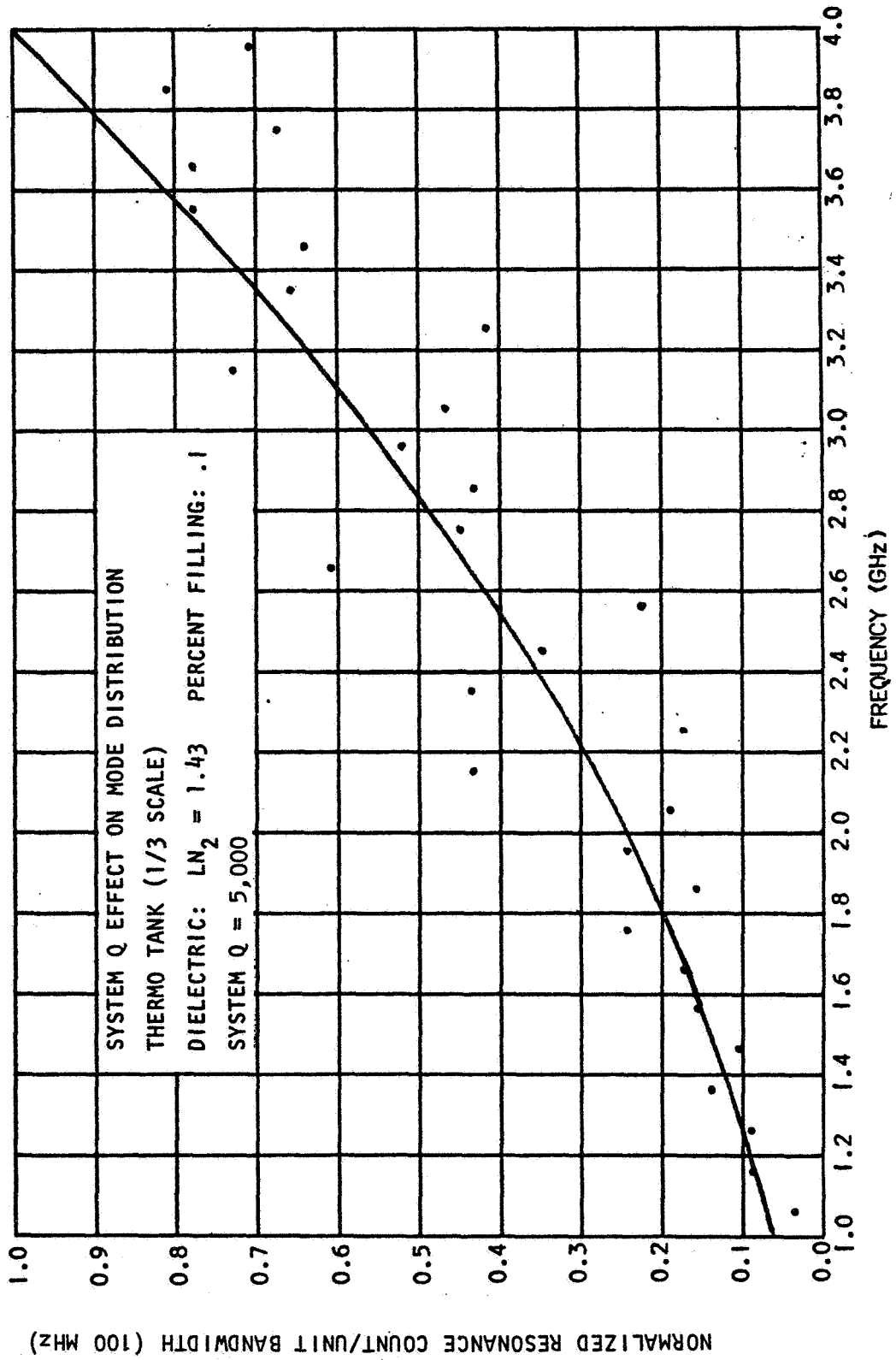
INTRODUCTION

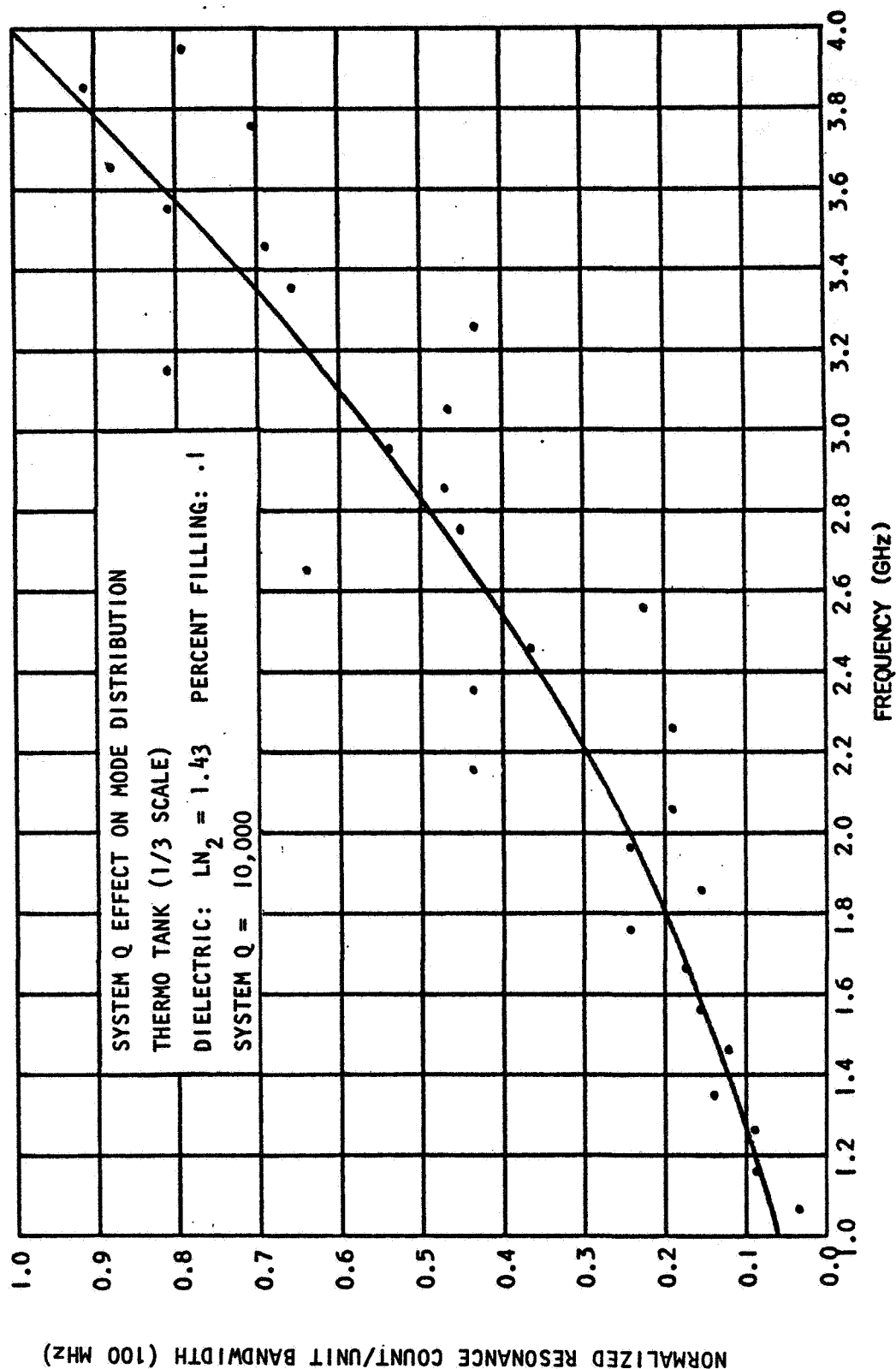
This appendix contains the graphical analysis of a statistical computer program which was run on the 1/3 scale THERMO tank partially filled with LN_2 . The graphs show the effect of System "Q" on the loading response and the mode distribution for various fillings and specific system "Q's". A study of these graphs provides information for the optimization of operating frequency band as well as system sensitivity.

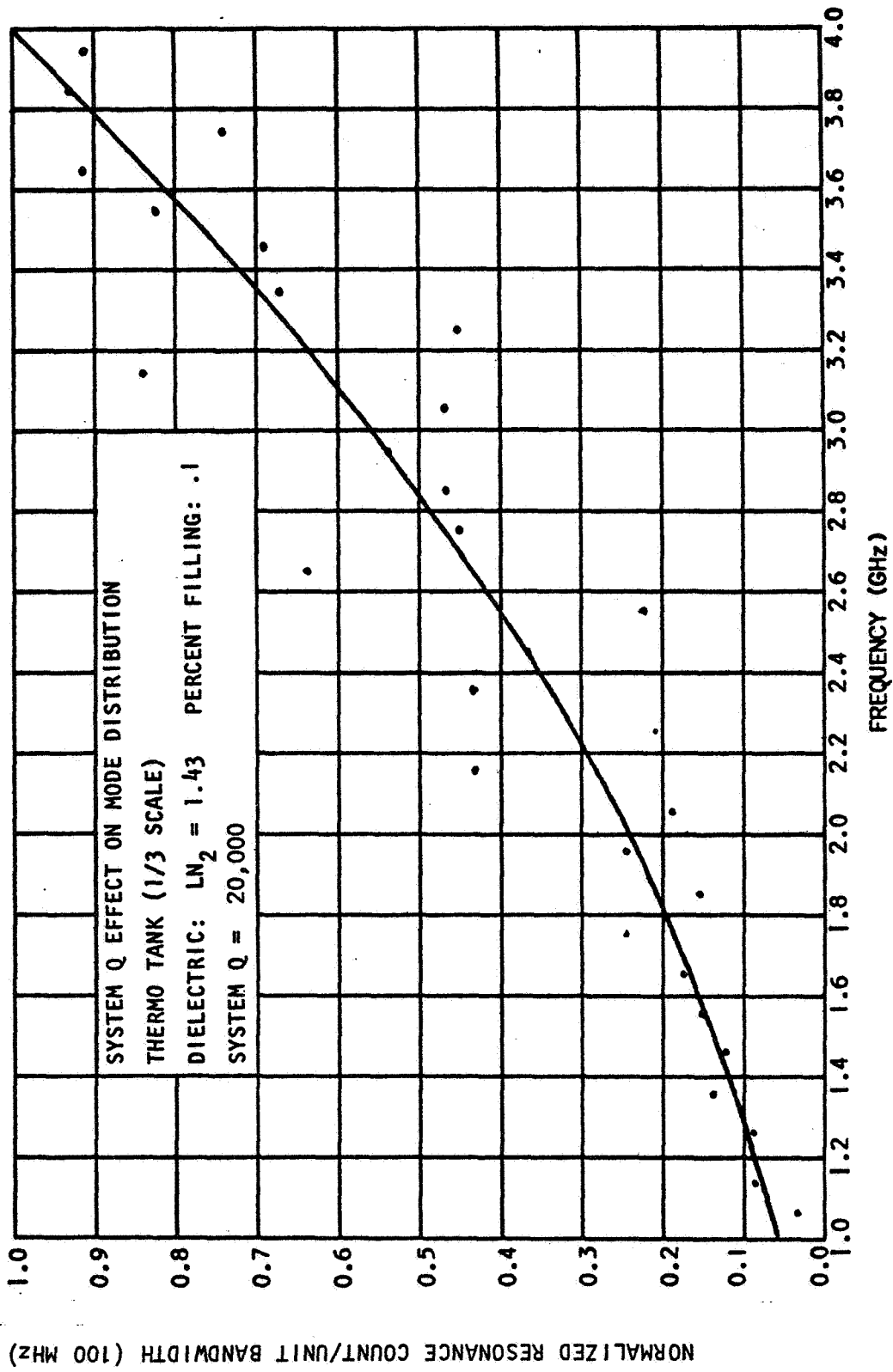


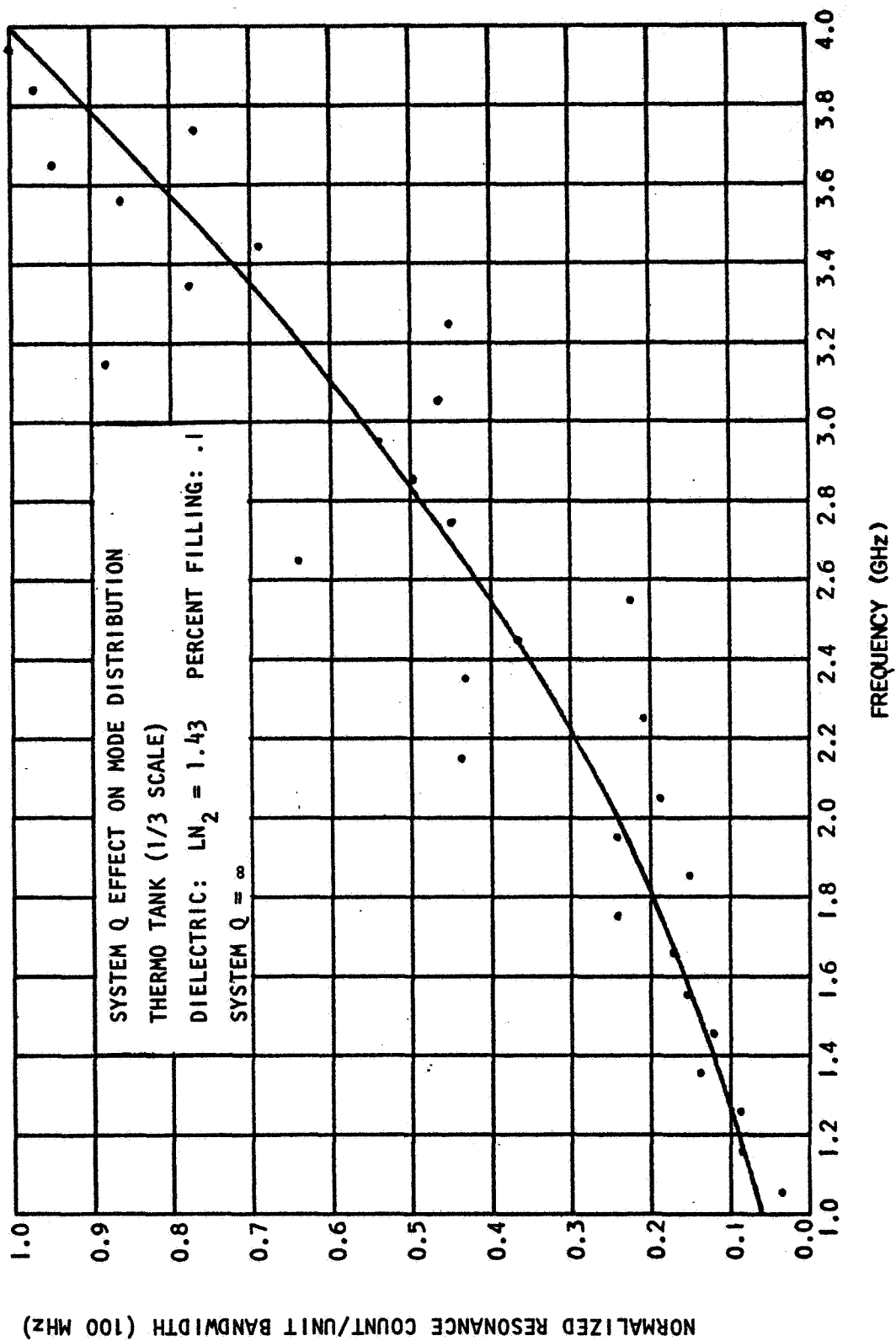


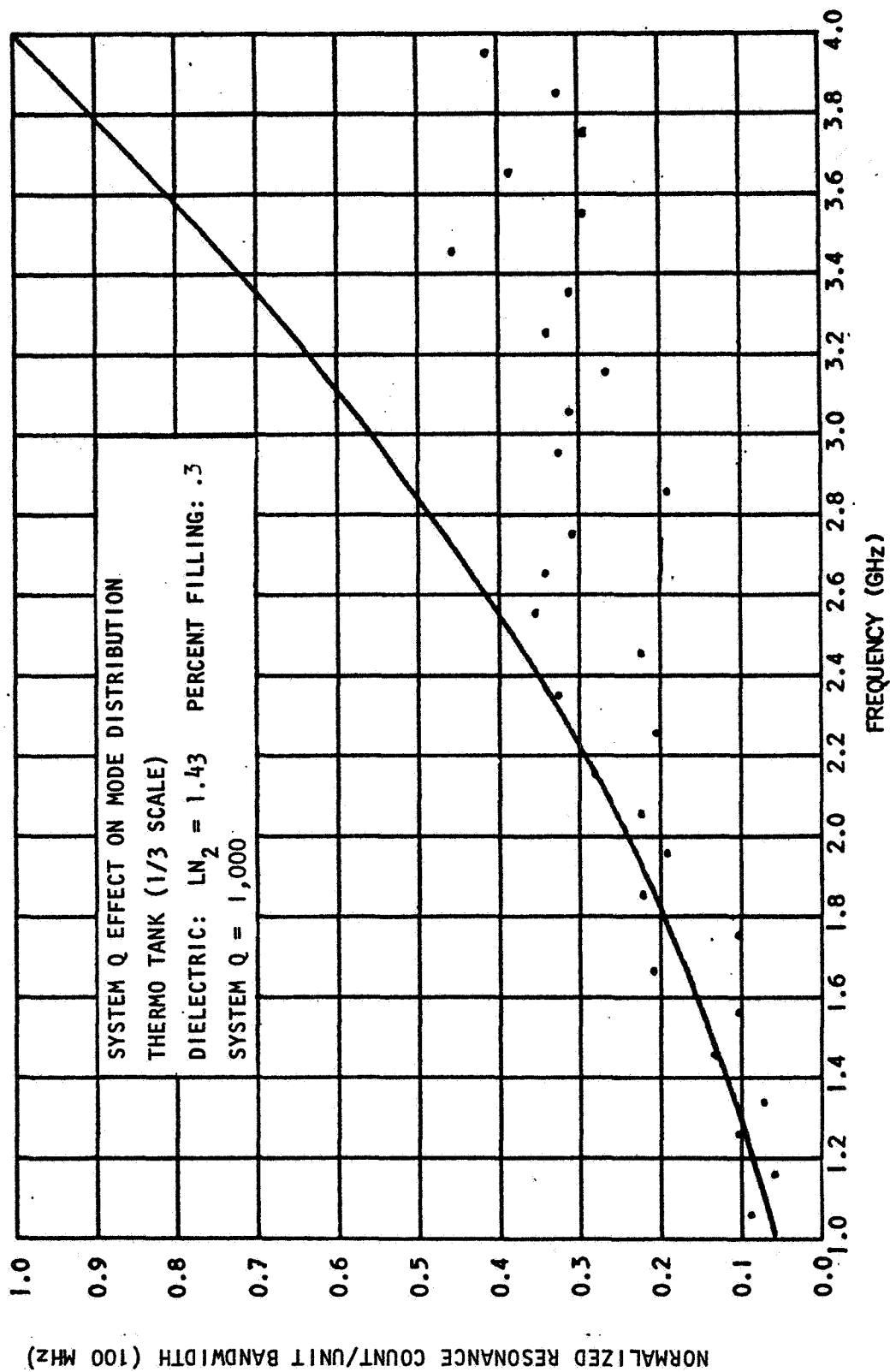


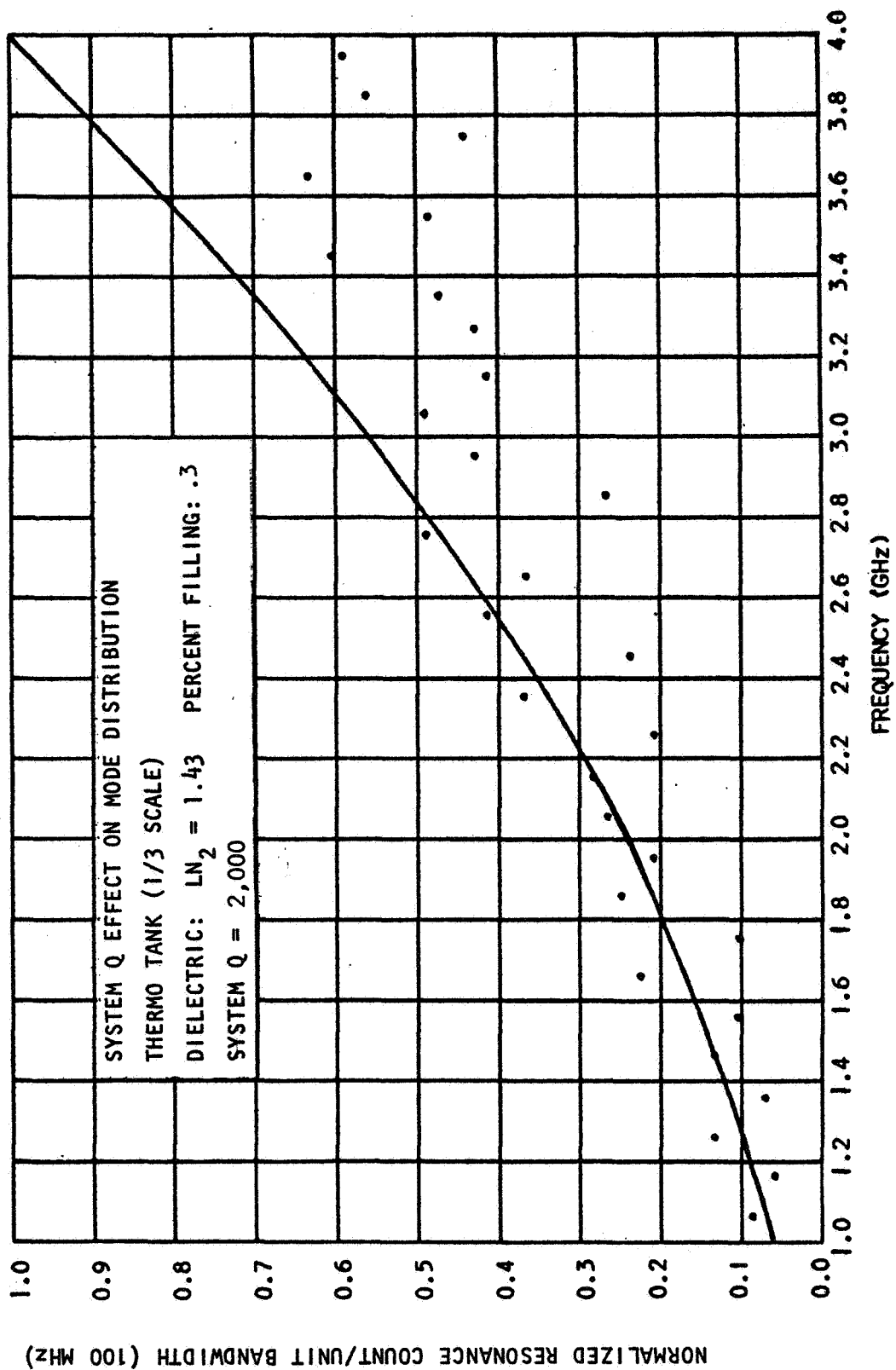


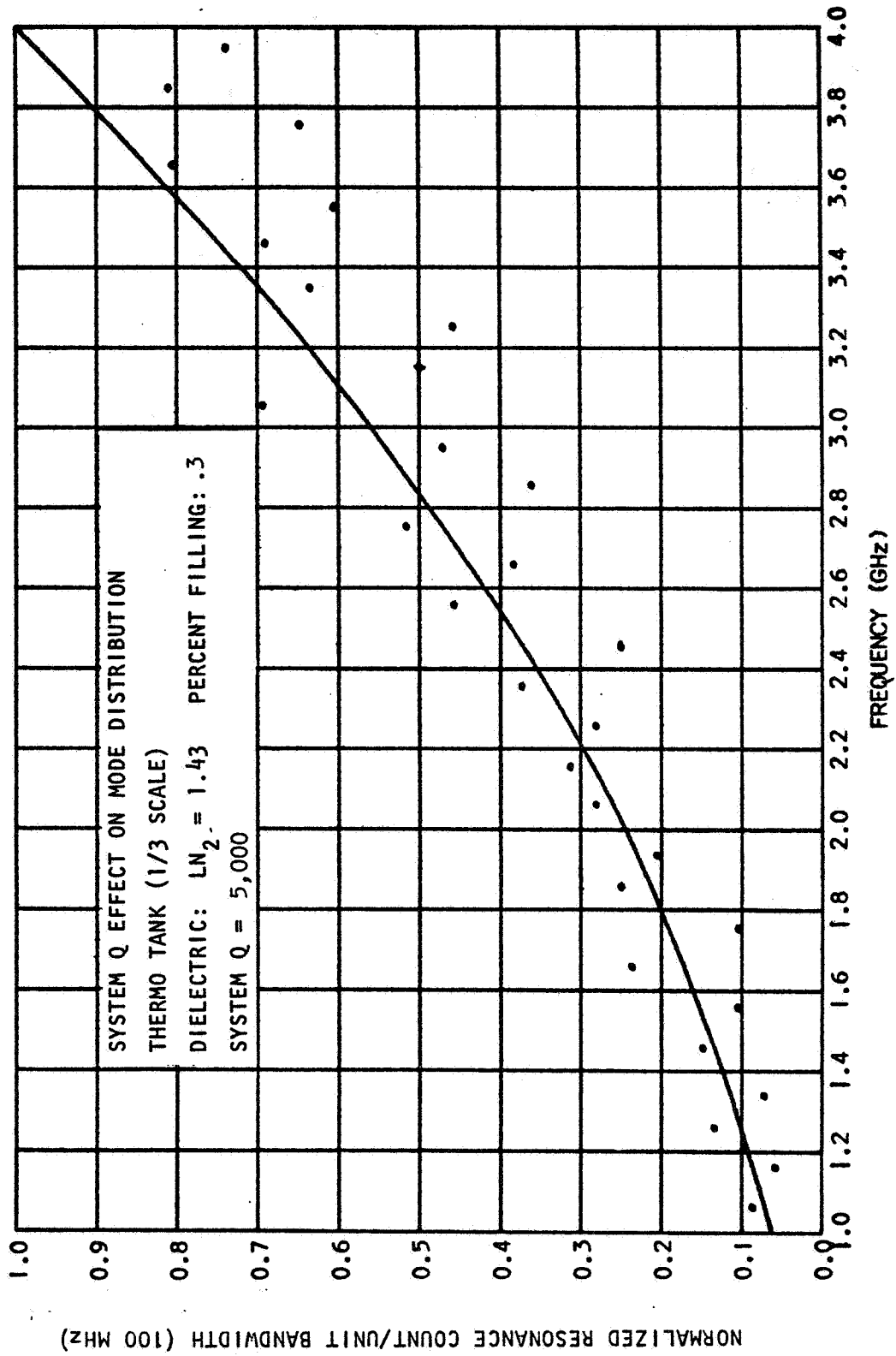


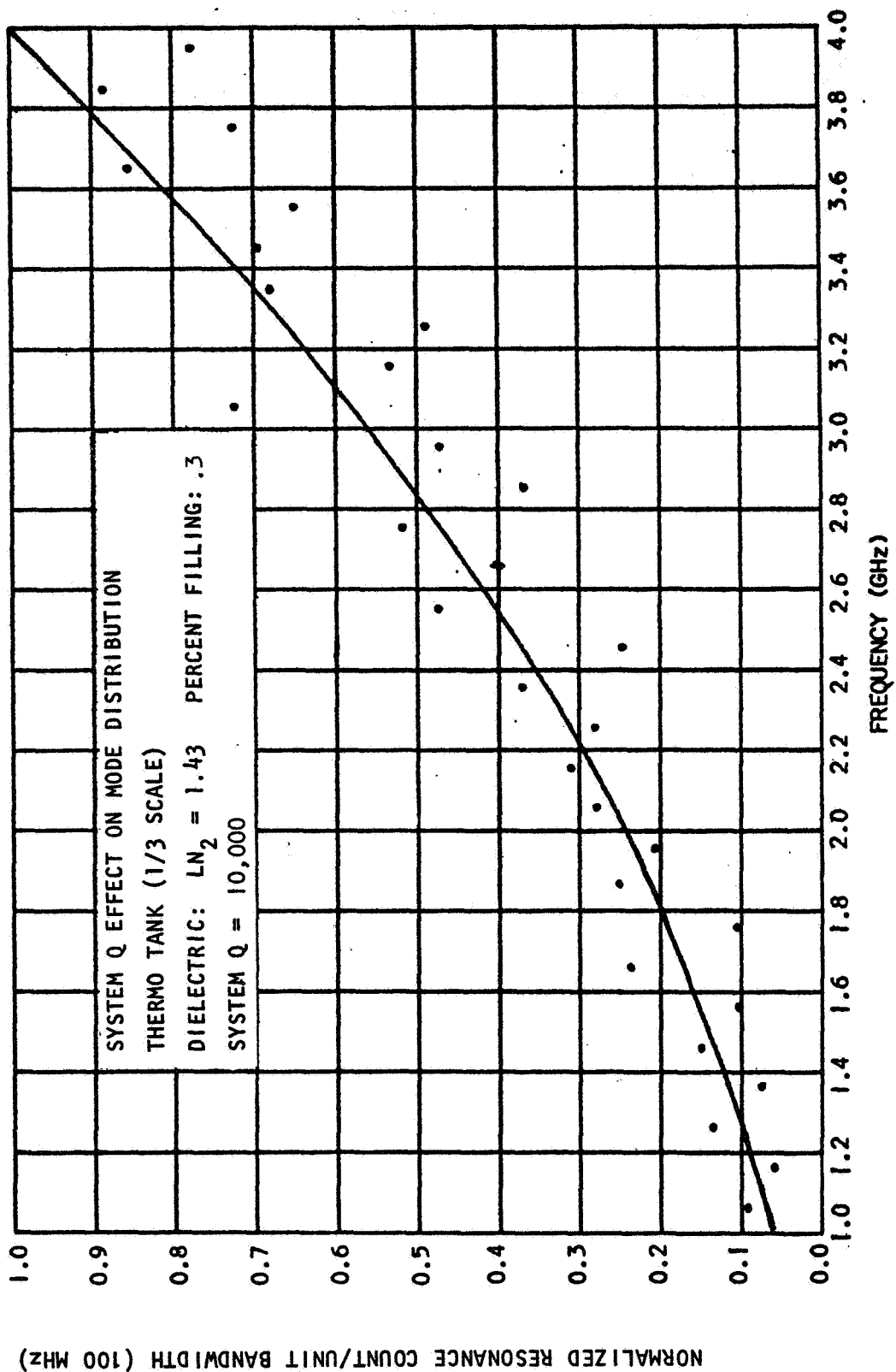


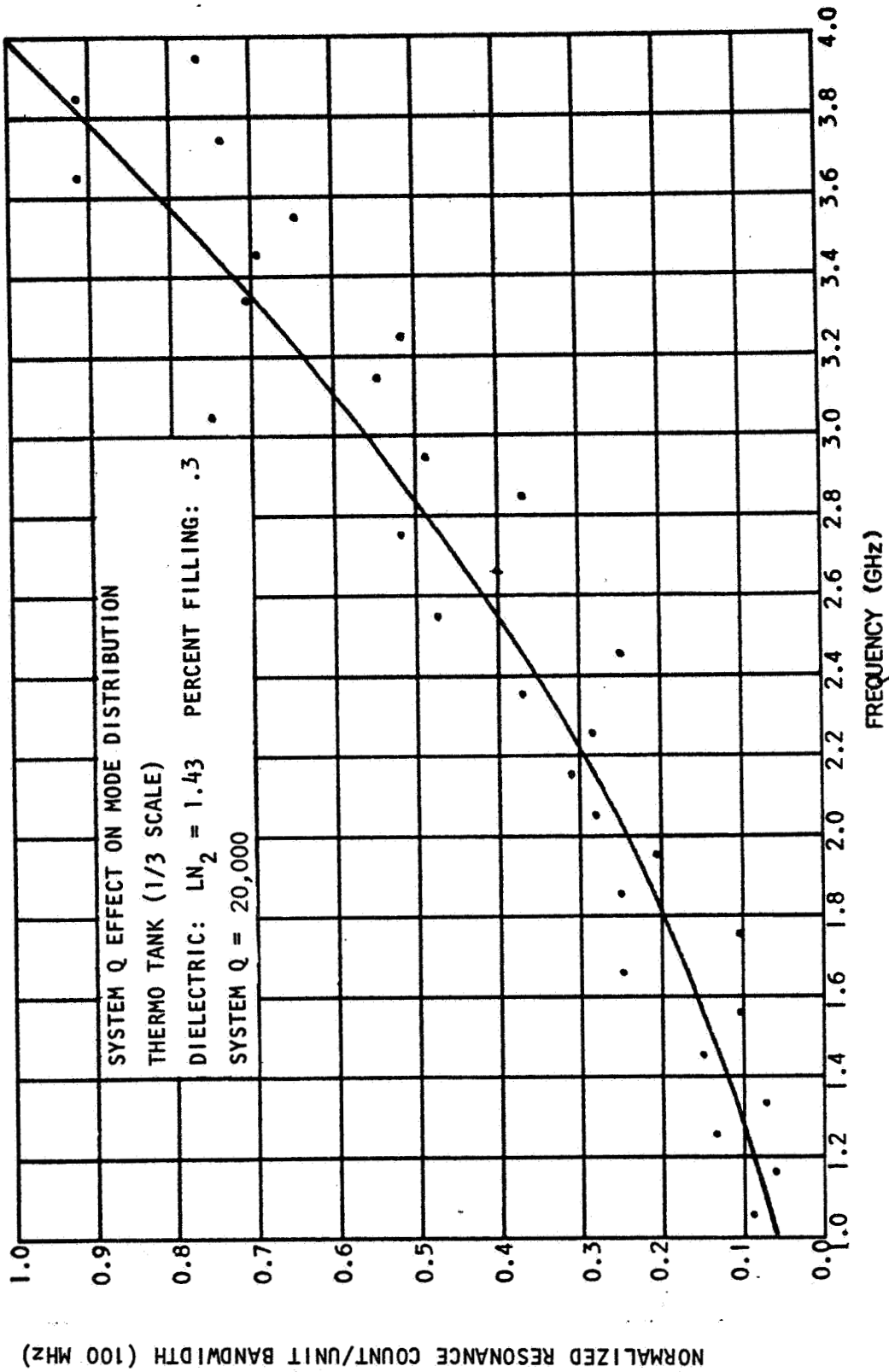


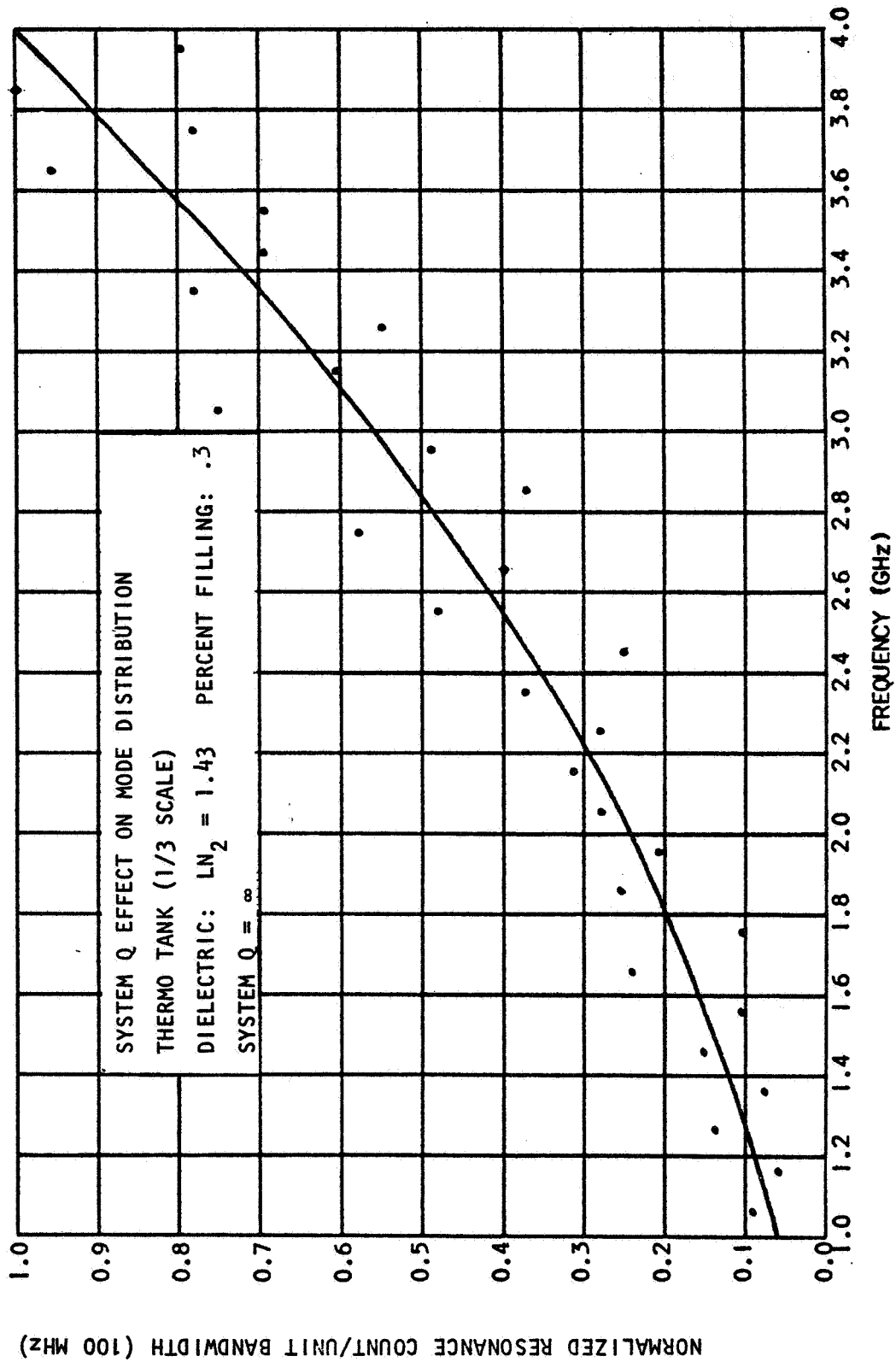


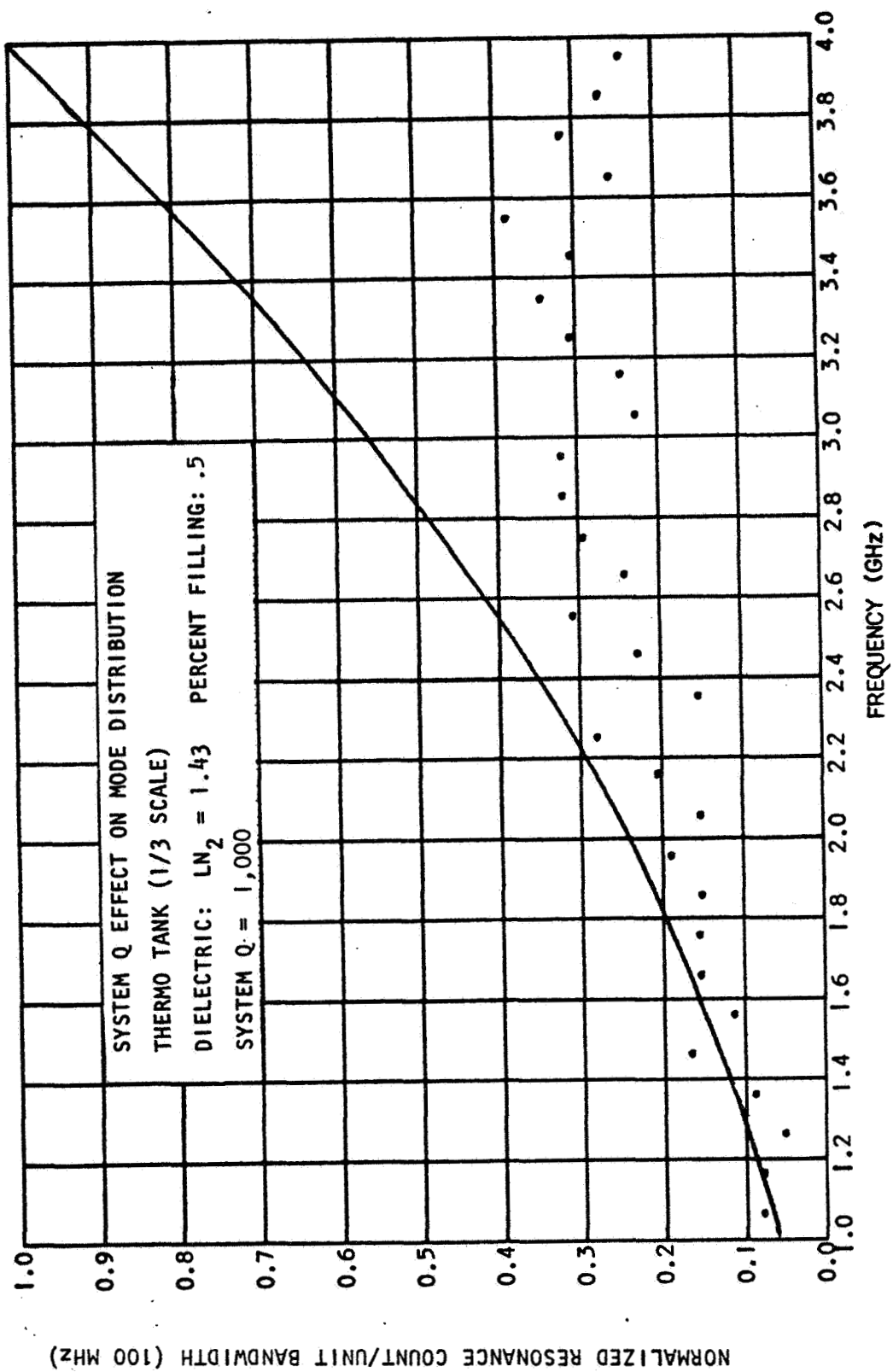


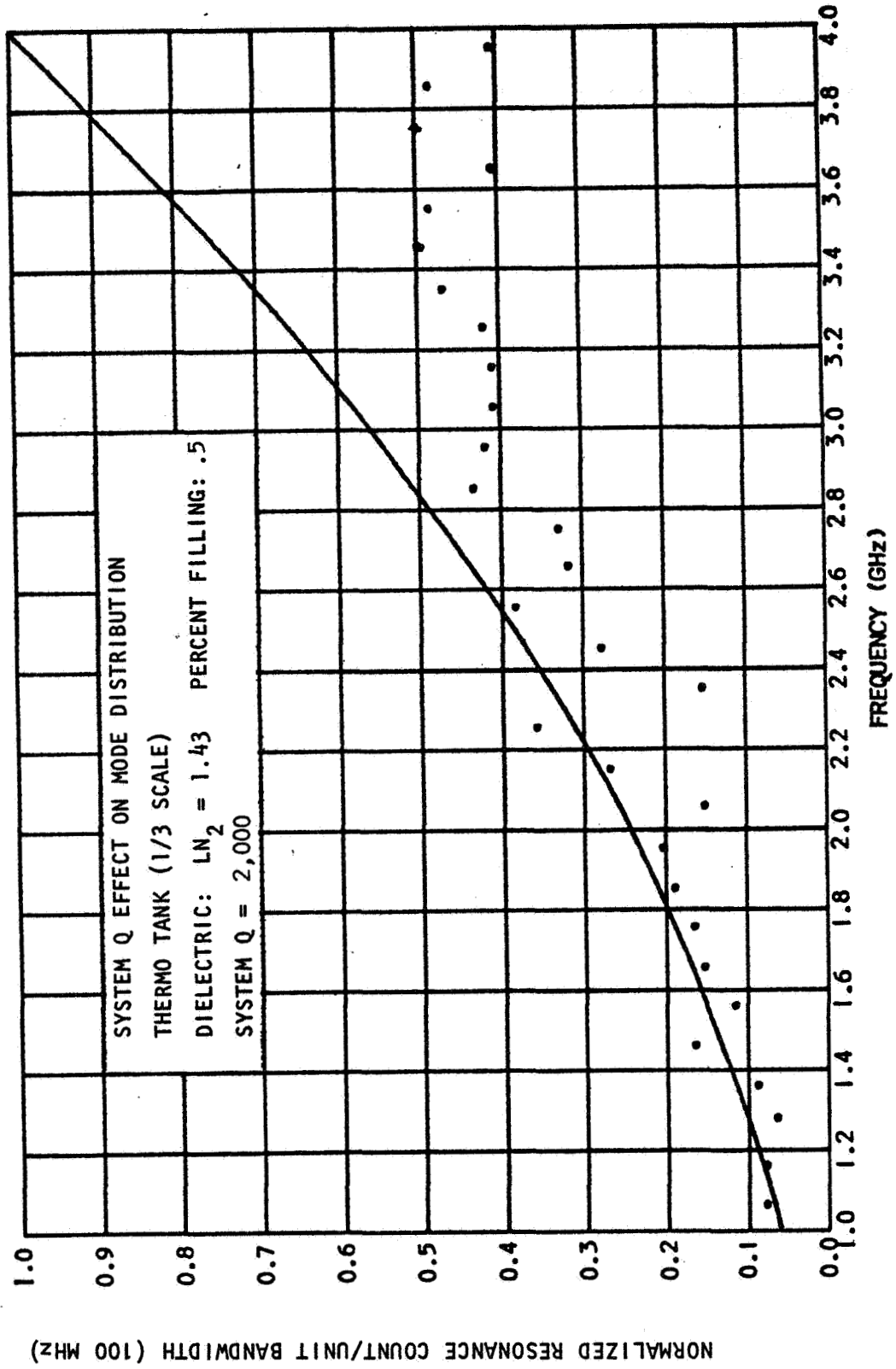


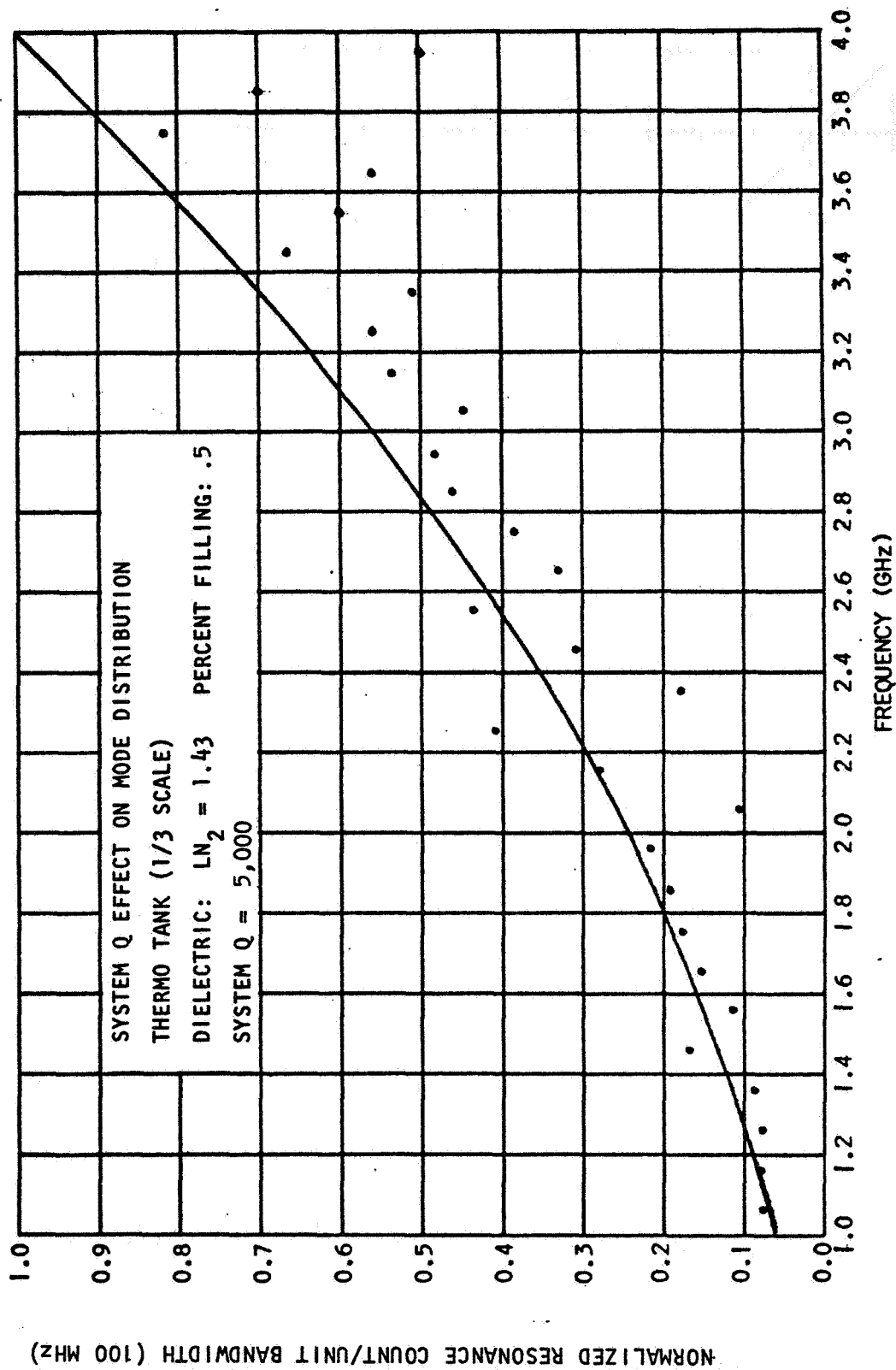


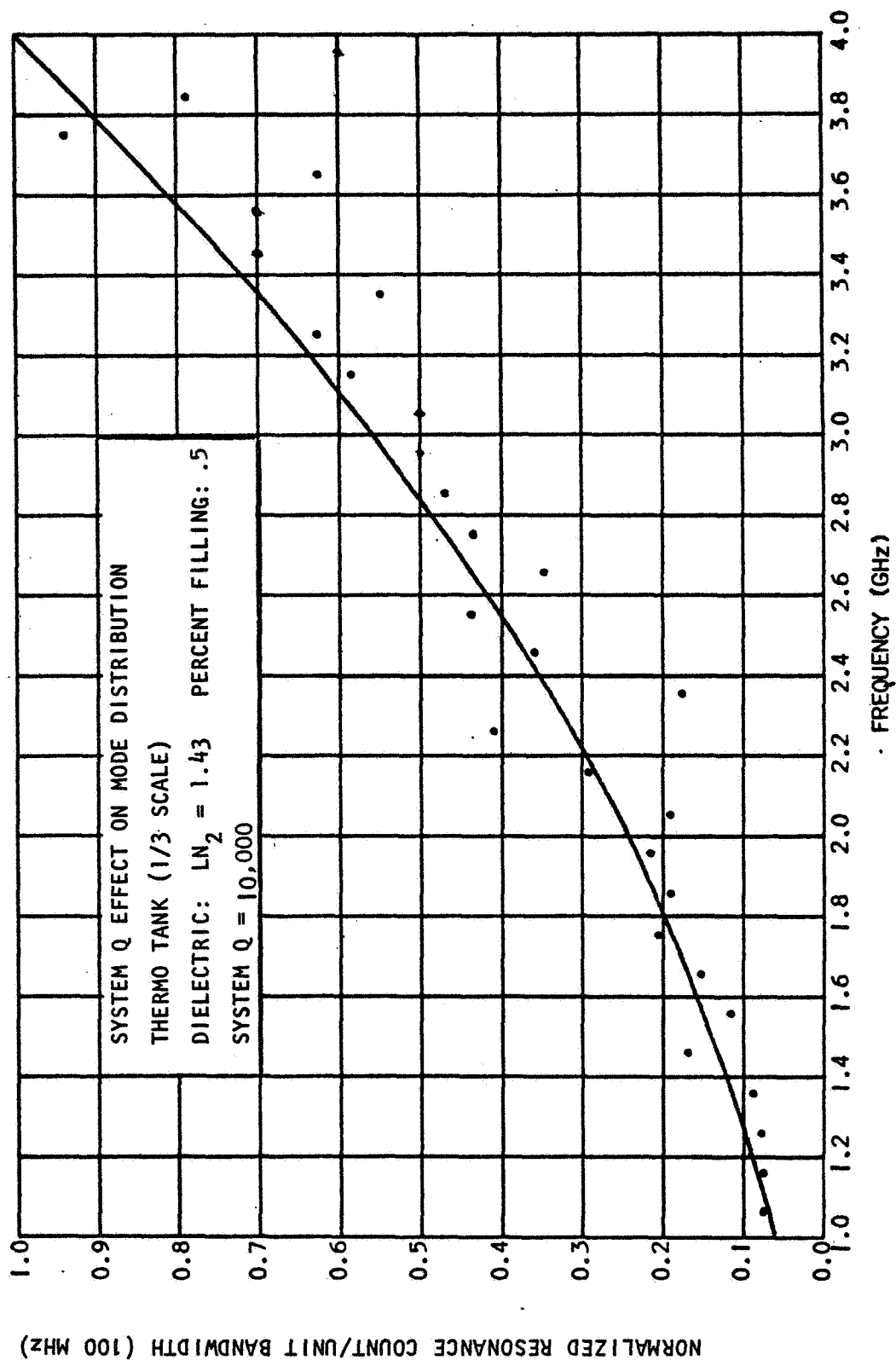


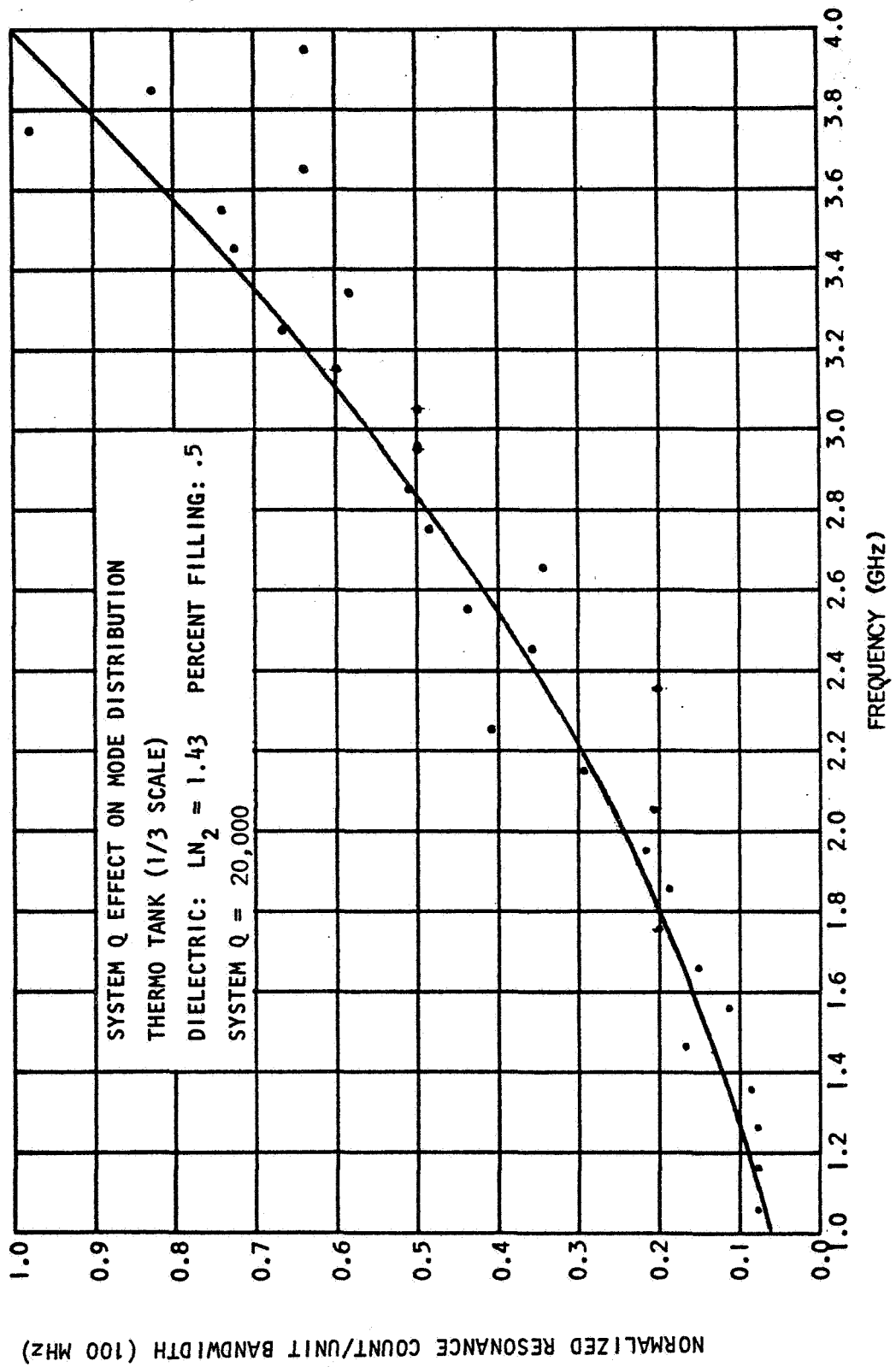


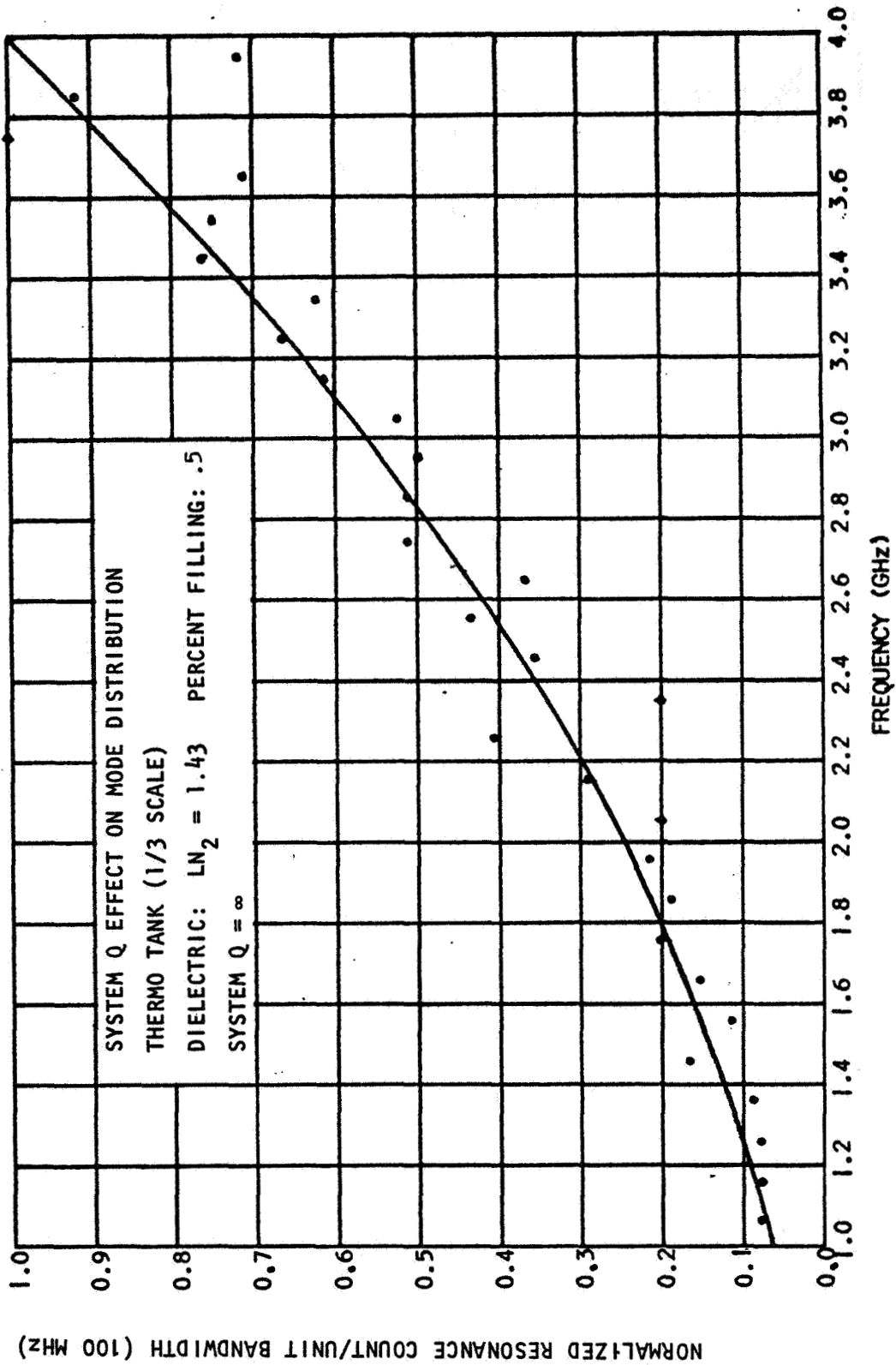


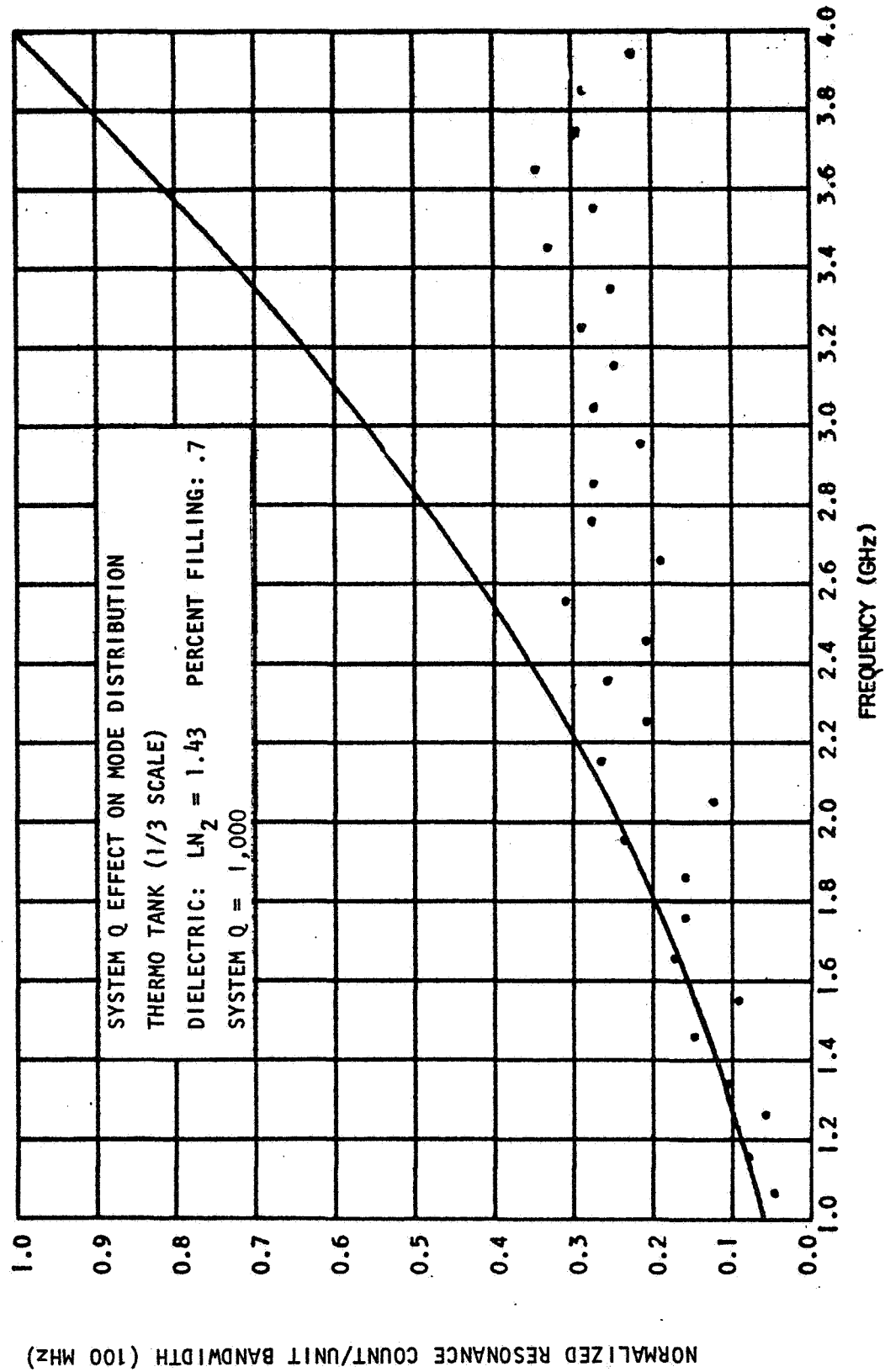


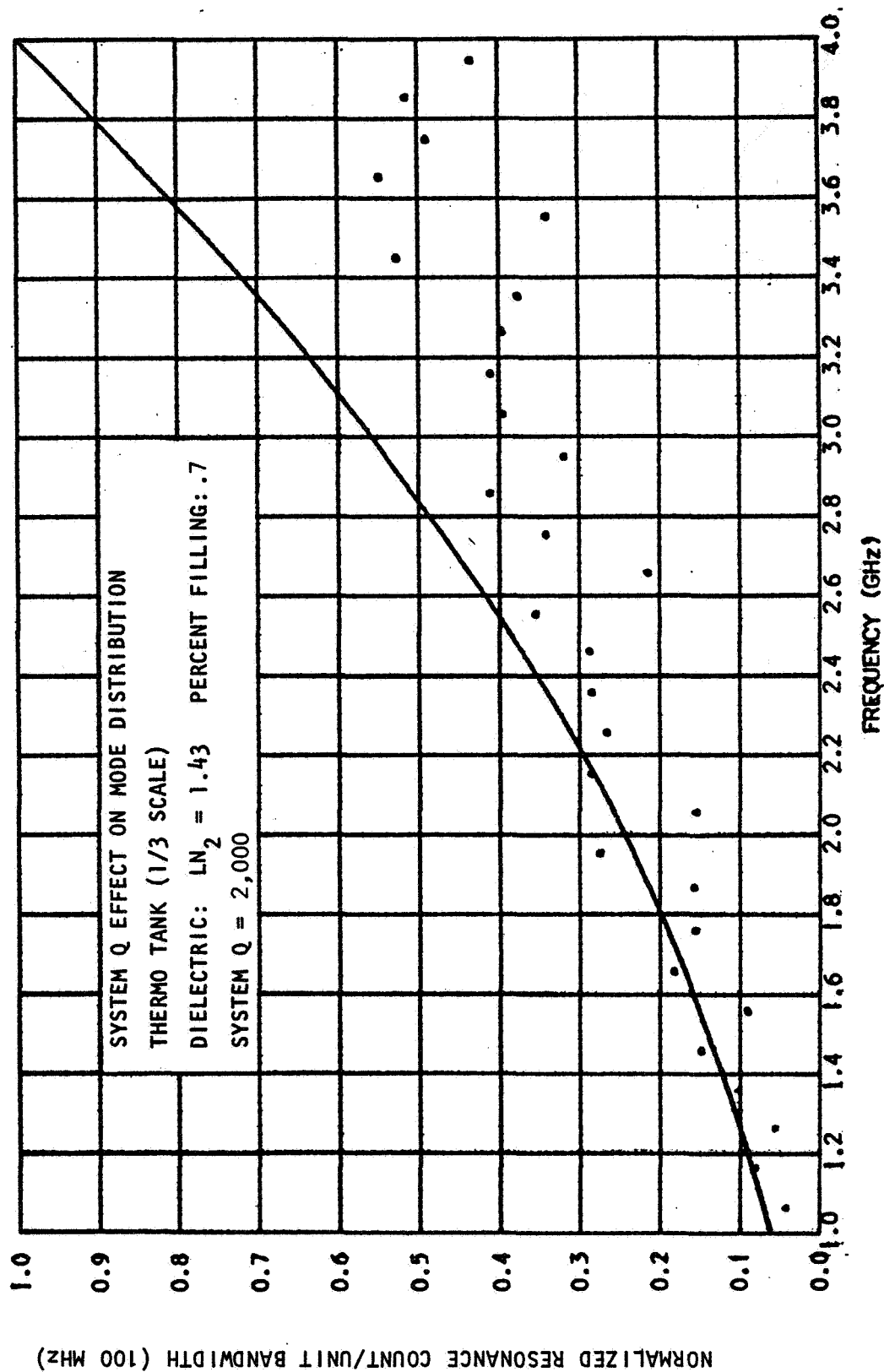


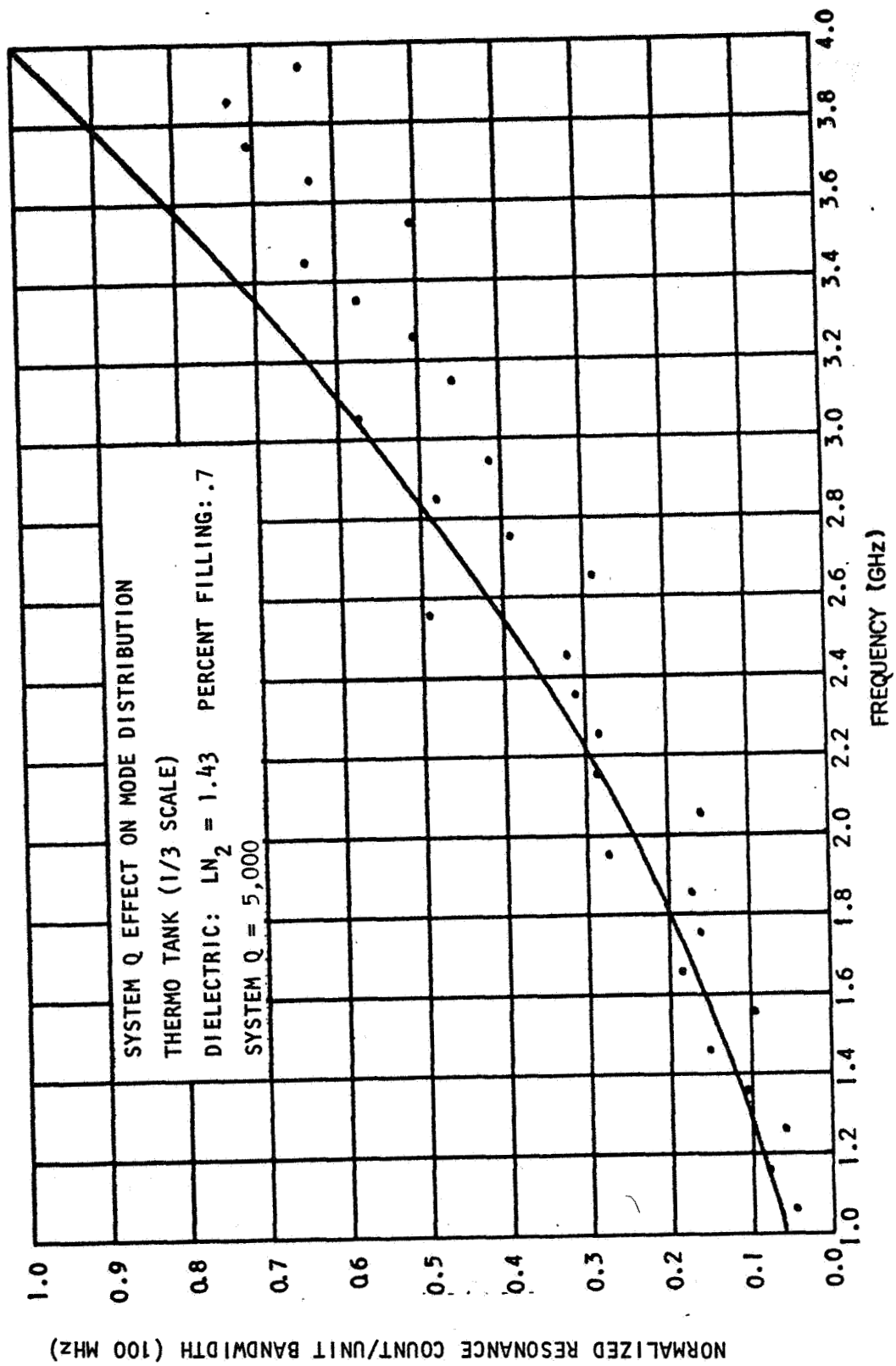


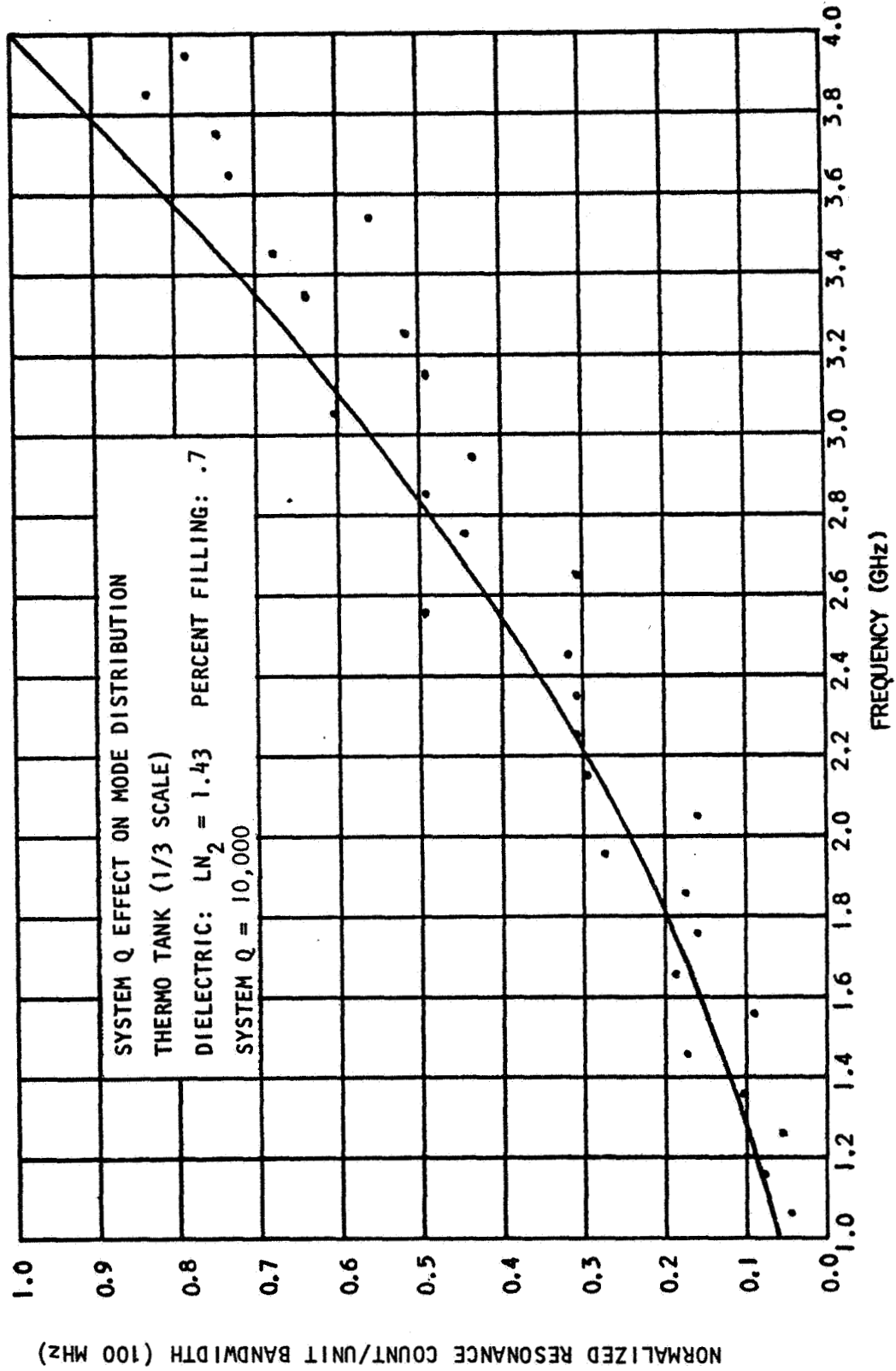


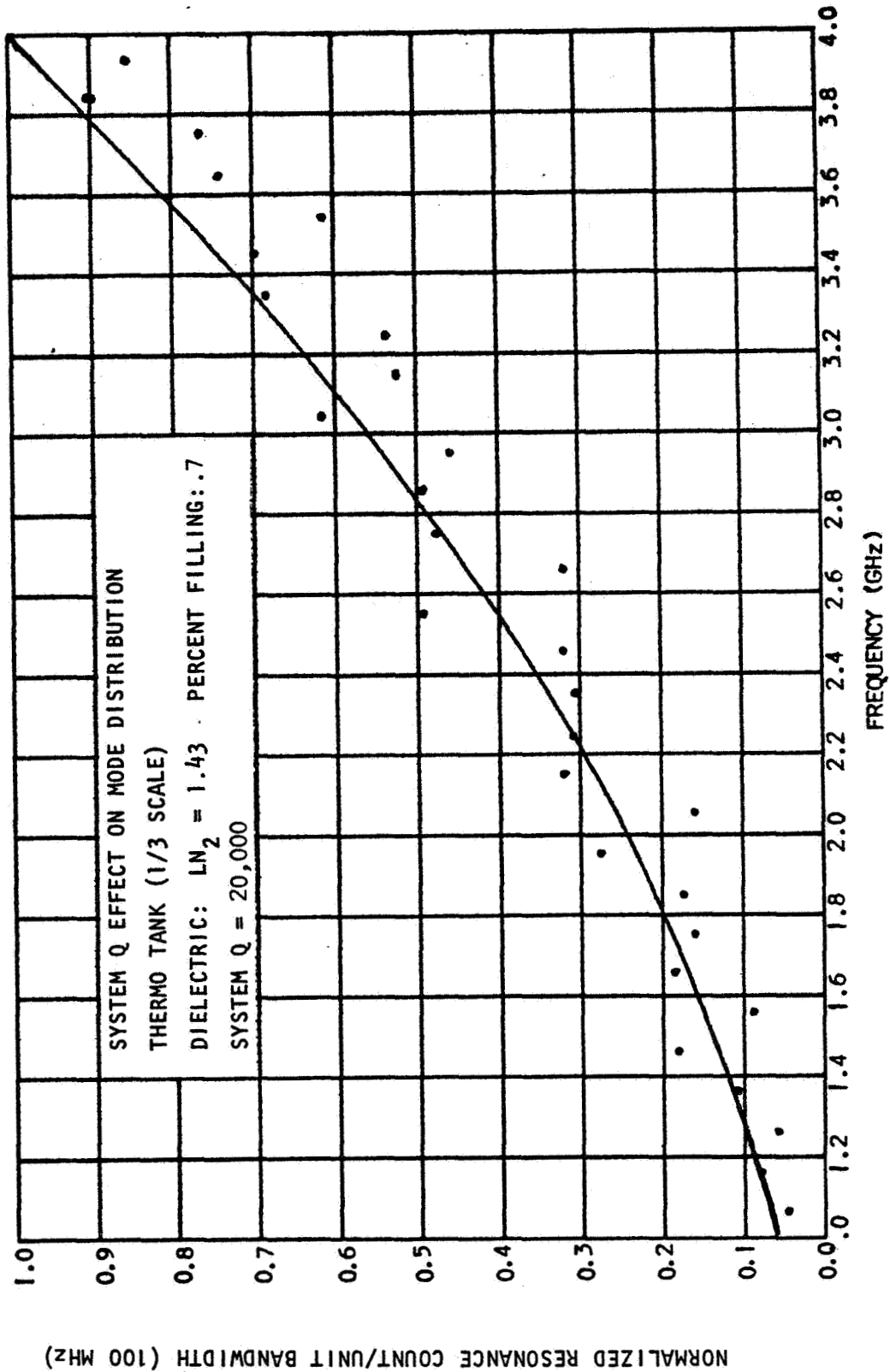


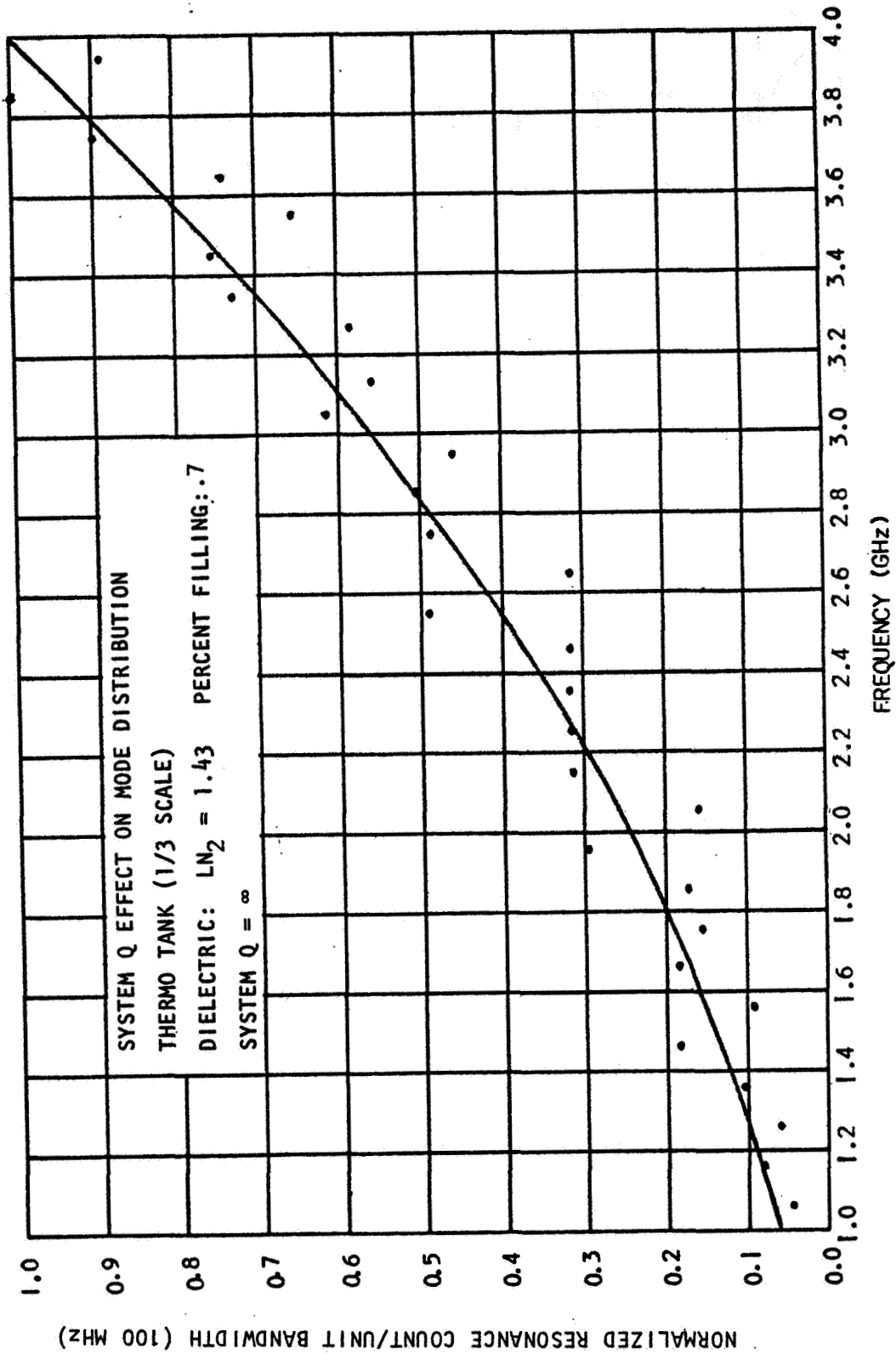


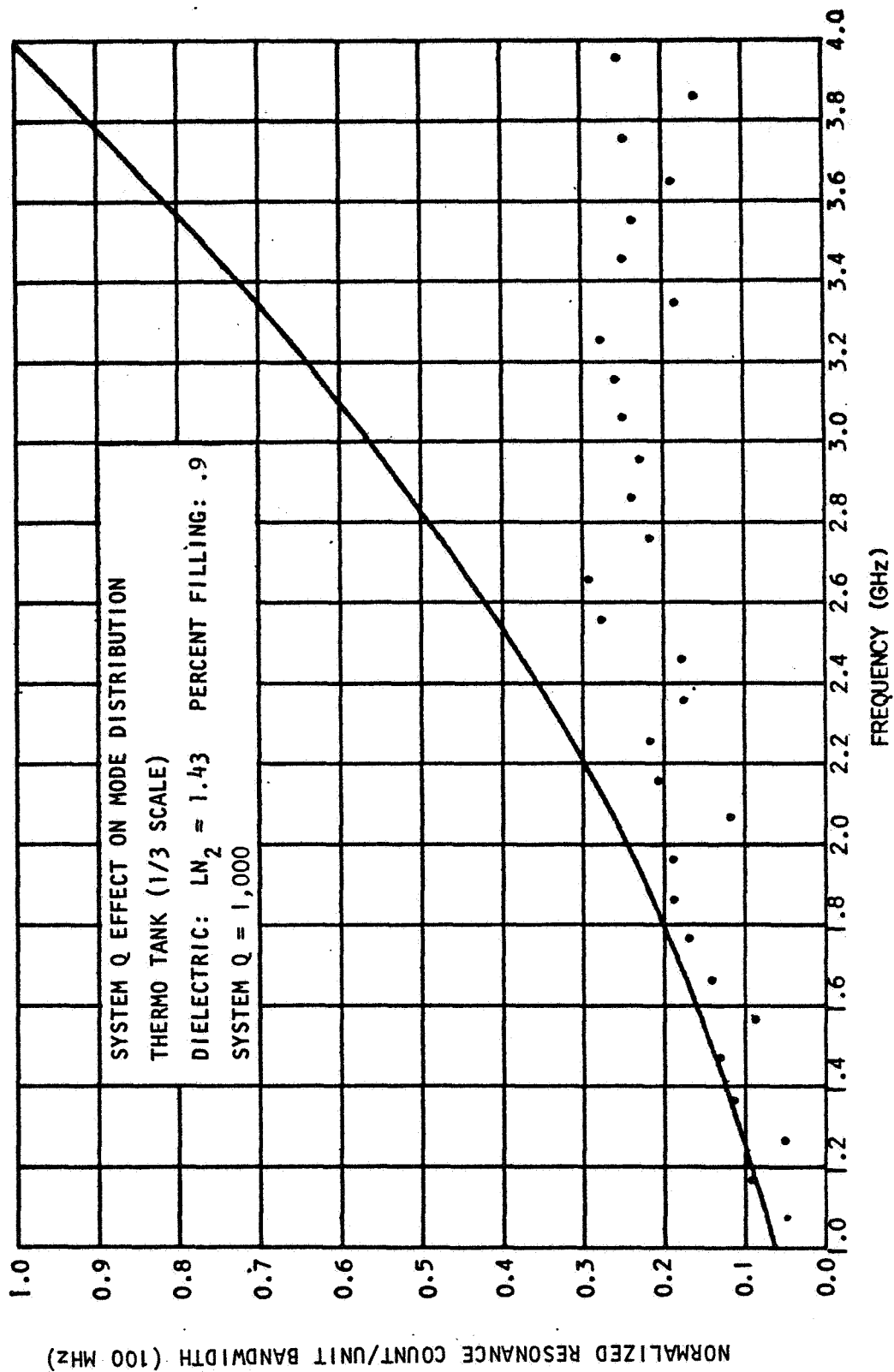


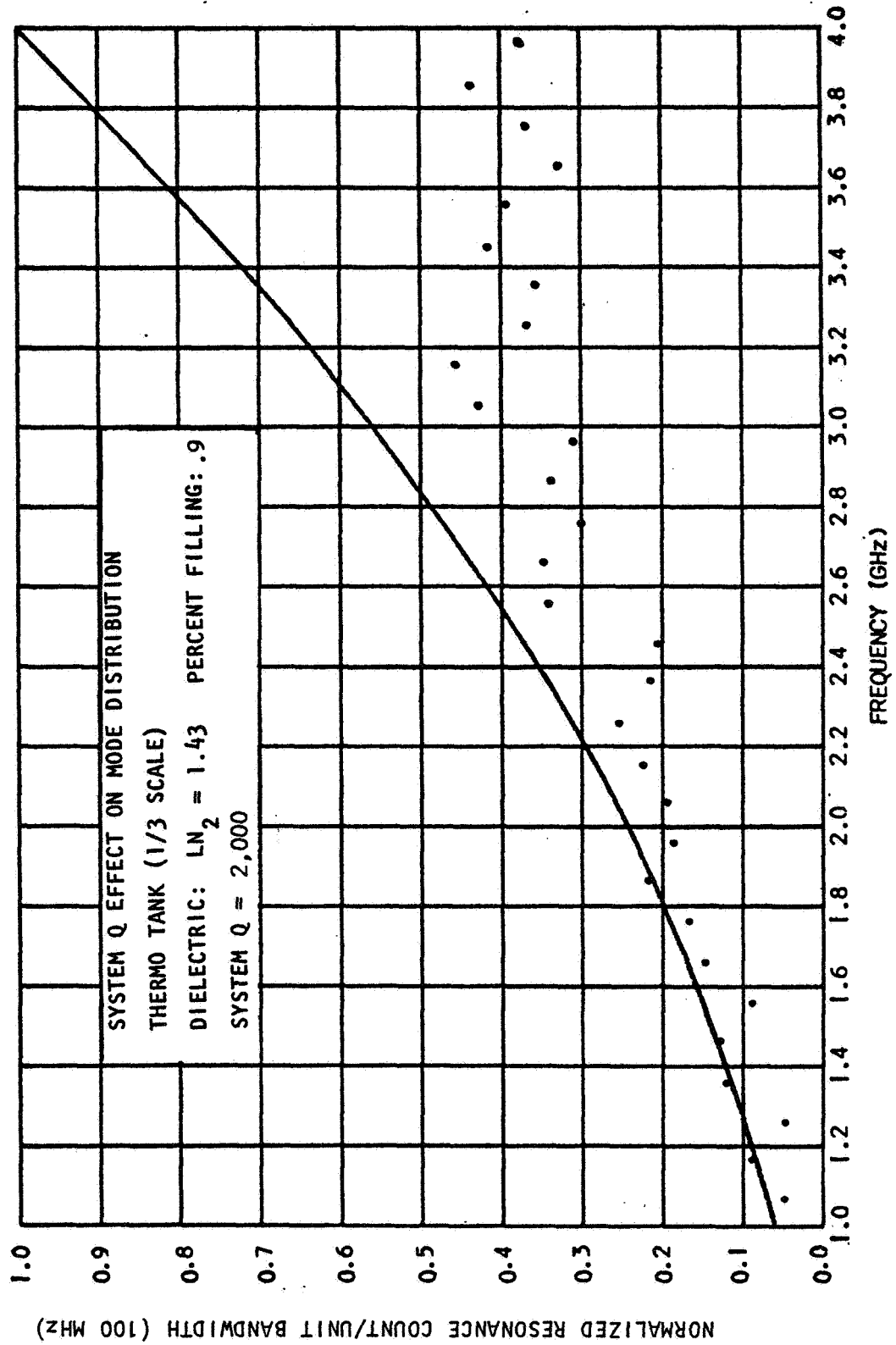


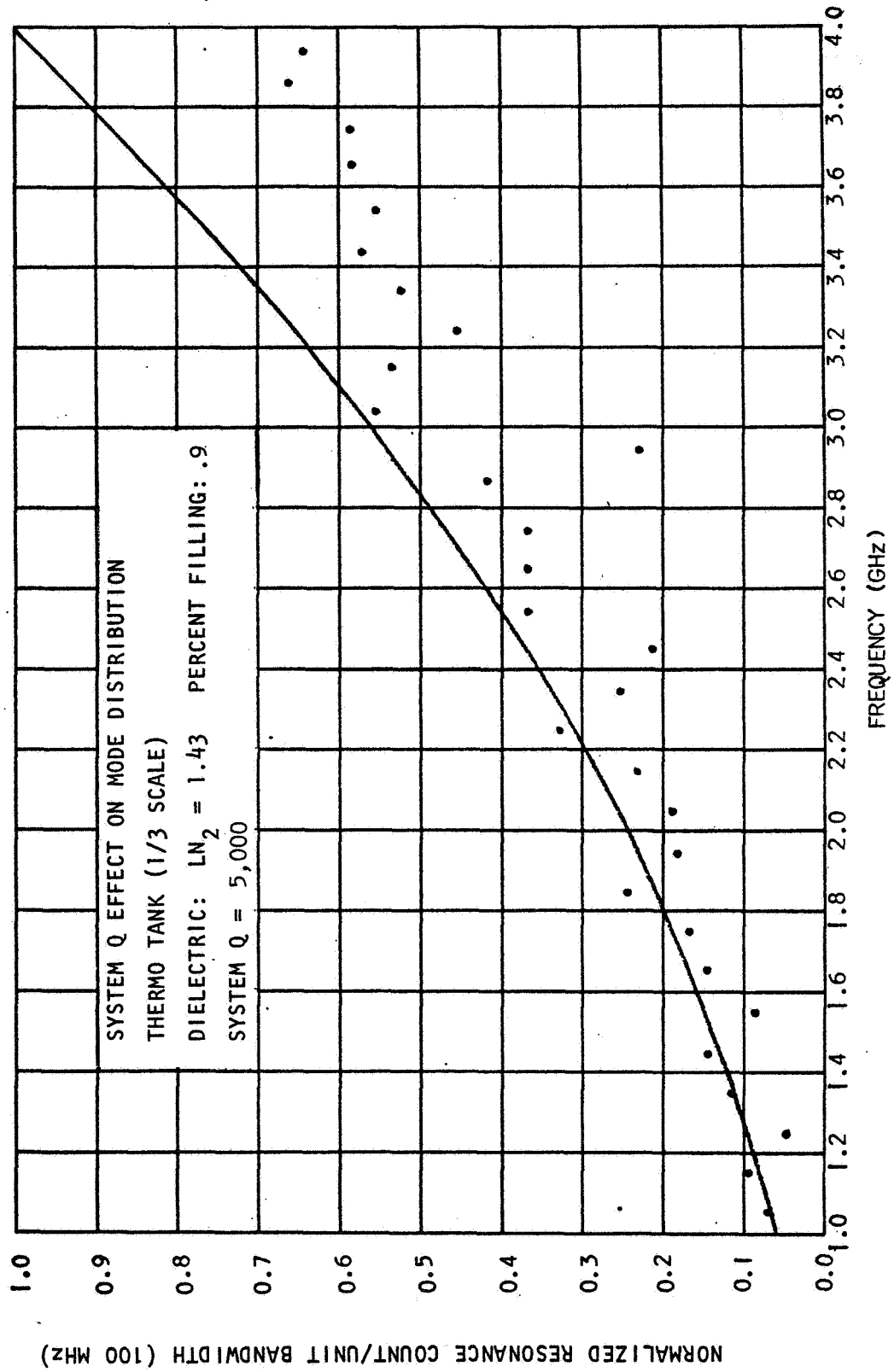


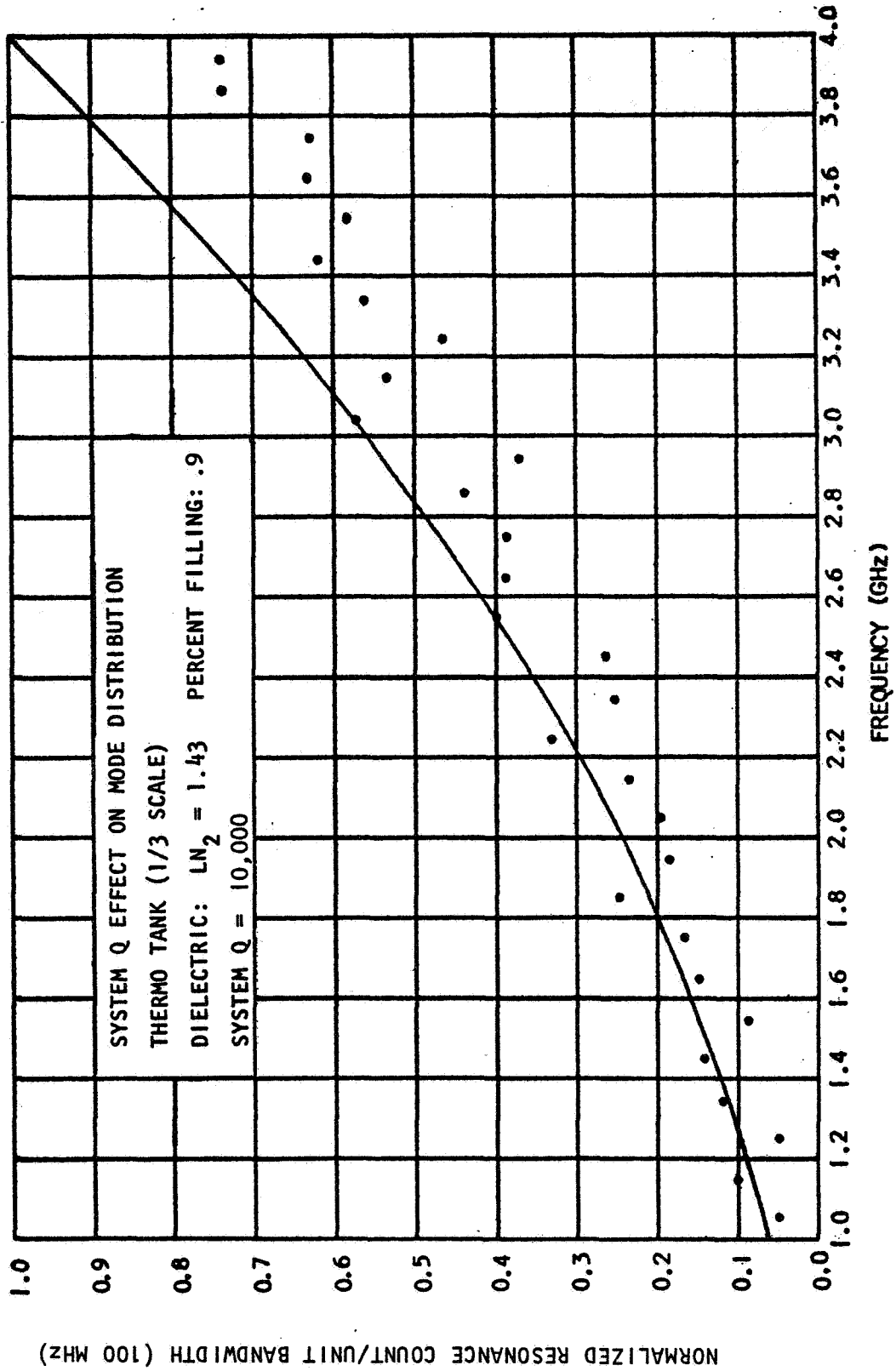


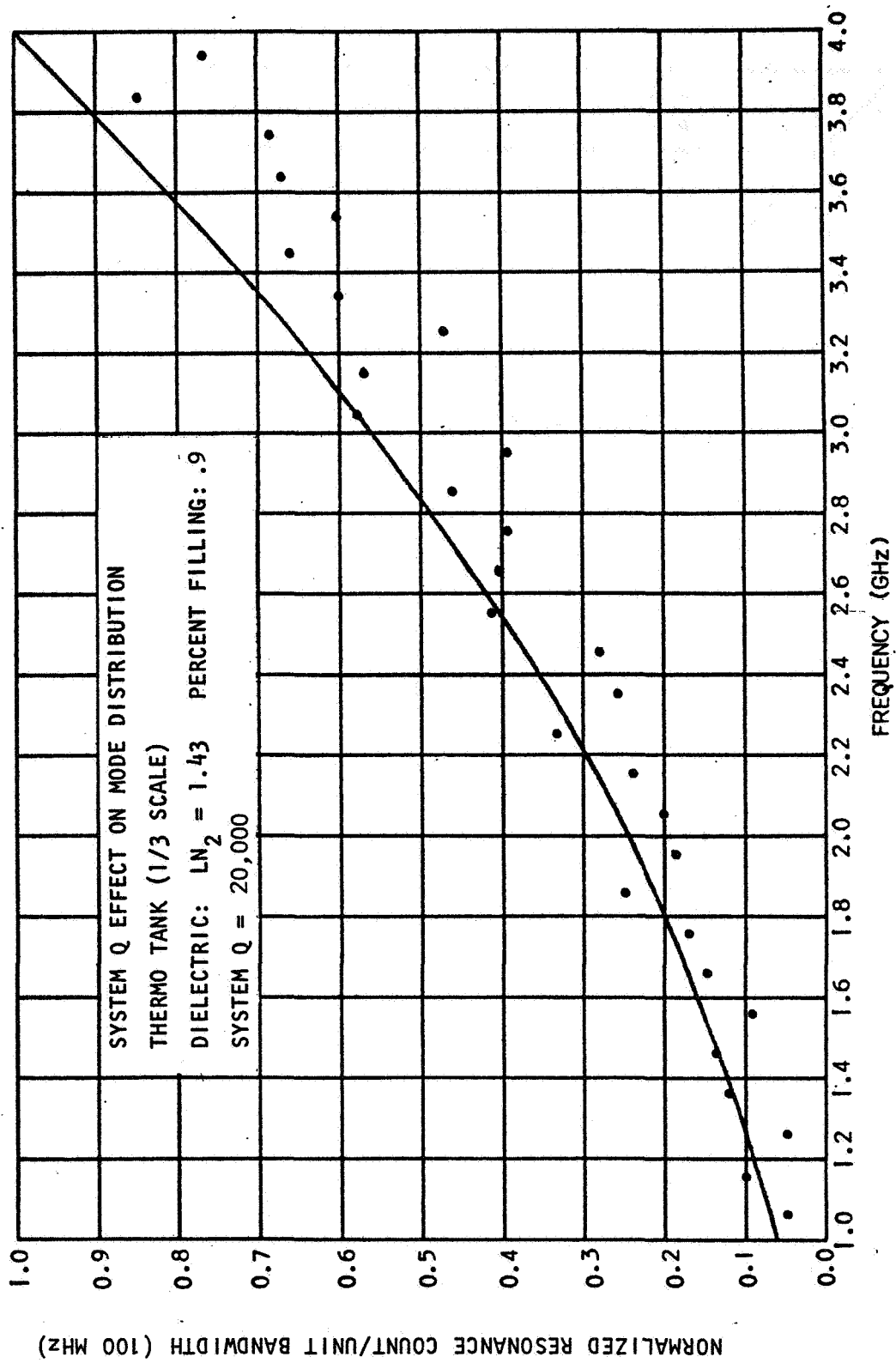


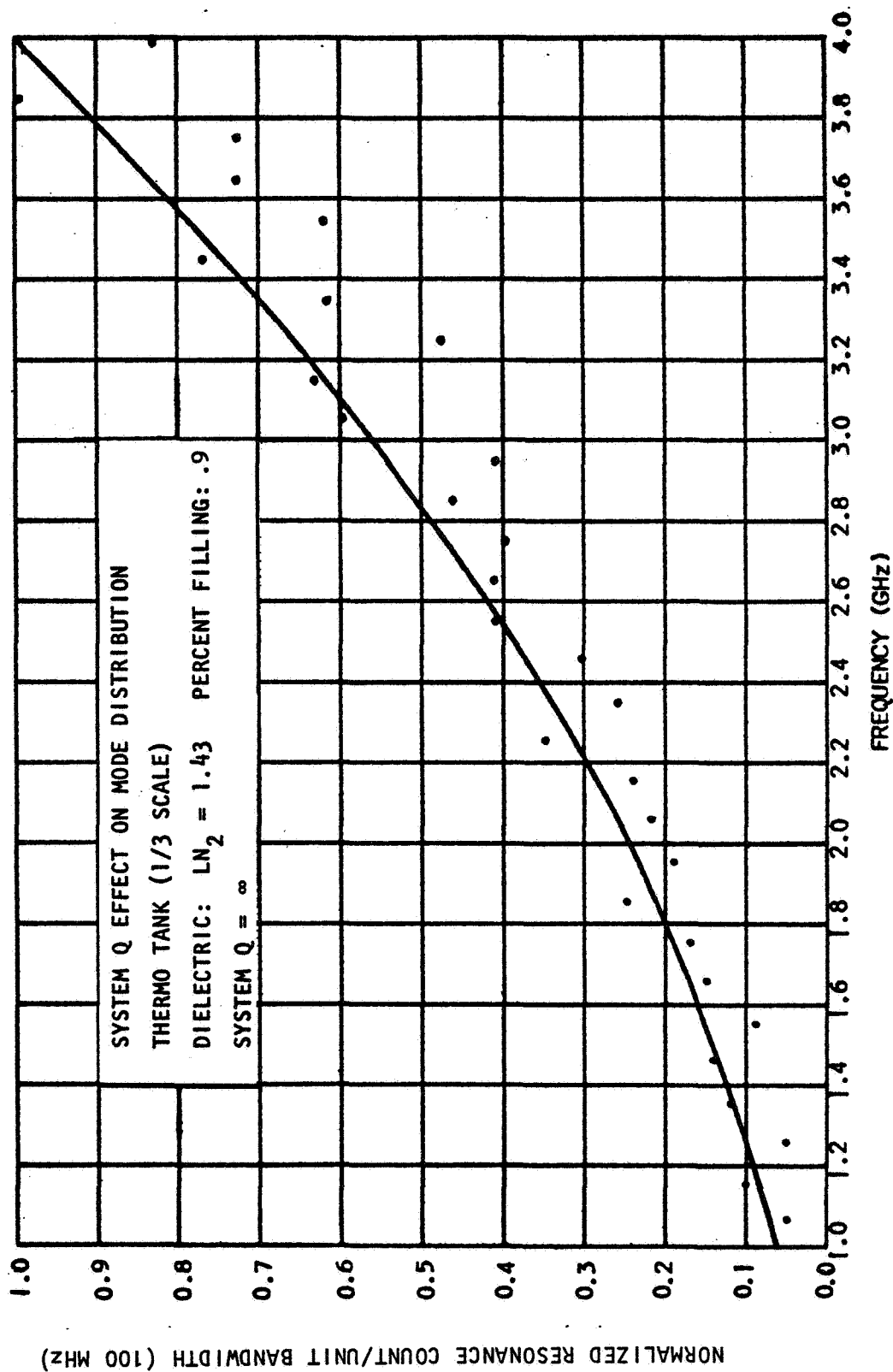












Although patent application Serial No. 708908 (Post & Brown) filed February 28, 1968, relates to an invention disclosed in data furnished to the Government in this Final Report, it is to be noted that this invention was not made (conceived or first actually reduced to practice) under this contract or in the performance of any work done upon an understanding in writing that this contract would be awarded. Accordingly, the rights acquired by the Government under this contract shall not include any rights, express or implied, in the aforementioned invention and this invention shall be deemed to be the exclusive property of the Bendix Corporation.